University of Nottingham

UK | CHINA | MALAYSIA

Mechanistic insights into the self-assembly and the interactions of supramolecular gels with biological systems

Maria Galini Faidra Angelerou (M.Sc.)

Submitted to The University of Nottingham for the degree of

Doctor of Philosophy

September 2018

Declaration

Unless otherwise acknowledged, the work presented in this thesis is my own. No part has been submitted for any other degree at The University of Nottingham or any other institution.

This project was part of the Centre of Doctoral Training in Targeted Therapeutics funded by the EPSRC (grant number EP/L01646X) and the experimental work was mainly conducted at the University of Nottingham (unless otherwise stated).

This doctoral dissertation was conducted under the supervision of:

Dr. Maria Marlow, Associate Professor at School of Pharmacy at the University of Nottingham, UK and

Dr. Mischa Zelzer, Assistant Professor at School of Pharmacy at the University of Nottingham, UK

Maria Galini Faidra Angelerou

September 2018

.."If you thought it would be a plan worth trying, I'd have to take your word it would help."

"You can't guarantee things like that! After all, when we had all the books we needed, we still
insisted on finding the highest cliff to jump off. But we do need a breather. We do need
knowledge. And perhaps in a thousand years we might pick smaller cliffs to jump off. The books are to remind us what asses and fools we are. They're Caesar's praetorian guard, whispering as the parade roars down the avenue, `Remember, Caesar, thou art mortal.' Most of us can't rush around, talking to everyone, know all the cities of the world, we haven't time, money or that many friends. The things you're looking for, Montag, are in the world, but the only way the average chap will ever see ninety-nine per cent of them is in a book. Don't ask for guarantees. And don't look to be saved in any one thing, person, machine, or library. Do your own bit of saving, and if you drown, at least die knowing you were headed for shore."..

Ray Bradbury, *Fahrenheit 451*

Acknowledgements

First and foremost, I would like to thank my scientific parents, Maria and Mischa for leading the way in these past three years and supporting every single one of my steps and decisions, giving me numerous opportunities and teaching me how to be a rigorous scientist.

There is a long list of friends and colleagues that supported this work at good and bad moments. I would like to cordially thank my lab friends, Litty, Rebeca, Ruggero, Amjad, Marina and Emanuele for supporting this work on a daily basis. Vasiliki and Fryni were always there for me to listen and advise, thank you for always being ready to help. My non-science friends Giorgos, Maria, Melina, Vasilis and my sister, Polyxeni that have been around to show me that there is still life outside the PhD world.

Lyko and Platon, having you is one of the biggest presents in my life. In good and bad moments you always challenged me to become a better person.

Benoit, there are no words to express what a precious, beautiful difference your presence made in my life. Thank you, have all the best of joy and luck in life.

Finally, there is nothing big enough to say to thank these two people that gave me the opportunity to write these words today. Thank you for showing how to unconditionally give, thank you for being the inspiring examples in my life.

To my most beloved teachers, my mother and father.

LIST OF PUBLICATIONS

Angelerou MGF, Frederix PWJM, Wallace M, Yang B, Rodger A, Adams DJ, Marlow M, and Zelzer M (2018) Supramolecular Nucleoside-Based Gel: Molecular Dynamics Simulation and Characterization of Its Nanoarchitecture and Self-Assembly Mechanism. *Langmuir* 34, 23, 6912-6921

Angelerou MGF, Yang B, Arnold T, Rawle J, Marlow M and Zelzer M. Hydrophobicity of surface-immobilised molecules influences architectures formed via interfacial self-assembly of nucleoside-based gelators. *Soft Matter,* 2018, **14**, 9851-9855

Angelerou MGF, Sabri A, Creasey R, Angelerou P, Marlow M, Zelzer M (2016) Surface-directed Modulation of Supramolecular Gel Properties. *Chemical Communications*; 52: 4298-4300

Johnson L, Angelerou MGF., Surikutchi BT, Allen S, Zelzer M, & Marlow M (2018). Low molecular weight nucleoside gelators: A platform for protein aggregation inhibition. *Molecular pharmaceutics*. (just accepted)

Angelerou MGF, Markus R, Paraskevopoulou V, Foralosso R, Clarke P, Alvarez CV, Chenlo M, Johnson L, Rutland C, Allen S, Brasnett C, Seddon A, Zelzer M and Marlow. Mechanistic insights into the encapsulation and release of model molecules with different properties from a supramolecular nucleoside gel *in vitro* and *in vivo* (under review)

Contents

Abbreviations

AFM Atomic Force Microscopy

ANOVA One-way Analysis of Variance

ALS aromatic group-linker- steroidal moiety

BSA Bovine Serum Albumin

CAB cholesteryl-4-(2-anthryloxy) butanoate

CD Circular Dichroism

Cy5-BSA cyanine5-Bovine Serum Albumin

DiI 1,1'-Dioctadecyl-3,3,3',3'-Tetramethylindocarbocyanine Perchlorate

DSC Differential Scanning Calorimetry

Fmoc Fluorenylmethoxycarbonyl

G' Storage/elastic modulus

G'' Loss modulus

GNL glycosyl-nucleoside lipids

GISAXS Grazing Incidence Small Angle X-Ray Scattering

GIWAXS Grazing Incidence Wide Angle X-Ray Scattering

IVIS In Vivo Imaging System

LC-MS Liquid Chromatography couple to Mass Spectrometry

LMWG Low Molecular Weight Gelator

LVE Linear-Viscoelastic

MW Molecular Weight

NMR Nuclear Magnetic Resonance

PBS Phosphate Buffer Serum

RT Room Temperature

SAFIN self-assembled fibrillar networks

s.c. Subcutaneous

TEM/SEM Transmission/Scanning Electron Microscopy

ToF-SIMS Time of Flight Secondary Ion Mass Spectrometry

USAXS Ultra Small Angle X-Ray Scattering

UV-Vis Ultra violet –visible

WCA water contact angle

XRD X-ray Diffraction

Table of Figures

General Abstract

Among the diversity of drug delivery systems for controlled release, supramolecular gels have recently attracted significant attention due to their biocompatibility and self-healing properties. Supramolecular gels consist of small organic molecules that self-assemble though non-covalent interactions into fibrillar networks that entrap high volumes of solvent (for hydrogels, water). This reversible nature of the interactions that holds the solid phase together is responsible for the dynamic nature of these materials and their responsiveness to multiple external stimuli. The presence of a third (or more) components in the system, apart from the gelator and the solvent, can bring major changes in the properties of the final gels, especially when large biomolecules are encapsulated such as proteins and nucleic acids. These changes are attributed to the interactions occurring among gelator, solvent and encapsulated molecule and it would be expected that any parameter that can affect these interactions can change the properties of the materials. This brings the focus of this work herein on the gelator/encapsulated component interface and the interactions occurring. We start with mechanistic investigations of the principles that govern the gel formation for a 2'-deoxycytidine-based gelator, describing the nanoarchitecture of the solid phase; a network of entangled fibres consisting of a hydrophobic core that generate hydrophilic cavities around them where the solvent mostly resides. On a higher level of complexity, we move on to studying the interactions on simple interfaces between gel and simple chemical functionalities and the effect that these chemical functionalities have on the properties of the self-assembled structures. The property of hydrophobicity and the presence of aromatic nuclei were found to directly affect the supramolecular structures formed. More

specifically, the surface properties Polar Surface Area (PSA) and the logP linearly relate with the formation of fibre bundles (fibre aggregation); higher fibre bundle radii are obtained as PSA increases and log P decreases. Additionally, the presence of an aromatic ring leads to higher fibre bundle diameters. Finally, we encapsulate molecules with different properties (a small hydrophobic dye, 1,1'-Dioctadecyl-3,3,3',3'-Tetramethylindocarbocyanine Perchlorate, and different proteins, insulin, lysozyme, β-lactoglobulin and Bovine Serum Albumin) into the supramolecular gels to identify the fibre/encapsulated molecule interactions as well as mechanistically elucidate the *in vivo* and *in vitro* release behaviour of these composite systems. The encapsulated molecules were found to directly interact with the fibres through non-covalent interactions (π-π stacking was identified) rather than get physically entrapped and they were released following the gel's erosion, maintaining their functionality, as demonstrated for insulin and lysozyme. A range of experimental techniques (and molecular dynamic simulations) are used, demonstrating the complementarity of different types of information that need to be accessed to ultimately gain a complete understanding.

Chapter 1

General Introduction

1.1 Introduction to gels

Several definitions have been proposed for gels in order to link their microscopic and macroscopic properties.[1-3] Based on them,[2] a gel has (1) a continuous microscopic structure with macroscopic dimensions throughout the time scale of the analysis and (2) its rheological properties are mostly solid-like despite that it is mainly liquid. In general, they consist of a solid network that limits the flow of the liquid phase and macroscopically behaves as a solid. A very common classification divides gels into chemical and physical gels. In chemical gels the components of the network are cross-linked through permanent covalent interactions whereas in physical gels the network components build the network through reversible, non-covalent interactions.[4]

1.2 Low Molecular Weight Gelators (LMWG) - definitions

Recently, there has been an increasing interest in supramolecular gels, due to their promising potential as conducting materials, materials for energy and information storage, catalysis and sensors[5-7] and for biological applications in tissue engineering, drug delivery, cell culture and gene therapy (Figure 1.1).[5, 8-9 10] Supramolecular gels are physical gels that consist of small organic components that associate through non-covalent interactions into 3D networks. These small organic molecules (with molecular weight smaller than 2000 Da)[11] are usually able, at concentrations lower than usually 0.1-10 wt %,[12] to gel water or organic solvents and form self-supportive

materials. These molecules, most often after the addition of a trigger, self-assemble into long one-dimensional structures that often interact to form structures of

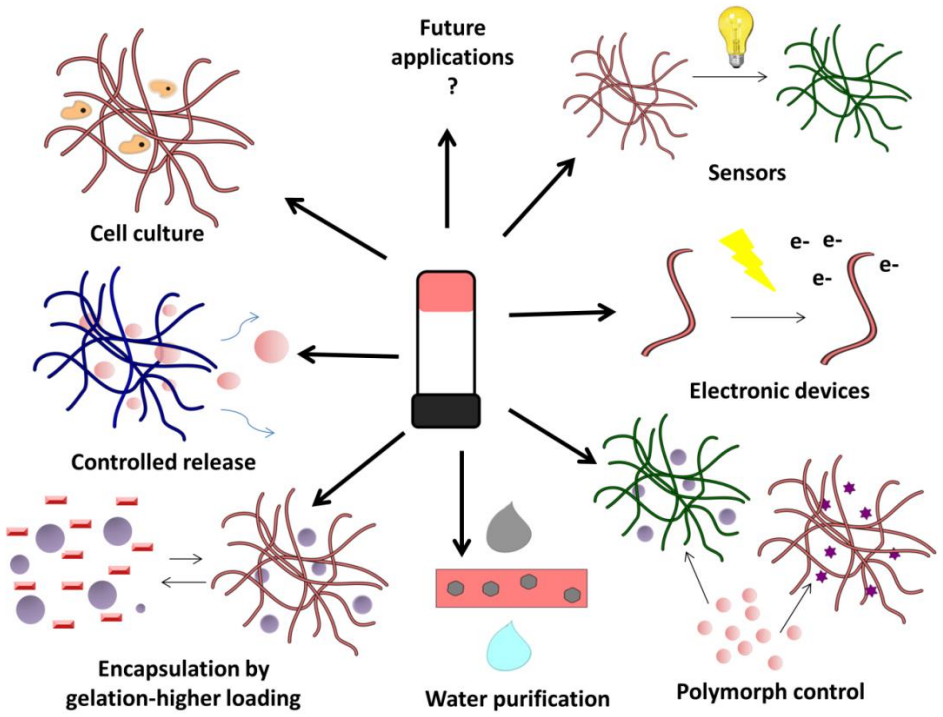

Figure 1.1: Overview of uses of supramolecular gels. Adapted from[13]

different geometries and architectures that ultimately result in an entangled network that can retain solvent volumes as high as 99 times their own.[7] At the nano-scale, this network consists of long one dimensional structures (fibres) entangled together with diameters ranging between a few nanometers to a few hundreds of nanometers,[14] forming high volume cavities where solvent molecules reside (Figure 1.2). Depending on the nature of the liquid phase, supramolecular gels divide into organogels (the liquid phase is an organic solvent) and hydrogels (water as the liquid phase). In an aqueous solvent system, these high water content materials are characterized by high biocompatibility and thus have a great potential for biologically relevant applications such as drug delivery and tissue engineering.[5, 9]

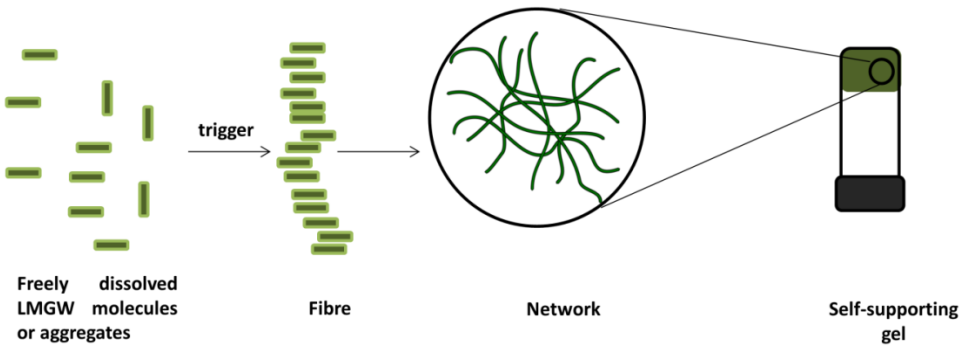

Figure 1.2: Simplistic representation of how supramolecular gels are formed after a trigger is applied. Green blocks represent the LMGW molecules/aggregates, potential triggers could be temperature or pH shifts, the presence of an enzyme or an ion. Adapted from [13, 15]

1.3 Classification of LMWG depending on the solvent system

Over the last two decades, there has been significant interest in LMWGs and numerous examples have been reported in the literature.[9] An interesting remark is that originally gelators were discovered by serendipity rather than design. In 1987, Lin and Weiss reported one of the first published in scientific journal example of organogelators, when they serendipitously observed that small amounts of cholesteryl 4-(2-anthryloxy)butyrate (CAB) gel organic molecules liquids.[16] However, significant attempts have been made to rationalize and predict gelators.[17-18] It is important to point out that most gelators have some structurally common features, the most important being their amphiphilic nature.[9] This property of amphiphilicity highlights the importance of solubility as a governing parameter of gelation[19] that will be discussed in detail later on. Several gelators have been described in the literature and will be discussed here based on the original molecule that was further modified/derivatized to gel organic solvents (organogelators)[20] or water (hydrogelators).[21]

1.3.1 Types of Organogels

One of the first reported organogels in the literature was cholesteryl-4-(2-anthryloxy) butanoate (CAB), the first cholesterol based gelator in a large family of ALS compounds, meaning compounds consisting of an aromatic group (A) connected through a functionalised linker (L) to a steroidal moiety (S), usually cholesterol (Figure 1.3, example structure (1)).[22-23] The prominent tendency of this type of gelators to aggregate is believed to relate to the molecular rigidity of the steroidal moiety as well as the presence of aromaticity and the hydrogen bond donors and acceptors.[24]

Another group of organogelators are fatty acid derivatives that have been extensively studied with the classic example of 12-hydroxystearic acid (2) and its derivatives.[25-26] Sugar (3),[27-28] aminoacid (4), [29-30] nucleoside(5) and urea (6) [31-32] derivatives have all been reported to possess organogelation properties. Example structures of these classes of organogelators are presented in Figure 1.3.

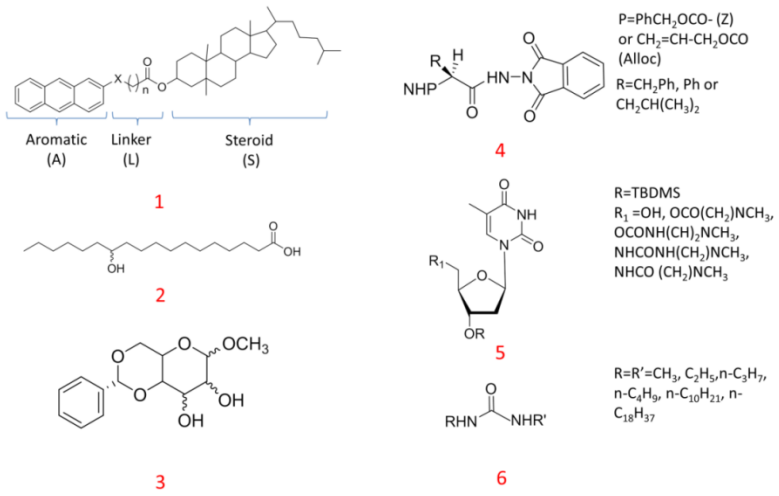

Figure 1.3: Example structures of organogelators: ALS gelators (1), 12-hydroxystearic acid (2), sugar-based dibenzylidenemonosaccharides (3) a family of phenylalanine derivatives (4)thymidine functionalised with urea, amides, carbamate and ester groups (5) urea-based compounds functionalised with n-alkyl chains and N-benzoyl-N'-aryl groups (6).

1.3.2 Types of Hydrogels

Hydrogelators are the materials of focus in this work and will be mainly discussed herein. In the design of hydrogelators, one of the first attempts reported to rationally synthesize a hydrogelator was by Hamilton, that converting a family of organogelators populated by urea derivatives into hydrogelators by adding hydroxyl groups.[33] Hamilton and Estroff were the first to categorize all molecules reported till 2003 to gel in aqueous media into amphiphiles, bolaamphiphiles, sugar-based and gemini surfactants (example structures are presented in Figure 1.4).[33] Amino acid and peptide derivatives are probably the most densely populated families of hydrogelators. Bradley et al reported a class of cystine based gelators,[34] whereas Suzuki and Hanabusa reported a family of L-lysine amphiphilic hydrogelators.[35-37] Nilsson and co-workers have extensively studied a group of fluorenylmethoxycarbonyl (Fmoc)-protected pentafluorophenylalanine derivatives

(Figure 1.4, example structure 11).[38-39] Furthermore, an important family of compounds to consider are the di- and tri-peptide derivatives. The Fmoc-diphenylalanine dipeptide (12)[40] was the first to be reported that gave rise to a library of Fmoc-dipeptides based on different amino acids(13).[18, 41] Later, several successful attempts were demonstrated with the substitution of the Fmoc group with naphthalene (14).[42-43] Another category of hydrogelators have been the carbohydrate-based amino acid derivatives where a few examples have been also reported.[44-45]

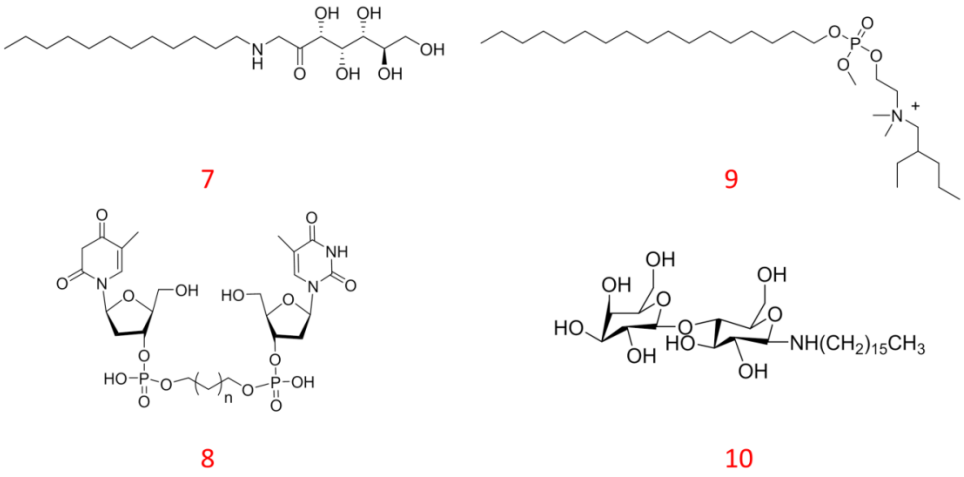

Figure 1.4: Example structures of an N-alkylaldonamide amphiphile (7) , a nucleotide bolaamphiphile (8) a gemini-surfactant (9) and a sugar-based disaccharide amphiphile (10) as categorised by Estroff and Hamilton.[12]

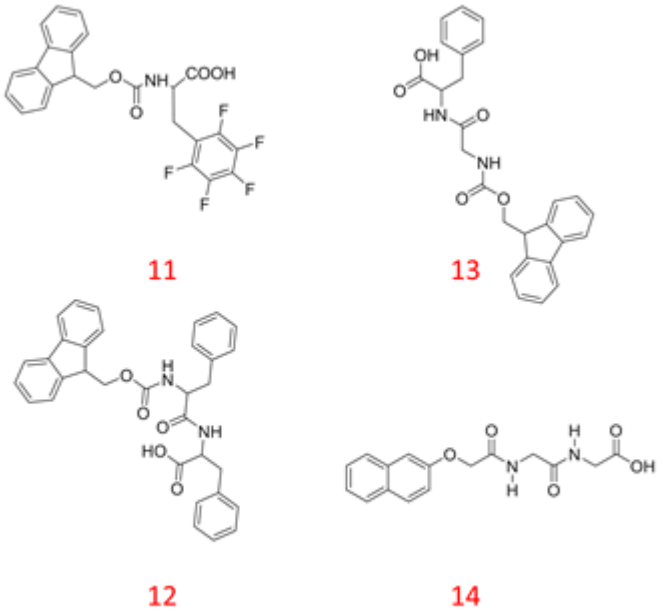

Figure 1.5: Examples of protected dipeptide-based gelators; (Fmoc)-protected pentafluorophenylalanine dipeptide (11), Fmoc-diphenylalanine dipeptide(12), Fmoc –glycine-phenylalanine dipeptide (13), naphthalene diglycine dipeptide (14).

1.3.2.1 Supramolecular gels of nucleobase, nucleoside and nucleotide analogues

Nucleobases are heterocycles that are important structural components of nucleic acids. They divide into two categories; purine and pyrimidine analogues that are nitrogen containing mono- and bi- cyclic systems that form hydrogen bonds (Figure 1.6). Due to their aromaticity they also tend to π-π stack. In the case of nucleotides and nucleosides, they consist of a nucleobase conjugated to a sugar moiety both prone to form hydrogen bonds. The distinctive element of the nucleotides compared to the nucleosides is that the

sugar is phosphorylated providing an extra element for interactions.[46]

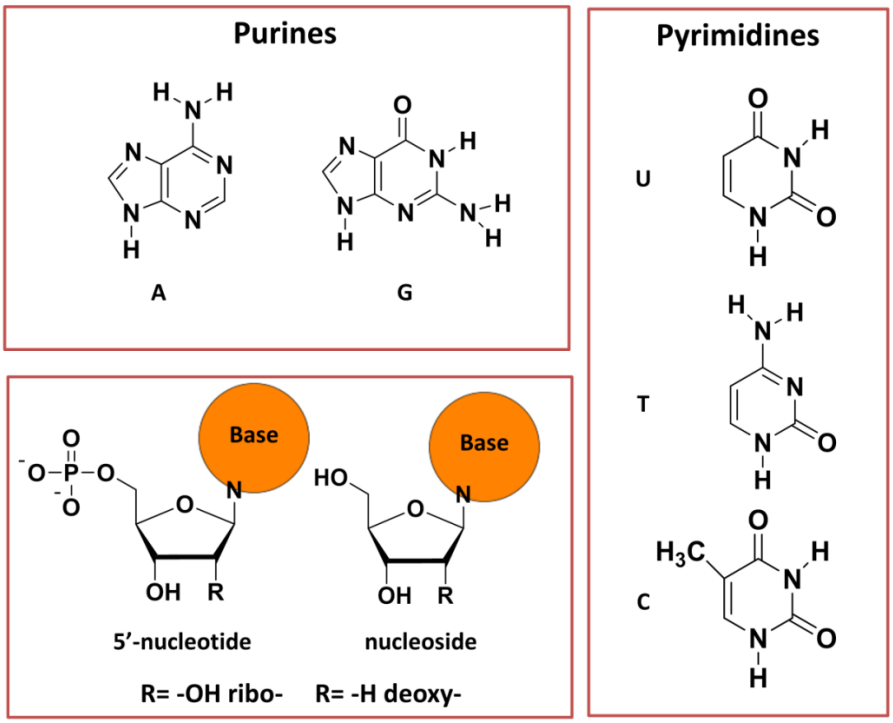

Figure 1.6: Structures of purines; adenine (A), guanosine (G), pyrimidines; uracil (U), thymidine (T) and cytidine (C) nucleotides and nucleosides. Adapted from.[46]

As has been mentioned previously, derivatisation is a common practice in the synthesis and design of new gelators. Derivatisation usually includes the addition of a hydrophobic moiety such as alkyl tails. Example of nucleoside-based derivatives are presented in Figure 1.7. Grinstaff and colleagues reported a diacylated uridinophosphocholine derivative (15)[47] that gave stable gels when the alkyl chain was 16 to 20 carbons long. Another example has been a group of benzyltriazole-modified 2'-deoxyuridine derivatives (16), where slight modifications to the gelator structure, such as the addition of a hydroxyl group, gave gels with very different gel stiffnesses.[48-49] In another example, a 2'-deoxyadenosine (17) was modified with a urea group at the sugar's 5'-position that formed a stable gel after one minute exposure to ultrasound.[50] In our group, a family of fatty acid-2' deoxycytidine conjugates (18)

were synthesized that formed gels with different mechanical properties depending on the alkyl chains.[51] This group of molecules and especially the N^4-octanoyl-2'deoxycytidine that forms a hydrogel will be extensively discussed in this work. More complex nucleic acid based gelators have also been reported, for example a uracil-cholesterol conjugate formed stable gels in organic solvents whereas an adenosine conjugate of oleanolic acid (19) gelled in mixtures of water/THF.[52] Additionally a family of novel glycosyl-nucleoside lipids (GNL) (20) was demonstrated to immobilise water and chloroform whereas in aqueous media these gelators successfully delivered oligonucleotides into human cells.[32, 53] Interestingly in the presence of the GNL gelator the internalisation of fluorescein labelled oligonucleotide was increased compared to the oligonucleotide alone. Another promising family of gelators consisted of nucleobase–peptide–glycoside conjugates that were suggested as promising biocompatible hydrogel drug delivery systems.[54] So far several successful attempts to generate nucleobase, nucleoside and nucleotide analogs that form supramolecular gels have been reported as reviewed by Peters and Davis.[46]

Finally, although bioderived gelators and especially amino acid/peptide-based ones are by far the most popular scaffolds for drug encapsulation due to their inherent biocompatibility,[9, 55] some examples of synthetic, non-bioderived LMW gelators with promising biological applications have also been reported. Perez-Garcıa and co-workers reported a gemini imidazolium amphiphile that showed controlled release profiles and improved anti-inflammatory efficacy for indomethacin compared to the drug alone.[56] Smith and colleagues reported 1,3:2,4-di(4-acylhydrazide)- benzylidene sorbitol (DBS-$CONHNH_2$) as a gelator able to encapsulate different anti-inflammatory

drugs, especially naproxen-loaded gels exhibited pH-dependent release.[57]

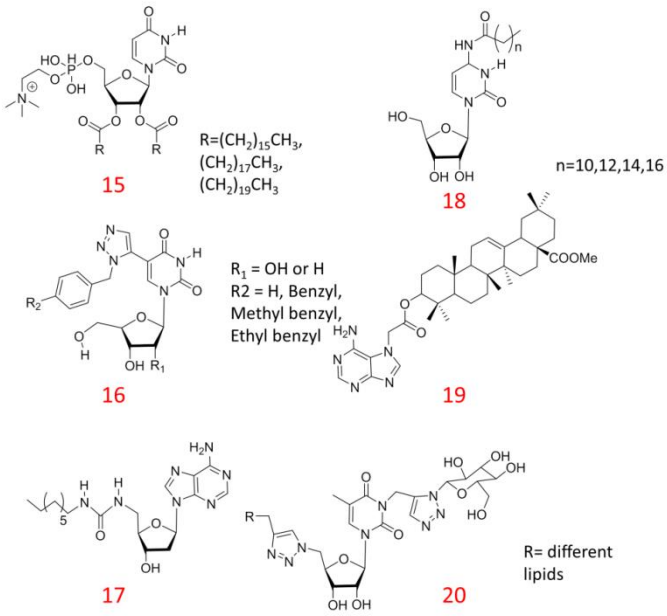

Figure 1.7: Examples of nucleoside-based derivatives. Diacylated uridinophosphocholine derivative (15) benzyltriazole-appended 20-deoxyuridine (16) 20-deoxyadenosine hydrogelator (17) fatty acid-2' deoxycytidine conjugates (18) adenine conjugates with oleanolic acid and (19) glycosyl-nucleoside lipids (20).

1.4 The thermodynamics of gelation

On a molecular level, LMW gelators interact through non-covalent interactions in order to form highly ordered structures in a hierarchical manner. To elucidate the principles that govern the formation of these nanostructures different mechanistic concepts have been suggested.

The most widely accepted approach is that gelation can be explained through crystallisation principles.[24] Especially for gelation due to cooling, the process is thought to follow certain pathway steps:[21] (i) cooling of the gelator's solution leads to the solution's supersaturation, (ii) that results in nuclei formation, (iii) nuclei growth into fibres, (iv) fibre branching and bundling, (v) formation of 3D fibrous

network through fibre entanglement. In an important piece of work, Meijer and colleagues demonstrated how π-conjugated molecules follow a nucleation-growth pathway to self-assemble into helical supramolecular fibrillary structures.[58]

The Avrami model[59-61] that was originally developed to describe crystallisation has been adopted by the supramolecular community to understand the kinetics of gelation due to the similarity between the two phenomena.[11, 62] This model can be mathematically expressed as:

$$1 - X(t) = \exp(-Kt^n)$$

where X(t) is the volume fraction of the gel phase, K is a temperature-dependent constant, n is the Avrami constant and t is the time. This model assumes that nucleation occurs randomly and homogeneously over the untransformed volume of the material and the growth of different domains happens independently to one another (Figure 1.8). The Avrami coefficient n can be related to the dimensionality of the object formed and ranges from 1 to 4; for example a value of 1 suggests one-dimensional growth, as would be expected for fibrils. This has been successfully calculated through kinetic data acquired from four different experimental techniques (circular dichroism, fluorescence, small-angle neutron scattering, and rheological methods) for a cholesterol-based system to be approximately one, confirming the one-dimensional growth.[63] More complex models introducing also a parameter for branching in the network formation have been applied by others.[21, 64]

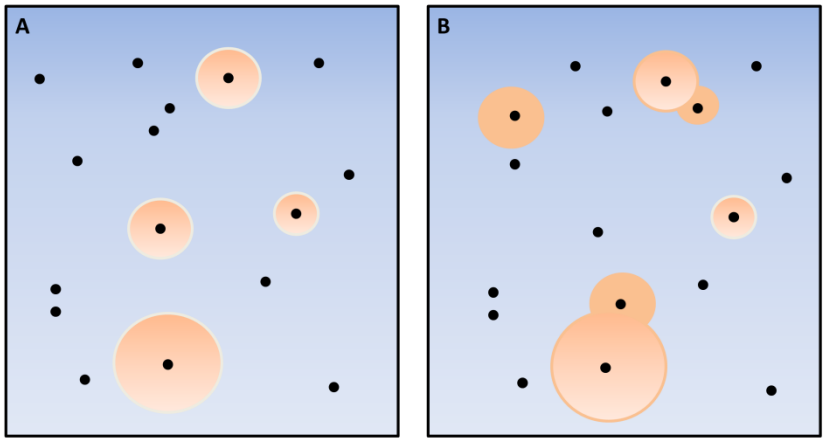

Figure 1.8: Representation of the Avrami model. Nucleation occurs randomly and homogeneously over the volume of the material and the growth of different domains happens independently to one another over time. Black dots represent the nucleation sites where nucleation initiates from and the pink spherical areas around them represent the growing new phase. Adapted from.[59]

Another demonstration of the nucleation fibre-growth mechanism was presented experimentally through a spherulitic network of the LMWG N-lauroyl-L-glutamic acid di-n-butylamide (GP-1).[65] Depending on the fibre branching intensity, the presence of clear boundaries among the different individual fibre networks can be identified. When the fibre branching is intense, distinct boundaries between fibre networks can be present whereas when fibre branching is less pronounced, fibre entanglement is more common and more elastic materials are produced. In the same work, it is demonstrated that there is an optimal temperature that can thermodynamically lead to a gel with optimal elasticity.

Furthermore, the gel state can be energetically seen as a kinetically trapped metastable state or a thermodynamic minimum.[66] In the former, as the amphiphilic

LMWG molecules transition into the energetically minimum crystal state, they get energetically trapped into a favourable intermediate state, the gel state. Since the gel state does not represent the overall thermodynamically minimum state (this is occupied by the crystal state), depending on the energetic barriers around this metastable state, this gel state can transition into the crystal state.[67] In the alternative scenario, the gel state might represent the thermodynamic minimum or even a local minimum between high activation barriers that turn the transition into the global minimum (the crystal state) impossible. [66] In a review, Adams and coworkers described the process of gelation as different transition pathways that, depending on the trigger (heat, pH, polarity switch or enzymatic action), can lead to different kinetically trapped states instead of the thermodynamic minimum.[68] In a different study, Stupp and colleagues used a peptide amphiphile to demonstrate that depending on the intermolecular repulsions, different metastable assemblies can be formed. In environments with low intermolecular repulsion, the assembled molecules form long fibres where β-sheets are thermodynamically favoured whereas monodisperse short fibres form at a metastable state. In high repulsion environment, an energy barrier was found to separate the thermodynamically favoured state and the kinetically trapped product.[69] These two different energetic states were found to interact with cells in a different way; the thermodynamic product was found to favour cell adhesion and improve cell survival whereas the metastable state prevented adhesion and could lead to cell death.

Through a different perspective, the self-assembly depending on the thermodynamic profile of the process can be classified into Equilibrium Self-Assembly (ESA) and Dynamic Self-Assembly (DySA).[70-71] ESA describes structures that find themselves at equilibrium state of a local or global entropy maximum whereas

there is no energy flow between the system and the external environment. DySA is a relatively new research field firstly proposed by Grzybowski, Stone and Whitesides.[72] When self-assembly is at thermodynamic equilibrium, the system's components eventually form a structure that is at the minimum of a thermodynamic potential (thermodynamic state). This state is determined by the thermodynamic parameters that are kept constant during the process. For example in an isothermal (temperature, T, constant) and isobaric (pressure, P, constant) process, when the number of molecules (N) is also constant, the self-assembly is driven energetically to reach the Gibbs free energy minimum G=H-TS (H is the enthalpy, S is the entropy) and if the difference between the two energetic states, $\Delta G<0$ the process is spontaneous. In another common scenario, for an isothermal and isochoric (T and V (volume) constant) process when the number of molecules (N) is also constant the self-assembly is driven energetically to reach the Helmholtz free energy F=U-TS (U is the internal energy), where the process is spontaneous if the difference between the two energetic states is $\Delta F<0$. The important point is that self-assembly can be related to enthalpic/energetic effects or entropic or both. DySA on the other side, is mostly encountered in biological systems, where an ordered self-assembled system due to a flux of energy (for example heat) resides away from equilibrium but still maintains a spatial organisation.

1.5 Triggers that induce supramolecular gelation

In order for LMWGs to self-assemble and ultimately form a supramolecular gel, a trigger is required. As presented in Figure 1.2, LMGW molecules are dissolved (fully dissolved or partially aggregated) in solution and they start to self-assemble only after a change in the pre-existing conditions occurs (Figure 1.9). The most frequent trigger is temperature. In this case, the LMWG molecules are subject to a heat-cool cycle in order to promote non-

covalent interactions with each other; increasing the temperature facilitates the solubilisation of the gelator that self-assembles into entangled networks when the temperature drops and the solubility decreases again (instead of crystallisation or precipitation). Another trigger that has also been widely applied has been the pH; at a certain pH a gelator molecule can have enhanced solubility compared to another. As reported N-protected nonpolar peptides have pKa values of about 3.5,[73] consequently at neutral pH, the α-carboxylic acid groups of the amino acids are negatively charged and self-assembly is unfavoured for several Fmoc-peptides, whereas they form gels in their non-charged state, at pH<3.5.[74] An important exception to this though has been Fmoc-diphenylalanine that was found to gel at neutral pH, this was attributed to the increase in the apparent pK_a value (compared to the usual values of 3.5) due to the self-assembly mechanism of this highly hydrophobic gelator. [75] In addition to these, another trigger that can alter the solubility of the LMWG as expected is a switch in the solvent polarity, for example the addition of water can trigger the hydrogel formation. For the widely reported Fmoc- FF, Mahler *et al* were the first to use this anti-solvent approach to form gels, Fmoc-FF was presolubilised in an organic solvent and with the addition of water solvophobic forces would drive the self-assembly. [40] Later on, Adams and co-workers demonstrated that the type of solvent as well as the ratio used can play a significant role in the mechanical properties of the self-assembled gel. [76] Finally in the presence of enzymes, functional groups that improve the solubility of the gelator get cleaved by the enzymes, resulting into its self-assembly. Interestingly, gel formation for some gelators has been induced through more than one trigger. For example, Fmoc-tyrosine forms stable gels after enzymatic dephosphorylation and pH switch, whereas for Fmoc-diphenylalanine a change in the solvent's polarity or a change in the pH can both induce gelation.[68] The trigger and consequently the process through which the self-assembly occurs has been shown to significantly affect the properties of the final

supramolecular gel (for example gel strength and nano-morphology).[68]

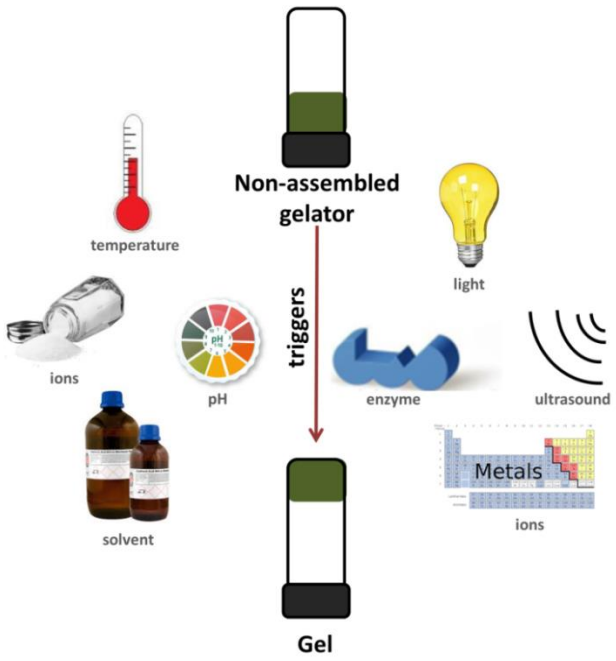

Figure 1.9: Schematic summary of the triggers that can induce the self-assembly of LMWG molecules into the formation of a gel.

1.6 Low molecular weight gelators – parameters that affect gelation

As mentioned above, the self-assembly process that eventually leads into gel formation is triggered by a change in the pre-existing conditions; from interaction of gelator only with the molecules of solvent (dissolved state) to the gelator's molecules interacting with each other (self-assembled state). Depending on the structural properties of the gelator, a change in the polarity of the solvent environment, a drop in the temperature, a shift in the pH and others can induce gelation.[77] As also mentioned before, a specific gelator can also be responsive to more than one trigger that can result in differences in the nanostructures formed. [68]

If one was about to consider the parameters affecting gelation, the concentration would be the one to discuss first. As has been previously described gelation occurs when concentrations are higher than the minimum gelation concentration (MGC) which is usually <2%.[13] The dependence of the structure formed and eventually gelation has been mechanistically demonstrated for nucleoside phosphocholine amphiphiles that gave gels only above specific concentrations.[47] The MGC is directly related to the solvent system and can vary depending on the solvent's polarity. The effect of the solvent composition over the properties of the final gel produced have been extensively explored.[13-14, 78-79]

It has also been widely demonstated[13] that temperature is a key parameter that affects gelation, most gels tend to melt above certain temperatures and that highlights the interdependence among MGC, solvent system and temperature. The effect of temperature was nicely demonstrated for nucleoside phosphocholine amphiphiles that formed helical fibres below the T_m (melting temperature) and lamellar structures above it.[47] When there are ionisable groups, pH can also affect the self-assembling process whereas when a gelator's molecules possess groups susceptible to enzymatic cleavage this can also trigger or potentially disrupt gelation (for example enzymatic degradation of peptide based gelators due to proteolytic enzymes[80]). Other parameters that have been reported to induce different responses from the supramolecular gels regarding their properties have been the light and sound[81-82] as well as the ionic strength of the buffer system used or the presence of an ion (for example metal atoms).[83-85] So far it has been clearly demonstrated that the properties of the final material (for example the mechanical properties) are process-dependent; they have been shown to heavily rely on the trigger used to initiate gelation[13, 68, 86] or the environmental conditions for example the cooling rate.[82]

As one can conclude and as has been previously demonstrated,[19] the changes in most of the above parameters mainly result in a change in the solubility of the gelator making this property of leading importance in the self-assembly. At this point, it is also important to note that some parameters are difficult to control, for example the moisture in the atmosphere or the precise room temperature resulting in different degrees of evaporation of the solvent when the system is exposed to the environment or different cooling rates. At the same time, different degrees of drying have been show to affect the conformation of the self-assembled structures in bulk at a different extent. [87] Other parameters, for example the effect of the different volumes of the gel formed or the properties of the container where the gel is being formed such as the surface properties (roughness, chemistry, hydrophobicity) or the container's shape, have on the self-assembly process and the final material's properties, have been generally neglected and only recently attracted reasonable attention.[88]

The effect that surface properties can have on the supramolecular self-assembly of bio-inspired LMW gelators such as proteins, peptide and nucleoside derivatives has been reviewed by our group. [88] Some examples have been published in the literature clearly describing that certain surface properties can affect surface-mediated self-assembly such as electrostatic interactions, hydrophilic/hydrophobic interactions, surface topology and roughness. [88] Saiani *et al* demonstrated the effect of surface charge on the self-assembled structures of the charged peptide AEAEAKAK; on negatively charged surfaces short, stiff rods were imaged with AFM whereas long fibres were observed on a TEM grid.[89] Additionally, diphenyl dipeptides were reported to exhibit different nanotube density and morphology on different surfaces made out of different materials such as PVC, glass, silicon, aluminium and mica substrates that was attributed to the substrates' hydrophobicity.[90-91] Further to this, diphenyl dipeptides were demonstrated

to self-assemble into nanofibers and microvesicles on glass surface and microporous membrane respectively. [92] Mayans *et al* reported that two surface properties (the hydrophobicity/hydrophilicity and the flatness/roughness) can play an important role on the dry film architectures of an FFF derivative.[93]

To explain these observations, two main mechanistic events have been suggested; the different degrees of adsorption of the self-assembling molecules onto the surface as well as the generation of nucleation sites at the surface. Based on the first scenario, depending on the intensity of the surface-gelator interactions, different degrees of adsorption of the gelator onto the surface will occur. If the gelator interacts strongly with the surface, increased local concentrations of the gelator next to the interface will take place that might result in different gelation kinetics or different self-assembled architectures. If the gelator-surface interactions are too weak, gelation is mainly going to proceed in solution (bulk gel). On the other hand, if the surface-gelator interactions are too strong, molecules will mostly adsorb onto the surface and intermolecular interactions will be prevented. Adsorption onto the surface can also orient molecules providing with a certain conformation that might favor or inhibit the self-assembly.

In the second scenario, the chemistry, roughness or topography on a surface can change the mobility of gelator's molecules generating nucleation sites that can locally promote gelation affecting the morphology of the supramolecular structures and the gelation kinetics. Generally, several observations on the effect of surface properties, mostly on the supramolecular architectures formed, have been made but no systematic correlations between effect-surface property or systematic experimental demonstration of the mechanism behind them have been made so far.

Finally, considering the susceptibility of these systems to this wide range of parameters, it is logical that for every system the effect of every possible factor cannot be controlled to the same extent, often resulting in the previously reported variabilities of gels' properties.[94] As expected, reproducibility in gel properties is of high importance especially when used for tissue engineering or drug delivery applications where high level of understanding and control of properties is required.

1.7 Low molecular weight gelators in drug delivery

Hydrogels have been widely used as drug delivery systems for controlled release.[9] Recently, various examples of supramolecular gels in drug delivery have been reported. Compared to polymeric gels, they were shown to demonstrate a range of advantages; they form reversibly and can be self-healing, they allow for fine tuning of their properties through several different stimuli and conditions, and they mostly involve mild conditions of gelation that do not compromise the stability of sensitive biopharmaceutical molecules such as proteins and nucleic acids during encapsulation (the crosslinking of polymeric gels can involve harsh conditions of gelation such as UV light or low pH to initiate cross-linking or the use of solvents).[9, 95-96 97] Currently there are two main strategies exploiting supramolecular gels as drug delivery systems, as presented in Figure 1.10.

- The therapeutic molecule is covalently (or through a functional linker) bound onto a functional group resulting in usually an amphiphilic compound. Following enzymatic cleavage, the active ingredient is gradually released (A).

- The therapeutic molecule is physically entrapped or interacts with the fibrillary network through non-covalent interactions and is released through diffusion or gel erosion (B).

In the first scenario an amphiphilic prodrug is generated that self-assembles in order to form a hydrogel. This strategy overcomes weaknesses such as low drug loading and burst drug release. The first example was a modified derivative of the antibiotic vancomycin where a pyrene group was introduced to drive the self-assembly process. [98] Another example used 6-aminoquinoline modified into a cyclohexane tris-amide scaffold.[99] The release of the therapeutic agent was evaluated in the presence of chymotrypsin. Additionally, LMWGs have been generated through covalently binding the non-steroidal anti-inflammatory drug ibuprofen with various dipeptides. The Gly-Gly derivative formed a stable hydrogel in water that significantly weakened in the presence of carboxypeptidase after one day incubation.[100] Further to this, different NSAIDs such as naproxen, flurbiprofen and ibuprofen were conjugated to aromatic amino acids and formed stable gels in water.[101]

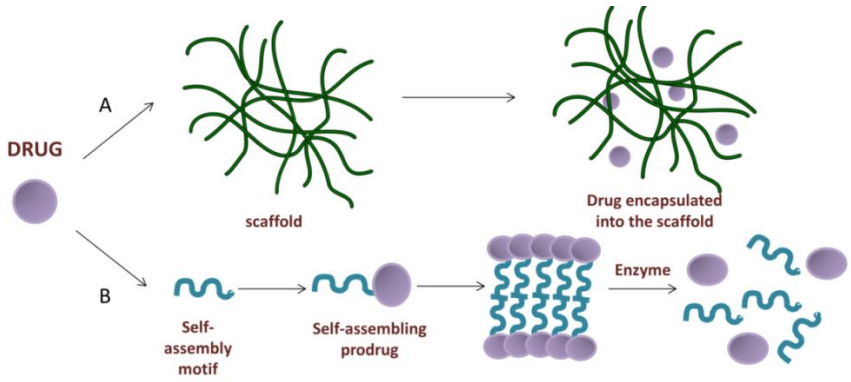

Figure 1.10: LMWG as drug delivery systems; (A) drug molecules encapsulated into self-assembled scaffolds and (B) drug covalently bound onto a self-assembly motif generating a self-assembling prodrug. In the presence of enzyme the drug will get released. Adapted from[9]

In the second strategy the hydrogel is used as scaffold to incorporate therapeutic ingredients and then release them in a controlled way. The drug either diffuses out of the self-assembled network or gets released through degradation of the network itself or a combination of both (Figure 1.11).

A first example of this strategy was presented by Vegner and colleagues where Fmoc-Leu-Asp hydrogels were used to incorporate adamantanamine and observe the immune response in rabbits (specific antibodies to adamantamine were produced) demonstrating the potential of this gel forming dipeptide for antigen presentation.[102] In a more recent example, Fmoc-phenylalanine and Fmoc-tyrosine showed that drug released followed Fickian's diffusion for these systems.[103-104] Furthermore, the hydrophobic drug camptothecin was encapsulated in a self-assembled peptide that demonstrated improved in vitro and in vivo efficacy inhibiting tumour growth.[105] The anticancer drug doxorubicin was also released in a controlled manner after incorporation in two oligopeptides that formed thermoresponsive hydrogels.[106]

Peptide based hydrogels have been shown to incorporate and release successfully in a controlled manner mostly small molecules. Due to the important advances in biopharmaceuticals,[107] significant progress has recently been reported using these self-assembling hydrogels for controlled release of large biomolecules such as proteins and nucleic acids. Li *et al* included this recent progress in the field in a very comprehensive review.[108] A very successful example of a self-assembling peptide used as a drug delivery system is acetyl-(Arg-Ala-Asp-Ala)$_4$-CONH$_2$ (PuraMatrix™, PM) that has demonstrated a broad range of clinical applications including cell culture, accelerated cartilage and bone growth, and regeneration of CNS, soft tissue, and cardiac muscle.[109-110] Specifically in drug delivery, Puramatrix® has successfully delivered several biologically-active agents (i.e. platelet rich plasma, proteins (growth factors, cytokines, insulin or antibodies) and siRNA in preclinical *in vivo* studies.[109, 111-112] Furthermore, Stupp and coworkers synthesized and developed a group of peptide amphiphiles able to deliver growth factors and other biomolecules.[96, 113] Another example with promising potential as biomaterials is MAX8, a β-hairpin peptide that consists of alternating valines and lysines and a glutamic acid at position 15 and was found to gel at physiological conditions (pH 7.4, 150 mM salt, and 37 °C).[114] MAX8 hydrogels were used to encapsulate a range of proteins and it was concluded that the release of positively charged and neutral proteins was mainly regulated by steric entrapment in the network whereas negatively charged proteins strongly interacted electrostatically with the positively charged fibrillar network.[115]

Unarguably, peptide based hydrogels have proven themselves as very promising delivery systems of small and large biomolecules and their applications have been extensively explored *in vitro* and *in vivo*. An important reason is that they consist of building blocks encountered in biology, the amino acids that are expected to be

biodegradable and biocompatible. As mentioned earlier, another class of building blocks that are bio-inspired and that have been proven to form stable hydrogels are nucleobase, nucleoside and nucleotide derivatives. Even if nucleobase, nucleoside and nucleotide-based hydrogels seem to have the same potential as the peptide-based ones, they have not attracted the same attention. So far, these type of gels have been evaluated for drug delivery[9, 46] and they have been shown to have great potential as injectable delivery systems,[116] delivering different classes of molecules ranging from small therapeutic molecules to macromolecules such as proteins and nucleic acids.[83, 117-118] Firstly, guanosine-based gels have been evaluated to successfully deliver small drug molecules in a controlled way. A guanosine-5'-hydrazide gel was able to encapsulate various pharmacologically active molecules such as acyclovir, vitamin C and vancomycin[119], whereas a 5'-deoxy-5'-iodoguanosine gel was reported to incorporate antivirals.[120] Additionally, thymidine-based gels have been shown as promising delivery systems of macromolecules where Kaplan *et al* demonstrated that a thymidine-based mechanoresponsive hydrogel can be used for the delivery of antibodies.[117] Furthermore, Ramin *et al* reported for the first time the sustained release of a small and a large molecule in vivo with no toxicity.[83] Additionally this hydrogel was shown to protect the integrity of a model protein for a period of a few days compared to the non-formulated protein in solution. This study has paved the way towards promising applications of nucleoside-based hydrogels as drug delivery systems. Interestingly, the authors reported that the two different molecules were released by a different mechanism, with the small hydrophobic molecule being released much slower compared to a larger more hydrophilic protein. Another example was a urea based-bolaamphiphile that was found to avoid the foreign body reaction after *in vivo* injection, providing more evidence on the safety of these materials.[116]

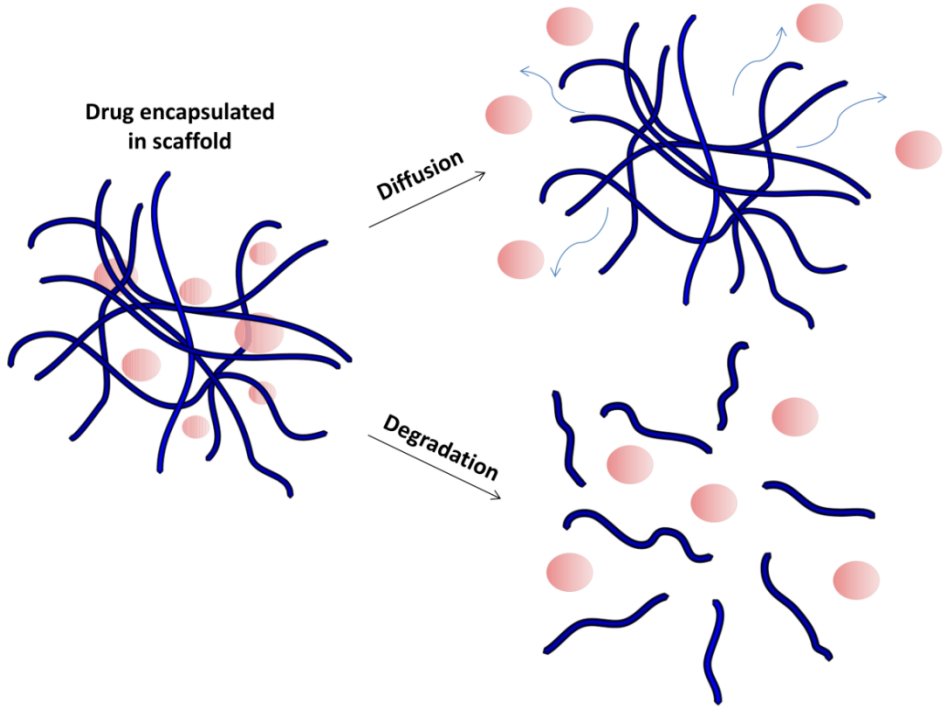

Figure 1.11: Mechanism of drug release after drug encapsulation in self-assembled gel scaffolds. The mechanism can be either diffusion of the drug out of the self-assembled network or degradation of the network itself or a combination of both.

1.8 Understanding the gelator-encapsulated molecules interactions

In a comprehensive review, Amabilino *et al* discussed the dynamic nature of supramolecular gels that is explained by the reversible non-covalent interactions that regulate the self-assembly.[7] Due to the dynamic nature of these materials, it is logical to expect that in the presence of different encapsulated molecules, the gelator molecules will interact with each other as well as with the encapsulated molecules and that this can potentially disrupt or strengthen the gel structure. Especially in the case of bulky biomolecules such as proteins and nucleic acids, that exhibit many functional groups able to interact with the gelator through electrostatic interactions, hydrogen bonding or π-π stacking, their presence could majorly change the interactions occuring that ultimately may result in the gel

formation. Considering the complexity of these biomolecules and the different ratios in the presence of these functional groups, a unique effect is expected on the gel structure from each one of the different encapsulated molecules. So far, several analytical techniques have been used to describe the effect that encapsulated molecules can have on the gel structure. Rheology is commonly used to detect differences in the gel stiffness or the gelation time in the presence and absence of the encapsulated molecules.[121-122] Microscopy techniques have managed to capture association of a nucleotide-based gelator with an oligonucleotide showing direct interaction between the gel fibre and the encapsulated molecule.[53] In another example, when camptothecin was encapsulated in a peptide-based amphiphilic gel the fibre diameter was found to increase to accommodate for the size of the encapsulated molecule.[105] In a different case, interactions between a sorbitol-based gel and naproxen were shown through the reduction of the gelation temperature (T_{gel}) by approximately 20 °C.[57] Although these studies clearly demonstrated the effect of the encapsulated molecule on the macro- or nano- properties of the gel, they have been incremental and have not managed to describe the full picture of the interaction and the overall effect on the whole structure.

Future applications of supramolecular gels require a deeper understanding of the *in vitro* and *in vivo* behaviour of these materials as well as very good reproducibility in their physicochemical properties. Considering the above, the effect that molecules with different structural levels of complexity can have on gel properties requires the design of appropriate simplified models that can give a straightforward insight into the interactions between gelator and the encapsulated molecule structures. So far, to study this effect, different proteins mixed with gels were evaluated at the nano to macro scale[121-122] and the effect that the protein characteristics (such as size,

chemistry, charge, conformation) can have on the properties of the bulk gel were described. Although these studies provide with unique observations, it is difficult to extract specific quantitative relationships between effect and property, as several properties are influencing the observed result every time. To address this, simple interfaces between surfaces, where a single property each time is being investigated, and supramolecular gels could provide with direct insight into property-effect relations.

1.9 Characterisation methods of supramolecular gels

In order to validly and accurately characterize and assess the properties of the supramolecular gels, it is important to be aware of the diversity of the techniques available, and the type of information (for example the scale or the property it evaluates) as well as its strengths and limitations. Characterisation of supramolecular gels requires the combination of different information on the different levels of structural associations.[123] As described before, single gelator molecules tend to interact on the molecular level with each other, eventually forming long fibrils (a few nanometers to a few hundreds nanometers), that will further assemble into higher order structures (up to a few microns) that will result in the formation of a network that will entrap solvent molecules. Macroscopic properties of the network along with the solvent system can be seen as the bulk gel. In this section, we will in detail refer to the methods that are available to characterise these gels and these are summarised in Figure 1.12.

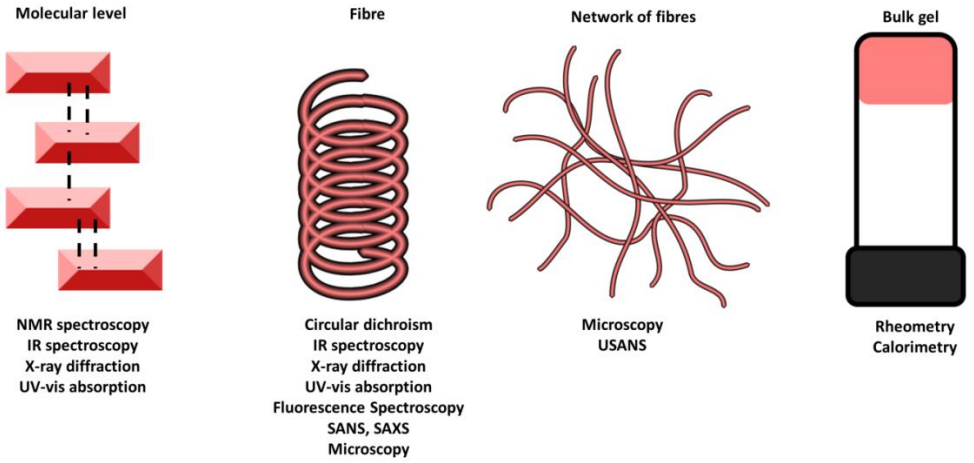

Figure 1.12: Range of techniques relevant to characterise the supramolecular gels on different scales providing with different levels of information; starting from the molecular level and proceeding to the formation of fibrils, the organisation of fibrils into higher order structures, and ultimately into the network of the entangled fibres that together with the liquid phase form the bulk gel. Adapted from [13]

1.9.1 Nuclear Magnetic Resonance (NMR) spectroscopy

Nuclear Magnetic Resonance (NMR) spectroscopy has been used extensively to assess the supramolecular gel formation[19, 124-125] and the mechanisms behind it. At the same time, as most LMWG are responsive to temperature and NMR data can be acquired at variable temperatures, NMR has been used to provide information on the effect of temperature.[14, 126] In the self-assembled fibres due to gelators' low mobility, the resonances are very broad and the solution-state proton NMR is not able to detect the assembled molecules' resonances. Through integration of the ^{1}H resonances of the gelator in solution over the ^{1}H resonances of the assembled gelators (against an internal standard), the relative amount of the gelator in solution versus the amount of the gelator in the assembled fibres can be quantified.[19, 127-129] Furthermore, saturation transfer difference (STD) NMR has been extensively used in order to study the molecule's exchange between assembled and mobile molecules in solution.[130-131] In this case, low power radiofrequency irradiation is used to selectively saturate the very broad ^{1}H resonances of the gel fibres. When molecules

are being exchanged with molecules participating in the gel fibres, they are subject to some of this saturation and hence are characterised by weaker ^{1}H NMR resonances compared to non-saturated samples. In addition to this, as mentioned earlier supramolecular gels are characterised by a gel-sol transition. By applying a temperature ramp and collect NMR data at different temperatures, the gel-sol transition can be measured and thus the functional groups that participate in gelation (the chemical groups participating in the assembled structures will slowly disassemble giving eventually stronger ^{1}H resonances), providing with an insight into the gelation kinetics.[14, 126] On a different note, NMR was used to probe the mesh size of supramolecular gels through comparing the diffusion coefficient of different size dextrans when immobilised in the gel and when in solution.[132] The size of the dextran that was immobilised (sterically hindered) by the gel network was correlated with the mesh size.

1.9.2 Spectroscopic techniques

Other spectroscopic techniques can provide unique information on different aspects of self-assembly, for example IR can detect hydrogen bond formation by detecting shifts between spectra of the assembled and non-assembled structures.[35, 133-134] In certain cases, for example peptide-based gelators, it can also give useful insight into the formation of secondary structures (for example formation of α-helix or β-sheet).[135] Similar types of information regarding the secondary structures can be provided by Circular Dichroism (CD). A necessary requirement for a CD active molecule is chirality, in certain cases the chromophore is not chiral itself but gives a CD signal due to vicinity to a chiral environment.[136-138] This is the reason why when a conformational change affects the chiral environment of the chromophore this can give a change in the CD signal and thus any conformational difference between the

assembled and the non-assembled state can be detected.[135] A caveat of CD is its high sensitivity where even small changes in the concentration can result in major differences in the CD spectra.[13] UV absorption can provide similar types of information, it is though hugely compromised due to background scattering as a result to the presence of several objects scattering light in the sample (fibres, aggregates or precipitates). Fluorescence is a very useful technique in order to probe π-π stacking of aromatic groups or aggregation of the fibres.[14, 126, 139] When aromatic groups stack together, a hydrophobic cavity gets generated that results in the displacement or molecules of water or oxygen that quench the fluorescence. This hydrophobic environment where the chromophores align together can give rise to a strong fluorescence emission.[14, 126] Indirectly, fluorescence spectroscopy can be useful to detect conformational changes occurring during gelation using fluorescent dyes. For example, hydrophobic fluorescent probes will fluoresce only in hydrophobic environments indicating the generation of hydrophobic pockets in the self-assembled structures in an aqueous solvent system.[140] Spectroscopic techniques are straightforward and flexible techniques allowing data collection at different temperatures as well as time-resolved experiments making them ideal for the study of gelation kinetics.

1.9.3 Scattering techniques

Another group of useful techniques to characterise these materials are the scattering techniques that can determine geometrical shapes,sizes and intra and inter molecular distances. Powder X-Ray diffraction is a usually easily accessible, straightforward way to quantify molecular and fibrillary spatial organisation but data can only be collected on dry gels.[135] The requirement for dry samples is an important compromise for these systems because as drying occurs, supersaturation

of the gelator in solution might result in precipitation or crystallisation of the gelator. Furthermore, Small Angle Scattering (SAS) techniques are very powerful tools in providing structural information in a broad range of distances (10 to a few hundreds of nanometers) for hydrated samples. For shorter and longer distances Wide and Ultra Small Angle Scattering instrumental setups are available. The data provided are usually fitted to a theoretical model describing a certain geometrical structure and the fitted parameters are estimated values of the geometrical characteristics of the nanostructures.[141] The theoretical model is usually chosen due to the geometrical structures observed, derived from a complementary technique, most often microscopy.[11] Good quality fitting can provide extra confidence that the right geometry was chosen. There are two sources of radiation widely used, X-Rays and neutrons. Due to the different way each radiation type interacts with matter (in principle X-rays interact with the atom's electron cloud whereas neutrons with the nuclei),[142] there are two major differences regarding the information acquired by the two radiation sources: (1) X-rays are less sensitive to lighter atoms compared to neutrons and (2) there is a significant difference between the neutron scattering lengths of deuterium and hydrogen. [143] Although in practice they provide with similar information for supramoleceular gels (geometries and dimensions of the nanostructures formed) they come with different advantages/disadvantages. X-Rays due to the high flux sources available at the moment can achieve good quality data in short period of collection time (sample exposure of a few sec) allowing for time resolved experiments. This high source intensity though can affect or be destructive to the sample. In contrast, SANS needs longer sample exposure times (up to hours) it allows for contrast manipulations giving the chance to resolve different structural features.[10] A limitation of the scattering techniques is that even if a relatively large volume of sample is analysed the output values are averaged for the population of

the objects and rarer/finer features can be potentially overlooked. To address this issue a complementary technique is required such as a microscopy.

1.9.4 Microscopy techniques

Microscopy techniques are fundamental tools in the visualisation of the nanostructures in the nano-and micro level. Electron Microscopy has revolutionised the accessible level of information since it can resolve single fibres with diameters of a few nanometers. In Figure 1.13, TEM images of a nucleo-lipid LMWG formed fibres are presented showing that valuable structural information can be extracted through EM that can significantly contribute to the characterisation of the nanoarchitectures. Although these techniques can contribute structural information, they come with significant compromises as sample preparation requires the sample to be dried, frozen or freeze-dried, processes that can alter the gel network. Fluorescence microscopy is a powerful imaging technique that allows for hydrated sample imaging at different conditions such as buffers or temperatures relevant to biological environments. An obvious condition is the sample to be fluorescent and when this is not the case functionalisation of the substrate or staining is required that can change the properties of the material. Additionally, even if superresolution fluorescence microscopy has achieved resolutions down to several nanometers, it is often not possible to measure the actual dimensions of the objects accurately due to limitations of the optics. Atomic Force Microscopy is also eventually establishing its place in the imaging of supramolecular gels.[56, 89] Although, subatomic features can be resolved, the actual geometry and dimensions are occasionally compromised due to geometry and dimensions of the tip that is being used. Whereas AFM is possible in liquid, it is usually much more time consuming as any floating objects in the liquid medium can misalign the laser on the tip and disrupt the imaging. Due to this, AFM

imaging is often performed on dry samples and hence compromises the value of data as previously described.

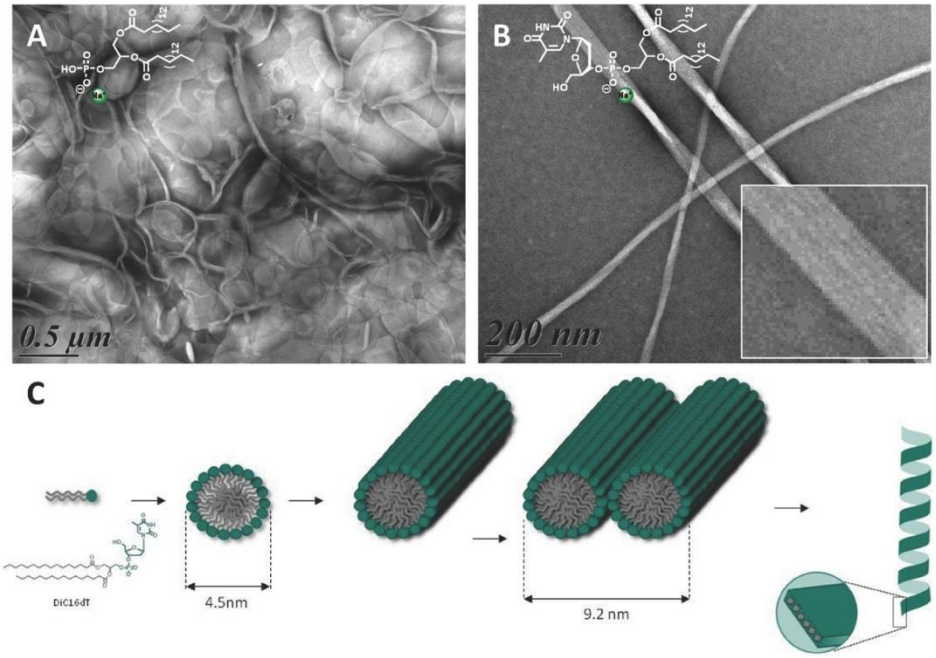

Figure 1.13: TEM images of: A) 1,2-dipalmitoyl-sn-glycerol-3-phosphate and B) Thymidine-3'-(1,2-dipalmitoyl-sn-glycero-3-phosphate)(6%, w/w) in NaCl 0.9%. Inset B) magnification of the TEM image. C) Suggested structure of supramolecular helical fibres. Reproduced with permission (Wiley Online Library).[83]

1.9.5 Techniques to characterise the bulk gel

As mentioned earlier, macroscopically the bulk gels are characterised by rheological viscoelastic properties. Oscillatory rheology is a routine way to describe the flow of supramolecular gels and can provide useful information about the strength of the gels and their property to reform their structure after the application of stress. [13, 55] Many other important parameters can be determined such as the effect of temperature on the gel strength or gelation time. Another bulk property characterising the bulk gel is the gelation temperature (T_{gel}), meaning the temperature at which the non-covalent crosslinks that maintain the gel structure fall apart due to thermal energy. Differential Scanning Calorimetry has been one of the

most well-established techniques to determine this thermal transition associated with gelation providing an accurate assessment of the T_{gel} particularly when there is a sharp transition phase. Temperature ramp experiments determining the T_{gel} are also possible with rheology.

1.9.6 Molecular dynamic simulations

In close complementarity to the experimental methods described earlier, molecular dynamic simulations are eventually finding their way in the toolkit of characterisation methods. Due to recent advances in computation power, larger length and time scale simulations are feasible providing a representative description of what is happening at the nanoscale. Insight into the early stages of the self-assembly process that are difficult to capture with experimental methods is a major advantage.[144-145] It is important to mention that any conclusions derived from computational calculations need to be correlated to experimental data and mutual confirmation of both approaches is necessary. Generally, computational methods investigating the self-assembly of supramolecular gelators constitute a broad, diverse research field that is not the focus of the present work, thus the technicalities of the field will not be further discussed.

1.9.7 Surface and interface-sensitive techniques

The above mentioned techniques can reveal information on different aspects of the supramolecular gels. In the present work, techniques that can reveal interfacial interactions between surfaces and gels are of particular interest. Interface-sensitive information can be revealed by the Grazing Incidence geometries of the abovementioned techniques, for example Grazing Incidence Small and Wide Angle Scattering techniques[146] or Grazing Incidence Fourier Transform InfraRed (FTIR).[147]

Atomic Force Microscopy (AFM) has been proven very useful to characterise the topography of thin gel films. AFM conjugated with FTIR or Raman have managed to reveal maps of chemical composition across surface areas of different materials.[148] Apart from the characterisation of the supramolecular structure on the one side of the interface, the properties of the substrate need to be clearly defined as well. AFM is a key technique in characterising the topography of the substrate as well as quantifying its roughness. In order to characterise the different chemical compositions on the top layer of the substrate, Time of Flight Secondary Ion Mass Spectrometry (ToF-SIMS) and X-ray photo electron spectroscopy (XPS) have been extensively used.[149] Whereas ToF-SIMS detects ions (charged fragments generated from molecules present on the surface), XPS provides the elemental composition of the top layer of the substrate. Addtionally, ToF-SIMS provides with qualitative/semi-quantitative information, whereas XPS is quantitative. Further to this, Water Contact Angle measurements provide a quantitative estimate of the affinity between water and substrate allowing for a relative characterisation of the surface hydrophobicity/hydrophilicity. Although the chemistry of the substrate influences the measurement's outcome, other parameters such as the surface roughness can also affect the outcome.[150]

1.10 Exploring the mechanism of gelation

So far we extensively described the broadness of the toolkit available to characterise supramolecular gels in order to ultimately be able to evaluate different mechanistic aspects of the association of the gel with the encapsulated molecules that can allow for tailored nanomaterials for drug delivery. Due to the flexible and dynamic nature of these materials (reversible non-covalent interactions are forming the assembly), each encapsulated molecule can have a unique effect on the gel structure. For this

reason, the gel structure, the gel properties as well as the mechanism of the self-assembly need to be well-defined and confidently described. Although in the literature there are several proposed models for the self-assembly mechanism, the driving forces and the final supramolecular structure obtained, most models are mainly inferred through certain selective experimental data that do not provide a detailed, confident picture of the studied material. In a landmark piece of work, Ulijn and colleagues were the first to give a clear picture of the self-assembly mechanism of the dipeptide Fmoc-FF. They used a range of spectroscopy and microscopy techniques to suggest a model architecture based on nanocylinders governed by π-π stacking and interlocked through β-sheet formation.[151] The modelled structures identified are presented in Figure 1.14.

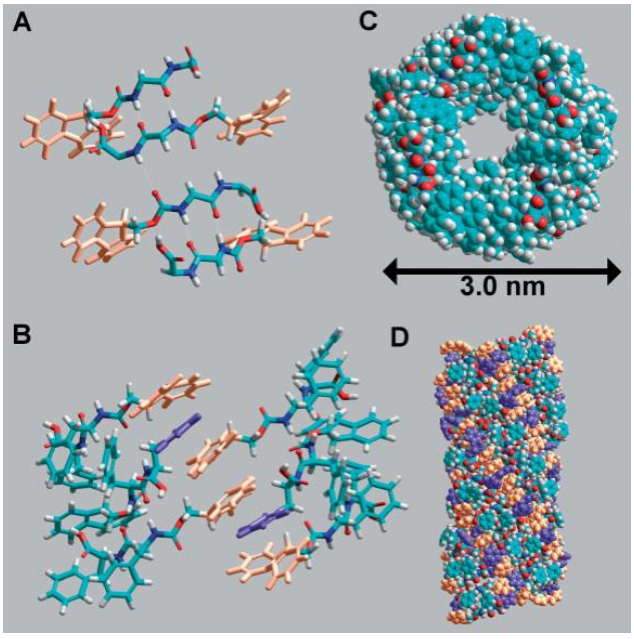

Figure 1.14: Model structure of Fmoc-FF peptides arranged in an anti-parallel b-sheet organisation (A), Fmoc groups interlocking to form p-stacked pairs with interleaved phenyl rings (B). Top view of cylindrical structure(C) and side view(D) In(a), (b) and (d) Fluorenyl groups are represented in orange and the phenyl groups are in purple. Reproduced with permission (Wiley Online Library).[151]

Regarding nucleic acid-based gelator self-assembly there have been scarce examples of evaluation of the assembly mechanism. In a very informative piece of work

though, Barthelémy and coworkers used a range of small angle X-ray scattering (SAXS), spectroscopic techniques and transmission electron microscopy (TEM) for a family of nucleoside phosphocholine amphiphiles to describe the supramolecular structures formed at different concentrations and different temperatures. The structure proposed for one of the nucleolipids used is presented in Figure 1.15. Ultimately, above a threshold concentration the amphiphiles with unsaturated alkyl chains assembled into an entangled network of fibres. The same gelators in organic solvent were organised into lamellar structures.[47] Other pieces of work evaluating the mechanism have been also reported mostly based on one or two techniques. For example, freeze-dried thymidine based gels were characterised by XRD to demonstrate that the headgroup of the gelator adapts a bent conformation to expose the hydroxyl groups towards the outside of the fibre.[152] Furthermore, Roviello *et al* investigated the supramolecular structures obtained through UV, CD, and light scattering for two thymidyl dipeptides.[153]

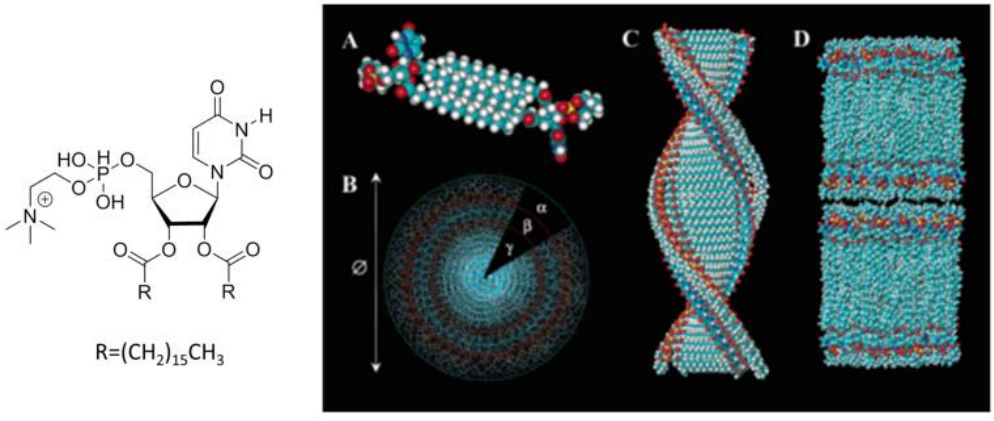

Figure 1.15: Suggested model illustrating DNA-like helical fibre and multilamellar molecular organisations in water formed by 1,2- Dipalmitoyluridinophosphocholine (left panel). Right panel; (A) Two molecules organised into the basic repeat unit of the helical fibre. (B) Top view of the strand presented in (C). (α corresponds to the hydrophilic domain (phosphocholines), β corresponds to uridine packing, and γ to the hydrophobic core. (C) Schematic illustration of the fibre. (D) Schematic illustration of a multilamellar organization. Adapted from[47]

Apart from the detailed description of the supramolecular structures formed, another very interesting question is the driving forces that direct the self-assembly. As mentioned earlier most of the hydrogelators have an amphiphilic nature and hydrophobic/solvophobic interactions and π-π stacking are mostly considered in the literature as the driving forces of the assembly. Most often, the nature of the interactions driving the assembly are inferred through the final conformations that the assembled molecules have whereas there are no actual experimental data suggesting it clearly. For example, for a naphthalene-dipeptide[43] and the Fmoc-diphenylalanine,[151] due to the prominent presence of the π-π stacking in the assembled structures it was inferred that these interactions are critical for the assembly. In a different approach eighteen different pentapeptides were synthesized to qualitatively demonstrate the necessity of aromatic nuclei for gelation to occur.[154] Molecular Dynamic simulations have been the only method so far to demonstrate clearly that hydrophobic interactions drive the self-assembly over time[155] whereas hydrogen bonds have been found to stabilise the assembled structures.[156]

1.11 Hierarchical self-assembly

In the simplistic approach that was previously discussed in Figure 1.2, LMWG molecules after dissolution in a solvent system and the application of a trigger, interact through non-covalent interactions and form first order structures, usually long one-dimensional structures, the fibrils. These first order structures most likely will assemble into higher order structures of various architectures[157] that will retain a large volume of solvent and form a gel. In the case of supramolecular gelators, structures with one dimensional order (fibres) that consist of building blocks such as

rods or discs[157] or lamellar phases[85] are frequently reported. Regarding the higher order structures that have been reported, there is a large variety of architectures such as helices[83] or beta-sheets[43, 151], ribbons or tapes[85] twisted or bundled together,[14] forming nanotubes or lamellar phases.[157] Significant work has been done in order to computationally predict first and higher order structures and the physicochemical parameters of the hierarchical assembly.[158] The architectures obtained have been shown to be directly connected with the mechanical properties of the final gels.[68] For example, the gel stiffness has been shown to directly relate to the individual fibre properties (thickness and length) as well as the way the fibres associate together (number of crosslinks, fibre distribution in space).[68] This highlights the importance of accurately describing the nanostructures' architectures and clearly understanding the mechanism of their formation.

1.12 Aims and objectives of the project

1.12.1 Limitations in the field

Supramolecular gels have been identified as promising materials in many research fields with potential applications in energy storage, electronics, photonics, sensors as well as tissue engineering and drug delivery. Especially for biomedical applications, where these materials are in direct contact with the human body for a potentially prolonged period of time, a high level of control and understanding of their properties is required. Considering these, we identified the following areas where further investigations could contribute to the already available knowledge:

(i) The self-assembly mechanism of nucleoside-based gelators is poorly understood. This prevents rational design and understanding of the self-assembly of these molecules.

(ii) The effect that different chemical functionalities have on the self-assembled structures has not been systematically explored. This is limiting the level of control over supramolecular gels that is required for the advanced applications of supramolecular gels.

(iii) The mechanism of encapsulation and release of bioactive molecules with different properties as well as the degradation profiles of the gels *in vitro* and *in vivo* have not been investigated. This is limiting the rational design of tailored supramolecular gels for drug delivery applications.

1.12.2 Challenges in the field

(i) Establish a detailed mechanistic understanding of the self-assembly mechanism of nucleoside-based gelators.

(ii) Establish a systematic mechanistic understanding of the interactions between specific chemical functionalities and the characteristics of the self-assembled architectures.

(iii) Elucidate the degradation mechanism of supramolecular gels *in vitro* and *in vivo,* as well as the mechanism of encapsulation and release of bioactives with different properties from the supramolecular gels.

1.12.3 Objectives of the project

(i) Determine the self-assembly mechanism of N^4-octanoyl-2'-deoxycytidine, a self-assembling and self-healing hydrogelator, and describe the molecular and supramolecular nanoarchitectures formed.

(ii) Determine the effect that different chemical functionalities (immobilised on substrates) have on the molecular and supramolecular architectures of thin gel films of different members of this cytidine-based gelators' family.

(iii) Determine the mechanism behind the encapsulation and release of model molecules with different properties from the supramolecular gel of N^4-octanoyl-2'-deoxycytidine *in vivo* and *in vitro.*

1.12.4 Aim of the project

This work focuses on the elucidation of the mechanistic principles underlying the interactions between a family of nucleoside-based gelators and biological systems with different levels of complexity.

Starting from comprehensively establishing the mechanistic principles that bring and hold together the self-assembled structures for a family of cytidine-based gelators, we aim to gradually build up our understanding of how the presence of different chemical functionalities interfere with the supramolecular structures. We will initially focus on the interface of supramolecular gels with different chemically modified substrates and study the effect of different chemical functionalities on the self-assembled structures in model interfaces. We will eventually move into bulk composite gel systems, where we will investigate how encapsulated molecules with complex chemistries can influence the properties of the final gel from a nano- to macro- level. Finally, we will assess the hydrogelator member of this cytidine-based family as a drug delivery system for the encapsulation of molecules with different properties *in vitro* and *in vivo*.

These objectives were addressed in three experimental chapters that have either been published already or are currently under review:

Chapter 2

A supramolecular nucleoside-based gel: Molecular dynamics simulation and characterization of its nanoarchitecture and self-assembly mechanism

Published in Langmuir, 2018, 34 (23), pp 6912–6921, DOI: 10.1021/acs.langmuir.8b00646

Chapter 3

Surface-mediated self-assembly: characterisation and modulation of gel properties for a family of cytidine-based gelators on model gel-substrate interfaces

First part

Surface-directed modulation of supramolecular gel properties

Published in *Chemical Communications*, 2016, 52, 4298-4300,

DOI: 10.1039/C6CC00292G

Second part

Hydrophobicity of surface-immobilised molecules influences architectures formed via interfacial self-assembly of nucleoside-based gelators

Published in *Soft Matter*, 2018,14, 9851-9855

DOI: 10.1039/C8SM01868E

Chapter 4

Mechanistic insights into the encapsulation and release of small molecules and proteins from a supramolecular nucleoside gel *in vitro* and *in vivo* (under review)

Chapter 2

A supramolecular nucleoside-based gel: Molecular dynamics simulation and characterization of its nanoarchitecture and self-assembly mechanism

Maria G. F. Angelerou,[†] Pim W. J. M. Frederix, [‡] Matthew Wallace, [∥] Bin Yang, [†] Alison Rodger, [§] Dave J. Adams, [⊥] Maria Marlow[†] and Mischa Zelzer, [† *]*

[†]University of Nottingham, School of Pharmacy, Nottingham, NG7 2RD, U.K.

[‡]University of Groningen, Faculty of Science and Engineering, Groningen 9747 AG, The Netherlands

[∥]University of East Anglia, School of Pharmacy, Norwich, NRT 4TJ, U.K.

[§]Macquarie University, Department of Molecular Sciences, NSW 2109, Australia

[⊥]University of Glasgow, School of Chemistry, Glasgow, G12 8QQ, U.K.

Author Contributions

The manuscript was written through contributions of all authors. MGFA conducted the major part of the experimental work including the fluorescence spectroscopy, circular and linear dichroism, time and temperature experiments as well as the synthesis and characterization of the gelator. PWJMF conducted the molecular dynamics. MW conducted the NMR experiment. BY and MGFA conducted the X-Ray Diffraction experiment. MGFA, MZ, MM, AR, DA contributed to the design, data interpretation and preparation of the manuscript. All authors gave approval to the final version of the manuscript.

Abstract

Among the diversity of existing supramolecular hydrogels, nucleic acid-based hydrogels are of particular interest for potential drug delivery and tissue engineering applications because of their inherent biocompatibility. Hydrogel performance is directly related to the nanostructure and the self-assembly mechanism of the material, an aspect that is not well-understood for nucleic acid-based hydrogels in general and has not yet been explored for cytosine-based hydrogels in particular. In this chapter, we use a broad range of experimental characterization techniques along with molecular dynamics (MD) simulation to demonstrate the complementarity and applicability of both approaches for nucleic acid-based gelators in general and propose the self-assembly mechanism for a novel supramolecular gelator, N^4-octanoyl-2'-deoxycytidine. The experimental data and the MD simulation are in complete agreement with each other and demonstrate the formation of a hydrophobic core within the fibrillar structures of these mainly water-containing materials. Further to this, as suggested by both experimental methods and MD simulations, solvophobic forces and π-π stacking direct the self-assembly whereas hydrogen bonds stabilise the self-assembled structures. The establishment of the mechanism for this cytidine-based gelator is a necessary step in order to proceed in further investigations of these materials in the following chapters. In Chapter 3, the effect of different non-covalent interactions on the self-assembled nanostructures will be investigated in simple model interfaces. The distinct duality of environments in this cytidine-based gel (hydrophobic core inside the fibres vs the hydrophobic cavities where the water resides) suggests the hypothesis that different molecules, both small hydrophobic drugs and biopharmaceuticals (proteins and nucleic acids), can be encapsulated in the gels for drug delivery applications as will be further explored in Chapter 4.

Objectives

Determine the self-assembly mechanism of N^4-octanoyl-2'deoxycytidine, a self-assembling and self-healing hydrogelator.

- Characterise the molecular and supramolecular architectures.
- Compare experimental and molecular dynamics data.
- Elucidate the forces mediating the self-assembly.

2.1 Introduction

In the last ten years, there has been increasing interest in supramolecular gels due to their potential applications as drug delivery systems, sensors and tissue engineering scaffolds.[9, 14, 53, 83, 126, 159-160] Derivatives of oligopeptides[135, 161] and nucleic acids i.e. nucleobases, nucleotides or nucleosides[46, 162] have been extensively investigated as supramolecular gelators for biological applications due to their inherent biocompatibility. Nucleic acid-based gelators in particular are attractive because they are expected to have improved stability towards enzymatic degradation compared to peptide-based gelators.

Nucleic acid-based gels are increasingly finding their way into applications in drug delivery. They can be promising injectable delivery systems[116] of small therapeutic molecules as well as macromolecules such as proteins and nucleic acids.[83, 117-118]

For example, guanosine-based gels have been used to deliver small drug molecules in a controlled way. A 5'-deoxy-5'-iodoguanosine gel was used to release antivirals,[120] and a guanosine-5-hydrazide gel was able to incorporate different pharmacologically active molecules including acyclovir, vitamin C and vancomycin.[119] Furthermore, thymidine-based gels have been reported in drug delivery systems for the release of macromolecules. Kaplan et al. presented a thymidine-based

mechanoresponsive hydrogel for the delivery of antibodies.[117] Ramin et al. demonstrated the sustained release of both a large and a small molecule in vivo for the first time.[83] Maisani et al. have also successfully demonstrated implantation of a thymidine-based composite hydrogel as a scaffold for bone tissue engineering.[163] Notably, among the existing examples of nucleic acid-based gels, guanine and cytosine derivatives are underrepresented and poorly investigated despite their attractiveness due to the possibility to access G-quadruplexes or i-motifs, ordered structures formed specifically by guanine and cytosine-rich nucleic acid sequences, respectively, that may provide cavities to host payloads in a gel.[162]

Maria's Marlow group has recently introduced a cytosine-based gelator, a fatty acid bound to a 2'-deoxycytidine, and reported the bulk mechanical properties of the resulting gels.[51] Importantly, we also demonstrated that the mechanical properties of the gel are affected by the surface that is in contact with the gelator solution during gelation.[164] Surface-assisted self-assembly has been recognized as a largely unexplored but significant factor in self-assembly and is receiving increasing attention,[165] not least due to the implications involved when formulating gels in situ or in the presence of other components such as macromolecules or particles.

To enable rational design of a class of gelators as well as the investigation and understanding of parameters that influence self-assembly and ultimately gel properties and application, it is essential to elucidate the self-assembly mechanism. In contrast to peptide-based gelators for which the self-assembly mechanism has been extensively explored,[135, 151] a detailed, experimentally supported understanding of the self-assembling mechanism of nucleic acid based gelators is lacking.

To date, evaluation of nucleic acid self-assembly typically plays an ancillary role where one or two techniques are used to investigate a specific component of the gelator. Barthélémy and co-workers reported SAXS data for an uracil based gelator

indicating strongly aggregated assemblies that were observed as fibers under TEM.[47] As an organogel, the same gelator displayed repeat periods (4.6 nm) that the authors interpreted to indicate orientation of the hydrophobic part of the gelator towards the organic solvent. In a later study, Barthélémy et al. used the mismatch in fiber diameter determined by SAXS and the length of the gelator obtained by CPK modelling to propose an interdigitated organization of a thymine based gelator.[53] Iwaura et al. used XRD data of freeze dried thymine-based gels to argue that the gelator headgroup bends to expose hydroxyl groups to the outside of the fibers.[152] Temperature-dependent transmittance and CD measurements have also been used to determine the gelation temperature of thymine, adenine and uracil-based gels.[152, 166] Banerjee et al. investigated the effect that different functional groups of self-assembling pyrimidine analogues can have of the final fibrillary network.[167] Roviello et al. used UV, CD and Light scattering to investigate the formation of supramolecular networks of two thymidyl dipeptides and assess their interactions with biomolecules.[153] To the best of our knowledge, no detailed investigation is currently available on the self-assembly organization or mechanism of cytosine based gelators. Moreover, while some data on other nucleic acid-based gelators exist, a comprehensive experimental and theoretical description of the contribution of all components in an amphiphilic nucleobase gelator has not yet been reported.

In this work, we systematically explore the self-assembly mechanism of the deoxycytidine derivative N^4-octanoyl-2'-deoxycytidine. This gelator is the only member of a class of thermoresponsive cytidine-based gelators developed by our group[133] that forms a self-healing hydrogel[51] and it has been reported as a promising candidate for applications in drug delivery (e.g as depots for controlled release via gel erosion and diffusion) and tissue engineering along with the macromolecular properties of the gel (e.g. rheology).[51]

Herein, we use a range of experimental approaches to identify the contribution of the different parts of the gelator to the self-assembly process to present the first complete experimental elucidation of the self-assembled organization of a nucleic acid based gelator. Molecular dynamics (MD) simulations are ideally suited to probe the initial stages of assembly as well as the dimensions and spectroscopic properties of fully assembled nanostructures.[168-170] They have been successfully applied to monolayers and bilayers of nucleolipids and their hybridization with single-stranded DNA.[171-172] Taking advantage of this, here we further combine our experimental dataset with MD simulations to demonstrate for the first time the complementary match of experimental and theoretical data for a nucleoside gelator. This combined approach enables us to propose a detailed, comprehensive model of the self-assembly of this cytidine-based gelator and paves the way for a rational design of this class of gelators.

2.2 Results and Discussion

Gels were formed from N^4-octanoyl-2'-deoxycytidine using a solvent mixture of 20:80% v/v ethanol:water. In the mixed solvent system used, the gelator forms a gel composed of cylindrical fibres (Figure 2.S1, ESI, this is further discussed in Chapter 3, Section 3.1.5.2). Whilst the gelator is able to form gels in water only[51] and does not form gels in organic solvents (e.g. methanol), the addition of ethanol in the solvent improves the solubility of the gelator, facilitating the preparation process and gives a transparent gel ideal for spectroscopy studies.

2.2.1 Self-assembly induces gelator fluorescence

For gelators that contain fluorescent moieties that are involved in the self-assembly process (e.g. Fmoc- or naphthyl-conjugated peptides), fluorescence

spectroscopy has been widely used to study their self-assembly processes.[15, 55, 161, 173-174] Unmodified nucleosides are not inherently fluorescent as shown for the example of 2'-deoxycytidine in Figure 2.1A. In contrast, *N*^{4}-octanoyl-2'-deoxycytidine, the modified 2'-deoxycytidine derivative used here, displays weak fluorescence (λ_{Ex} = 326 nm, λ_{Em} = 367 nm, see Figure 2.S2 for excitation and emission spectra) in methanol where the molecule is fully soluble (Figure 2.1B), suggesting fluorescence might be a useful tool to monitor self-assembly of this nucleoside gelator into structures where the aromatic moiety is protected from water.

In a mixture of 20:80% v/v ethanol:water, where *N*^{4}-octanoyl-2'-deoxycytidine forms a supramolecular gel,[51] the intrinsic fluorescence indeed shows a marked increase compared to *N*^{4}-octanoyl-2'-deoxycytidine in methanol and 2'-deoxycytidine in ethanol/water (Figure 2.1). This suggests that the self-assembled environment enhances the fluorescence of *N*^{4}-octanoyl-2'-deoxycytidine leading to aggregation-induced emission,[14] likely due to an increase in the π-π interactions of the aromatic rings in the nucleobase that protects the molecule's fluorescent chromophore from solvent-induced quenching and leads to a strong emission at 357 nm (Figure 2.1B, black trace). Because of the significant difference in fluorescence intensity between the solution and the gel sample, we postulate that the increase in fluorescence intensity is more likely to be related to the self-assembled state affecting quenching rather than any solvent-induced changes in molecular fluorescence.

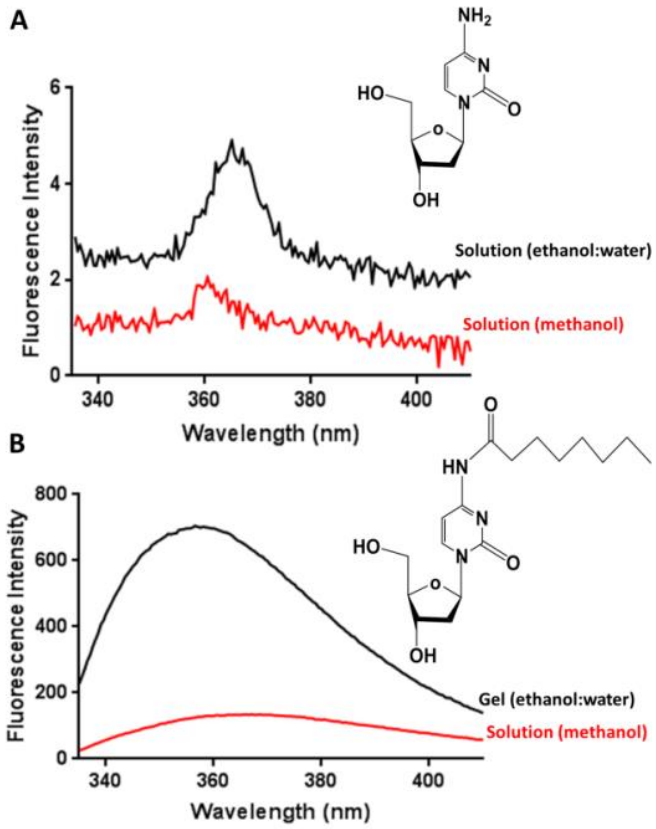

Figure 2.1: Fluorescence emission spectra of (A) 2'-deoxycytidine and (B) N^4-octanoyl-2'-deoxycytidine at a concentration of 14 mM in either 20:80% v/v ethanol:water (black trace) or methanol (red trace) upon excitation at 326 nm.

To gain further understanding of the arrangement of the nucleobases in the gel, Circular dichroism (CD) experiments were performed. Aromatic nucleobase monomers are achiral molecules that become CD active due to their proximity to the chiral sugar.[136] As with double-stranded DNA, when the chiral nucleosides stack, they gain further CD intensity if the assembly is helical. As explained in detail in the ESI, circular and linear dichroism data confirmed the π-π stacking interactions of the nucleobases in the gel state.

2.2.2 Hydrophobic domains are formed in the gel fibers

For nucleoside-based amphiphiles, limited evidence has been provided to describe how their hydrophobic parts interact with each other. The presence of hydrophobic environments in the fibers of a cholic acid-based gel has been confirmed in the past through fluorescence by incorporating 8-anilinonaphthalene-1- sulfonic acid into the supramolecular system.[175] Nile red, a poorly water-soluble dye that dissolves and fluoresces strongly in hydrophobic environments[176] was therefore added to the gels to investigate if hydrophobic pockets are present in the self-assembled structures. After excitation of the gel containing Nile red at 540 nm, strong fluorescence at 630 nm was obtained (Figure 2.2A, red trace) that was absent in the control sample (Figure 2.2A, black trace) where a lower intensity peak at 660 nm was observed. Super resolution fluorescence microscopy showed that the fluorescence signal is spatially arranged in fiber-like structures (Figure 2.2B). These data clearly demonstrate the presence of a well-defined hydrophobic environment within the fibre structure.

2.2.3 The effect of temperature on the self-assembly

As noted above, two different fluorescence signals (the gelator's intrinsic fluorescence and the fluorescence of an incorporated dye) can be related to π-π stacking related exclusion of solvent and the association of the dye with the hydrophobic part of the gelator, respectively. By monitoring the effect of the temperature on the two different fluorescence signals, we can understand how the hydrophobic interactions contribute to the self-assembly formation and how they relate to each other.

The change in fluorescence emission intensities of the gelator itself with temperature (λ_{Ex} = 326 nm) is presented in Figure 2.3. The intrinsic gel fluorescence is high at room temperature, but drops drastically as

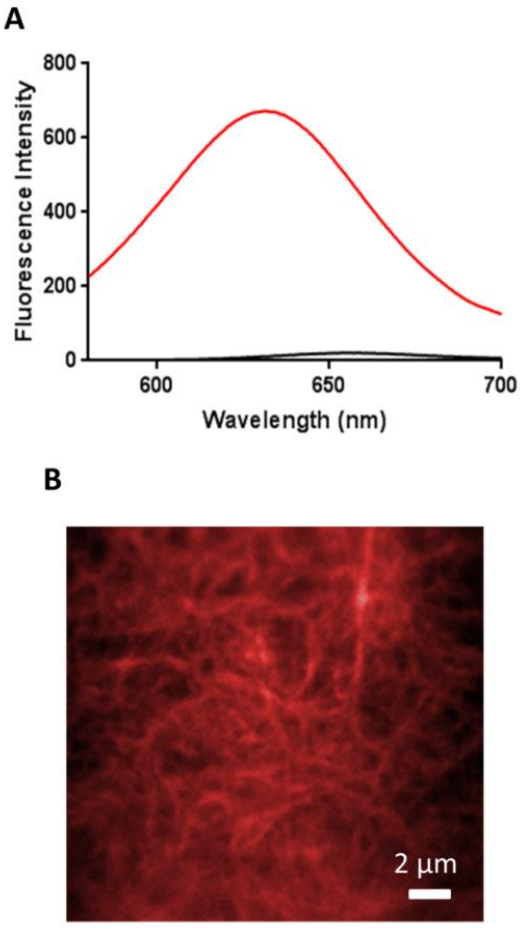

Figure 2.2: (A) Fluorescence emission spectra (λ_{Ex} = 540 nm) of Nile Red (approximately 0.1 mM) in ethanol:water (20:80% v/v) (black trace) and the gel after the incorporation of Nile Red in ethanol:water (red trace). (B) Super Resolution Fluorescence Microscopy image of gels after the incorporation of Nile Red.

the temperature increases and flattens out after 40 ˚C. Visual inspection (using the 'vial inversion test'[177]) showed that this temperature coincides with transition of the gel into a solution and confirms that the intrinsic gelator fluorescence at room temperature is related to the presence of self-assembled structures. A control experiment monitoring the change of the fluorescence signal over time at a constant

temperature (ESI Figure 2.S9) demonstrates that the differences observed in Figure 2.3 cannot be explained by thermal instability of the gel and are indeed related to the change in temperature. Fluorescence therefore also provides a direct route to study the behavior of the nucleobase in the self-assembly process and supports the hypothesis that during self-assembly π-π stacking of the nucleobases occurs.

The same experiment was conducted on gels containing Nile red (Figure 2.3; control experiment of Nile Red alone is presented in Figure 2.S10, ESI), after excitation at two different wavelengths; 326 nm (intrinsic fluorescence from the gelator) and 540 nm (fluorescence from Nile red).

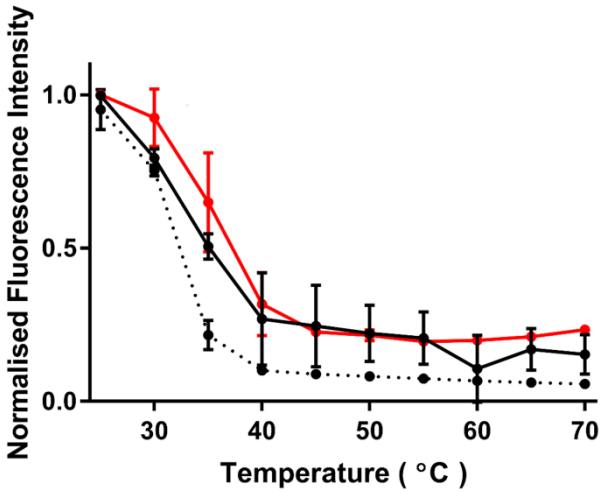

Figure 2.3: Temperature dependent change in fluorescence emission intensities of N^4-octanoyl-2'-deoxycytidine gelator during the gel-sol transition (heating up from 25 to 70 ˚C). Gels in ethanol:water (20:80% v/v) after excitation at 326 nm and emission at 382 nm (inherent gelator fluorescence, dashed trace) and gels after the incorporation of Nile Red in ethanol:water (20:80% v/v) after excitation at 540 nm and emission at 625 nm (Nile Red fluorescence, red trace) and after excitation at 326 nm and emission at 360 nm (inherent fluorescence in presence of Nile Red, black trace). The intensities were normalised to the highest observed value in each condition. The bars represent the standard deviations (number of repeats N=3).

There is a small shift in the transition temperature between the gel containing a dye (black trace) and the plain gel (dashed trace) both after excitation at 326 nm, even

at this low concentration of dye, suggesting that the dye is having a stabilizing effect on the gel structure. When the gels containing the dye were excited at the two different wavelengths, the data matched closely, indicating that Nile Red is interacting with the hydrophobic, aromatic part of the gelator.

NMR spectroscopy has been used extensively to elucidate supramolecular gel formation[19, 124-125] and hence was used here to further study the effect of temperature on self-assembly. In the gel state, the resonances of the gelators are very broad due to the low mobility of the gelators in the self-assembled fibers. The assembled gelator's resonances are therefore not visible by solution-state ^{1}H NMR. Thus, the fraction of mobile gelator in solution in a sample can be determined by integration of the ^{1}H resonances

of the gelator against an internal standard. This approach allows quantification of the relative amount of gelator in solution versus the amount of gelator in the assembled fibers.[19, 128-129, 178] In addition, saturation transfer difference (STD) NMR has been proven useful as a tool to study the exchange between assembled gelator molecules and mobile molecules in solution.[127, 130-131] In this technique, the very broad ^{1}H resonances of the gel fibers are selectively saturated with low-power radiofrequency irradiation. Molecules in exchange with the gel fibers receive some of this saturation and therefore exhibit weaker ^{1}H NMR resonances in the ^{1}H NMR spectrum recorded immediately after saturation compared to non-saturated samples.

In Figure 2.4, NMR integrals and STDs of proton signals for gel samples are plotted as a function of temperature. Protons have been assigned and grouped into

aromatic, aliphatic and deoxyribose (sugar) (ESI, Figure 2.S11). STD effects are quantified as described in ESI, Figure 2.S11 and Equation 2.S1. A strong STD effect indicates the existence of a significant exchange between free and assembled gelator molecules.[127, 130] Between 25 ˚C and 45 ˚C, strong STD effects are observed while integration of the gelator resonances indicates that only a fraction of the gelator molecules are NMR-visible. A significant population of the gelator is therefore aggregated at these temperatures while a degree of exchange exists between the assembled gelators and those in solution. Above 55 ˚C, no STD effects are observed and no increases in the NMR integrals with temperature relative to an internal standard are discernible. The gelators therefore have a high degree of mobility at these temperatures with no NMR-invisible assemblies present. Below 35 ˚C, the STD effects are saturated and there is no clear change with temperature.[178]

As discussed above, the gelator's fluorescence is directly related to the π-π stacking whereas the NMR data shed light into the mobility of the gelator's molecules. The discrepancy in the dissociation temperatures observed between the fluorescence (40 ˚C) and NMR (45 ˚C) may indicate that even if the π-π interactions become weaker (fluorescence data), the gelator molecules are still, to some extent, assembled (NMR data).

As the temperature increases, the NMR integrals increase until they plateau while the STD effects decrease to zero. The difference between the initial NMR integrals (at temperatures < 35 ˚C) and the integrals at higher temperatures (> 55 ˚C) is greater for the aromatic protons than the aliphatic resonances. This observation indicates that at lower temperatures (< 35 ˚C), the aromatic group has a much lower mobility in the self-assembled fibers than the alkyl chain.[179] At lower temperatures,

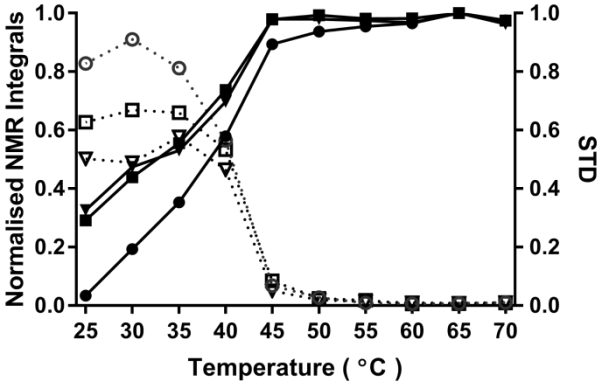

Figure 2.4: Plots of ^{1}H NMR integrals measured on *N*^{4}-octanoyl-2'-deoxycytidine gels against temperature. STDs are also plotted (dashed traces). Trimethylsilylpropanoic acid (TSP) was used as the reference for integration. Different groups of the gelator's protons are presented; aromatic (circles), deoxyribose (triangles) and aliphatic (squares).

the integrals of the deoxyribose resonances overlap slightly with those of the aliphatic tail (ESI, Figure 2.S11), thus precluding a detailed comparison of the integrals of the deoxyribose resonances with those of the aromatic and aliphatic resonances. The alkyl chain resonances chosen for this integration did not overlap significantly with the deoxyribose resonances.

2.2.4 Tracking self-assembly through fluorescence properties

The fact that the fluorescence can be associated with the hydrophobic part of the molecule can give us valuable information on how the self-assembly process progresses during gel formation.[140] Tracking these two fluorescence signals (the gelator's intrinsic fluorescence and the dye's fluorescence) over time can provide a direct way to measure the gelation time and the gel's stability with time.

Gelator solutions (with and without the dye), after incubation at 60 ˚C, were directly pipetted into a cuvette and the intensity of the fluorescence was measured over time (Figure 2.5). For the gel (without the dye, red data), the fluorescence is of low intensity until the onset of the gel formation where the

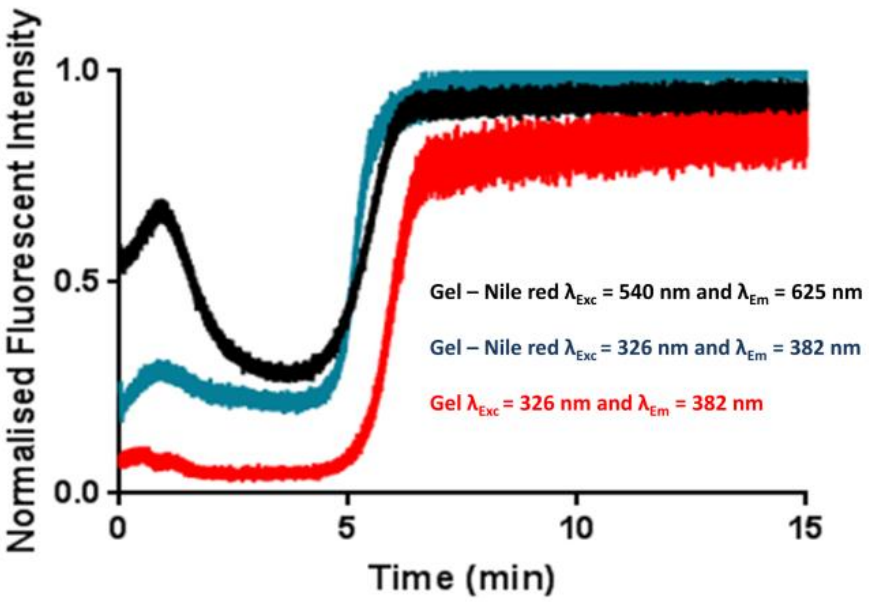

Figure 2.5: Gel formation; normalized fluorescence emission intensity vs time during gel formation (cooling down process from 60 ˚C to 25 ˚C). Fluorescence of gels in ethanol:water (20:80% v/v) upon excitation at 326 nm and emission at 382 nm (with (blue trace) and without nile red (red trace)) and fluorescence of gels after the incorporation of Nile Red in ethanol:water upon excitation at 540 nm and emission at 625 nm (black trace). The intensities were normalized to the highest observed value.

signal increases rapidly and levels off again as the gel forms. However, two small peaks are present at early time points, suggesting the formation of initial oligomers, presumably related to early stage π-π interactions. The intensity of these peaks eventually drops probably due to reorganisations of the oligomers before the final gel formation when the intensities plateau.

With respect to the gel containing Nile red, we excited at two different wavelengths, 326 nm (λ_{Em} = 382 nm for the gelator's intrinsic fluorescence) and 540 nm (λ_{Em} = 625 nm for Nile red fluorescence). There is strong fluorescence emission at 2 minutes in both cases (black data at 540 nm and blue data at 326 nm), probably due to the temporary generation of localized hydrophobic environments that decreases and increases again, leveling off when the gel is fully formed at 7 minutes. This suggests a complex process of initial assembly and reorganization into stable

extended structures. Even if accurate time lengths cannot be measured due to experimental limitations (there is approximately 30 seconds of uncertainty due to variations between sample preparation and starting the measurements), the three data sets almost overlay (the data where the dye is present are slightly shifted to earlier times further indicating its role in stabilizing the gels). The fact that all the data start leveling out at approximately the same time point (7 minutes) confirms that the turning point in the fluorescence traces corresponds to the time required for gelation. Visual observations confirm the fact that the gel is formed (and becomes self-supporting within the first 10 minutes).[51] Gelation time is usually measured through rheology measurements that involves the application of strain.[38, 135] Measuring gelation time through fluorescent emission is a non-invasive way to determine gelation time in this system, that gives an advantage since no strain is applied during the gel formation so no mechanical perturbation to the structure formed.

2.2.5 Probing the nanostructures

To gain further insight into the local packing of the molecules after assembly, N^4-octanoyl-2'-deoxycytidine xerogels were prepared and analyzed by X-Ray powder diffraction (Figure 2.6). Four main peaks can be identified. The first two sharp peaks at 2theta 5.19˚/17.0 Å and 7.86˚/11.2 Å (ratio 2:3) could indicate a lamellar structure with a d-spacing of 34 Å (ratio 1:2:3, suggesting the diameter of the fiber and the dimension of a single molecule at approximately 17 Å). However, data collection at lower 2theta to confirm assignment of the structures was not possible due to instrumental constraints and hence unambiguous identification of the lamellar

structure was not possible. In addition to this, drying induced artefacts such as fiber aggregation could affect the results. [180]

Two broad peaks at 20.5˚ and 26.0˚ (and a shoulder at ~14.4˚) dominate the spectrum in Figure 2.6, corresponding to spacings of 4.3 and 3.4 Å (and 6.1 Å). The gelator molecules self-assemble into loose, flexible structures, held together through π-π interactions and hydrogen bonds. Considering this, these two broad peaks are attributed to the different spacings of the nucleobases along the fiber axis, supported by different N–H–O bonds formed between the gelator molecules.

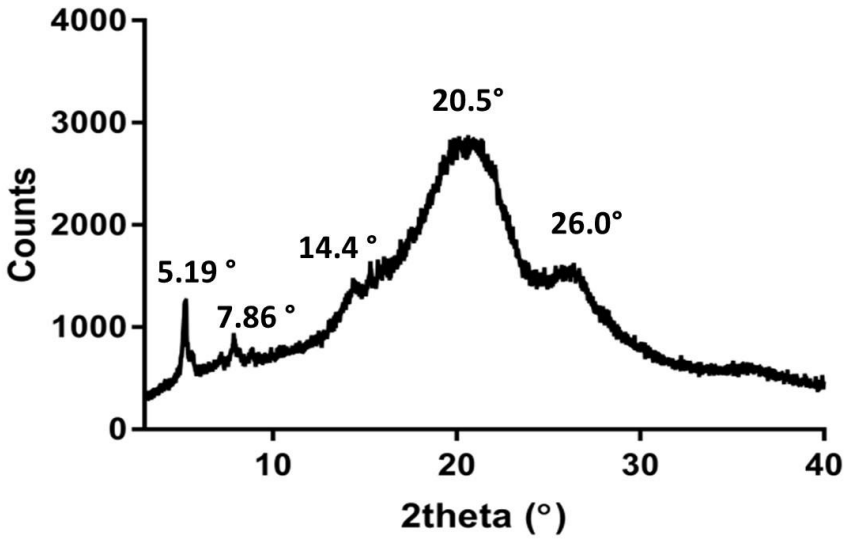

Figure 2.6: Powder X-Ray diffraction data obtained from xerogels of *N*[4]-octanoyl-2′-deoxycytidine.

Since X-ray powder diffraction data did not conclusively allow estimation of the fiber diameter and could only be performed on dried samples, small angle neutron scattering (SANS) data for the wet gels were acquired to estimate the diameters of the fibers formed. The data were fitted to a flexible cylinder model with a polydisperse cross section. The results are presented in Figure 2.S12, ESI. All parameters for the best fit are shown in Table S1. The fitting result indicates that the

radius of the main unit of which the gel is composed is about 6.88±0.05 nm, giving a fiber diameter of approximately 14 nm. As the calculated maximum length of an individual gelator molecule (1.7 nm, see MD section below) is an order of magnitude smaller than the measured fiber diameter, it is reasonable to assume that SANS did not measure individual fibers but that the gel architecture is complex and composed of multiple fibers. Hierarchical self-assembly into structures of increasing complexity has been clearly demonstrated in the past for nucleobase-based amphiphiles. Baldelli et al. reported the self-assembly of 1,2-dilauroyl-phosphatidyl-uridine into cylindrical aggregates that under suitable conditions would form giant worm-like micelles entangled into a network.[181] Moreau et al. demonstrated how the hexagonal packing of helical structures formed by 1,2-dipalmitoyluridinophosphocholine could result in fibers.[47]

2.2.6 Probing the self-assembly through molecular dynamics

In order to understand the mechanism of the self-assembly on the nanoscale in more detail we performed molecular dynamics (MD) simulations of gelator molecules in 20:80% v/v ethanol:water. For the self-assembly simulations, 50 or 150 molecules of gelator were randomly placed in a small periodic box of water and ethanol (Figure 2.7A) and the simulations were run for 150 and 350 ns, respectively. In the low concentration simulation, gelator molecules formed small aggregates within 5 ns, where the molecules were preferentially organized in a parallel fashion, maximizing aliphatic-aliphatic and parallel-displaced π-π contacts (Figure 2.7B). Note that the solvent distribution around the aggregates was not homogeneous: aliphatic tails were mainly solvated by ethanol, while the cytosine bases were mainly solvated by water, and the deoxyribose group environment was well represented by the

overall solvent composition. In the final assembly ethanol was observed in the periphery of the fiber (nucleobases) but did not penetrate to the hydrophobic core. The aggregate size continuously increased by creating small micelle-like assemblies (Figure 2.7C). These assemblies had a transient nature, often reordering or dissociating until all molecules were in a single, flexible aggregate resembling a micelle (Figure 2.7D). When the concentration of the gelator molecules was tripled, a similar assembly path was observed, but it resulted in a one-dimensional assembly that stretched across the periodic boundary of the simulation box (Figure 2.S13). This fiber or worm-like micelle still exhibited a large degree of heterogeneity though, which could be caused by the limited simulation time or the inherent flexible nature of the fibers as observed in the experiments.

To confirm the stability of the fibrous structures and also gain a better insight into the characteristics of the interactions between molecules, we designed a nanostructure by pre-ordering different numbers of gelator molecules into a fibrous structure in a chiral fashion (see Figure 2.8A), based on common patterns observed in the spontaneous assembly simulation. MD simulations for 150 ns revealed that

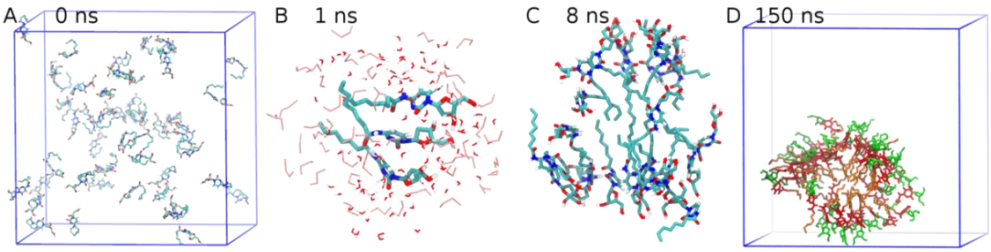

Figure 2.7: Snapshots from an MD simulation of the self-assembly of 50 gelator molecules in ethanol:water. (A) Starting point of randomly dispersed gelator molecules. Periodic boundary conditions are indicated by the blue cube. Solvent is omitted for clarity. (B) From 0-5 ns, small aggregates of parallel-aligned gelator molecules were observed. Note that the hydrophobic tail is preferentially solvated by ethanol (pink), while the polar nucleobases are stacking and solvated by water. (C) Transient micellar structures are observed from 5-150 ns. (D) Endpoint of a 150 ns simulation displaying a micellar assembly. Green: deoxyribose red: nucleobase, orange: aliphatic tail.

flattening of the fiber was observed, but the base-base stacking and hydrogen bonding, and the tail-tail interactions remained mostly stable near the middle of the fiber (Figure 2.8B and 2.8C).

As the X-ray data represent the distances between planes of electron densities, distances obtained through the MD can be compared with the assignments of the pXRD data, as summarized in ESI, Table 2.S2. To compare the simulated structures to the experimental results intra-fiber distances were measured by means of radial distribution functions (RDF, ESI Figure 2.S14). The RDF maximum representing the length of the molecule, from 5' carbon to final tail carbon, was found at 17–18 Å, in accordance with the pXRD analysis (half of the d-spacing of the suggested lamellar structure), molecules are in an extended conformation. Additionally, the diameter of the fiber, represented by a maximum in the RDF between two 5'-carbon atoms of the deoxyribose moiety, was found to be 36 Å, again indicating the SANS measurements represent bundled fibers. To give an insight into the representative distances

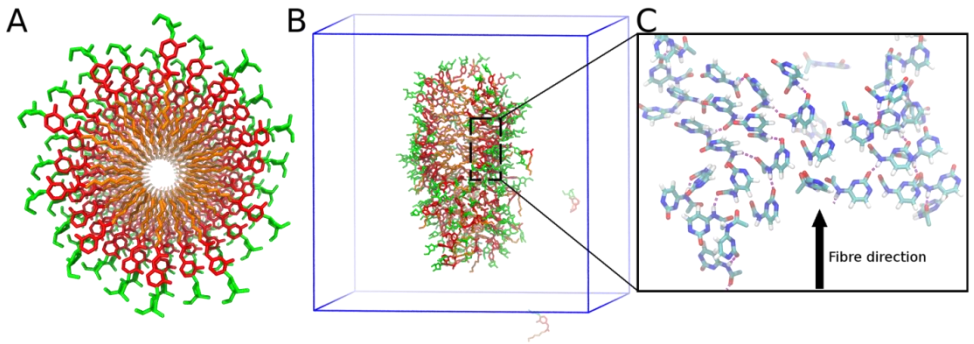

Figure 2.8: Snapshots from an MD simulation of 160 pre-ordered gelator molecules in ethanol:water. (A) Chiral starting structure. Green: pentose, red: nucleobase, orange: aliphatic tail. (B) Final structure after 50 ns. Periodic boundary conditions are indicated by the blue cube. Solvent is omitted for clarity. (C) Expansion of only the cytosine bases in the fiber indicating H-bonding (in purple) and parallel-displaced π-π-stacking.

of the intermolecular hydrogen bonds, the following distances were measured; 0.39 nm (amide C – amide N, or 0.28 nm amide O – amide N), 0.31 nm (base N(3) – amide N), and 0.27 nm (base O(2) – amide N). These hydrogen bond distances were encountered in different frequencies as presented in ESI, Figure 2.S15. The broad range of intermolecular hydrogen bond distances, as suggested by the pXRD data, can be supported by the different potential hydrogen bond acceptors proposed by the MD. The aromatic base stacking was found to be fairly flexible with RDF maxima at 3.6 and 5.1 Å (closest and center-center distance, respectively). Similar lengths of the molecule and distances between atoms of neighboring molecules were also found in the structures that were formed spontaneously from solvated gelator molecules, although in lower intensities because of the more pronounced heterogeneity (ESI, Figure 2.S14). Taken together, these MD data demonstrate the spontaneous formation of fibrous nanostructures with length scales matching those obtained from experimental observations, thus confirming that the proposed fiber structures are reasonable.

2.3 Conclusions

In the present work, experimental data along with molecular dynamic simulations were used together to indicate the self-assembling mechanism and the nanoarchitecture of the fiber of a novel nucleoside (cytosine-based) gelator. The gelator molecules, driven by solvophobic forces, initially assemble into oligomeric structures then rearrange to orient themselves into a cylindrical fiber with the aliphatic chains towards the core, the nucleobases stacked together and the hydrophilic sugars towards the external surface of the fiber, whereas hydrogen bonds are stabilizing the structure. A dual environment is formed, displaying hydrophobic cores within the fiber and hydrophilic cavities surrounding them. While

some structural elucidation of the self-assembly of nucleoside-based gels exist, this is the first report of the self-assembly of a cytosine based gelator. Moreover, this work demonstrates that the traditionally less well established molecular modelling of nucleobase gelators is a powerful approach to deduce information about the self-assembly of nucleic acid based gelators and matches well with experimental data.

The architecture of the present cytidine-based gel presents promising opportunities for the encapsulation of small hydrophobic molecules (e.g. anticancer drugs) as well as the stabilization of hydrophilic biopharmaceuticals (e.g. therapeutic proteins or peptides) in drug delivery applications. The ability to measure, predict and rationalize nucleobase gelator self-assembly provided by this work opens the way to a rational design of a previously unexplored class of nucleobase gelators based on cytidine for biomedical applications.

2.4 Experimental Section

2.4.1 Materials

2'-Deoxycytidine (lot #SLBN6031, 99% (HPLC)) and Nile Red (lot 47H3445) were purchased from Sigma Aldrich. The gelator was synthesized according to procedures reported previously.[51] Solvents (HPLC grade) were obtained from Fischer Scientific. Analysis of the gelator was performed by NMR and LC-MS (ESI Figure 2.S16 and 2.S17) and purity was determined as 98% (LC-MS).

2.4.2 Gel preparation

In a glass container (14 cm diameter), water (300 mL) was equilibrated at 60 ˚C. The solvent mixture was prepared by mixing milliQ water and ethanol (80:20% v/v). 6.00±0.01 mg of N^4-octanoyl-2'-deoxycytidine were pre-weighed in 1.5 ml HPLC vials. 1.2 mL of the solvent mixture was pipetted into the vials to give a 5mg/mL

mixture. The vials were placed in the preheated water not in direct contact with the bottom of the container for 2 minutes. The vials were removed and mildly agitated and left to rest on the bench for 30 seconds. Consequently, the required volume for the analysis was placed in a suitable container until a transparent gel was produced.

2.4.3 Gels containing Nile Red

Nile Red (0.32 mg) was suspended in in premixed solvent (20:80% v/v ethanol:water, 10 mL) and sonicated for 15 minutes. The gels were prepared as above using the stock solution of Nile Red as solvent. A freshly made stock solution was prepared for each experiment.

2.4.4 Super resolution fluorescent microscopy

Samples were prepared according to the standard protocol, 5 µL of the warm gelator solution were pipetted onto a clean coverslip. Images were recorded with a Zeiss Elyra PS1 with a 561nm laser: 0.1 % power100x/NA1,46 TIRF objective, with EMCCD camera in laser wide field mode, using TIRF illumination; 35 ms camera exposure time, LBF -561/642 filters.

2.4.5 Fluorescence spectroscopy

Spectra were recorded at a Cary Eclipse Fluorescence Spectrophotometer. The spectra were recorded with scan rate 30 nm/min, averaging time 1 sec and data interval 0.5 nm. Spectra of 14 mM 2'-deoxycytidine and N^4-octanoyl-2'-deoxycytidine were recorded at room temperature (in premixed solvent 20:80% v/v ethanol:water and methanol) after excitation at 326 nm. The excitation slit was set at 2.5 nm and the emission slit at 5 nm.

2.4.6 Circular and Linear Dichroism

Samples of 2'-deoxycytidine were prepared at concentrations of 4.2 mM in methanol and ethanol:water (20:80% v/v) in 1 mm cuvette, whereas samples of N^4-octanoyl-2'-deoxycytidine were prepared at 3.5 mM in methanol and 14 mM in ethanol: water 20:80% v/v in 1 mm cuvette and 0.1 mm demountable cuvette, respectively. Circular and linear dichroism spectra were recorded simultaneously at a Jasco J-815 instrument. The acquisition parameters were; bandwidth 2 nm, data pitch 0.2 nm, scanning speed 100nm/min and each spectrum was the product of averaging 4 accumulations.

2.4.7 Fluorescence temperature experiment

Spectra of the gels (5 mg/mL in premixed solvent 20:80% v/v ethanol:water) were recorded at 25, 30, 35, 40, 45, 50, 55, 60, 65 and 70 ˚C, with 326 nm excitation and 382 nm emission wavelengths. The excitation slit was set at 2.5 nm and the emission slit at 5 nm. Temperature experiments of the gels after the incorporation of the Nile Red (5 mg/mL in premixed stock solution 20:80% v/v ethanol:water) were recorded at same temperatures as before with 540 nm excitation and 625 nm emission wavelengths. The excitation slit was set at 5 nm and the emission slit at 5 nm. An excitation spectrum was recorded for the gels (5 mg/mL in premixed solvent 20:80% v/v ethanol:water) and the emission wavelength was set at 382 nm. The excitation slit was set at 2.5 nm and the emission slit at 5 nm.

2.4.8 Kinetics experiment

The gel was prepared according to the standard protocol and immediately transferred into the sample holder to record the fluorescent spectrum. Data points were collected for 40 minutes. For the gel, the excitation slit was set at 2.5 nm and the emission slit at 5 nm, the excitation wavelength was 326 nm and the emission 382 nm. For the gel after the incorporation of the Nile Red, the excitation slit was set at 5 nm and the emission slit at 5 nm, the excitation wavelength was 540 nm and the emission 625 nm, averaging time 0.0125 ns.

2.4.9 Powder X-ray Diffraction

Gels were prepared according to the general preparation method mentioned before and left to fully dry at room temperature. Powder X-ray diffraction (pXRD) patterns on the dry gel were collected over the 2theta range of 3-40o on a PANalytical X'pert diffractometer using Cu-Kα1 radiation (λ=1.5406Å).

2.4.10 Molecular dynamics simulations

Molecular dynamics simulations were performed using the GROMACS 4.6.7 package.[182] Force field parameters for the cytidine derivative were based on a combination of the 2'-deoxycytidine and aliphatic tail parameters of the GROMOS54a8 force field.[183-184] After a short energy minimization, simulations of a pre-ordered fiber (50 ns) or 50/150 randomly dispersed amphiphiles (150 ns) in a periodic box of 10 x 10 x 10 nm filled with a pre-equilibrated SPC water / ethanol mixture[185] were run in the NPT ensemble with time steps of 1 fs. Bonds involving hydrogens were constrained using the LINCS algorithm, [186] except from water bonds

which were constrained using the more efficient SETTLE algorithm. [187-188] Center of mass motion of the system was removed every 100 steps. Temperature was kept at 298 K using the velocity-rescaling thermostat[188] (τT= 1.0 ps) and pressure at 1.0 bar using the Berendsen barostat[189] (τp= 1.5 ps). Van der Waals and electrostatic forces were cut off at 1.4 nm using the Verlet list scheme; long-range electrostatic interaction were treated using a Barker-Watts reaction field with εRF = 62. Visualisation of the simulations was done using the VMD program v. 1.9.3.[190] Radial distribution functions were calculated on the final one-third of the simulations using the GROMACS package with a bin width of 0.002 (see ESI for further details).

2.4.11 NMR experiment

To prepare a sample for analysis by NMR spectroscopy, 4 mg of N^4-octanoyl-2'-deoxycytidine was weighed into a 1.2 mL HPLC vial. A solution of 80% D_2O/20% ethanol-d6 was then added to the vial to create a 5 mg/mL mixture of N^4-octanoyl-2'-deoxycytidine. The vial was then placed in a water bath at 60 ˚C for 2 minutes, whereupon the vial was removed from the bath, gently shaken and stood for 30 seconds. The solution was then injected into a pre-heated 5 mm NMR tube using a preheated 1 mL polypropylene syringe fitted with a 200 µL polypropylene pipette tip. The NMR tube had been preheated by placing it in the water bath. The syringe was preheated by placing it in a 10 mm NMR tube which was immersed in the bath. A 2 mm (O.D) capillary (New Era Enterprises, New Jersey, USA) containing 20 mM 3-(trimethylsilyl)propionic-2,2,3,3-d4 acid sodium salt (TSP) in D_2O was then inserted into the sample when still liquid. A clear gel formed in the tube within 10 minutes. After 1 hour had elapsed, the sample was transferred to the spectrometer for analysis.

NMR experiments were performed on a Bruker Avance II 400 MHz wide bore spectrometer operating at 400.20 MHz for ^{1}H. TSP (0 ppm) was used a reference for all spectra. The sample was heated in 5 ˚C increments, with a seven minute equilibration time at each temperature prior to acquiring NMR data. ^{1}H integrals were measured from spectra obtained in 4 scans using a 30˚ excitation pulse, a relaxation delay of 40 s and a signal acquisition time of 4 s. The total acquisition time was 2 minutes and 56 seconds. STD spectra were acquired using a 90˚ excitation pulse and a signal acquisition time of 4 seconds. The relaxation delay was set at 8.1 s with presaturation applied during the last second at -5 ppm (on resonance) and at -250 ppm (off resonance). Presaturation was delivered using twenty Gaussian pulses of 50 ms duration and peak powers of 380 Hz. The separation between the pulses was 1 ms. On and off-resonance spectra were acquired alternately in 4 scans at each frequency. 8 dummy scans were acquired prior to signal acquisition. The total acquisition time for STD spectra was thus 3 minutes 16 seconds.

2.5 Supporting Information

2.5.1 Nano-architecture of the gels

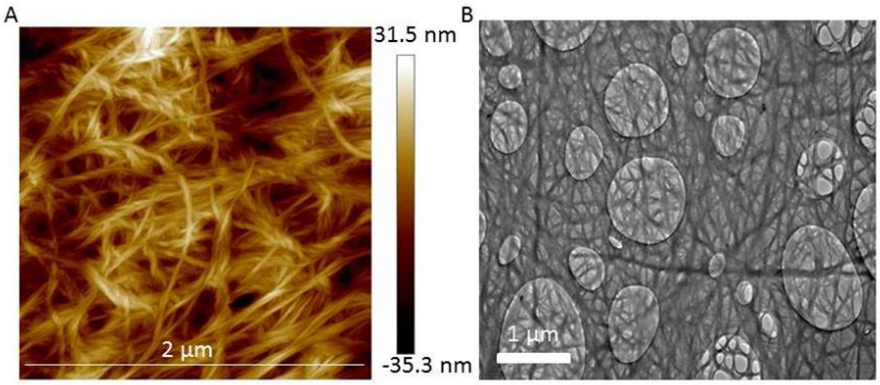

Figure 2.S1: Nanoarchitecture of N^4-octanoyl-2'-deoxycytidine gel in ethanol:water (20:80%); Atomic Force Microscopy images of dried gels (A) and Transmission Electron Microscopy images (B) showing tubular structures (the oval structures originate from the sample holder). Numeric values of the fibre diameters are summarized in Table 2.S2.

2.5.2 Fluorescence properties of the gelator

To help understand the fluorescence properties of the gelator, the excitation spectrum of the gel is presented in Figure 2.S2. Three peaks are present at 225 nm, 265 nm and 326 nm at room temperature. The emission spectra after excitation at these three wavelengths show emission maxima at the same wavelength (360 nm). Excitation to the lowest excited state (i.e. excitation at

326 nm) results in the highest quantum yield emission so this is used in our further analysis.

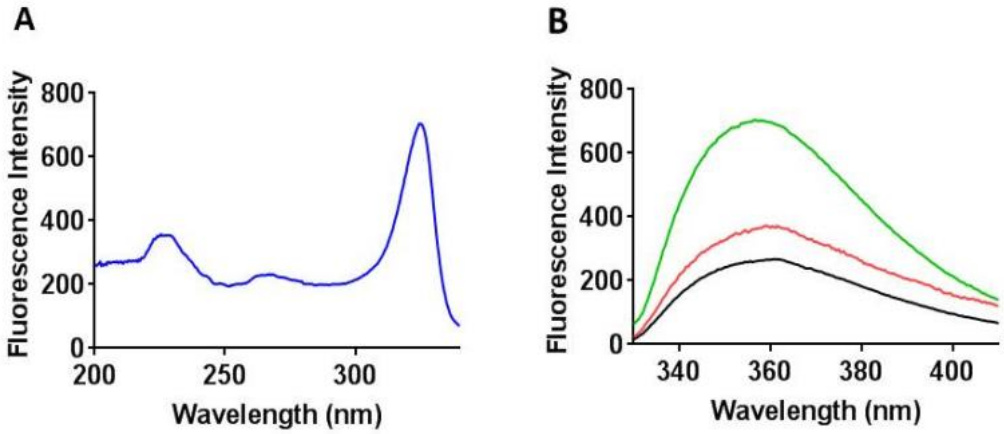

Figure 2.S2: Fluorescence spectra of N^4-octanoyl-2'-deoxycytidine in ethanol:water (20:80% v/v). (A) Excitation spectrum (emission at 382 nm) and (B) emission spectrum after excitation at 225 nm (red trace), 265 nm (black trace) and 326 nm (green trace). Number of repeats, N=3.

2.5.3 Circular and Linear Dichroism investigations of the gel formation

In Figure 2.S3A, two almost identical CD spectra of 2'-deoxycytidine in two different solvent systems; 20:80% v/v ethanol:water (black trace, gel state) and methanol (red trace, gelator in solution) are presented. These spectra are in accordance with the literature.[137] The different solvents can therefore be assumed not to change the electronic structures of the deoxycytidine chromophore significantly.

In Figure 2.S3B, the spectrum of N^4-octanoyl-2'-deoxycytidine dissolved in methanol (red trace) presents similar features to that of 2'-deoxycytidine with the 280 nm peak apparently shifting about 20 nm to the red. The main 320 nm peak in the fluorescence excitation spectrum (Figure 2.S2A) together with the CD intensity in this region actually indicate that there is a new transition due

to the amide group of the octanoyl-tail. The spectrum of the gel induced by water:ethanol is at first sight quite different from those of the monomers. What we observe is consistent with the changes one would expect from π-π stacking interactions, namely a shift of a few nanometers to the red together with exciton couplets. An exciton couplet for an isolated transition has zero CD signals where the monomers have a maximum and there is a sharp transition about this point from positive to negative or conversely. In our case we have overlapping transitions, so any exciton doubles the complexity of a spectrum. The 326/315 nm exciton couplet in the gel spectrum (black trace, Figure 2.S3B) is particularly clear and so a good indicator of the formation of a gel in ethanol:water but not in methanol. The 300/280 nm and 240/230 nm couplets are also indicative of the gel. The 220 nm region is more complex. In the 2'-deoxycytidine samples (Figure 2.S3A), the polarisation at 269 nm is oriented along the sugar/amine axis (Figure 2.S4). This polarisation is presumably similar to the polarisation at 280 nm in the monomer spectrum (Figure 2.S3B, red trace), and in the gel (Figure 2.S3B, black trace).

Along with the CD data, Linear dichroism (LD) data were also collected to confirm that LD signal is not dominating the CD spectra (Figure 2.S5 and 2.S6).

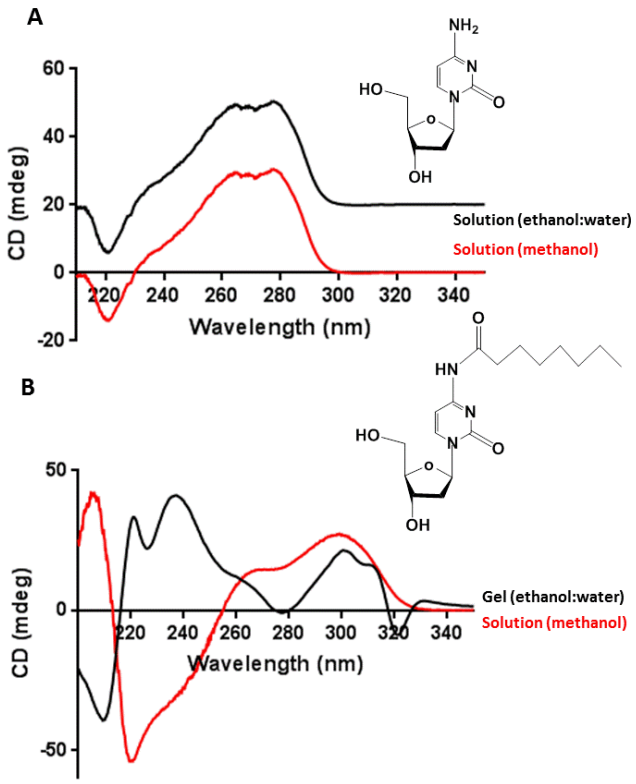

Figure 2.S3: Circular dichroism spectra of 2'-deoxycytidine (A) and *N*[4]-octanoyl-2'-deoxycytidine (B) (ethanol:water curve displaced by 20 mdeg for clarity). (A) 2'-Deoxycytidine dissolved in methanol (red trace) and in a mixture of ethanol:water (20:80% v/v) (black trace) in a 1 mm pathlength cuvette (the black trace is displaced from zero for clarity). (B) *N*[4]-Octanoyl-2'-deoxycytidine dissolved in methanol (red trace) and at the gel state in a mixture of ethanol:water (20:80% v/v) (black trace corresponds to a single measurement of the spectrum of the gel) in a 0.1 mm pathlength cuvette.

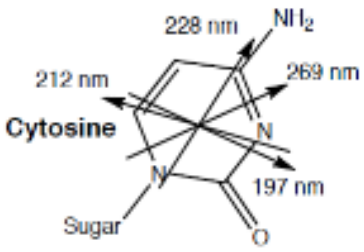

Figure 2.S4: Transition polarisations for UV transitions of cytosine.[136]

Linear Dichroism is a useful tool to detect orientation in a sample. To minimise alignment of gel fibres due to mounting of the sample in the demountable cuvette, the gel was formed before the top window was placed on top. Nonetheless, all samples showed an LD signal (Figures 2.S5 and 2.S6) and a difference between the horizontal and vertical direction was apparent. A negative signal corresponds to a transition preferentially vertically oriented in the instrument used. All transitions polarised along the light path are invisible. The prevalence of positive LD signals indicates that the cytidine transitions are preferentially polarised in the horizontal direction. This suggests that the fibre direction is preferentially horizontal in all samples. The positive peak at 300 nm corresponds to the second component of the exciton arising from the lowest energy transition. Overall, the fibres tend to be present in an oriented fashion but comparison of Figures 2.S3B and 2.S5 show the LD signal is not dominating the CD spectrum despite its larger magnitude. The transition polarisations are indicated for cytosine in Figure 2.S4. We assume they shift to longer wavelengths when substituted and that they shift even further when π-π stacked. The shapes of the spectra suggest both different fibre orientations and different degrees of stacking. Despite our best efforts it is clear there is sample to sample differences and preferential orientation.

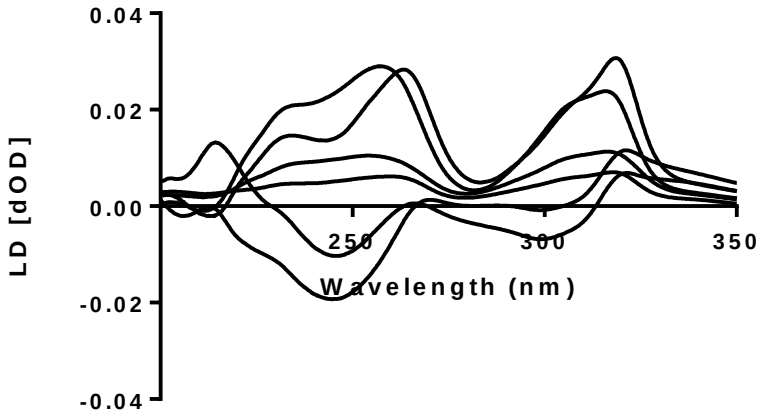

Figure 2.S5: Linear Dichroism spectra of N^4-octanoyl-2'-deoxycytidine gels in a mixture of ethanol:water (20:80% v/v). Different traces correspond to different repeats of the gel in a 0.1 mm pathlength cuvette.

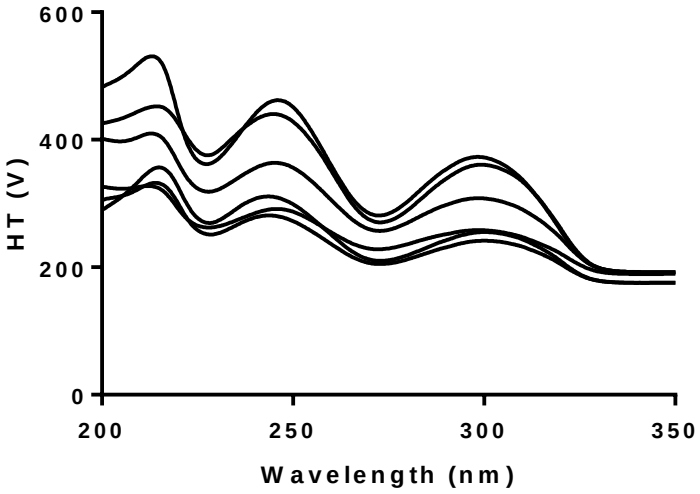

Figure 2.S6: HT Voltage values against wavelength corresponding to the CD and LD data presented above. Values lower than 600 V are considered to provide reliable measurements.

The LD data suggest two types of structure form. The one dominating the two middle spectra of Figure 2.S5 has the cytidines stacked like DNA with the stack oriented vertically (so all the transitions absorb more horizontally than vertically polarised light) making a positive LD spectrum. The other structure is more complex having positive and negative signals. We speculate this is due to a dominance of different twists in the π-π stacking to accommodate the

deoxyribose and octanoyl-tail, possibly as a consequence of subtle differences in sample preparation; this would require further investigation. A linear stacked structure can also form presumably depending on subtle difference in preparation methodology.

2.5.4 Variability of the molecular arrangement in the stacked nucleobases

Interestingly, different batches of gels gave different emission spectra after excitation at 326 nm (Figure 2.S7), with a single band shifting between 360 nm to 382 nm, suggesting a flexible/variable π-π stacking conformation which will be discussed in more detail later. We presume one (the 380 nm sample) has more π-π stacking which stabilises the lowest excited state as in duplex versus single stranded DNA. Because of this variability in the emmission maximum, the apparent blue shift (362 nm to 357 nm) of the emission maxima of the gelator in solution and the gel state (Figure 2.1B) is not significant enough to draw any conclusions. Because of the significant difference in fluorescence intensity between the solution and the gel sample, we postulate that the increase in fluorescence intensity is more likely to be related to the self-assembled state affecting quenching rather than any solvent-induced changes in molecular fluorescence.

Variation from sample to sample was also apparent in both CD and fluorescence data, indicating some inherent variability in the spectroscopic properties of these structures in the gels. Relative intensities of the peaks varied between gel batches (Figure 2.S7), though showed consistent features (similar peak positions). The overall CD intensity variations (Figure 2.S8) are

presumed to be largely due to variations in path length due to assembling a demountable cell for each experiment, but the differences in relative intensities and even signs also indicate variability in the secondary structures of the gels. This is presumably a consequence of the flexibility and hence different orientations that the nucleobases can take which can seed different structures. The CD spectra are similar in the longer wavelength region of the spectrum but differ noticeably in the region (below 240 nm) which, in mixed sequence DNAs, changes for different polymorphs and structures such as triplex and quadruplex structures.

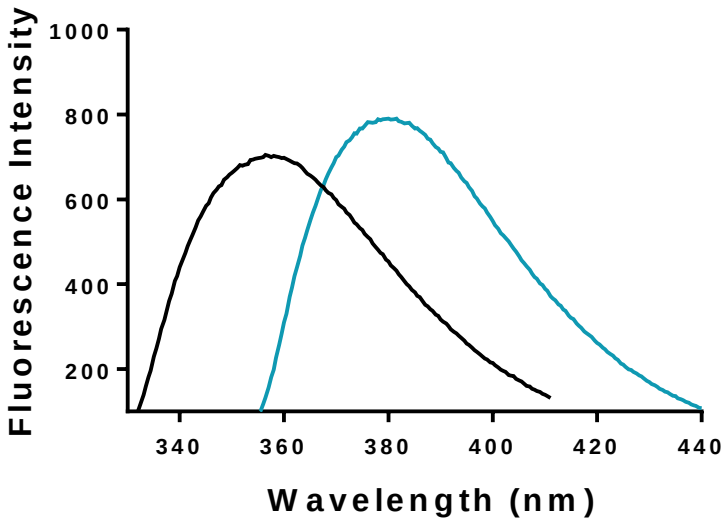

Figure 2.S7: Fluorescence emission spectra of two different batches of gels after excitation at 326 nm.

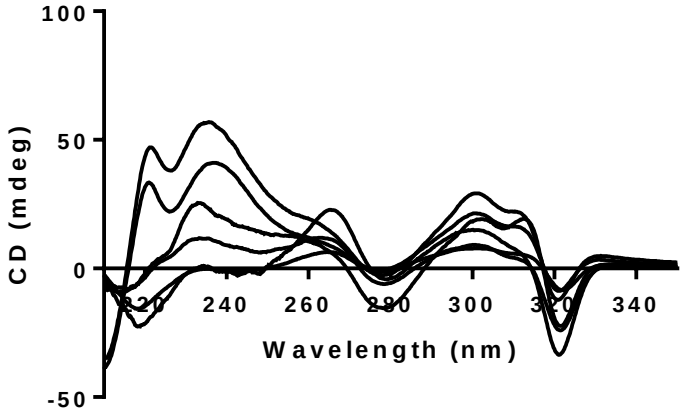

Figure 2.S8: Circular dichroism spectra of N^4-octanoyl-2'-deoxycytidine showing different repeats of the gels prepared in a mixture of ethanol:water (20:80% v/v) (different black traces) in a 0.1mm pathlength cuvette suggesting a flexible structure between the stacked nucleobases.

2.5.5 Effect of temperature over time on the self-assembly induced fluorescence

To confirm that the decrease in fluorescence intensity is solely dependent on the dissociation of the stacked nucleobases and that the gel is stable at a certain temperature over time, the fluorescence intensity was measured at different time points over the course of a temperature experiment (40 minutes). The temperature of 32 ˚C was selected as it corresponds to the temperature at the middle of the slope (Figure 2.3) and would therefore present the worst-case scenario as it shows the highest sensitivity (and hence variability) to changes in the fluorescence signal due to structural changes in the gel. Although higher temperatures are likely to show a more severe impact on gel stability, for our gel the fluorescence intensity has almost non-measurable values after 40 ˚C, making it impossible to detect any changes by fluorescence. As presented in Figure 2.S9, the differences observed on the gel's fluorescence at different temperatures (black trace) cannot be explained by thermal instability of the gel and the observations in Figure 2.3 are indeed related to the change in temperature.

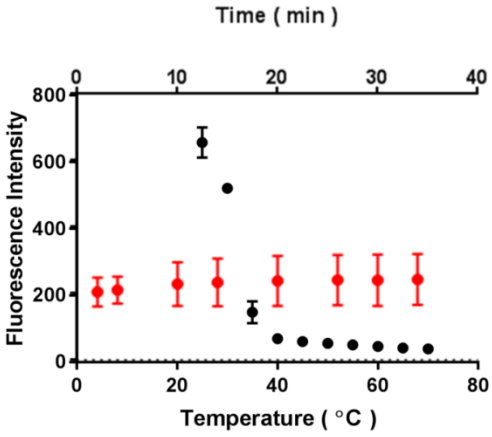

Figure 2.S9: Fluorescence intensity of gels over time at 32 ˚C (red trace, top axis) and gels at different temperatures (black trace, bottom axis) in ethanol:water; excitation at 326 nm and emission at emission maxima (358 nm for red trace and 360 nm for back trace). The bars represent the standard deviations (number of repeats, N=3). The top and bottom axis are not correlated, they have been plotted on the same graph for convenient comparison of the datasets.

2.5.6 The effect of temperature on the self-assembly

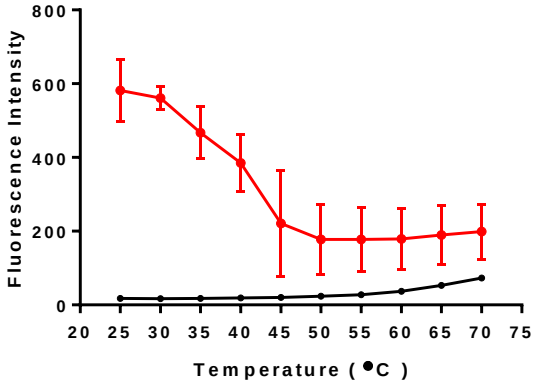

Figure 2.S10: Temperature-dependent change in fluorescence emission intensities during the gel-sol transition. Gels after the incorporation of Nile Red in ethanol:water; excitation at 540 nm and emission at 625 nm (Nile Red fluorescence, red trace). Nile Red in ethanol:water; excitation at 540 nm and emission at 625 nm (Nile Red fluorescence, black trace). The error bars represent the standard deviations (number of repeats, N=3).

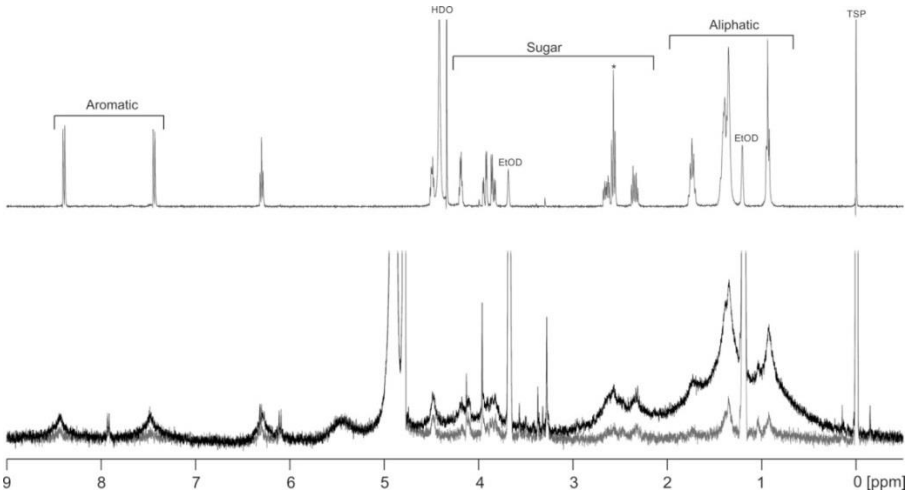

Figure 2.S11: ^{1}H NMR spectra of *N*^{4}-octyl-2'-deoxycytidine gel at 70 ^{o}C (upper) and 25 ^{o}C (lower), recorded with presaturation applied at -5 ppm (on resonance, grey) and at -250 ppm (off resonance, black). The spectra at 25 ^{o}C have been scaled vertically by a factor of 16 relative to the upper spectra. The peak marked * is the terminal CH_2 of the alkyl chain adjacent the carbonyl and cannot be analysed separately from the sugar resonances. The integrals of the EtOD resonances have been subtracted from the gelator integrals plotted on Figure 5. To accomplish this, the EtOD resonances were integrated relative to Trimethylsilylpropanoic acid (TSP) at 70^{o}C. These normalised integrals were then subtracted from the gelator regions at each temperature. Due to the broadness of the gelator peaks at lower temperatures, accurate integration and STD measurements of the EtOD resonances were not possible.

STD effects plotted on Figure 2.5 are defined as:

$$STD = \frac{I_0 - I_{Sat}}{I_0} \quad \text{(S1)}$$

where I_{Sat} and I_0 are the integrals obtained from spectra recorded with on resonance (-5 ppm) and off resonance (-250 ppm) presaturation respectively.

2.5.7 Analysis of the SANS data

The small angle neutron scattering (SANS) data for the gel can be fitted to a flexible cylinder model with a polydispersed cross section (Figure 2.S12) and all parameters

for the best fit are shown in Table 2.S1. The fitting result indicates that the radius of the fiber constituting the gel is about 68.8 ± 0.5 Å with a polydispersity of 0.22 ± 0.01, a Kuhn Length of 377 ± 10 Å and an average fiber length of 1515 ± 50 Å. The volume fraction of the fiber is as low as 0.048%.

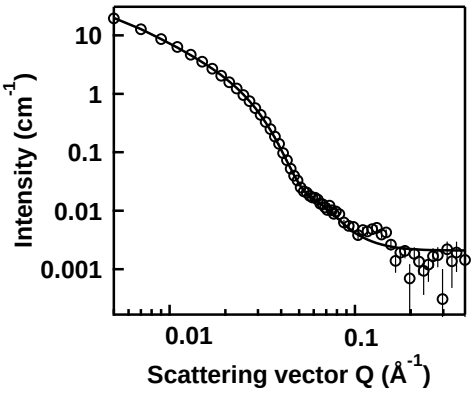

Figure 2.S12: SANS profile for the gel formed by *N*[4]-octanoyl-2'-deoxycytidine gelator. The continuous line is a fit to the model described as above.

Table 2.S1: The model fit parameters generated by fitting the customised flexible cylinder model to the data in NIST SANS analysis package. The chi squared value is 2.17.

Parameter	**Value**
Scale	0.00048±0.00001
Countour Length (Å)	1515 ± 50
Kuhn Length (Å)	377 ± 10
Radius (Å)	68.8 ± 0.5
Polydispersity of Radius	0.22 ± 0.01
Background (cm^{-1})	0.0020 ± 0.0001

2.5.8 Molecular Modelling of the self-assembled structures

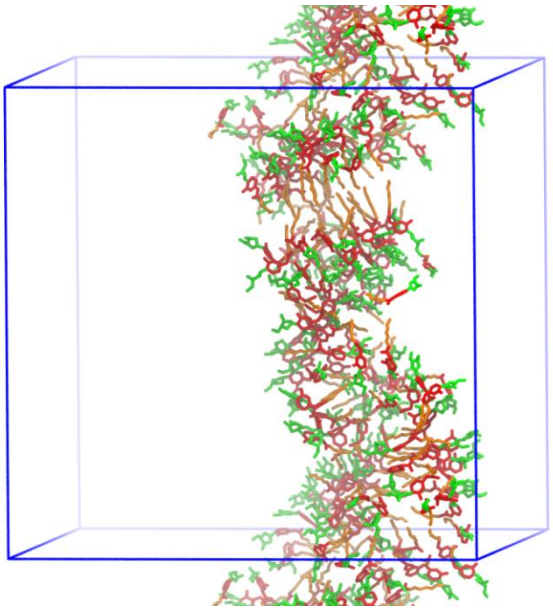

Figure 2.S13: Snapshot of a 350 ns MD simulation of the self-assembly of 150 gelator molecules in ethanol:water displaying a one-dimensional assembly with local order. Periodic boundary conditions are indicated by the blue cube. Solvent is omitted for clarity. Green: deoxyribose, red: nucleobase, orange: aliphatic tail.

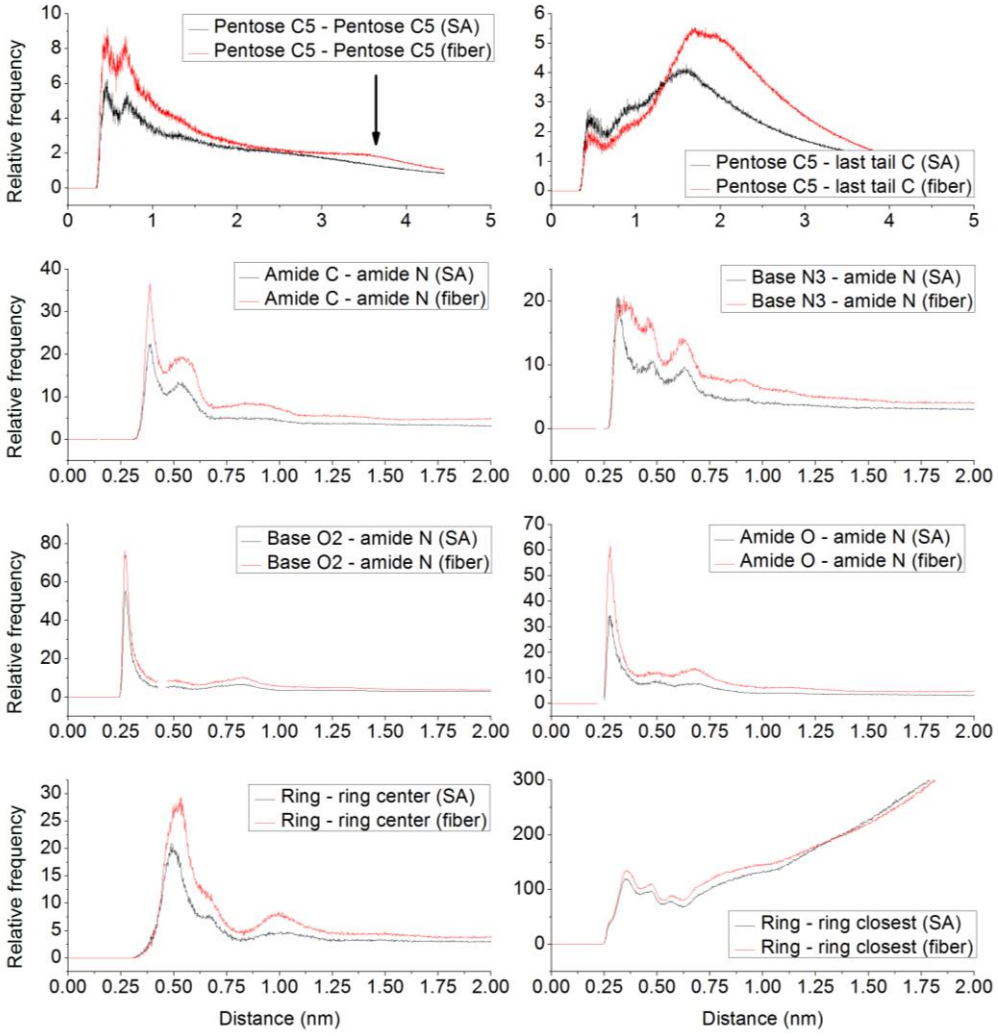

Figure 2.S14: Radial distribution functions for the fiber simulation (160 gelator molecules, red traces) and the self-assembly simulation (150 gelator molecules, black traces). The relative frequency of specific distances occurring is plotted in bins of 0.002 nm. Only the last 100 ns of the simulation time were taken into account. For nucleobase center, the center of mass of any non-H atoms in the ring was used. The area under the curves was normalised to the total number of interactions, except for ring-ring closest distances from any nucleobase ring non-H atom to any other nucleobase ring non-H atom. The maxima are at 0.46/0.68 nm (C5'- C5'), 1.7 nm (fiber, pentose C5' to last carbon of tail), 0.39 nm (amide C-N), 0.31 nm (base N3-amide N), 0.27 nm (base O2 – amide N), 0.28 nm (amide O – amide N), 0.5 nm (base center-center) and 0.36 nm (base closest distance). The arrow in the deoxyribose-deoxyribose RDF plot indicates the local maximum representing the fiber diameter of 3.6 nm.

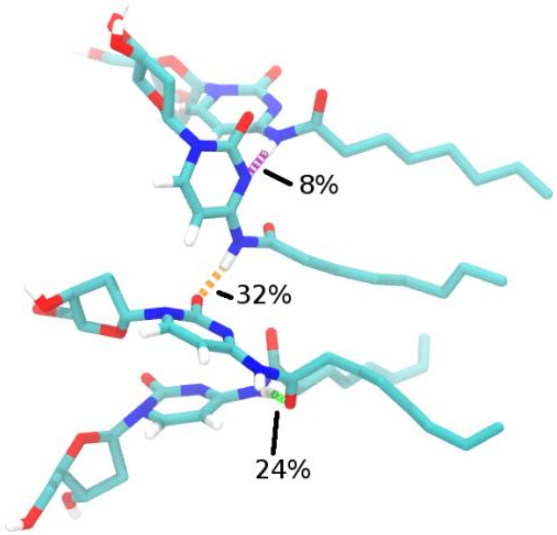

Figure 2.S15: Snapshot of different H-bonds at the end of the fiber simulation. The numbers indicate the occupancy of the specific H-bond during the last 100 ns of the simulation, using a cut-off distance of 0.35 nm and a maximum acceptor-H-donor angle of 30 degrees. For the 150 molecules self-assembly simulation, the occupancies are 11% (base N - amide NH), 33% (base O - amide NH) and 17% (amide O - amide NH). The remaining percentage of molecules is not H-bonded within the cut-offs or H-bonding with solvent.

Table 2.S2: Summary and assignments of the distances obtained from MD and pXRD.

distance	MD	pXRD
Hydrogen bonds	3.9 Å (amide C – amide N, or 2.8 Å amide O – amide N) 3.1 Å (base N3 – amide N) 2.7 Å (base O2 – amide N)	4.3 and/or 3.4 Å[a]
π-π stacking	3.6 and 5.1 Å (closest and center-center distance, respectively)	
Fibre diameter	36 Å	34 Å[b]
Molecular length	17-18 Å	17 Å[c]

[a] measured experimentally

[b] d-spacing calculated through the ratio 1:2:3 (at 2theta 5.19˚/17.0 Å and 7.86˚/11.2 Å, ratio 2:3) suggesting a lamellar structure, attributed to the fibre diameter.

[c] estimated as half the fibre diameter (half of the d-spacing) corresponding to the fibre radius or the molecular length.

2.5.9 Structural characterisation of the gelator

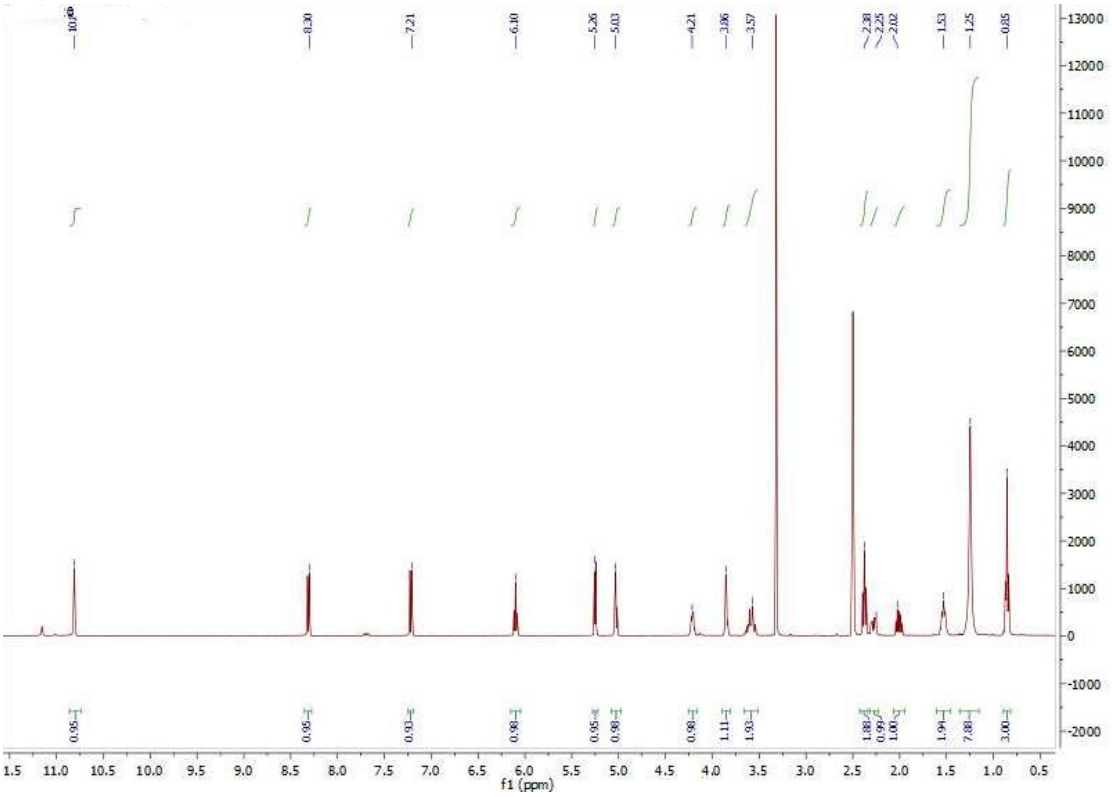

Figure 2.S16: ^{1}H NMR spectrum of *N*^{4}-octanoyl-2'-deoxycytidine in deuterated DMSO. Details of the peak assignment can be found in previously published work.[51]

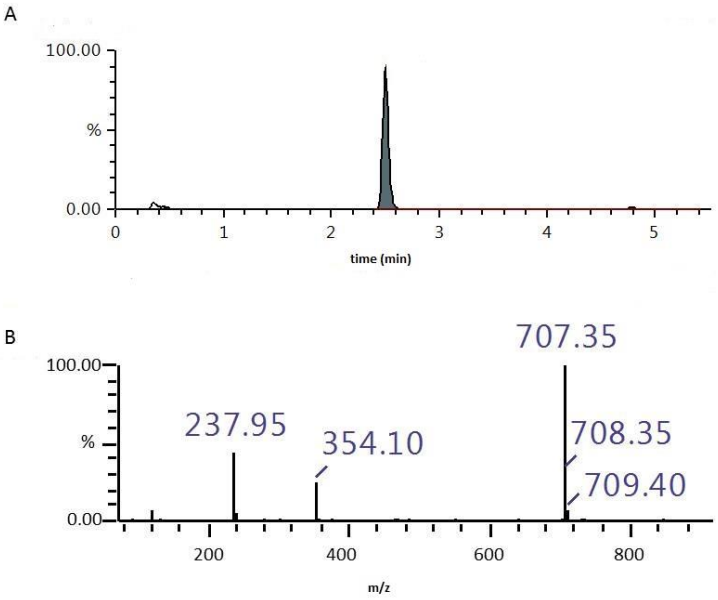

Figure 2.S17: LC-MS analysis of *N*^{4}-octanoyl-2'-deoxycytidine in methanol. Purity determined from the chromatogram as 99% (by height) and 98% (by area) by UV at 254 nm (A). MS spectrum with main ions detected at m/z 237.95 [*N*^{4}-octanoyl-cytosine + H]$^+$, 354.10 [M+H]$^+$ and 707.35 [2M + H]$^+$.

2.6 General conclusions

In this chapter the mechanism of the self-assembly was established for the N^4-octanoyl-2'-deoxycytidine gelator that will set the basis for further investigations of these materials in the coming chapters. Driven by solvophobic forces, the gelators' molecules first assemble into oligomeric structures and eventually orient themselves into cylindrical structures with the aliphatic chains towards the fibre's core, the nucleobases stacked together and the hydrophilic sugars protruding on the external surface of the fibre. In addition, hydrogen bonds are further stabilizing the self-assembled structure. This fine balance of weak non-covalent interactions that holds the self-assembled structures together, in the presence solvent molecules, defines the reversible, dynamic nature of the supramolecular gels. Further to this, the arrangement of the molecules into fibrillar structures generates a dual environment, demonstrating hydrophobic cores inside the fibres and surrounded by the hydrophilic cavities where the water molecules reside. This dual environment suggests that molecules with different properties (size, charge, hydrophobicity/hydrophilicity) can be encapsulated for drug delivery applications and this will be further discussed in Chapter 4. The presence of encapsulated molecules with complex structures can influence this fine balance of interactions that holds the assembled structures together and directly affect the properties of these dynamic materials. To understand the effect that different encapsulated molecules can have on the self-assembled structures and having already established how the self-assembled structures form, in Chapter 3, we move to simple interfaces between chemically modified surfaces and supramolecular gels and directly describe how different chemistries relate to the self-assembled structures.

Chapter 3

Surface-mediated self-assembly: characterisation and modulation of gel properties for a family of cytidine-based gelators on model gel-substrate interfaces

Abstract

Supramolecular gels are physical gels that form through non-covalent interactions. These non-covalent interactions lead to rather dynamic materials that gel when a fine balance between the gelator-gelator interactions and the gelator-solvent interactions is achieved. As expected the presence of any additional molecule during the self-assembly process, can shift this balance towards materials that do not gel, or form weaker or stronger gels (compared to the gel alone). In Chapter 3, in order to test the hypothesis that different chemical functionalities can structurally affect the supramolecular gel formation and ultimately its mechanical properties, we generated different simple flat interfaces between differently chemically modified surfaces and gels. We used different members of the cytidine-based family of gelators, flat surfaces modified with single chemical functionalities and different surface-sensitive techniques to explore the interfacial interactions of these simple systems. In the first part, we used one gelator, the N^4-tetradecanoyl-cytidine, on two very different surfaces, a very hydrophilic one (functionalised with hydroxyl groups) and very hydrophobic structures (functionalised with aromatic groups ie. phenyl) to demonstrate that different chemistries can significantly affect the physical properties (diameter of the fibres formed) and mechanical properties of thin gel films in the dry state. In the second part, we expanded our studies into interfaces formed by a range of surfaces with different chemistries and different 2'-

deoxycytidine-based gelators to demonstrate that different chemical functionalities can affect the structural associations of gelator molecules into first order (unit fibres) and higher order (fibre bundles) structures in the wet state. These investigations on simple interfaces suggest that chemical functionalities can alter the final properties of supramolecular gels highlighting the need for detailed mechanistic investigations in composite systems of supramolecular gels encapsulating therapeutic molecules for drug delivery applications.

Objectives

Determine the effect that different surface chemical descriptors have on the molecular and supramolecular architectures of thin gel films

First part

- Generate two differently modified surfaces and characterise their properties
- Determine the physical properties (morphology) of the dry gel films (the diameter of the fibres) on the two different surfaces
- Determine the nanomechanical properties of the dry gel films on the two different surfaces

Second part

- Generate a range of different chemistries on surfaces related to the gelators' structure and characterise their properties.
- Generate a range of different theoretically and experimentally determined parameters to describe the different surface chemistries
- Characterise the molecular and supramolecular structures on the gel-surface interface

- Identify the key surface descriptors that directly correlate with the characteristics of the architectures formed

First part

Surface-directed modulation of supramolecular gel properties

Maria Galini Faidra Angelerou [a], Akmal Sabri [a], Rhiannon Creasey [b], Polyxeni Angelerou [c], Maria Marlow [a] and Mischa Zelzer[a,d] *.*

[a.] University of Nottingham, School of Pharmacy, Nottingham NG7 2RD E-mail: pazmem@exmail.nottingham.ac.uk and pazmz@exmail.nottingham.ac.uk

[b.] School of Chemistry, University of Queensland, St Lucia, Australia, 4067

[c.] Delft University of Technology, Delft, School of Civil Engineering, 2628 CD, Delft

[d.] National Physical Laboratory, Teddington, Middlesex, TW11 0LW

Author Contributions

The manuscript was written through contributions of all authors. MGFA and AS have conducted the experimental work. MGFA, MZ, MM and RC have contributed to the design, data interpretation and preparation of the manuscript. PA contributed in the data processing of the AFM nanomechanical characterisation. All authors have given approval to the final version of the manuscript.

3.1.1 Introduction

Supramolecular materials are under intense investigation in many areas such as conducting materials, energy and information storage, tissue engineering, sensors, coatings or catalysis[9, 159-160]due to their ability to self-heal (ability to reform after the application of shear stress that destroys the gel structure), mimic biological functionalities and form structures with precise nano-scale order and interactions.[5]

The functionality and application potential of supramolecular materials is closely linked to their chemical, physical and mechanical properties which in turn are affected by processing conditions and gelation triggers such as concentration, pH, temperature, solvent and enzymes.[77, 92, 191]

Among the factors affecting supramolecular self-assembly, the influence of the surrounding material surface on bulk gel properties has received little attention. The effect of surfaces on the formation of self-assembled monolayers is well established[192] and a recent example demonstrated that the structure of a surface (i.e. graphite) can provide a template for monolayer formation and guide 2D self-assembly of molecules (p-terphenyl-3,5,3'',5''-tetracarboxylic acid)with matching dimensions.[193]

As surfaces can template and influence the self-assembly of monolayers we hypothesised that material surfaces may also have the potential to influence self-assembly of gelators and hence affect the properties of the resulting gels. To date the interplay between surface properties and bulk gelation is poorly understood and existing reports mostly focus on confinement of the self-assembly trigger to the surface. For example, it was shown that self-assembly can be triggered with surface immobilised enzymes to form fibres[194] or electrochemically to form gel films.[195] A direct influence of surface morphology on self-assembly was observed when diphenylalanine was placed in contact with either glass or a microporous mixed cellulose ester membrane, where the gelator formed nanofibres and microvesicles, respectively.[92, 196]

Although the material surface has been recognised to play an important role in the self-assembly process[62] the effect of this interaction on gel properties has not yet

been demonstrated. Here, we report for the first time a direct relation between material surface properties and the physical properties of a gel film formed on the surface (Figure 3.1.1).

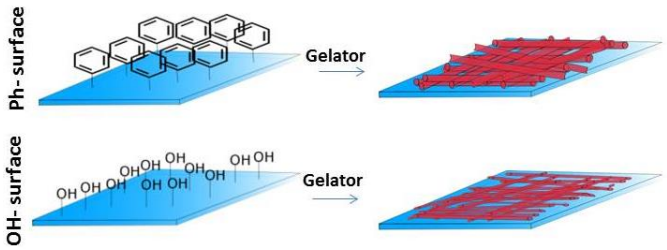

Figure 3.1.1: Schematic of the experimental setup. Two surfaces (left) with different hydrophobicity were used as substrates for gel formation; a very hydrophobic functionalized with phenyl groups (top) and a very hydrophilic functionalized with hydroxyl groups (bottom). After the application of the gelator on the substrate a fibrillar network was formed (right).

3.1.2 Results and Discussion

To investigate the effect of surface properties on physical dry gel characteristics we formed gel films from one recently synthesized cytidine derivative, the N-(1-((2R,4S,5R)-4-hydroxy-5-(hydroxymethyl)tetrahydrofuran-2-yl)-2-oxo-1,2-dihydropyrimidin-4-yl)octanamide) (C14-cytidine)14 on surfaces displaying two different chemical functionalities. The gelator is currently under investigation as a class of drug delivery system with low toxicity[133] and we expect that its amphiphilic nature would enable it to interact differently with surfaces of high or low hydrophobicity.

Piranha cleaned glass was used as a polar surface (WCA measurements gave 24 ± 2°) and silanisation of that glass surface with trimethoxyphenylsilane introduced phenyl groups providing a hydrophobic (WCA measurements gave 82 ± 2°) surface. ToF-SIMS analysis confirmed the presence of phenyl-groups. The linear ion fragments $C_4H_3^+$ and $C_5H_3^+$ have previously been reported as characteristic ToF-SIMS ions from

phenyl-surfaces[197] and their intensity was significantly increased on the surface after silanisation (Figure 3.1.2A), confirming chemical modification of the surface. The topography of the surfaces was measured by AFM (Figure 3.1.2B). The OH- surface was smooth and featureless, while the Ph-surface displayed a structured topography.

Gel films were formed on the two surfaces using the C14-cytidine (Figure 3.1.3A) using an anti-solvent approach ie, dissolving the gelators in ethanol and then adding the ethanol solution to water. The gelator is soluble in ethanol at the required concentration and temperature but insoluble in water. The gelator formed a fibrillar network (Figure 3.1.3B). AFM data (see Figure 3.1.S1 in ESI) showed that on both surfaces the C14-cytidine formed a micrometer thick gel film (1.0 ± 0.2 µm).

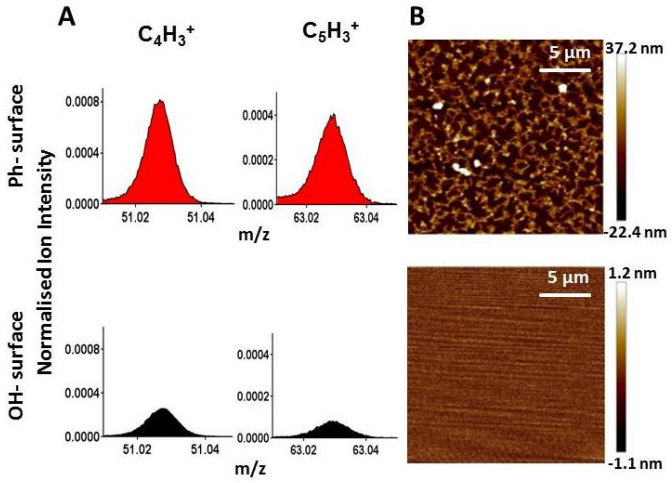

Figure 3.1.2: Surface analysis on the OH- and Ph-surfaces. (A) ToF-SIMS shows the presence of characteristic ions for phenyl groups on the Ph surfaces at m/z = 51 ($C4H3^+$) and m/z = 63 ($C5H3^+$). Spectra were normalised to the total ion counts. (B) AFM images showing different topographies on the OH- and the Ph-surface.

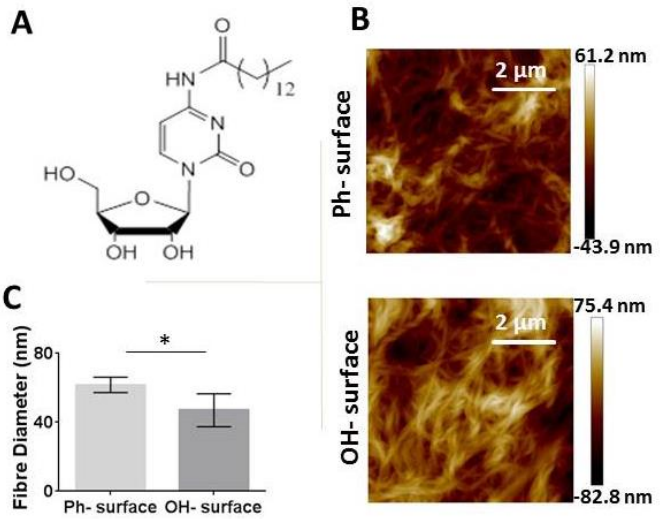

Figure 3.1.3: The structure of C14-cytidine (A). AFM images of the gel structure formed by the two gelators on either the OH- or Ph-surface (B) and significantly different (unpaired t-test, $p < 0.05$) diameters of gel fibres determined from the AFM images (C). N=60 fibres measured on each condition.

In order to evaluate if the gel films are homogeneous over the whole sample, AFM images were taken at extreme points across the sample and the fibre diameters were determined (Figure 3.1.S3 in ESI). The gels' fibre diameters were found to be comparable at various locations on both surfaces, confirming that gelation occurred uniformly over the whole surface.

To establish if surface properties affect the physical and mechanical properties of the self-assembled cytidine gelator, AFM was used to measure the diameter of the self-assembled fibres as well as the Young's modulus of the gel film. When comparing the fibre diameter of both gelators on the two surfaces, significantly larger values were obtained on the Ph- surface (61.7 ± 4.4 nm) than on the OH- surface (47 ± 9 nm) (Figure 3.1.3C). This indicates a different interaction between the gelator molecules and the surface that ultimately leads to differences in the self-assembly pathway and the molecular architecture of the gels. The mechanism behind this is currently unclear and will be subject of future investigations. Preliminary data (SI, Section 3.1.5.4) were also obtained for the fibres in the bulk gel

under the same conditions but showed no significant difference. The extent of the effect of surface along the gel thickness requires further work.

To investigate if the different fibre architectures are accompanied by different mechanical properties in the gel films, the relative mechanical properties (Young's modulus) of gels obtained on the two surfaces were measured via nanoindentation with AFM. Nanoindentation measurements can be used for films as thin as 1 µm[198] and are therefore suitable for the present gel films (thickness: 1.0 ± 0.2 µm).

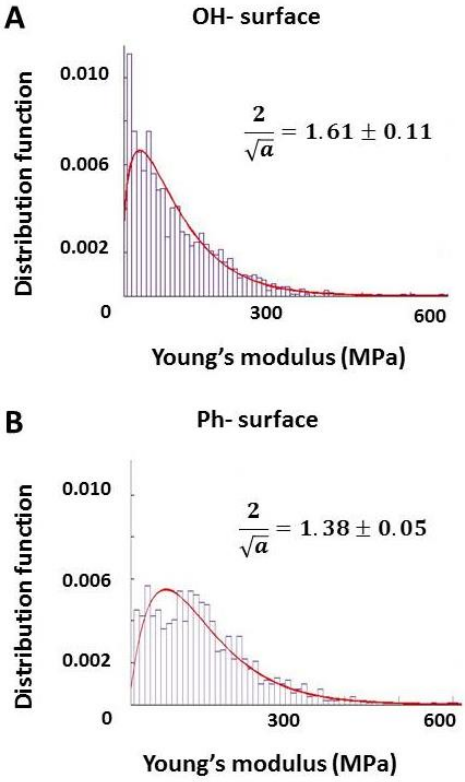

Figure 3.1.4: Histograms of the Young's modulus (determined by AFM) fitted with distribution functions for the C14-cytidine gel films on the OH-surface (A) and the Ph-surface (B).

The data was plotted as histograms and fitted to a gamma distribution (p-value < 0.01). The distributions of the stiffness measurements and the skewness of the

curve fits (α values) are presented in Figure 3.1.4. The Young's moduli measured on both samples are distributed over the same range (10 – 600 MPa). The relatively high Young's moduli (values in the kPa range are typical for solvated gels measured in bulk[199]) can be explained by the fact that these gels have been dried and their mechanical properties measured as thin films on solid substrates rather than bulk conditions. The datasets for each surface were compared through the parameter α which is indicative for the skewness of the distribution. An unpaired t-test (p-value < 0.10) showed that the skewness was significantly different (t=2.696, df=4) on each surface. These results quantitatively demonstrate a distinct difference in the distribution of stiffness values of gel films obtained on different surfaces, indicating that gel films on Ph-surfaces (more hydrophobic and rougher) are stiffer than those on OH-surfaces (more hydrophilic, smoother).

3.1.3 Conclusions

The effect of different surfaces on supramolecular dry gel film properties was investigated and quantified for the first time. We show that the gelator formed dry gels with different fibre diameter and different dry gel stiffness. This demonstrates a direct relationship between surface and gel properties, highlighting the importance of surface properties (different chemistries and presence/absence of topography) in self-assembly and providing new means for control over gel functionality. These investigations were though conducted on dry gel films, obscuring the observation of solely the effect of the surface and not the combination of the effect of surface as well as drying.

3.1.4 Experimetal Methods

3.1.4.1 Materials

13 mm diameter borosilicate microscope cover glasses (Lot: 30473832) were purchased from Marienfeld GmbH and Co KG, Germany.

Sulphuric acid 95-97% w/v BP analytical grade was purchased from Sigma Aldrich (Lot: SZBE2510V). Hydrogen peroxide 100 volumes >30% w/v laboratory reagent grade were purchased from Fisher Chemicals (Lot 1525019). Methanol HPLC grade (Lot 1541331), Acetone HPLC grade (Lot 1413194), Propan-2-ol analytical reagent grade (Lot 1416700), Toluene analytical reagent grade (Lot: 1529541) were purchased from Fischer Chemicals UK. Triethoxyphenylsilane (purity 98%) was purchased from Aldrich Chemistry UK (Lot: #MKBR4637V). All water used was milli Q (18.2 MΩ·cm) ultrapure water.

3.1.4.2 Surface modification

3.1.4.2.1 Preparation of hydroxyl- surfaces

Microscope cover glasses were placed onto a metal rack and were sonicated sequentially in methanol, acetone and propan-2-ol for two minutes in each solvent using Ultrawave Sonicator, Scientific Laboratory Supplies (Lot 37474994). After sonicating, the cover glasses were blow dried using pressurised air. The slides were then treated with piranha solution (3:1 of 97% H_2SO_4 : 30% H_2O_2) for 30 minutes. The cover glasses were rinsed using water and blow dried using pressurized air. The piranha etched vials were prepared in the same way as described above.

3.1.4.2.2 Preparation of phenyl- surfaces

Freshly piranha etched slides were placed in a metal rack and immersed in a 1% v/v triethoxyphenylsilane solution and left to react in an oven at 70°C for one hour. The cover glasses were then rinsed sequentially with toluene, acetone and water and blow dried using pressurised air.

The vials after the piranha cleaning were immersed in a 10% v/v triethoxyphenylsilane in toluene followed by the steps as described before.

3.1.4.3 Gel preparation

3.1.4.3.1 C14-cytidine.

To form the gelator stock solution 2.5 mg C14-cytidine and 150 µl ethanol were added into a glass vial, the solution was sonicated for 2 minutes and then heated at 60°C until the gelator was fully dissolved.

3.1.4.3.2 Gel film formation

The modified glass slides were heated on a heating mantle to 60°C. 9 µl of the hot gelator stock solution (60°C) was pipetted onto the modified glass slides using a micropipette. This was immediately followed by the addition of 21 µl of water (also heated to 60°C beforehand) onto the glass slides. The gel films formed on the surfaces were left to cool to room temperature. The samples were stored in a desiccator overnight.

3.1.4.3.3 Gel formation in vials

The modified glass vials were heated on a heating mantle. 90 µl of the hot gelator stock solution (60^{o}C) was pipetted onto the modified glass slides using a micropipette. This was immediately followed by the addition of 210 µl of water (also heated to 60^{o}C beforehand) . The gel formed were left to cool to room temperature. The samples were stored in a desiccator overnight.

3.1.4.4 Water Contact Angle Measurement

The water contact angle (WCA) measurement for the hydroxyl- and phenyl- glass surfaces were performed on a CAM 200 Optical Contact Angle Meter KSV Instrument LTD using CAM200 software. Water droplets were placed on the surfaces and 20 images were taken in 1 sec intervals. Each image was fitted to the circle model and the resulting right and left contact angles were averaged out. At least three measurements were taken on each sample. The WCA measurements are presented as average ± standard deviation (SD).

3.1.4.5 ToF-SIMS analysis

ToF-SIMS analysis was performed using a ION-TOF TOF-SIMS IV instrument (Münster, Germany). 3 mm x 3 mm raster scans (with 256 x 256 pixels) were obtained using 25 keV Bi_3^+ primary ions with charge compensation. The data was analysed with Surfacelab 6. Positive ion mass spectra were calibrated with m/z 1 (H^+), 15 (CH_3^+), 29 ($C_2H_5^+$), 43 ($C_3H_7^+$) and 57 ($C_4H_9^+$). The analysed areas were divided into four 1.5 mm x 1.5 mm quadrants. For each quadrant, the area under the curve for ions of interest ($C_4H_3^+$ and $C_5H_3^+$) was determined and normalized to the total ion intensities (Table 3.1.S1).

Table 3.1. S1: Intensities of ions characteristic for the phenyl group measured on both the OH- and the Ph-surface.

	Normalised Area			
	$C_4H_3^+$		$C_5H_3^+$	
R.O.I.	Ph- surface	OH- surface	Ph- surface	OH- surface
1	0.0219	0.0065	0.0068	0.0032
2	0.0216	0.007	0.007	0.0034
3	0.0215	0.0073	0.007	0.0036
4	0.0219	0.0076	0.007	0.0038
mean ± SD	0.0217±0.0002	0.0071±0.0004	0.0070±0.0001	0.0035±0.0002

3.1.4.6 AFM imaging

The modified cover glass with and without gels were imaged using a Bruker AFM Probe D300 atomic force microscope in tapping mode (75 kHz, spring constant 3 N/m, cantilever thickness: 3µm, scan rate: 0.5 Hz, target amplitude: 3.0 V). Each image consists of 512 line scans. At least one AFM image was obtained from each of the three repeat samples that were prepared for each gelator/surface combination.

3.1.4.7 AFM nanoindentation

The mechanical properties were measured on an MFP3D Asylum Research Atomic Force Microscope using contact mode and a trigger point of 0.2 mV. A Multi75 Al probe was used with glass bead of a radius of 12.5 µm attached to the cantilever. The spring constant k was experimentally determined as 4.322 N/m and the cantilever resonant frequency 75 kHz. The sensitivity was calculated to be 113 m/V using the InVOLS method where plain clean glass was used as a substrate. The gels were left to dry in a desiccator and were measured within 3 days. For each of the

two different surfaces three samples were prepared and five force maps of 16x16 force curves were acquired on a 25x25 µm area. The force curves were then fitted according to the JKR model and the Young's modulus was calculated using the Asylum Research software (version 13). The values for each sample were batch exported to generate three histograms for each type of surface. Young's modulus values of less than 10 MPa were results of bad curve fits as determined individually and thus excluded from the datasets.

The fitting of each histogram was performed using Matlab R2014a and the goodness of fit was tested using the Kolmogorov – Smirnov test function kstest (level of significance 1%). All six datasets fitted the gamma distribution. To compare the Young's modulus distributions of the datasets, the skewness (α) of the fitted gamma distributions was used and a two-tailed student's unpaired t-test (p-value < 0.10) was performed on the datasets (n=3) and the data are presented in Table 3.1.S2.

Table 3.1.S2: Skewness values (α) for the gamma distributions fitted to the Young's modulus values obtained from C14-cytidine gel films.

	skewness	
sample	**OH- surface**	**Ph- surface**
1	1.72	1.4
2	1.46	1.44
3	1.63	1.31
mean ± SD	1.60 ± 0.11	1.38 ± 0.05

3.1.5 Supplemetary Information

3.1.5.1 Gel thickness measurements

The gel thickness was determined using Atomic Force Microscopy in tapping mode (cantilever resonant frequency of 75 kHz, spring constant of 3 N/m, cantilever

thickness of 3µm and scan rate 0.1 Hz) assessed after scratching the gel in the areas where the force maps were generated with a 21 G needle. Gwyddion 2.41 software was used to analyse the data. On each area a strip with a width of 128 pixels was selected to generate an average line profile. The distance between the cursors was used as the gel height and the measurements were averaged out to determine the thickness of the material (ESI, Figure 3.1.S1). The gel thickness was estimated from nine areas and is displayed as mean ± standard deviation (SD).

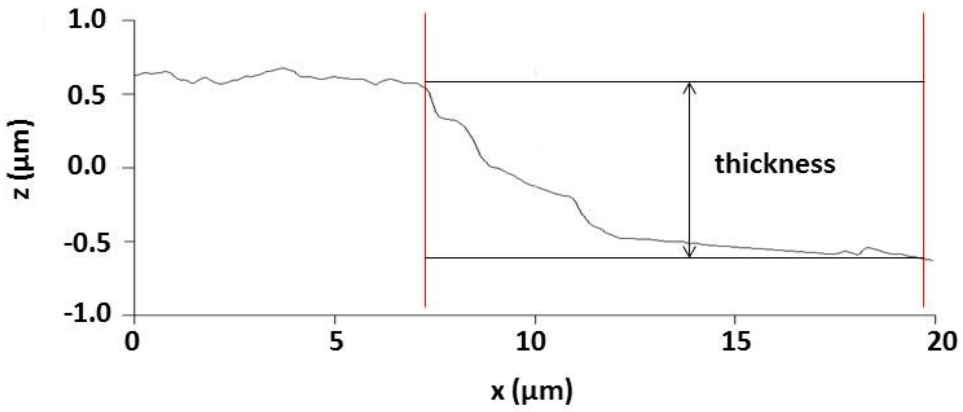

Figure 3.1.S1: Typical line profile of scratched gel films obtained by AFM to measure the thickness of the gel film. The vertical axis (z) represents the height (µm) of the sample and the horizontal axis (x) the horizontal distance (µm).

3.1.5.2 Determination of Fibre Diameter

The fibre diameter was estimated using Nanoscope Analysis 1.5 software by measuring the fibre width presented in Figure 3.1.3 in the main document. Using a flattened by the software image of 2 x 2 µm, a fibre on the gel surface was selected and the cross section was plotted by the software. The cursors were placed as indicated in S. Figure 2 and the distance between the two cursors was measured by the software and reported as fibre diameter. One AFM image was obtained from

each of the three repeat samples that were prepared for each gelator/surface combination. 20 fibres were measured for each image.

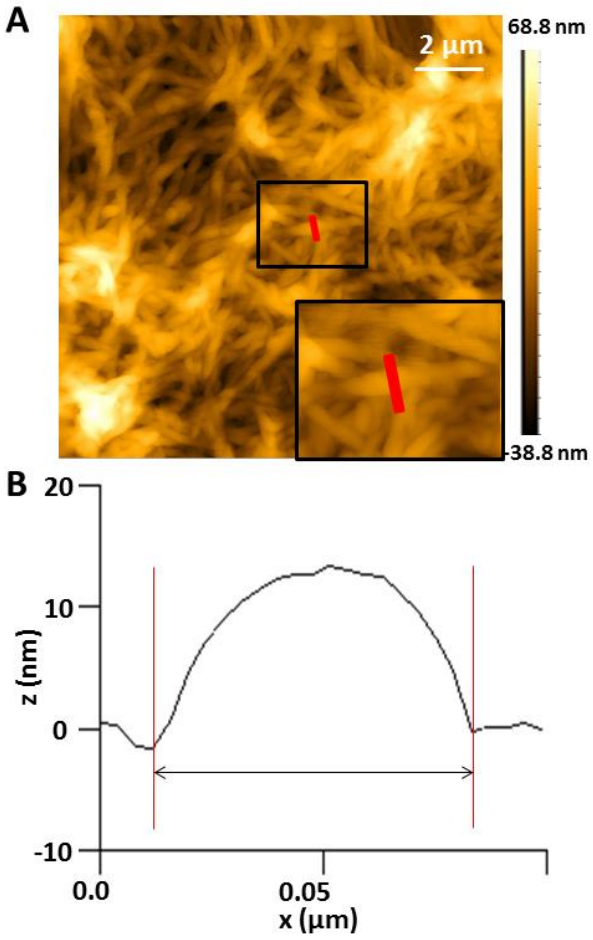

Figure 3.1.S2: Procedure for the determination of the fibre diameters. Lines were drawn across fibres on the AFM images (A) to generate line profiles across the fibre widths (B). The fibre edges were determined and the distance between the fibre endpoints was measured to obtain the fibre diameter. The inset in the image (A) is a magnification of the area framed in black. In the line profil (B) the vertical axis (z) represents the height of the sample and the horizontal axis (x) the horizontal distance. The authors though recommend a more accurate way of measuring the fibre diameter; through the estimation of the distance measured at the Full Width at Half Maximum (GWHM) of the bell-shaped curve, given by the fibre.

3.1.5.3 Gel homogeneity

To determine if the gel fibres are uniform across the whole sample area, AFM images were taken at the edge, the centre and middle between the edge and the centre (midpoint) of the sample (S. Figure 3). The width of 20 gel fibres per sample was measured to determine if fibre diameters vary across the sample. Statistical analysis (One way ANOVA, p-value < 0.05) showed no significant difference.

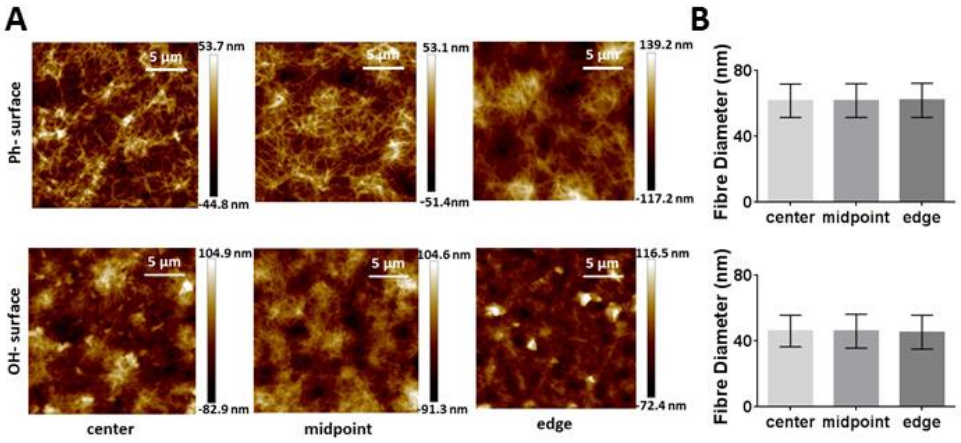

Figure3.1.S3: AFM images (A) and fibre diameters (B) of gel films measured in the centre, at the midpoint and the edge of the gel films.

3.1.5.4 Fibre measurements in bulk gel

Preliminary data were obtained for the fibres in the bulk. The modified vials were prepared and characterised qualitatively by WCA images. Gels were prepared in a piranha etched and a phenyl- silanised vial and left overnight. Gel pieces were removed out of the bulk gel gently and placed on a microsope slide. The samples were left for a day to dry before imaged with AFM in the same way as described before. 6 images were obtained for each condition and 5 fibres were measured on

each one of them. Statistical analysis (One way ANOVA, p-value < 0.05) showed no significant difference.

Second part

Hydrophobicity of surface-immobilised molecules influences architectures formed via interfacial self-assembly of nucleoside-based gelators

Maria Galini Faidra Angelerou,[a] Bin Yang,[a] Tom Arnold,[b,c,d,e] Jonathan Rawle,[b] Maria Marlow[a] and Mischa Zelzer*[a]*

aDepartment of Pharmacy, University of Nottingham, Nottingham, NG2 7RD, United Kingdom. E-mail: maria.marlow@nottingham.ac.uk, mischa.zelzer@nottingham.ac.uk.

bI07 Diamond Light Source Ltd, Harwell Science and Innovation Campus, Didcot, Oxfordshire, OX11 0DE, United Kingdom

cEuropean Spallation Source ERIC, P.O Box 176, SE-221 00 Lund, Sweden

dSTFC, Rutherford Appleton Laboratory, Chilton Didcot, OX11 0QX , UK

Author contributions

The manuscript was written through contributions of all authors. MGFA and BY have conducted the experimental work. MGFA, MZ, MM, TA and JR have contributed to the design, data interpretation and preparation of the manuscript. All authors have given approval to the final version of the manuscript.

3.2.1 Introduction

Supramolecular gels have attracted significant interest as conducting materials, materials for energy and information storage, catalysis and sensors[5-6]and for biological applications in tissue engineering, drug delivery, cell culture and gene therapy.[5, 8-9]A key requirement for the application of supramolecular gels is the fabrication of highly controlled nanoarchitectures that can perform predefined functions.

Surface-mediated self-assembly has recently emerged as a promising new approach to address this challenge as it aims to harness the universal presence of interfaces to influence the outcome of the self-assembly process.[88, 165] Despite its promise, surface-mediated self-assembly has not yet demonstrated its full potential because our understanding of the underpinning relationship between surface properties and gel functionality is very limited. Surface properties such as hydrophilicity, roughness, charge and structure have been implicated in affecting self-assembly of small molecular weight gelators, leading to adaptation of different architectures,[90-91, 93]geometries[92] or mechanical properties[200] of the self-assembled materials. However, currently data is unable to predict surface-supramolecular material property relationships.

To address this lack of mechanistic understanding and enable rational design of interfacial self-assembled structures, two challenges have to be met. Firstly, the structure of self-assembled architectures at interfaces rather than the bulk have to be measured. Here, we employ grazing angle incidence scattering on gel films for the first time to obtain insight in the self-assembled structures formed in a gel film. Secondly, correlations between surface parameters and supramolecular material

properties have to be established. Here, we are correlating the structural data from the gel obtained by grazing incidence scattering with a range of experimental and theoretical descriptors of the surface to elucidate determinants that underpin the control imparted by surfaces on the self-assembly process (Figure 3.2.1).

We hypothesize that the chemical similarity between the gelator and the surface chemistry leads to interference of the surface with the driving forces that underpin the self-assembly. Hydrophobic and solvophobic interactions have been reported as key driving forces in self-assembly.[14, 68, 118, 155-156, 200] Previously, we have shown that an alkyl-modified derivative of cytidine produces gel films with different mechanical properties on a hydrophilic and a hydrophobic surface. [164]AFM measurements showed that the dried gels displayed fibres with larger diameters on the hydrophobic than on the hydrophilic surface.

3.2.2 Results and Discussion

To test the hypothesis that hydrophobic surface interactions play a key role we first needed to establish if altering the

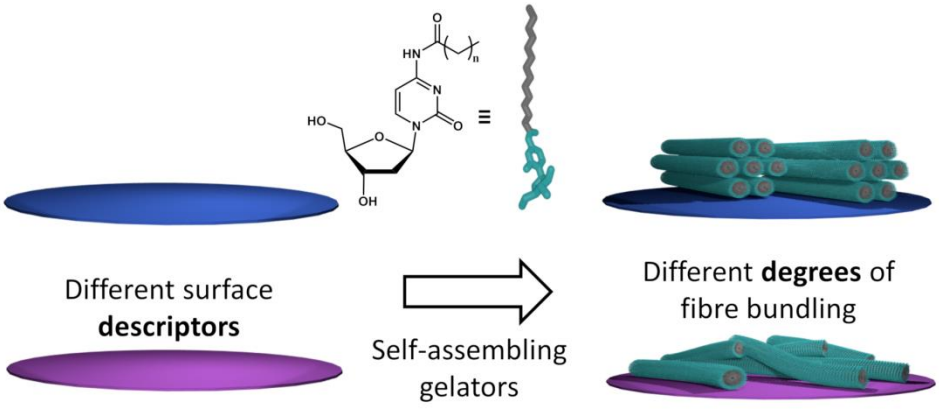

Figure 3.2.1: Conceptual overview of the work investigating the correlations between different surface descriptors and the self-assembly of different 2'-deoxyxytidine-based gelators (The 2'-deoxycytidine moiety is coloured green and the alkyl chain grey).

chemical composition of the hydrophobic alkyl tail in the gelator is directly related to a change in fibre architecture, i.e. a change in fibre diameter. Four derivatives of a 2'-deoxycytidine-based gelator with varying alkyl chain lengths (C8-dCyt, C10-dCyt, C12-dCyt and C14-dCyt with 8, 10, 12 and 14 carbon atoms, respectively, Figure 3.2.S1, SI) were synthesised and used to prepare gel films on piranha cleaned silicon wafers (OH surfaces). The OH surfaces (surfaces covered with hydrophilic hydroxyl groups) were characterized with AFM (Figure 3.2.S2, SI) and water contact angle (WCA) measurements (Table 3.2.S1, SI), showing that the surfaces are very hydrophilic (WCA= 4.7 ± 0.7˚) and smooth (R_q= 1.031 ± 0.167 nm) with no topographical features.

All four gelators self-assemble into fibrous structures (Figure 3.2.S3, SI) and form gel films on the OH surfaces. To determine the structure of the gel, time resolved grazing incidence wide angle X-ray scattering (GIWAXS) data were collected (Figure 3.2.S4, SI). Grazing incidence X-ray scattering is well-established to determine film structures on surfaces;[201-202]here we capitalize on the suitability of our samples to undergo GI X-ray scattering analysis (low surface roughness) to study the interfacial structures of supramolecular gel films for the first time.

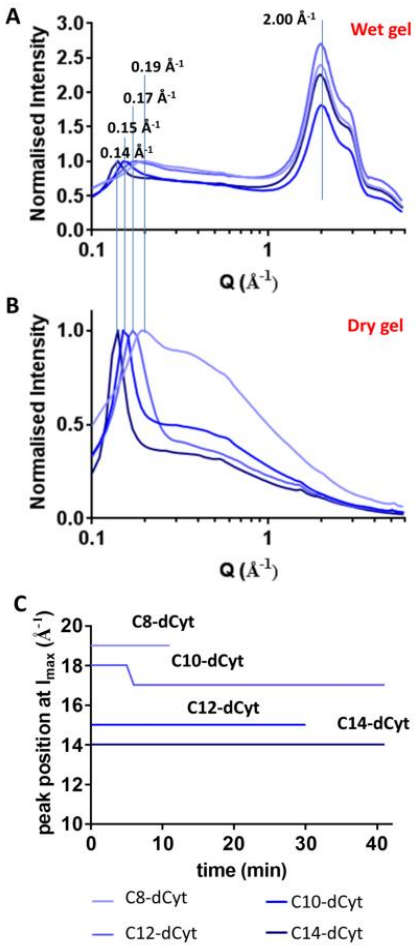

Figure 3.2.2: GIWAXS data of the (A) first (wet sample) and (B) last (dry sample) pattern for all four gelators. Values are normalized to the maximum peak intensity at Q= 0.14 Å^{-1}, 0.15 Å^{-1}, 0.18 Å^{-1} and 0.19 Å^{-1}, for C14-dCyt, C12-dCyt, C10-dCyt and C8-dCyt, respectively. (C) Peak position at maximum intensity as determined from the GIWAXS data is plotted over time for the four gelators. The peak at 2 Å corresponds to water.

The first GIWAXS pattern (wet sample, Figure 3.2.2A) has a prominent broad peak at 2.00 Å^{-1} with a shoulder at 2.86 Å^{-1} that corresponds to water.[203]Its disappearance over time indicates that drying occurs on all samples. The last pattern (dry sample, Figure 3.2.2B) shows distinct, sharp peaks at low Q at 0.19 Å^{-1} (33.1 Å), 0.17 Å^{-1} (36.9 Å), 0.15 Å^{-1} (41.8 Å) and 0.14 Å^{-1} (44.8 Å) that relate to the unit fibre diameter (the first ordered structural unit formed by the gelator, Table 3.2.S2, SI). Comparison between the first (wet sample) and the last (dry sample) pattern shows the same scattering peaks (a minor shift of 2 Å was only observed for the C10-dCyt gelator)

and indicates that the samples are unaffected by the drying process (Figure 3.2.2C). The maintenance of the peak position and enhanced scattering contrast in air favours the subsequent use of dry gel patterns.

For calculation of the fibre diameter, based on previous work for similar nucleolipid systems that form fibrous (cylindrical) structures[118, 204]a hexagonal packing is assumed (Figure 3.2.S5, SI). The calculated C8-dCyt fibre diameter of 38 Å is in close agreement with molecular dynamics simulations (36 Å) reported previously.[200] Increasing the alkyl chain length of the gelator causes the calculated fibre diameter to increase linearly from 42.6 Å to 48.3 Å and 51.7 Å for C10-dCyt, C12-dCyt and C14d-Cyt, respectively (Figure 3.2.S6, SI). This confirms that the alkyl chain length directly impacts the diameter of the self-assembled fibres.

To investigate the arrangement of molecules inside the fibres, the positions of the peak maxima from the GIWAXS data of the dry gels (Figure 3.2.2B) were identified (Table 3.2.S3, SI). All samples showed peak maxima at similar positions that can be assigned structurally in the same manner (Table 3.2.S3, SI), suggesting that the alkyl chain length does not affect the molecular arrangement within the fibres.

The ability of single fibres to associate with each other and form higher order structures such as helices, ribbons, twists and bundles is well documented.[46, 118, 126, 158]In order to explore association of fibres formed by the four different nucleoside based gelators, we used GISAXS. A typical GISAXS time-resolved pattern is presented in Figure 3.2.S7, SI. In agreement with the GIWAXS data, broad peaks corresponding to the unit fibre diameter develop during drying with maximum intensities at Q=0.19 $Å^{-1}$, 0.170 $Å^{-1}$, 0.15 $Å^{-1}$ and 0.140 $Å^{-1}$ for the C8-dCyt, C10-dCyt, C12-dCyt and C14-dCyt, respectively (Figure 3.2.S8 and 3.2.S9, SI). The first collected pattern (wet gel)

was fitted to a flexible cylinder model as previously reported for the C8-dCyt bulk gel,[164]yielding radii of 59.6 ± 0.7 Å, 53.8 ± 1.6, 50.2 ± 0.3 and 61.5 ± 0.3 Å for the C8-dCyt, C10-dCyt, C12-dCyt and C14-dCyt gels, respectively. The corresponding fibre diameters are significantly larger than the fibre unit diameter reported above, suggesting the formation of higher order structures (fibre bundles). In accordance with previous literature,[87, 180] fibre aggregation due to drying was observed over time on our samples but the effect is not significant at early time-scales (Section 10, SI). Consequently the observed differences in fibre bundle dimensions are related to the different structures of the gelators.

After establishing that the self-assembled structure of the alkyl modified cytidine gelator can be modulated by changing the alkyl chain length we tested the hypothesis that the chemical composition of the surface could exert a similar effect on the self-assembly process. Surfaces were prepared to match specific chemical entities present in the nucleoside gelators; (i) the hydrophobic alkyl chain, (ii) different parts of the nucleoside and (iii) the presence or absence of aromaticity (Figure 3.2.S10, SI).

Surfaces were functionalized with alkyl chains containing 8 or 18 carbons (C8 and C18), ethylamine (EtNH2), deoxycytidine (dCyt), cytidine (Cyt) cyclohexyl (cHex) and benzyl (Benz) groups. Surface modification was confirmed by water contact angle (WCA) measurements (Table 3.2.S1, SI), ToF-SIMS (Figure 3.2.S11 and 3.2.S12, SI) and AFM (Figure 3.2.S2, SI). All surfaces showed no significant topography and very low surface roughness (R_q < 1.2 nm), making them suitable for GI measurements.

Two of the four gelators, the most hydrophobic (C14-dCyt) and the most hydrophilic (C8-dCyt), were selected to investigate their interaction with the different surfaces.

Both gelators self-assemble into fibrous structures (Figure 3.2.S13 and 3.2.S14, SI) and form gels on all surfaces.

GIWAXS data were collected on dry gel films formed on all surfaces (Figure 3.2.3). Only dry films were analysed because the water peak obscures the GIWAXS patterns of wet gels and the peak positions on dry and wet films are comparable. The same peaks present in the GIWAXS patterns of C8-dCyt and C14-dCyt on the OH surface were found on all other surfaces, suggesting that neither the unit fibre nor the orientation of the molecules inside the fibres are affected by these surfaces.

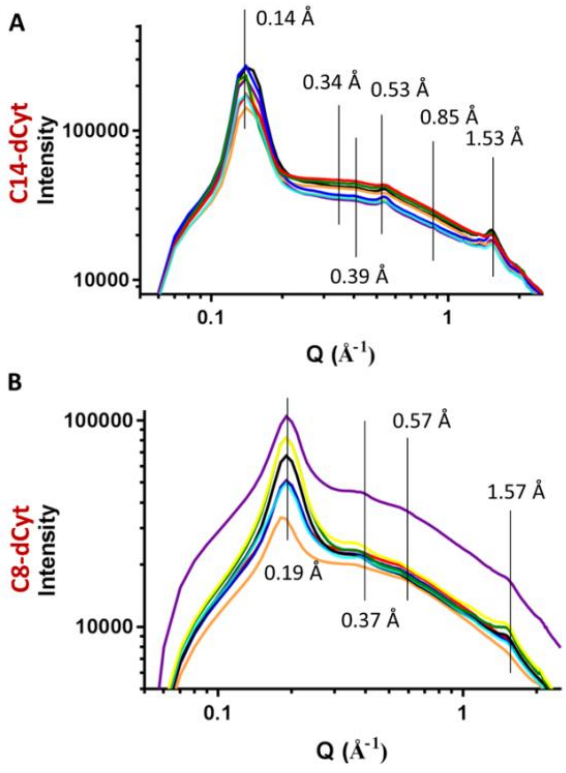

Figure 3.2.3: GIWAXS traces of the dry gels for the two gelators C14-dCyt (A) and C8-dCyt (B) on all the surfaces; cHex (light blue), OH (red), C8 (green), dCyt (blue), Cyt (orange), Benz (purple), C18 (yellow), EtNH2 (black). Peaks are labelled with Q values in $Å^{-1}$.

To investigate the effect of different surfaces on the higher order structures we collected GISAXS patterns. Peak positions at Q= 0.14 $Å^{-1}$ (C14-dCyt) and 0.19 $Å^{-1}$ (C8-dCyt) remained constant during drying, i.e. drying does not change the unit fibre diameter. In contrast, the surface modifications resulted in different fibre bundle radii (Figure 3.2.S15, SI) that cannot be explained by drying effects (Section 10, SI). These fibre bundles were presumably formed by association of individual fibres. This suggests that the effect of the surface is not related to a direct interference in the self-assembly of the gelator molecules. Instead, the surface influences fibre-fibre aggregation which subsequently leads to the formation of thicker fibre bundles.

To exploit surface-mediated self-assembly in the rational design of fibre and gel properties, it is necessary to build a more detailed conceptual understanding of the underpinning surface-gelator interactions from which design rules can emerge. To identify key surface parameters that underpin the observed effect on fibre bundle aggregation, we expressed the chemistry presented on our surfaces with a range of descriptors and tested for correlation of these parameters with the measured fibre bundle radii.

Structural descriptors (number of rotatable bonds), experimental (WCA, R_q) and theoretical (logP, polar surface area (PSA)) parameters (Table 3.2.S6) were used for linear regression analysis (Table 3.2.S8, SI). PSA and logP correlate linearly with the fibre radii (Figure 3.2.4), as demonstrated in SI, table 3.2.S8. Gels deriving from C14-dCyt showed better correlations with the surface properties compared to gels derived from C8-dCyt. Longer aliphatic chains have previously been reported to lead to more effective packing of molecules.[14, 126]This in turn improves the quality of scattering patterns and likely contributes to a more accurate fibre radii

determination and higher confidence in the correlations for C14-dCyt compared to C8-dCyt.

Higher fibre bundle radii are obtained as PSA increases and logP decreases, i.e. fibre bundle radii are releated to the hydrophobicity of the immobilised molecules. This is contrasted by the lack of correlation between fibre bundle radii and WCA values, which are descriptors of surface hydrophobicity. Unlike PSA and logP that relate to molecular properties, the WCA is a reflection of surface hydrophobicity, which also depends on surface coverage, orientation of immobilised molecules and surface roughness, among other factors. It is therefore likely that the self-assembly process is more sensitive to the nature of the immobilised molecule than the composition of the surface as a whole. The relationship between fibre bundle radii and aromaticity was tested with a t-test ($P<0.05$). The presence of an aromatic ring leads to higher fibre bundle diameters, also supporting the concept that specific chemistries affect fibre bundle formation.

3.2.3 Conclusions

In summary, we used GIWAXS and GISAXS to investigate the interfacial interactions between a class of gelators with different hydrophobicities and surfaces with a range of different chemistries for the first time and determine how these parameters affect the final supramolecular structures formed on the surfaces. We demonstrated that the size of the hydrophobic alkyl chain directly affects gel fibre diameter. In contrast, the chemical nature of the surface did not influence the fibre diameter but affected the aggregation of fibres only for the most hydrophobic gelator, C14-dCyt. This leads to formation of fibre bundles with radii whose size correlates with the hydrophobicity of the surface immobilised molecules (logP, polar

surface area, aromaticity). The fact that the fibre radii do not correlate with experimental descriptors of the overall surface (WCA, R_q) indicates that the chemical nature of the immobilised molecules is more important than the overall surface properties. We believe that identifying the nature of the surface-gelator interactions and the parameters that control them will enable significantly improved design of self-assembly processes and their tailoring to emerging applications in material and life sciences.

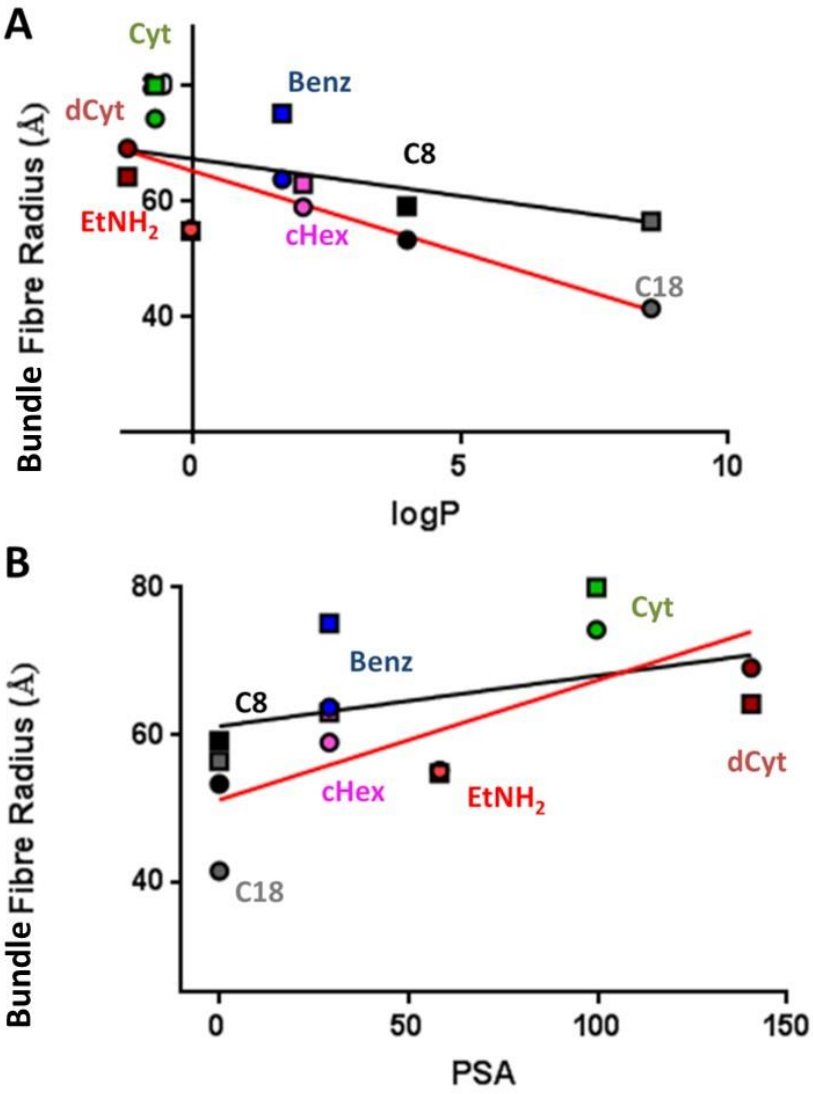

Figure 3.2.4: Linear Regression analysis between bundle fibre radius of both gelators and (A) logP, R2=0.7678 (C14-dCyt, represented by circles and red trace) and R2=0.2087(C8-dCyt, represented by squares and black trace) and PSA R2=0.6181 (C14-dCyt, represented by circles and red trace) and R2=0.1448 (C8-dCyt, represented by squares and black trace). The datapoints are labelled to indicate the respective surface chemistry: alkyl chains containing 8 or 18 carbons (C8 and C18), ethylamine

(EtNH2), deoxy-cytidine (dCyt), cytidine (Cyt) cyclohexyl (cHex) and benzyl (Benz) groups (Figure 3.2.S10, SI).

3.2.4 Experimental methods

3.2.4.1 Materials

2'-Deoxycytidine [lot #SLBN6031, 99% [high-performance liquid chromatography (HPLC)] was purchased from Sigma Aldrich. All the gelators were synthesized according to procedures reported previously.[51] Solvents (HPLC grade) were obtained from Fischer Scientific. Analysis of the gelator was performed by NMR and liquid chromatography−mass spectrometry (LC−MS) (Supporting Information Figures 3.2.S18, 3.2.S19), and purity was determined as >98% (LC−MS). Silicon Wafers - Reclaim Grade P(Boron) (PI-KEM Limited, Product Code: SILI0029W), 4" Diameter,425-550 µm thick, P(Boron), 0-100 ohm cm, Single Side Polished. (3-Aminopropyl)trimethoxysilane, 97% (Alfa Aesar, product code: A1128422)Sulphuric acid 95-97% w/v BP analytical grade was purchased from Sigma Aldrich. Hydrogen peroxide 100 volumes >30% w/v laboratory reagent grade were purchased from Fisher Chemicals. Methanol HPLC grade, Acetone HPLC grade, Propan-2-ol analytical reagent grade, Toluene analytical reagent grade were purchased from Fischer Chemicals UK. water used was milli Q (18.2 MΩ·cm) ultrapure water DIC purum, ≥98.0% (GC) (Sigma-Aldrich, product code: 38370).N,N-Dimethylformamide anhydrous, 99.8% (Sigma-Aldrich, Product code: 227056). Triethylamine, ≥ 99.5% (Sigma-Aldrich, Product code: 471283). n-Octyltrimethoxysilane, 97+% (Alfa Aesar, Product code: 42698). Trimethoxy(octadecyl)silane technical grade, 90% (Sigma Aldrich, Product code: 376213).Succinic anhydride≥99% (GC), (Sigma Aldrich, product code: 239690).Cyclohexanecarboxylic acid, 98% (Product code: 101834). Benzoic acid ACS reagent, ≥99.5% (Product code: 242381)

3.2.4.2 Gel film preparation

The gelators were weighed out in 1.5 ml scintillation vials and ethanol was added to achieve a stock concentration of 25 mg/ml. The vial was transferred on a preheated hotplate at 60 °C and heated up for 2 minutes (complete dissolution). Water was added to achieve a final concentration of 5 mg/ml and the sample was immediately transferred onto a silicon wafer for further analysis.

3.2.4.3 Surface modification

To create the differently modified surfaces, cleaned silicon wafers were used as substrates. The samples were placed in petri dishes and cleaned by sequentially sonicating them for five minutes in methanol, acetone and isopropanol. The substrates were then dried using compressed air and clean, hydrophilic surfaces covered with hydroxyl groups were accomplished via piranha cleaning. 30 ml Piranha solution of 1:3 of H_2O_2/H_2SO_4 was added to a glass petri dish containing the samples and left for 30 minutes. The samples were rinsed with Millipore ultrapure water and dried with compressed air.

The synthetic pathways for all surfaces are presented in Figure **3.2.**S20. Amine terminated surfaces (NH_2) were generated via silanisation of the slides with (3-aminopropyl) trimethoxysilane (APTMS). The slides were incubated in a glass petri dish in 20 ml of a 1 % solution of APTMS in toluene at room temperature for 1 hour, followed by washing with toluene, acetone and Millipore ultrapure water and drying under compressed air.

To immobilise different parts of the nucleoside, amino-terminated surfaces (NH_2) were incubated in a glass petri dish in 15 ml of anhydrous DMF with 1.5 g succinic anhydrite and 20 µl of trimethylamine at room temperature overnight and then

rinsed with DMF, acetone, methanol and water to produce carboxylic acid-terminated surfaces (COOH). In the last step of the modification the carboxylic acid terminated surfaces prepared before were incubated overnight in a glass petridish in 15 ml of DMF and 90 µl of diisopropylcarbodiimide (DIC) with 20 mM of 2'-deoxycytidine (for the deoxycytidine terminated surfaces, dCyt) and ethylamine hydrochloride (ethylamine- terminated surfaces, $EtNH_2$) at room temperature overnight. For the cytosine- terminated surfaces (Cyt), we incubated overnight in a glass petridish in 15 ml of anhydrous DMSO and 90 µl of diisopropylcarbodiimide (DIC) with 20 mM of cytosine at room temperature overnight. For the cyclohexane- and benzene- terminated surfaces, the amino-terminated surfaces were incubated in 15 ml of anhydrous DMSO with 90 µL DIC and 20 mM of cyclohexanoic acid and benzoic acid at room temperature overnight. The different alkyl terminated surfaces were incubated in 25 ml of toluene 5% *n*-octyltrimethoxysilane and *n*-octadecyltrimethoxysilane at 70 ˚C for 1 h. When at room temperature surfaces were shaken on a Heidolph Rotamax 120 Orbital Shaker at 20 rpm for 16 hours. After incubation, the slides were rinsed in the solvent of incubation, methanol, acetone and Millipore water.

3.2.4.4 Surface characterisation

3.2.4.4.1 Water Contact Angle (WCA) measurements

Water contact angle (WCA) measurements were used to monitor changes in surface properties. The WCA was determined with a KSV Cam200 Optical Contact Angle Meter. The Cam200 was set up to record 10 frames at a speed of one frame per second for each droplet. The WCA of the droplet in each frame were then calculated

using the circle fitting method by Cam200. The first two values were excluded and the other eight were averaged. The WCA measurements are presented as average ± standard deviation (SD).

3.2.4.4.2 ToF-SIMS analysis

ToF-SIMS analysis was performed using an ION-TOF TOF-SIMS IV instrument (Münster, Germany). 3 mm x 3 mm raster scans (with 256 x 256 pixels) were obtained using 25 keV Bi_3^+ primary ions with charge compensation. The data was analysed with Surfacelab 6. Positive ion mass spectra were calibrated with m/z 1 (H^+), 15 (CH_3^+), 29 ($C_2H_5^+$), 43 ($C_3H_7^+$) and 57 ($C_4H_9^+$). Spectra were manually analysed and major peaks were identified and assigned to mass fragments by the software algorithm. The analysed areas were divided into four 1.5 mm x 1.5 mm quadrants. For each quadrant, the area under the curve for ions of interest was determined and normalized to the total ion intensities (ESI Table 3.2.S3).

3.2.4.5 Atomic Force Microscopy Imaging

The modified cover glass with and without gels were imaged using a Bruker AFM Probe D300 atomic force microscope in tapping mode (75 kHz, spring constant 3 N/m, cantilever thickness: 3 µm, scan rate: 0.5 Hz, target amplitude: 3.0 V). Each image consists of 512 line scans. At least one AFM image was obtained from each of the three repeat samples that were prepared for each gelator/surface combination.

3.2.4.6 Grazing incidence wide angle X-ray scattering (GIWAXS) and grazing incidence small angle X-ray scattering (GISAXS)

GIWAXS and GISAXS experiments were performed on the I07 beamline, Diamond Light Source,[205] Didcot, UK using a Pilatus P2M detector. Surfaces were aligned and time-resolved GIWAXS experiments were started immediately after spreading of the

solution on the surface using X-rays with an energy of 18 keV and a wavelength of 0.68728 Å to achieve a Q-range of 0.05 $Å^{-1}$ to 5.8 $Å^{-1}$. The sample-detector distance was 30 cm. For time resolved GISAXS experiment, patterns with a Q-range of 0.027-0.6 $Å^{-1}$ were obtained using an X-ray energy of 14.5 keV and a wavelength of 0.85507 Å. The sample-detector distance was 3 m. In both cases the incident angle was 0.08°, just below the critical angle for the substrate and ensuring surface sensitivity. For GIWAXS, 20 µL of warm gelator solution were spread on each surface whereas 10 µL were used for GISAXS. The different sample volumes in the GISAXS experiment were in order to achieve shorter drying times for all the time-resolved data to be collected. Samples were initially aligned before spreading the solution and time-resolved data were recorded directly after the solution was spread. A pattern was collected every two minutes.The first pattern collected from GISAXS data was fitted using SasView-4.1 as explained in the Supplementary Information. Statistical analysis was performed with GraphPad Prism 7 and the outcome is tabulated on SI, Table 3.2.S8.

3.2.5 Supplementary Information

3.2.5.1 Structures of nucleoside-based gelators

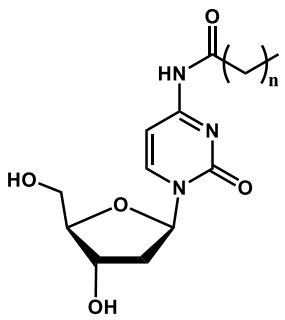

Figure 3.2.S1: Structure of the nucleoside-based gelator with different alkyl chain lengths; C8-dCyt (n=6 carbon atoms), C10-dCyt (n=8 carbon atoms) , C12-dCyt (n=10 carbon atoms) and C14-dCyt (n=12 carbon atoms)).

3.2.5.2 AFM images of all the surfaces

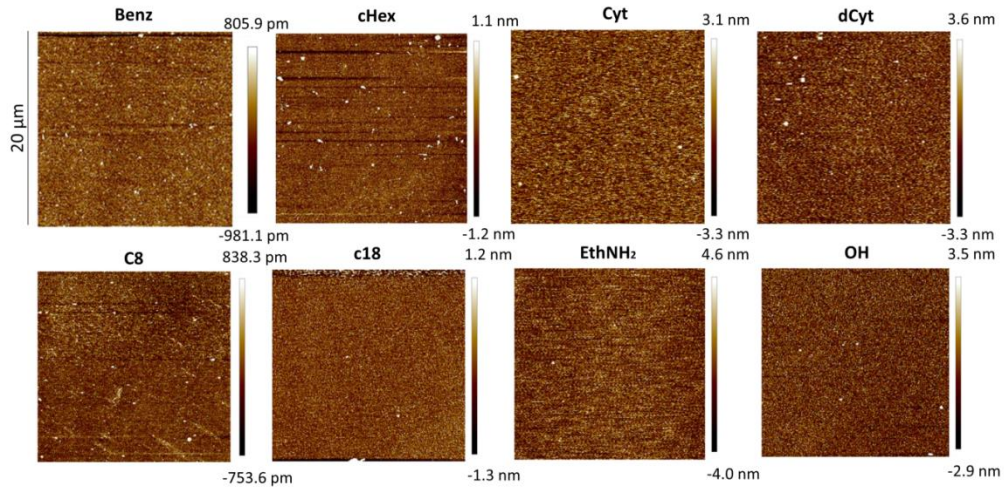

Figure 3.2.S2: AFM images of the differently modified surfaces. Each image represents a square with dimensions of 20 µm x 20 µm. Different surface chemistries; alkyl chains containing 8 or 18 carbons (C8 and C18), ethylamine ($EtNH_2$), deoxy-cytidine (dCyt), cytidine (Cyt) cyclohexyl (cHex) and benzyl (Benz) groups and piranha cleaned (OH).

3.2.5.3 Surface properties

Table 3.2.S1: Values for characteristic properties of different surfaces derived from experimental measurements. Roughness average (R_a) and Root mean square roughness (R_q) were determined experimentally through Atomic Force Microscopy (AFM) images (figure 3.2.S1) and Water Contact Angle(WCA) determined experimentally.

property / surface	R_q (nm)	R_a (nm)	WCA (°)
Benz	0.391 ± 0.093	0.195 ± 0.005	57.6 ± 1.2
cHex	0.676 ± 0.078	0.26 ± 0.021	55.1 ± 1.9
C8	0.346 ± 0.035	0.183 ± 0.006	74.7 ± 1.6
C18	0.306 ± 0.078	0.228 ± 0.064	72.8 ± 2.7
$EtNH_2$	0.904 ± 0.275	0.659 ± 0.303	67.3 ± 6.5
dCyt	1.041 ± 0.092	0.709 ± 0.081	34.5 ± 1.6
Cyt	0.698 ± 0.237	0.548 ± 0.208	35.5 ± 1.2
OH	1.031 ± 0.167	0.717 ± 0.059	4.7 ± 0.7

3.2.5.4 AFM images of xerogels on all the surfaces

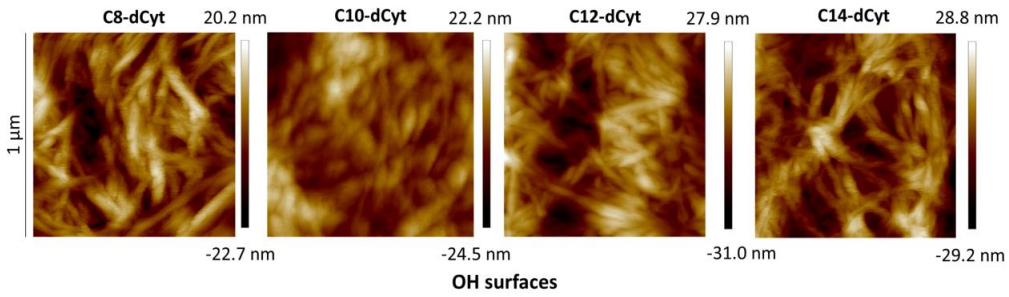

Figure 3.2.S3: AFM images of dry gels on different surfaces; gels formed by four gelators with different alkyl chain lengths on OH surfaces.

3.2.5.5 Time-resolved GIWAXS and GISAXS

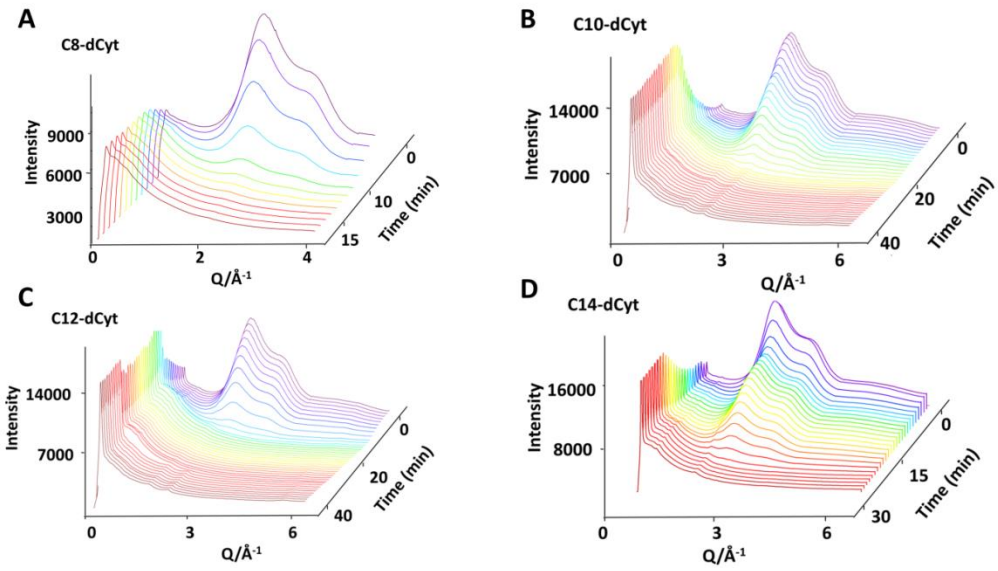

Figure 3.2.S4: Time resolve GIWAXS pattern of gels formed by for four different cytosine based gelators with varying aliphatic chain lengths on clean silicon wafers; (A) C8-dCyt, (B) C10-dCyt, (C) C12-dCyt and (D) C14-dCyt.

Table 3.2.S2: Definitions of fibre unit and fibre bundle as used in this work.

Unit fibre 	First-order cylindrical structure that consists of oriented gelator molecules; the lipophilic alkyl chain of each molecule is towards the core of the fibre whereas the hydrophilic sugar points towards the external surface
Fibre bundle 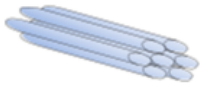	Higher-order cylindrical structures that consists of unit fibres associated together

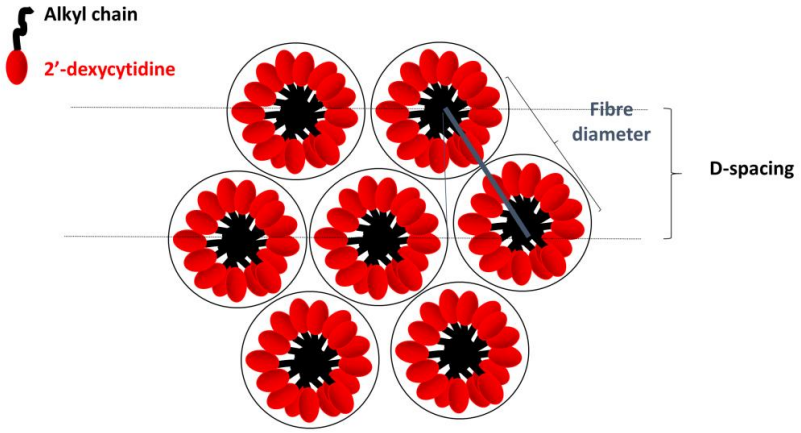

Figure 3.2.S5: Proposed hexagonal packing for unit fibres. D-spacing determined experimentally is presented and the fibre diameter is calculated trigonometrically as proposed.

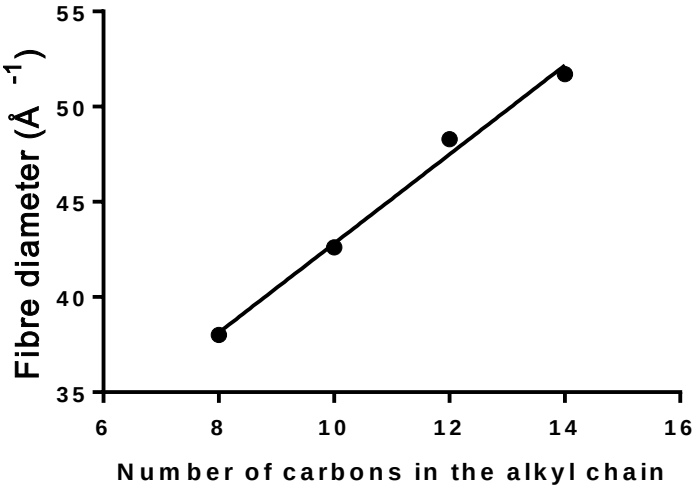

Figure 3.2.S6: Fibre diameter against number of carbons in the alkyl chain (R^2=0.9915). Fibre diameter values were determined through the GIWAXS patterns as explained in Figure 3.2.S5.

Table 3.2.S3: Reflection peaks, Q-ratio, D-spacing and assignments to the fibre structures of thin gel films of the four gelators on piranha cleaned silicon wafers in GIWAXS setup.

Reflection peaks ($Å^{-1}$)	Q ratio	D-spacing ($Å^{-1}$)	Assignment to fiber structures
0.19, 0.38 **(C8-dCyt)** 0.17, 0.35, 0.53, 0.68, 1.07 **(C10-dCyt)** 0.15, 0.3, 0.45, 0.6 **(C12-dCyt)** 0.14, 0.28, 0.42 **(C14-dCyt)**	1:2 1:2:3:4:6 1:2:3:4 1:2:3	33 36.9 41.8 44.8	D-spacing related to the hexagonal packing
0.55 **(for all gelators)**		11.4	D-spacing related to the hexagonal packing
1.53 **(for all gelators)**		4.1	the N-H-O bond spacing of the gelator along the fiber axis or the distance between the stacked nucleobases

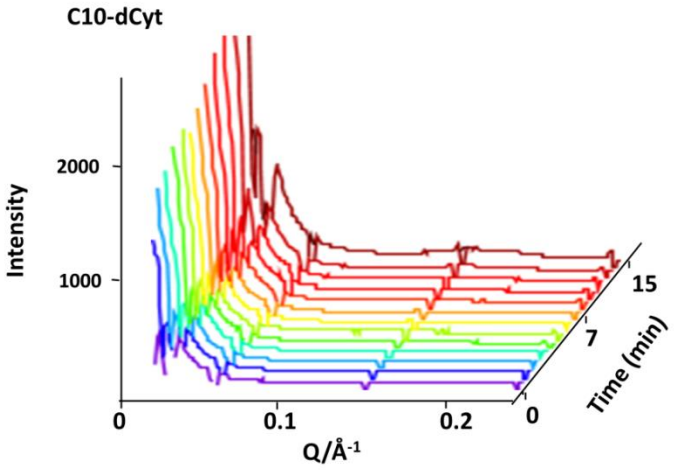

Figure 3.2.S7: Time resolved GISAXS pattern of gels formed by C10-dCyt on a clean silicon wafer. Data points between 0.030 $Å^{-1}$ - 0.048 $Å^{-1}$ and 0.062 $Å^{-1}$ - 0.074 $Å^{-1}$,0.156 $Å^{-1}$ - 0.158 $Å^{-1}$ and 0.246 $Å^{-1}$ - 0.247 $Å^{-1}$ are missing due to masking by the reflective beam-stop and the spaces between the detector plates, respectively.

The ability of single fibers in supramolecular gels to associate with each other and form higher order structures such as helices, ribbons, twists and bundles

is well documented.[14, 46, 118, 158] In order to explore association of fibers formed by the four different nucleoside based gelators, we used GISAXS. An example of a GISAXS time-resolved pattern is presented in SI, Figure 3.2.S7. A broad peak with a maximum intensity approximately at Q=0.19 $Å^{-1}$, 0.170 $Å^{-1}$, 0.15 $Å^{-1}$ and 0.140 $Å^{-1}$ for the C8-dCyt, C10-dCyt, C12-dCyt and C14-dCyt, respectively, develops for all gel samples during drying (SI, Figure 3.2.S8). As presented in SI, Figure 3.2.S9 due to the peak distortion as a result of the 2D detector gaps, the intensity maxima are hard to be accurately determined, there is thought a clear peak shift in agreement with the trend followed in the GIWAXS setup. These peaks correspond to the lowest Q peak observed in the GIWAXS experiment. This confirms that these peaks are not artifacts introduced by the proximity of the beam stopper.

The first collected pattern was fitted according to the model flexible cylinder as previously reported for the C8-dCyt bulk gel.[200] Fitting GISAXS data to a model requires dilute samples[141] that was why the first collected pattern was selected. Grazing Incidence data has been previously fitted to theoretical models to acquire geometrical parameters.[146] The structures of all four gels could be modelled as flexible cylinders with radii of 59.6 ± 0.7 Å, 53.8±1.6, 50.2±0.3 and 61.5±0.3 Å for the C8-dCyt, C10-dCyt, C12-dCyt and C14-dCyt gels, respectively. These radii are considerably larger than the radius of a single fibre formed by the respective gelator, suggesting the presence of fibre bundles as previously reported for the C8-dCyt bulk gel.[200] Aggregation phenomena as previously reported[87, 180] could also be observed as previously reported, as the sample is directly exposed to the environment and drying could start immediately after spreading the sample.

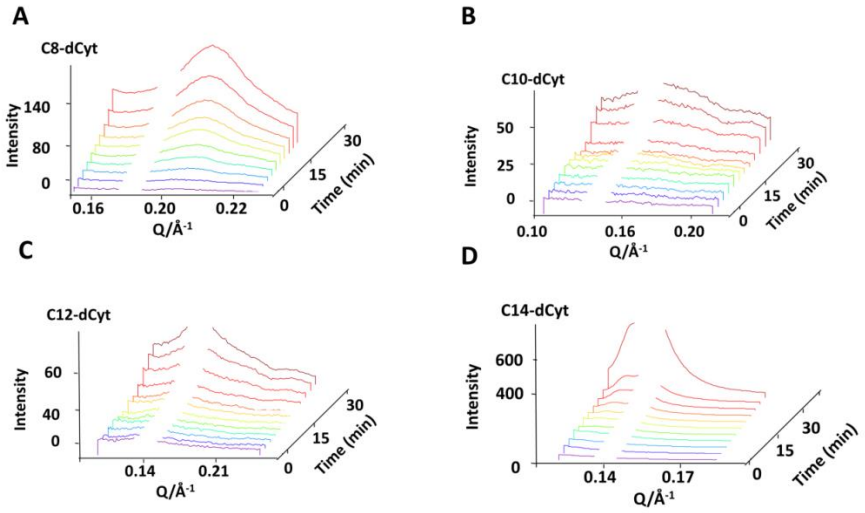

Figure 3.2.S8: Selected Q-range of time resolved GISAXS patterns of gels formed by for four different cytosine based gelators with varying aliphatic chain lengths on clean silicon wafers ; (A) C8-dCyt, (B) C10-dCyt, (C) C12-dCyt and (D) C14-dCyt. Data points between 0.156 $Å^{-1}$ - 0.158 $Å^{-1}$ are missing due to the spaces between the 2D detector plates.

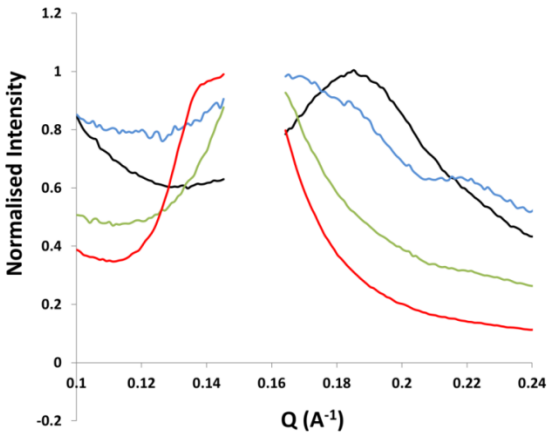

Figure 3.2.S9: Selected Q-range of GISAXS patterns of dry gels (last pattern collected) formed by four different cytosine based gelators with varying aliphatic chain lengths on clean silicon wafers; C14-dCyt (red trace), C12-dCyt (green trace), C10-dCyt (blue trace) and C10-dCyt (black trace). Data points between 0.156 $Å^{-1}$ - 0.158 $Å^{-1}$ are missing due to the spaces between the detector plates on the 2D detector.

3.2.5.6 Different surface chemistries

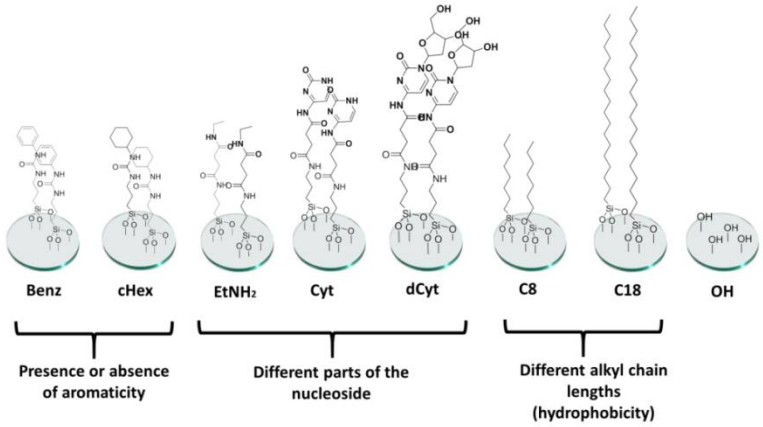

Figure 3.2.S10: Different chemistries developed and characterised on the silicon wafers and labels used for the different surface chemistries. Different surface chemistries; alkyl chains containing 8 or 18 carbons (C8 and C18), ethylamine ($EtNH_2$), deoxy-cytidine (dCyt), cytidine (Cyt) cyclohexyl (cHex) and benzyl (Benz) groups and piranha cleaned (OH).

3.2.5.7 ToF-SIMS Analysis

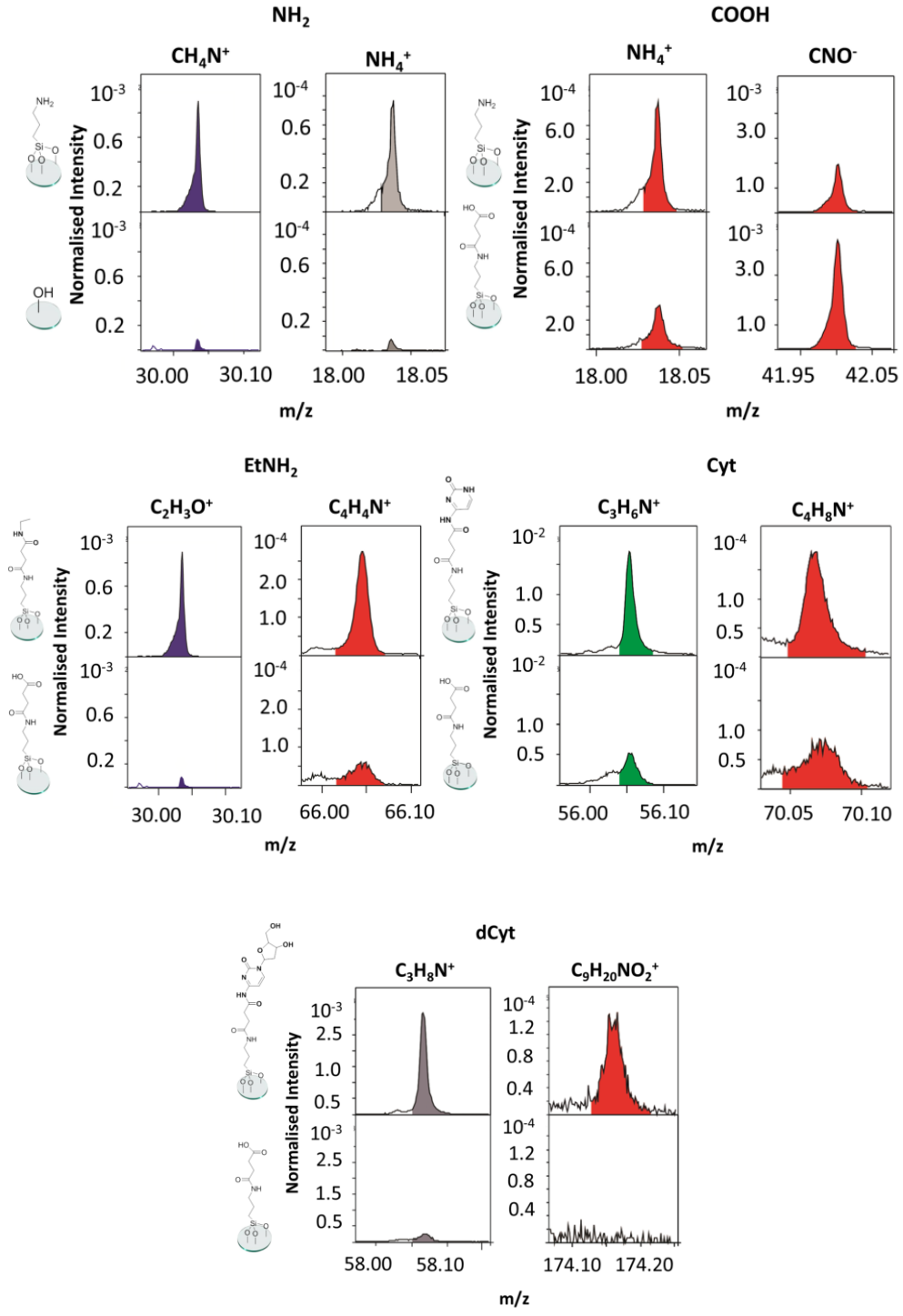

Figure 3.2.S11: Characteristic ions obtained by ToF-SIMS demonstrating the different chemistries on each surface. Two ions indicative for the annotated surface modification before (bottom) and after (top) the last surface modification step are shown for each surface. Surface chemistries of the relevant samples are shown to the left of the spectra. Different surface chemistries; ethylamine ($EtNH_2$), deoxy-cytidine (dCyt), cytidine (Cyt) cyclohexyl (cHex) and benzyl (Benz) groups and piranha cleaned (OH).

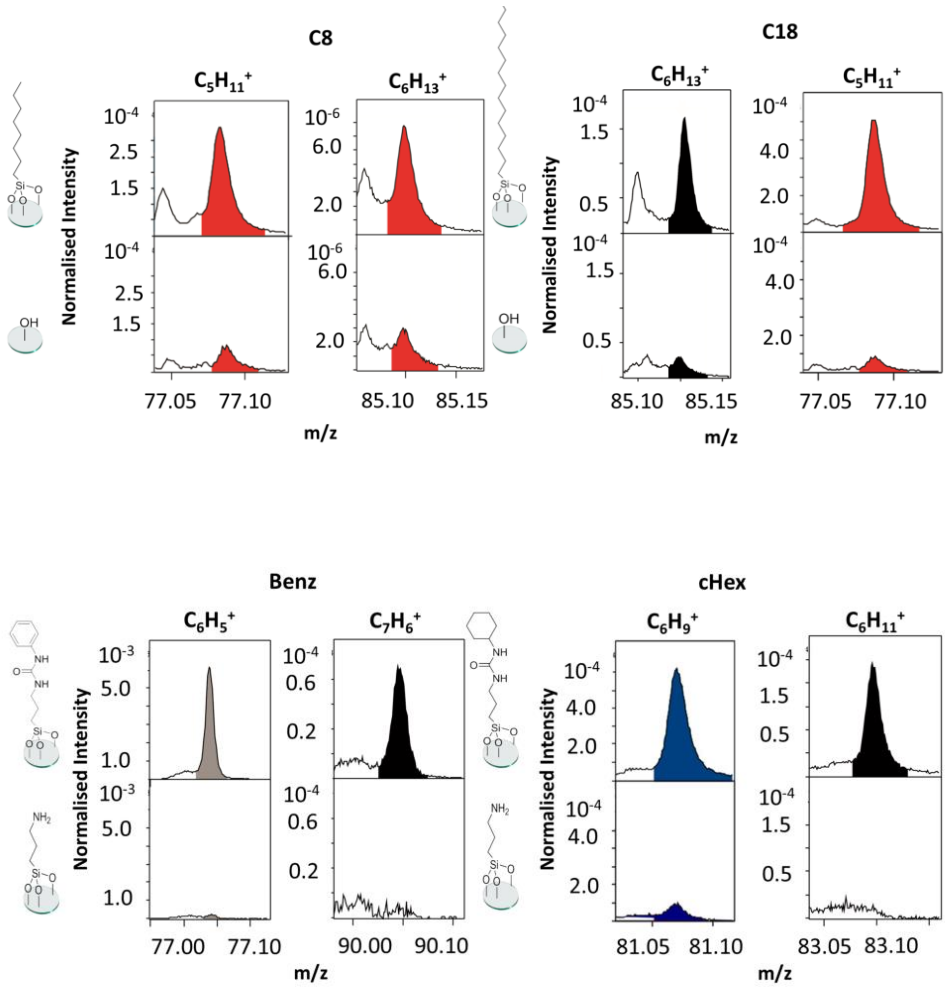

Figure 3.2.S12: Characteristic ions obtained by ToF-SIMS demonstrating the different chemistries on each surface. Two ions indicative for the annotated surface modification before (bottom) and after (top) the last surface modification step are shown for each surface. Surface chemistries of the relevant samples are shown to the left of the spectra. Different surface chemistries; alkyl chains containing 8 or 18 carbons (C8 and C18), cyclohexyl (cHex) and benzyl (Benz) groups and piranha cleaned (OH).

Table 3.2.S4: Ions of interest (Figure 3.2.S11) distribution on four regions of interest (R.O.I.).

NORMALISED INTENSITY FOR IONS (MASS, STANDARD DEVIATION)						
	$C_2O_3^+$ (43.0203, 57.1)		$C_4H_4N^+$ (66.0379, 61.5)		$C_3H_6N^+$ (56.0516,37.1)	
R.O.I.	$EtNH_2$	COOH	$EtNH_2$	COOH	Cyt	COOH
1	3.26E-02	1.58E-02	3.28E-03	1.03E-03	1.98E-02	8.54E-03
2	3.17E-02	1.76E-02	3.42E-03	1.01E-03	1.96E-02	9.06E-03
3	3.78E-02	1.53E-02	3.32E-03	1.31E-03	1.99E-02	7.43E-03
4	3.47E-02	1.87E-02	3.38E-03	1.26E-03	1.98E-02	8.45E-03
mean	0.0342	0.0169	3.40E-03	1.15E-03	1.98E-02	8.37E-03
SD	0.0027	0.0016	6.00E-05	2.00E-04	1.30E-04	6.80E-04
	$C_3H_8N^+$ (58.0672, 35.7)		$H_{20}NO_2^+$ (174.1655,69		$C_4H_8N^+$(70.0654,3.5)	
R.O.I.	dCyt	COOH	dCyt	COOH	Cyt	COOH
1	3.20E-02	4.41E-03	3.07E-04	2.81E-05	3.45E-03	2.04E-03
2	2.92E-02	3.79E-03	2.88E-04	1.10E-05	3.43E-03	2.38E-03
3	3.41E-02	4.84E-03	3.52E-04	2.90E-05	3.52E-03	1.80E-03
4	2.96E-02	4.37E-03	3.07E-04	3.12E-05	3.50E-03	2.13E-03
mean	3.12E-02	4.35E-03	3.13E-04	2.48E-05	3.48E-03	2.09E-03
STD	2.29E-03	4.31E-04	8.00E-05	9.31E-06	4.20E-05	2.40E-04
	CH_4N^+ (30.0331,-25.6)		NH_4^+ (18.0351, 70.7)		NH_4^+(18.0351, 70.7)	
R.O.I.	NH_2	OH	NH_2	OH	COOH	NH_2
1	7.16E-02	8.30E-03	7.08E-03	9.37E-04	0.003491	7.08E-03
2	7.02E-02	6.49E-03	6.68E-03	7.51E-04	0.003344	6.68E-03
3	7.15E-02	8.59E-03	6.72E-03	9.79E-04	0.003594	6.72E-03
4	7.20E-02	4.43E-03	6.62E-03	4.93E-04	0.003489	6.62E-03
mean	7.13E-02	6.95E-03	0.00677	7.90E-04	3.48E-03	6.77E-03
STD	7.80E-04	1.92E-03	0.000206	2.22E-04	1.03E-04	2.06E-04
					CNO- (15.9944, -67.2)	
					COOH	NH_2
					5.08E-02	2.02E-02
					5.10E-02	1.99E-02
					4.90E-02	2.02E-02
					4.97E-02	1.99E-02
					0.050146	2.01E-02
					0.000957	1.60E-04

Table 3.2.S5: Ions of interest (Figure 3.2.S12) distribution on four regions of interest (R.O.I.).

NORMALISED INTENSITY FOR IONS (MASS, STANDARD DEVIATION)						
	$C_5H_{11}^+$ (71.0879,33.1)		$C_6H_{13}^+$ (85.1052,47.2)		$C_7H_6^+$ (90.0464, -0.4)	
R.O.I.	**C18**	**OH**	**C18**	**OH**	**Benz**	**OH**
1	6.49E-03	1.93E-03	2.07E-03	6.11E-04	6.81E-02	1.78E-04
2	6.61E-03	2.87E-03	2.05E-03	8.66E-04	6.50E-02	1.58E-04
3	6.37E-03	1.83E-03	2.04E-03	5.94E-04	7.16E-02	1.50E-04
4	6.52E-03	1.26E-03	2.04E-03	3.90E-04	7.15E-02	1.29E-04
mean	6.50E-03	1.97E-03	0.00197	6.15E-04	6.91E-02	1.54E-04
STD	9.90E-05	6.67E-04	0.000667	1.95E-04	3.15E-03	2.00E-05
	$C_6H_9^+$ (81.0699, 46.8)		$C_7H_5^+$ (89.0372, -15.8)		$C_6H_5^+$ (77.0376,-12.8)	
R.O.I.	**cHex**	**OH**	**cHex**	**OH**	**Benz**	**OH**
1	1.21E-02	1.96E-03	1.11E-03	4.13E-04	6.81E-02	3.96E-03
2	1.20E-02	1.96E-03	1.13E-03	4.06E-04	6.50E-02	3.98E-03
3	1.23E-02	1.80E-03	1.35E-03	3.46E-04	7.16E-02	3.58E-03
4	1.22E-02	1.80E-03	1.08E-03	3.42E-04	7.15E-02	3.53E-03
mean	1.22E-02	1.88E-03	1.17E-03	3.77E-04	6.91E-02	3.76E-03
STD	0.000129	9.24E-05	0.000123	3.8E-05	0.003152	0.000241
	$C_5H_{11}^+$(71.0879,-19)		$C_6H_{13}^+$(85.1052,-11.6)			
R.O.I.	**C8**	**OH**	**C8**	**OH**		
1	5.00E-03	2.54E-03	1.38E-03	3.48E-04		
2	4.68E-03	1.59E-03	1.32E-03	5.16E-04		
3	4.76E-03	1.64E-03	1.31E-03	5.08E-04		
4	3.71E-03	1.14E-03	1.03E-03	7.33E-04		
mean	4.54E-03	1.73E-03	1.26E-03	5.26E-04		
STD	5.72E-04	5.85E-04	1.54E-04	1.58E-04		

3.2.5.8 AFM images of xerogels on all the surfaces

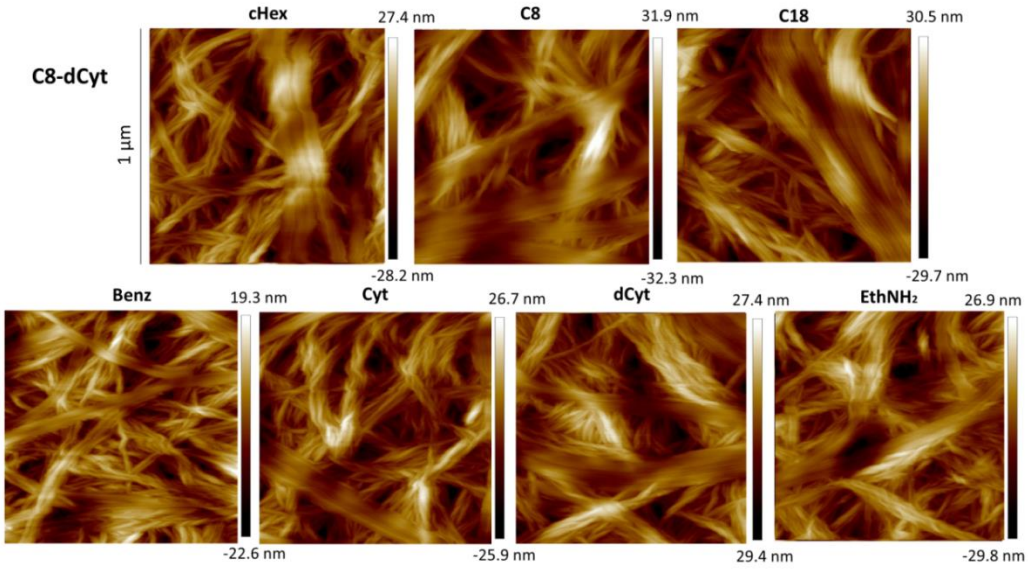

Figure 3.2.S13: AFM images of gels on different surfaces; gels formed by C8-dCyt on surfaces displaying different chemistries. Different surface chemistries; alkyl chains containing 8 or 18 carbons (C8 and C18), ethylamine ($EtNH_2$), deoxy-cytidine (dCyt), cytidine (Cyt) cyclohexyl (cHex) and benzyl (Benz) groups and piranha cleaned (OH).

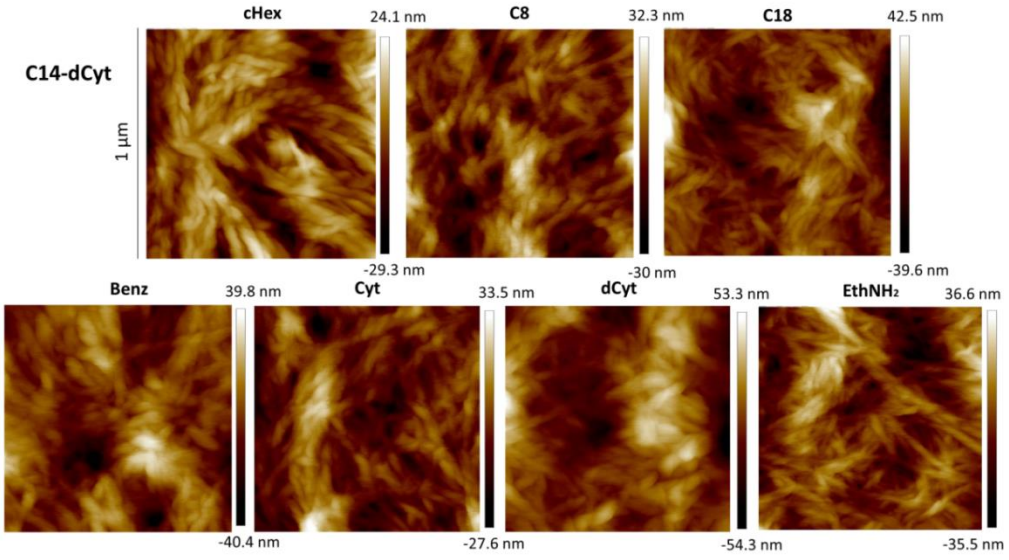

Figure 3.2.S14: AFM images of gels on different surfaces; gels formed by C14-dCyt on surfaces displaying different chemistries. Different surface chemistries; alkyl chains containing 8 or 18 carbons (C8 and C18), ethylamine ($EtNH_2$), deoxy-cytidine (dCyt), cytidine (Cyt) cyclohexyl (cHex) and benzyl (Benz) groups and piranha cleaned (OH).

3.2.5.9 Linear Regression analyses

Table 3.2.S6: Independent variables used in the Linear Regression analyses. As independent variables, measured surface parameters (WCA, R_q), theoretical properties of the immobilized molecules (logP, polarizable surface area, calculated by ChemDraw Professional version 16.0) and structural descriptor (number of rotatable bonds, number of aromatic rings) were used

	INDEPENDENT VARIABLES					
property / surface	logP	R_q (nm)	R_a (nm)	WCA (°)	NRB	PSA
Benz	1.675	0.391±0.093	0.195±0.005	57.6±1.2	4	29.1
cHex	2.064	0.676±0.078	0.26±0.021	55.1±1.9	4	29.1
C8	4	0.346±0.035	0.183±0.006	74.7±1.6	5	0
C18	8.558	0.306±0.078	0.228±0.064	72.8±2.7	15	0
$EtNH_2$	-0.034	0.904±0.275	0.659±0.303	67.3±6.5	8	58.2
dCyt	-1.218	1.041±0.092	0.709±0.081	34.5±1.6	10	140.56
Cyt	-0.7	0.698±0.237	0.548±0.208	35.5±1.2	8	99.66
OH	0	1.031±0.167	0.717±0.059	4.7±0.7	0	31.5

Table 3.2.S7: Dependent variables used in the Linear Regression analyses.

	DEPENDENT VARIABLES	
radius / surface	C14-dcyt	C8-dcyt
Benz	63.768±0.206	75.176±2.5447
cHex	59.008±1.570	63.383±0.11998
C8	55.101±0.44506	59.147±2.7044
C18	41.522±3.4419	56.467±1.348
$EtNH_2$	55.184±3.0752	54.832±0.96758
dCyt	69.127±0.872	64.231±1.6068
Cyt	74.306±0.593	80±0.0000001
OH	61.487±0.30014	59.588±0.654619

Table 3.2.S8: Statistical output including parameters after testing each idependent variable against a dependent one with Linear Regression analysis.

C14-dCyt	logP	WCA	PSA	NRB	R_q
Best-fit values ± SE					
Slope	-2.813 ± 0.6918	-0.2642 ± 0.1341	0.1626 ± 0.05715	-0.8039 ± 0.8424	17.26 ± 11.68
Y-intercept	65.23 ± 2.592	73 ± 7.381	51.19 ± 4.028	65.15 ± 6.726	48.08 ± 8.538
X-intercept	23.19	276.3	-314.8	81.04	-2.785
1/slope	-0.3555	-3.785	6.151	-1.244	0.05792
95% Confidence Intervals					
Slope	-4.591 to -1.035	-0.5923 to 0.06394	0.01566 to 0.3095	-2.865 to 1.257	-11.32 to 45.85
Y-intercept	58.57 to 71.9	54.94 to 91.06	40.83 to 61.54	48.69 to 81.6	27.19 to 68.97
X-intercept	14.85 to 59.67	149.7 to +infinity	-3749 to -138.3	27.28 to +infinity	-infinity to -0.6093
Goodness of Fit					
R square	0.7678	0.3928	0.6181	0.1318	0.2669
Sy.x	5.742	8.497	7.364	10.16	9.337
Is slope significantly non-zero?					
F	16.53	3.881	8.092	0.9108	2.184
DFn, DFd	1, 5	1, 6	1, 5	1, 6	1, 6
P value	0.0097	0.0963	0.0361	0.3768	0.1899
Deviation from zero?	Significant	Not Significant	Significant	Not Significant	Not Significant
Equation	Y = -2.813*X + 65.23	Y = -0.2642*X + 73	Y = 0.1626*X + 51.19	Y = -0.8039*X + 65.15	Y = 17.26*X + 48.08

C8-dCyt	logP	WCA	PSA	NRB	R_q
Best-fit values ± SE					
Slope	-1.282 ± 1.117	-0.1012 ± 0.1476	0.06881 ± 0.07479	-0.2926 ± 0.7961	-3.156 ± 12.08
Y-intercept	67.32 ± 4.185	69.14 ± 8.123	61.19 ± 5.271	66.03 ± 6.356	66.18 ± 8.83
X-intercept	52.49	683.4	-889.3	225.7	20.97
1/slope	-0.7798	-9.884	14.53	-3.418	-0.3169
95% Confidence Intervals					
Slope	-4.154 to 1.589	-0.4623 to 0.2599	-0.1235 to 0.2611	-2.241 to 1.655	-32.71 to 26.4
Y-intercept	56.56 to 78.08	49.27 to 89.02	47.64 to 74.74	50.48 to 81.58	44.58 to 87.79
X-intercept	17.41 to +infinity	187.4 to +infinity	-infinity to -193.3	35.06 to +infinity	2.614 to +infinity
Goodness of Fit					
R square	0.2087	0.07265	0.1448	0.02201	0.01125
Sy.x	9.27	9.351	9.637	9.603	9.656
Is slope significantly non-zero?					
F	1.318	0.47	0.8464	0.135	0.06825
DFn, DFd	1, 5	1, 6	1, 5	1, 6	1, 6
P value	0.3028	0.5186	0.3998	0.7259	0.8026
Deviation from zero?	Not Significant	Not Significant	Not Significant	Not Significant	Not Significant
Equation	Y = -1.282*X + 67.32	Y = -0.1012*X + 69.14	Y = 0.06881*X + 61.19	Y = -0.2926*X + 66.03	Y = -3.156*X + 66.18

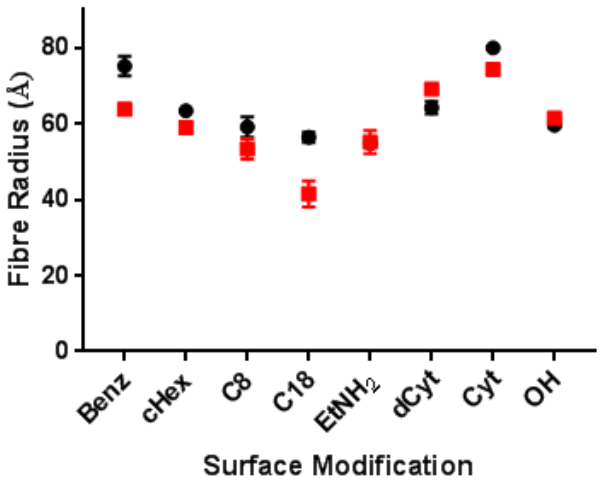

Figure 3.2.S15: Fibre radii of wet gels on two gelators (black squares (C8-dCyt) red circles (C14-dCyt)) prepared on surfaces with different chemical functionalities obtained from GISAXS data (fitting error is presented for each data point). To compare between the two gelators, Tukey's multiple comparisons test ($P < 0.05$) was performed and no significant difference was observed. Different surface chemistries; alkyl chains containing 8 or 18 carbons (C8 and C18), ethylamine ($EtNH_2$), deoxy-cytidine (dCyt), cytidine (Cyt) cyclohexyl (cHex) and benzyl (Benz) groups and piranha cleaned (OH).

3.2.5.10 Effect of sample drying in data collection and interpretation

Drying has been previously reported to induce fibre aggregation for some gelators,[180] and can contribute the orientation and alignment of gel fibres.[206] Hence the possibility of the presence of drying effects have to be considered in the interpretation of the present data.

The Grazing Incidence geometry used here was operated with an incident angle of 0.08°. This angle is just below the critical angle for the substrate and ensures surface sensitivity. Consequently, the measurements took place on the gel-surface interface rather than the gel-air interface, making the data less susceptible to drying

processes that occur at the gel-air interface. To minimise the time between gel application on the surface and the start of the measurement, beam alignment was performed before depositing the gel on the surface and measurements were initiated immediately after gel deposition and collection time for each pattern was 2 seconds, allowing rapid acquisition of the first pattern before drying effects can be established. Higher-order fibre association was then assessed using the first pattern of the time-resolved experiment which corresponds to a wet sample with minimal to no drying effects.

To experimentally demonstrate that drying effects are negligible in the first time-resolved pattern, fibre bundle radii of from the first pattern of gels prepared on piranha cleaned surfaces were compared with those determined for the second pattern (2 minute time interval). Pirhana cleaned surfaces are significantly more hydrophilic than all the other surfaces and the warm solution of the hydrophilic gelator spreads more compared to the rest of the surfaces, resulting in increased surface area exposed to air and thus increased and faster drying effects.

The radii acquired for were; 59.588 ± 0.654619 Å (0 min) and 60.363 ± 0.19862 Å (2 min) for C8-dCyt and 61.487 ± 0.30014 Å (0 min) and 61.302 ± 0.14393 Å (2 min) for C14-dCyt (fitting parameters are presented in Table 3.2.S10). This demonstrate that the fitted radii did not change within the course of the two first minutes and drying effects are negligible when the first time-resolved patterns are compared. Drying effects can therefore not explain differences in the first patterns observed between samples.

3.2.5.11 Fitting approach GISAXS

The first pattern collected from GISAXS data was fitted using SasView-4.1 to the Kratky-Porod flexible cylinder model (Figure 3.2.S16) and an example fitting is presented in Figure 3.2.S17.[207-208] SAXS in the GI geometry have been previously fitted as reported in the literature using theoretical models.[146]

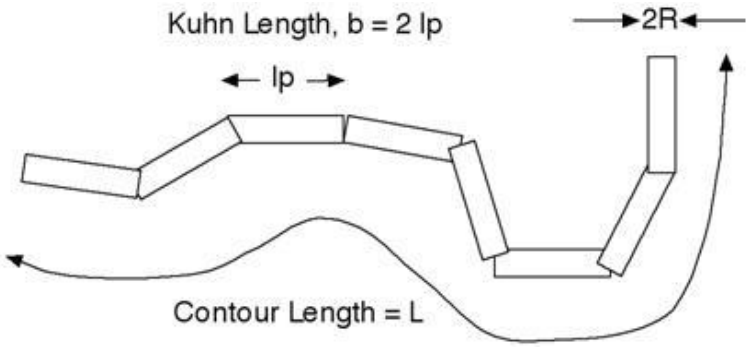

Figure 3.2.S16: Schematic representation of Kratky-Porod flexible cylinder model used as a fitting model for the GISAXS data.

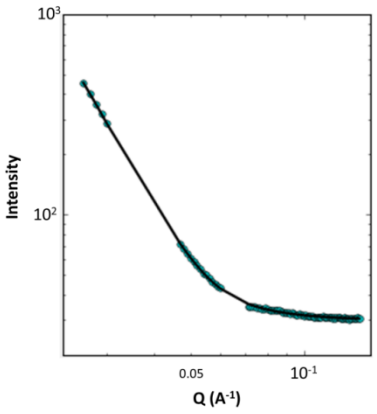

Figure 3.2.S17: Representative GISAXS pattern of wet C8-dCyt gel on OH surface, the solid line on the pattern is a fit to the data with a Kratky-Porod flexible cylinder model. Data points between 0.030 $Å^{-1}$ -

0.048 $Å^{-1}$ and 0.062 $Å^{-1}$ - 0.074 $Å^{-1}$ are missing due to masking by the reflective beam-stop and the spaces between the detector plates, respectively.

Table 3.2.S9: The model fit parameters generated by fitting the GISAXS pattern of gels formed on the different surfaces with a Kratky-Porod flexible cylinder model in the SasView-4.1 analysis package.

Gelator	C8-dCyt	C10-dCyt	C12-dCyt	C14-dCyt
	OH	OH	OH	OH
Scale	5.9825±0.095376	2.0175±0.0093582	1.8541±0.015445	10.817±0.050224
Background	29.832	20.947	27	33
Length	1.2335E+32±3.5738E+33	507.69±32.474	3.79E+15±6.58E+15	1.32E+05±6.78E+04
Kuhn length	98.193±0.6364	131.31±1.5796	98.982±1.2874	134.63±4.2096
Radius	59.588±0.654619	53.829±1.6456	50.206±0.29695	61.487±0.30014
Schulz distribution of radius	0.29679±0.022256	0.89783±0.0073768	0.000001439±0.0036674	0.46187±0.0013729
Chi^2/Npts	0.13	1.12	3.5	1.87

Table 3.2.S10: The model fit parameters generated by fitting the GISAXS pattern of gels formed on the different surfaces with a Kratky-Porod flexible cylinder model in the SasView-4.1 analysis package.

Gelator	C14-dCyt				
	Benz	cHex	dCyt	Cyt	EtNH2
Scale	13.245±0.064	2.052±0.396	5.272±0.024	2.057±0.011	1.7257±0.096
Background	37.231	42.562	37.33	41.45	23.038
Length	33650±8040	1.40E+14±6.65E+14	8.10E+41±7.68E+41	1.55E+44±1.61E+44	7.50E+24±1.00E+08
Kuhn length	63.443±2.160	105.36±8.09	111.06±1.1449	116.17±1.2031	112±7.3625
Radius	**63.768±0.206**	**59.008±1.570**	**69.127±0.872**	**74.306±0.593**	**55.184±3.0752**
Schulz distribution of radius	0.382±0.005	0.267±0.042	0.600±0.005	0.365±0.005	0.35756±0.0419
Chi^2/Npts	0.3	0.7	0.3	0.4	0.05
Gelator	C14-dCyt			C8-dCyt	
	C8	C18	OH	C8	C18
Scale	2.5396±0.011745	1.0761±0.14233	10.817±0.050224	5.8076±0.20967	4.3451±0.48517
Background	43.669	48.47	33	33.54	26.986
Length	5.47E+35±4.69E+35	4.01E+02±5.29E+03	1.32E+05±6.78E+04	8.17E+10±1.00E+08	5.67E+20±1.58E+22
Kuhn length	75.939±0.50502	100.37±15.404	134.63±4.2096	53.808±4.2126	102.62±6.2522
Radius	**55.101±0.44506**	**41.522±3.4419**	**61.487±0.30014**	**59.147±2.7044**	**56.467±1.348**
Schulz distribution of radius	0.20079±0.0066877	0.60371±0.038536	0.46187±0.0013729	0.63497±0.52347	0.041355±0.02275
Chi^2/Npts	1.7	1.2	1.87	0.64	0.013
Gelator	C8-dCyt				
	Benz	cHex	dCyt	Cyt	OH
Scale	15.815±0.76759	13.146±0.54997	11.937±0.37097	15.425±1.004	5.9825±0.095376
Background	32.644	29.783	29.878	31.779	29.832
Length	9.53E+08±1.47E+10	1.10E+22±1.00E+08	3.55E+12±1.00E+08	1.06E+46±2.01E+47	1.2335E+32±3.5738E+33
Kuhn length	117.42±5.3623	101.78±3.5611	107.51±3.6385	107.34±1.5184	98.193±0.6364
Radius	**75.176±2.5447**	**63.383±0.11998**	**64.231±1.6068**	**80±0.00000010937**	**59.588±0.654619**
Schulz distribution of radius	0.38466±0.0045008	0.39587±0.33032	0.37619±0.0063078	0.51276±0.04749	0.29679±0.022256
Chi^2/Npts	7.2	3.5	1.1	4	0.13
Gelator	C8-dCyt				
	$EtNH_2$				
Scale	3.7907±0.1297				
Background	63.463				
Length	5.01E+9±1.00E+08				
Kuhn length	61.807±4.7398				
Radius	**54.832±0.96758**				
Schulz distribution of radius	0.63757±0.041084				
Chi^2/Npts	1.5				

Table 3.2.S11: The model fit parameters generated by fitting the GISAXS pattern of gels formed on the OH surfaces at 0 min and 2 min with a Kratky-Porod flexible cylinder model in the SasView-4.1 analysis package.

Gelator	C14-dCyt - OH surface	
	0 min	**2 min**
Scale	10.817±0.050224	23.736±0.026
Background	33	33
Length	1.32E+05±6.78E+04	2.36E+37±5.57E+36
Kuhn length	134.63±4.2096	112.74±0.477
Radius	**61.487±0.30014**	**61.302±0.144**
Schulz distribution of radius	0.46187±0.0013729	0.42408±0.001
Chi^2/Npts	1.87	3.8
Gelator	C8-dCyt - OH surface	
	0 min	**2 min**
Scale	5.9825±0.095376	8.778±0.02839
Background	29.832	32.14
Length	.2335E+32±3.5738E+3	3.96E+38±3.258E+38
Kuhn length	98.193±0.6364	94.804±1.029
Radius	**59.588±0.654619**	**60.363±0.19862**
Schulz distribution of radius	0.29679±0.022256	0.30879±0.001098
Chi^2/Npts	0.13	1.65

3.2.5.12 Synthesis and characterisation of the gelators

The four different gelators were synthesized according to the protocol published before[51] and characterisation data are presented below.

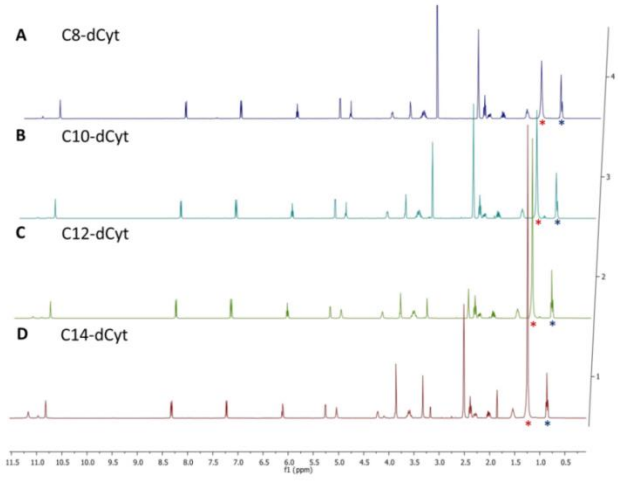

Figure 3.2.S18: 1H NMR traces for the four different gelators, demonstrating the similarity in the structures of the four molecules. The peak intensities are normalised to the peak at δ 0.86 (3H, CH3) of C8-dCyt (blue asterisk) confirming the difference in the alkyl chain lengths when compared to the peak at δ~1.25 (CH2-(CH2)x-CH3) with x = 20 hydrogen atoms for C14-dCyt, x=16 for C12-dCyt, x=12 for C10-dCyt and x=8 for C8-dCyt (red asterisk). Spectra have been setoff to demonstrate the difference in the relative intensities. Spectra have been assigned in detail in previously published work.[51]

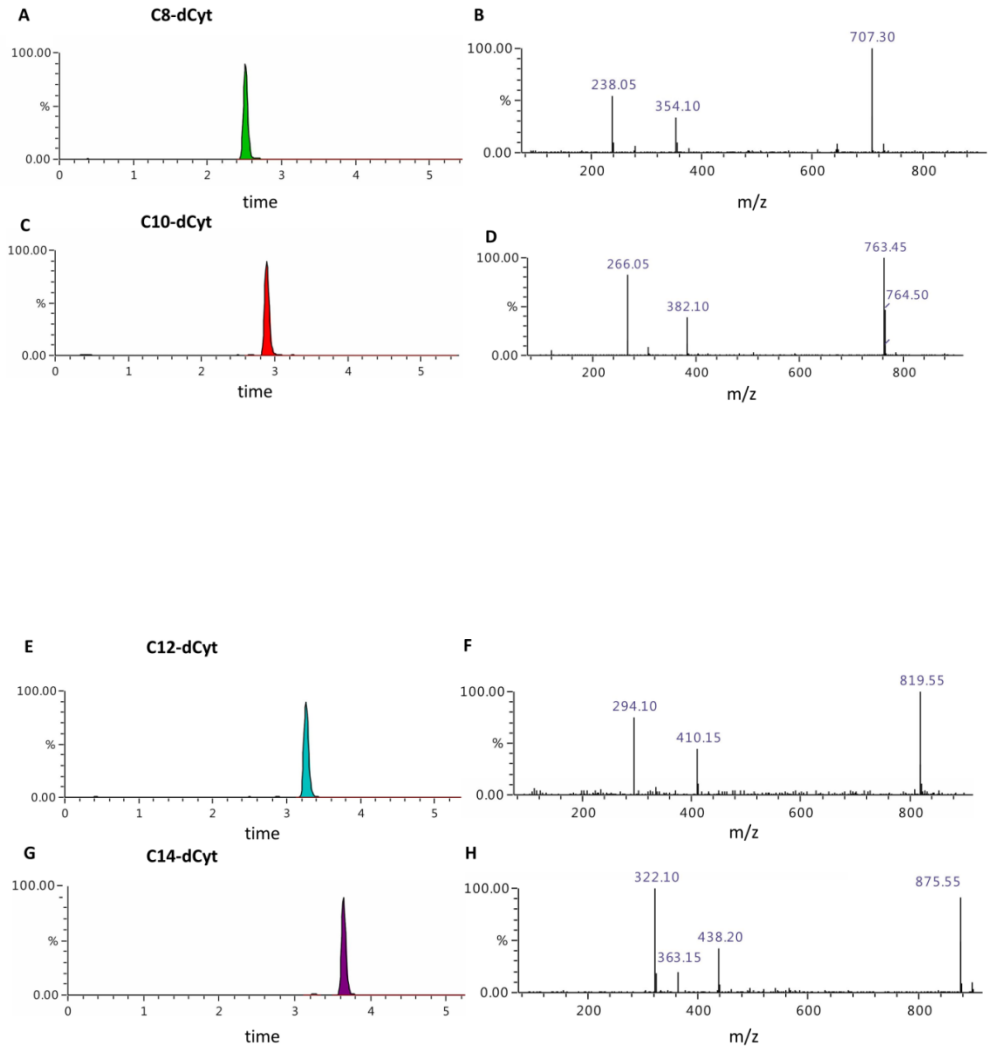

Figure 3.2.S19: LC-MS analysis of different gelators in methanol. Purity determined from the chromatogram as >99% (by height) and >98% (by area) by UV at 254 nm for (A) C8-dCyt, (C) C10-dCyt, (E) C12-dCyt and (G) C14-dCyt. MS (+) spectrum with main ions detected for (B) C8-dCyt at m/z 238.05 [N^4 -octanoylcytosine + H]$^+$, 354.10 [M+H]$^+$ and 707.30 [2M + H] $^+$, (D) C10-dCyt at m/z 266.05 [N^4 -decanoylcytosine + H]$^+$, 382.10 [M+H]$^+$ and 763.45 [2M + H] $^+$,(F) C12-dCyt at m/z 294.10 [N^4 -dodecanoylcytosine + H]$^+$, 410.15 [M+H]$^+$ and 819.55 [2M + H] $^+$, (H) C14-dCyt at m/z 322.10 [N^4 -tetradecanoylcytosine + H]$^+$, 438.20 [M+H]$^+$ and 875.55 [2M + H] $^+$.

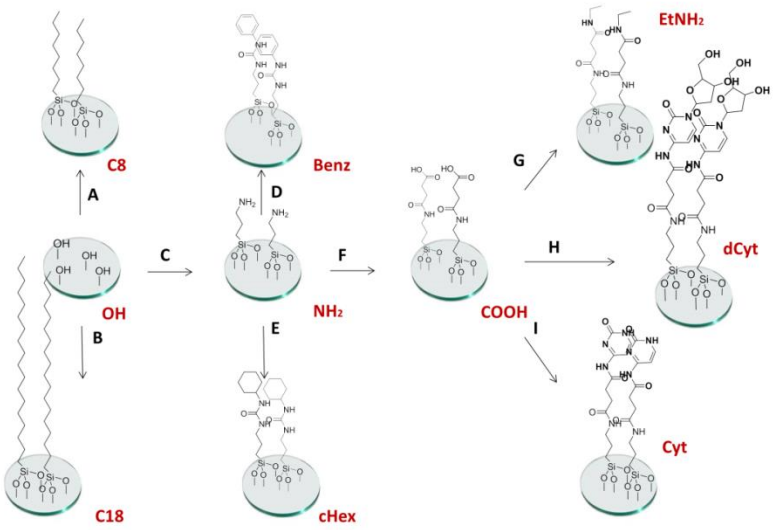

Figure 3.2.S20: Synthetic pathways for the different surfaces. Piranha cleaned surfaces were incubated in 25 ml of toluene 5% v/v (A) n-octyltrimethoxysilane and (B) n-octadecyltrimethoxysilane at 70 ˚C for 1 h. (C) Piranha cleaned surfaces were incubated in 1 % v/v with (3-aminopropyl) trimethoxysilane (APTMS) in toluene at room temperature for 1 h. (F) Amino-terminated surfaces were incubated in 15 ml of anhydrous DMF with 1.5 g succinic anhydrite and 20 µl of trimethylamine at room temperature overnight. In the last step of the modification the surfaces prepared before we incubated overnight in glass petridish in 15 ml of DMF AND 90 µl of diisopropylcarbodiimide (DIC) with 20 mM of (H) 2'-deoxycytidine and (G) ethylamine hydrochloride at room temperature overnight. (I) Carboxy-terminated surfaces in 15 ml of anhydrous DMSO and 90 µl of diisopropylcarbodiimide (DIC) with 20 mM of cytosine at room temperature overnight. For the cyclohexane and benzene- terminated surfaces the amino-terminated surfaces were incubated in 15 ml of anhydrous DMSO with 90 µL DIC and 20 mM of (E) cyclohexanoic acid and (D) benzoic acid at room temperature overnight.

3.3 General Conclusions

In this chapter, we investigated how different chemical functionalities can influence the self-assembly formation. In the first part, thin gel films of N^4-tetradecanoyl-cytidine were formed on two very different surfaces (a very hydrophobic surface functionalised with phenyl groups, and a very hydrophilic one, functionalised with hydroxyl groups) to demonstrate with AFM imaging and AFM nanoindentation measurements that the physical (fibre diameter) and mechanical properties of dry films are significantly different on the two surfaces. The first part of this work demonstrated for the first time that surface chemistry has a direct effect on the physical and mechanical properties of dry thin films of supramolecular gels. The value of the conclusions though was limited by three important factors: (1) only two different surface chemistries were tested, (2) gel films were studied in the dry state and (3) even if the gel thickness was very low (< 1 μm), the air-gel interface was characterised and not the gel-substrate.

In the second part, in order to generate a systematic investigation on the effect that different surface chemistries can have on the self-assembled structures, we expanded the study into gel films of different 2'-deoxycytidine based gelators (with different degrees of hydrophobicity) and surfaces with a range of different chemistries. Acknowledging the limitations of the dry state, gels were studied on the wet state with GISAXS and GIWAXS directly on the gel-substrate interface. Different descriptors of the surface chemical functionalities were generated, determined either experimentally or theoretically, and the key parameters that relate directly to the self-assembled structures formed were identified through linear regression analyses. The logP value and the polar surface area (PSA) of the surfaces were found to linearly relate to the diameter of the fibre bundles of the N^4-tetradecanoyl-2'-

deoxycytidine. This work identified linear correlations between hydrophobic surfaces and lower degrees of fibre bundling and suggests that modulating the hydrophobic forces can provide extra control of the self-assembly. Overall, it was demonstrated that different chemical functionalities can alter the properties of the self-assembled structures suggesting the hypothesis that encapsulated molecules with complex chemistries are likely to interact with the gel and alter its final properties. The effect that different encapsulated molecules can have on this cytidine-based gel will be discussed in Chapter 4.

Chapter 4

Mechanistic insights into the encapsulation and release of small molecules and proteins from a supramolecular nucleoside gel *in vitro* and *in vivo*

Maria Galini Faidra Angelerou,[a] Robert Markus,[b] Vasiliki Paraskevopoulou,[a] Rugerro Foralosso,[a] Philip Clarke,[c] Clara V Alvarez,[d] Miguel Chenlo,[d] Litty Johnson,[a] Catrin Rutland,[e] Stephanie Allen,[a] Christopher Brasnett,[f] Annela Seddon,[f,g] Mischa Zelzer*[a] and Maria Marlow*[a]

[a] *School of Pharmacy, University of Nottingham, UK*

[b] *SLIM Imaging Unit, Faculty of Medicine and Health Sciences, School of Life Sciences, University of Nottingham, Nottingham NG7 2RD, UK*

[c] *School of Medicine, University of Nottingham, Queen's Medical Centre, UK*

[d] *School of Medicine, University of Santiago de Compostela, Spain,*

[e] *School of Veterinary Medicine and Science, Faculty of Medicine, University of Nottingham, Sutton Bonington, UK,*

[f] *HH Wills Physics Laboratory, Tyndall Avenue, University of Bristol, BS8 1TL*

[g] *Bristol Centre for Functional Nanomaterials, HH Wills Physics Laboratory, Tyndall Avenue, University of Bristol, BS8 1TL*

Author contributions

The manuscript was written through contributions of all authors. MGFA performed the experimental work unless stated. MGFA and VP performed the SDS-PAGE analysis. MGFA and RF labelled BSA. MGFA and LJ performed the release studies. CVA and MC designed and conducted the insulin functionality assay. MGFA, AS and

CB conducted the SAXS experiment. CR conducted the histological analysis. MGFA and RM conducted the fluorescence microscopy imaging. MGFA and PC conducted the in vivo study. MGFA, MZ, MM and SA have contributed to the design, data interpretation and preparation of the manuscript. All authors have given approval to the final version of the manuscript.

Abstract

Supramolecular gels have recently emerged as promising biomaterials for the delivery of a wide range of bioactive molecules; from small hydrophobic drugs to large biomolecules such as proteins and nucleic acids. Although they have been widely reported to deliver several different molecules in a controlled way, the mechanism of encapsulation and release remains unknown. In this chapter, we use the nucleoside-based hydrogelator, N^4-octanoyl-2'-deoxycytidine, as a drug delivery system for proteins with different properties and a hydrophobic dye to elucidate *in vitro* and *in vivo* how these materials interact, encapsulate and eventually release bioactive molecules. So far, we demonstrated the mechanistic principles behind this hydrogelator's self-assembly (Chapter 2) and we showed that different chemical functionalities can influence the way nucleoside-based gelators self-assemble and ultimately alter their mechanical properties on simple interfaces (Chapter 3). Here, we hypothesize that in more complicated composite systems of supramolecular gels, the mechanism of encapsulation is based on the direct, non-covalent interactions between the gelator and the different encapsulated molecules, and that their presence significantly affects the properties of the supramolecular gel. We additionally speculate that the different properties of the encapsulated molecules (size, charge, hydrophobicity/hydrophilicity) can diversify their release profiles from the gel *in vitro* and *in vivo*. In order to address these questions, we employ

fluorescence microscopy and spectroscopy as well as Small Angle X-ray scattering, to show that the encapsulated molecules directly interact with the hydrogelator (rather than get physically entrapped in the gel network) and eventually get released as the gel erodes. The ability of these materials to protect proteins against enzymatic degradation is demonstrated here for the first time. Released proteins were proven to be functional *in vitro*. Real-time fluorescence microscopy revealed that the properties of the encapsulated molecules (small hydrophobic dye vs large protein) have a significant effect on their release profile and the degradation profile of the gel itself, results that were confirmed *in vivo*. *In vivo*, the gel was found to completely degrade after two weeks and no signs of inflammation were detected, demonstrating its *in vivo* safety. Ultimately, this study provides a solid demonstration of how bioactive molecules with different properties can significantly impact the supramolecular gel's nano- and macro- properties, establishing the need for mechanistic investigations in order for these materials to reach their maximum potential in the challenging of drug delivery.

Objectives

Determine the mechanism behind the encapsulation and release of molecules with different properties from the supramolecular gel of N^4-octanoyl-2'-deoxycytidine *in vivo* and *in vitro*

- Demonstrate the gel degradation mechanism of the supramolecular gel of N^4-octanoyl-2'-deoxycytidine.
- Demonstrate the encapsulation and release mechanism of model compounds from this supramolecular gel.

- Assess the *in vitro* and *in vivo* performance of the supramolecular gel of N^4-octanoyl-2'-deoxycytidine as a drug delivery system.

4.1 Introduction

Hydrogels for biomedical applications such as tissue engineering and drug delivery are widely reported [209-211]. Hydrogels are traditionally divided into polymeric gels that consist of covalently cross-linked polymer networks and supramolecular gels, consisting of fibrillar networks formed through non-covalent interactions [2]. Recently, supramolecular gels have attracted significant attention in drug delivery, especially in the delivery of biologics [108], where they were shown to present a number of advantages over the polymer based gels; they allow for fine tuning of their properties through several different parameters, they can be self-healing, and they mostly involve mild conditions of gelation that do not compromise the stability of sensitive biopharmaceutical molecules such as proteins and nucleic acids during encapsulation [9, 95-96]. On the other hand, the crosslinking of polymeric gels can involve harsh conditions of gelation such as UV light or low pH to initiate cross-linking or the use of solvents which has been proven detrimental for the functionality of biopharmaceuticals [97].

Bioinspired gelators based on peptides[212] and nucleic acids are popular candidates for drug delivery systems[9, 46] because of their inherent biocompatibility due to their high water content and their self-healing properties [9]. For example Puramatrix®, a self-assembling acetyl-(Arg-Ala-Asp-Ala)$_4$-$CONH_2$ peptide that forms a stable hydrogel after increasing the pH and the ionic strength, has been employed for a broad range of pre-clinical applications and has successfully delivered several biologically-active agents such as proteins (growth factors, cytokines, insulin or

antibodies) and siRNA in pre-clinical *in vivo* studies [109, 111-112]. Peptide-based gels however have been shown to be susceptible to proteolytic enzymatic degradation and chemical modifications are necessary to improve their biostability [80, 213-214]. Nucleoside-based gelators are proposed as a novel alternative modality that would be stable against proteolytic enzymes.

Nucleoside-based gels have recently been introduced as injectable delivery systems that can reform in situ after injection at the site of action [116], delivering different classes of molecules from small therapeutic molecules to macromolecules such as proteins and nucleic acids [83, 117-118]. For example, a guanosine-5'-hydrazide gel was able to encapsulate various pharmacologically active molecules such as acyclovir, vitamin C and vancomycin[119], whereas a 5'-deoxy-5'-iodoguanosine gel was reported to incorporate antivirals [120]. Additionally, Kaplan et al. demonstrated that a thymidine-based mechanoresponsive hydrogel can be used for the delivery of antibodies [117]. A urea based-bolamphiphile was found to avoid the foreign body reaction after *in vivo* injection, demonstrating the ability of these types of gels to be immunocompatible [116]. Ramin et al. reported the sustained release of a small hydrophobic fluorescent dye and a fluorescently labelled protein through a nucleotide lipid containing thymidine and 1,2 –dipalmitoyl-sn-glycerol phosphate paired with different cations with no toxicity *in vivo* [83]. Additionally this hydrogel was shown to protect the integrity of the model protein *in vivo* for a period of a few days compared to the non-formulated protein, successfully demonstrating the potential of these materials. Interestingly, the authors reported that, despite their size, the small hydrophobic molecule was released more slowly compared to the larger, more hydrophilic protein, raising questions over the influence that the properties of the

molecules of interest can have on the encapsulation mechanism and the behaviour of the final formulation.

Due to the dynamic nature of these materials [7], molecules with different properties (molecular weight, charge, hydrophobicity etc.) are expected to interact with the low molecular weight gelator and critically alter the properties of the final gel material. Previously, in a simplified model system, we demonstrated that thin films of a nucleoside-based gelator in contact with surfaces displaying different chemical functionalities adapted different mechanical properties [164]. Here, we postulate that complex interfaces of the gelators with chemically diverse molecules such as proteins could have similar significant effects on the final gel properties and behaviour, regarding the syringeability, self-healing properties, release profile and functionality of the encapsulated molecules and finally the degradation of the gel.

Herein, we use the well-understood, self-healing nucleoside-based hydrogelator N^4-octanoyl-2'-deoxycytidine[51, 200] developed in our group (SI, Figure 4.S1), to encapsulate a broad range of molecules (a small hydrophobic molecule and several proteins) and characterize its performance as a drug delivery system *in vivo* and *in vitro*. This nucleoside-based gelator was previously shown to encapsulate a hydrophobic dye (model molecule for hydrophobic drugs) selectively into the hydrophobic core of the fibres [200]. Here we mechanistically investigate how proteins with different properties associate with the gel nanofibers and, for the first time for a supramolecular gel, we report the detailed mechanism of encapsulation and release of therapeutically relevant molecules and erosion of the gel. After release, we demonstrate that functional proteins (lysozyme and insulin) retain their biological activity *in vitro*. Furthermore, the ability of the gel to improve the stability of a model protein in the presence of proteolytic enzymes compared to the protein

alone is demonstrated for the first time. Finally, the release of a small hydrophobic dye and a fluorescently labeled protein as well as their effect on the gel degradation profile are studied *in vitro* and *in vivo*.

4.2 Results and Discussion

4.2.1 Formation of stable, self-healing gels that release proteins through gel erosion

Proteins are complex macromolecules with a diversity of chemical groups exposed on the surface or buried in their core depending on the nature of the surrounding environment. Two major properties that tend to define their behaviour in solution are their molecular weight (MW) and isoelectric point. In order to investigate the potential of the hydrogel to act as a drug delivery system for the controlled release of different proteins we incorporated four model proteins at the same concentration (SI, Figure 4.S2). Bovine Serum Albumin (BSA), β-lactoglobulin (β-lact) and insulin (ins) are negatively charged at physiological pH (PBS, pH 7.4) but possess different MWs whereas β-lactoglobulin and lysozyme (lys) have similar/comparable MWs but are negatively and positively charged, respectively, at physiological pH. Stable gels were obtained after encapsulation of all proteins, (SI, Figure 4.S3).

This hydrogelator has been previously reported to be self-healing [51]. This is an important condition for the syringeability of the gel and its ability to reform *in situ*. Rheology measurements have been extensively used in the literature to simulate the shear stress during syringing [51, 83, 115-116]. Here we perform time dependent rheology measurements to investigate if the presence of the protein is preventing the ability of the gel to self-heal. The protein containing gels were subjected to alternating strains; 0.2% (1200 sec) where the gel retains its structure and then at 500% strain (30 sec) where the gel structure breaks down and after that a relaxation period

follows (strain 0.2%, 1800 sec) that allows the gel to reform as presented in Figure 4.1A. The ability of the gel samples to reform after disruption of the gel structure was quantitatively evaluated by comparing the mechanical strength recovery ratio of the different gels (storage modulus after gel disruption ratioed by initial storage modulus). The mechanical strength recovery was 84 ± 15% (gel), 71 ± 20% (gel with lysozyme), 80 ± 10% (gel with β-lactoglobulin), 86 ± 10% (gel with BSA) and 84 ± 19% (gel with insulin). Statistical analysis (ANOVA ($P<0.05$), $N = 5$) of each gel with protein as compared to a gel only control showed no significant difference suggesting that the presence of protein is not affecting the ability of the gel to self-heal, an important finding that suggests the syringeability of the gel after protein encapsulation. The effect of the different protein on the gel's stiffness is presented in SI, Figure4.S4, demonstrating that only gel containing insulin has significantly lower stiffness compared to the rest of the gels.

Supramolecular gels have been proven promising materials for the sustained release of drugs [9, 46]. In order to investigate the potential for controlled release of different proteins through this nucleoside-based gel, we performed *in vitro* release studies. Gels with and without the proteins were brought in contact with PBS at 37 °C and samples of the supernatant were taken at different time points. The concentration of the proteins at each time point was determined using the colorimetric Bradford assay, measuring the absorbance at 595 nm[215] and the gelator's concentration was quantified through its UV absorbance at 295 nm (Figure 4.1B). Interestingly, the release profiles of all proteins followed the same trend, regardless of the different proteins' properties, that was the same as the physical degradation profile of the gel. For polymeric gels both diffusion and erosion/degradation have been reported to regulate the release depending on the

formulation [97]. For example, for Pluronic gels encapsulating the therapeutic proteins insulin[216] and IL-2[217], it was demonstrated that gel erosion underpins the release mechanism. To date, for supramolecular gels the protein release mechanisms have been identified as diffusion of the molecule out of the gel [104, 114] whereas gel erosion has not been reported so far. Especially for supramolecular peptide-based gels, it has been previously demonstrated that proteins with different properties mainly diffused through the gel and had different release profiles depending on their properties [115], whereas no data have been reported so far on the release mechanism of nucleoside-based gels. For this nucleoside-based gel, the correlation of the kinetics of the protein release and gel degradation profile as well as the independence of the release profile on the type of the encapsulated protein, strongly suggest that erosion is the main mechanism by which proteins leave the gel. Macroscopic images of the gel eroding over time are presented in SI, Figure 4.S5.

In order to study the gel erosion on the nanoscale, we used Atomic Force Microscopy (AFM). Gels not containing proteins were incubated in PBS at 37 °C and after 4 h incubation samples drawn from the supernatant were imaged with AFM at 37 °C in PBS. Individual fibres were captured floating in the supernatant (Figure 4.1C) demonstrating that intact fibres leave the bulk gel during gel erosion in a biologically relevant environment.

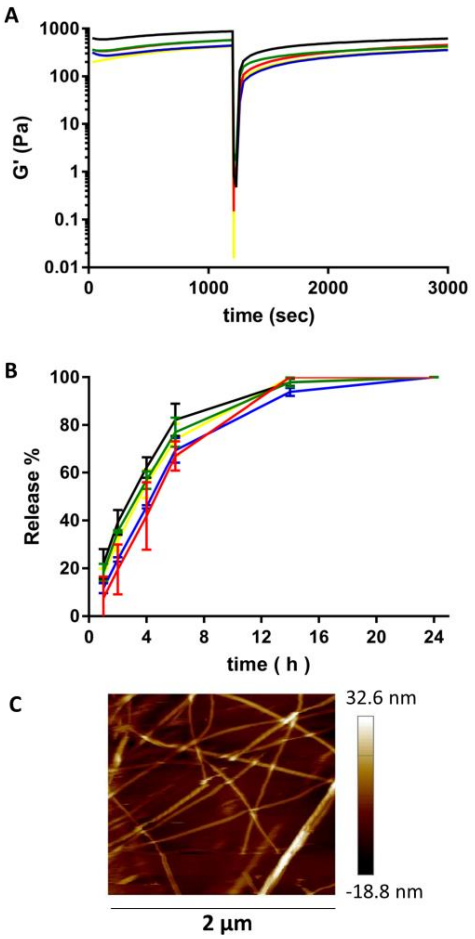

Figure 4.1: Formation of stable, self-healing gels able to deliver different proteins in a sustained way. (A) Oscillatory rheology time recovery data of the protein containing gels; BSA (blue), β-lactoglobulin (red), lysozyme (green), insulin (yellow) and gel alone (black trace). Data were recorded for 1200 sec (γ= 0.2 %) and then the gel was disrupted for 30 sec (γ=500%), the gel was left to reform for 1800 sec (γ= 0.2 %) at 37 °C, ω was maintained constant at 5 rad/s. (B) Release profiles of different proteins from the gel; blue (BSA), β-lactoglobulin (red), lysozyme (green), insulin (yellow) and gel alone (black trace). 0.5 ml of protein containing (30 µM) gel (0.5% w/v) were incubated with 1 ml PBS at 37 °C. The protein concentration was determined at certain time points using a Bradford assay at 595 nm [215]. The gelator concentration was determined at 295 nm. (C) AFM images of gel fibres (gel alone at concentration 0.5% w/v) on mica imaged in the release medium (PBS) after 4 h incubation at 37 °C. 0.5 ml of gel (0.5% w/v) were incubated with 1 ml PBS at 37 °C.

4.2.2 Prevention of protein enzymatic degradation

Proteins are prone to enzymatic degradation in the presence of the various proteolytic enzymes within the tissues [218]. One of the main goals of protein encapsulation in gels is protecting them from enzymatic degradation. To date, it has been extensively suggested but never clearly shown how gels can prevent protein degradation. In this work, in order to investigate if the nucleoside based gel can protect the protein's integrity from enzymatic degradation, we exposed the protein containing gels to two model proteolytic enzymes, α-chymotrypsin[219] and pepsin [220]. These enzymes are encountered in the human body, are readily available and inexpensive. Bovine Serum Albumin was chosen as the model protein due to its relative high molecular weight that would allow for a clear demonstration of the protein breakdown into shorter protein fragments in SDS-PAGE separation.

To demonstrate that after encapsulation in the gel the protein remains intact for longer compared to the protein in solution alone in the presence of enzymes, samples of gels containing proteins (G) and samples of the protein in solution alone (P) were incubated for different time periods (1 h, 4 h and 1 day) in the presence of enzymes before analysing them via SDS-PAGE (Figure 4.2). In the presence of both enzymes, when the highlighted band that corresponds to BSA was compared between protein with and without the gel at every time point, there was a noticeable decrease in the band intensity for the protein alone, revealing the decrease in the amount of intact protein. At the later time points, the band intensity is fading for the protein in the gel as well. This eventual decrease in the total amount of protein in both the gel and solution could be attributed to enzymes eventually diffusing into the gel, BSA partially diffusing out of the gel, the gel slowly eroding or a combination of all three processes.

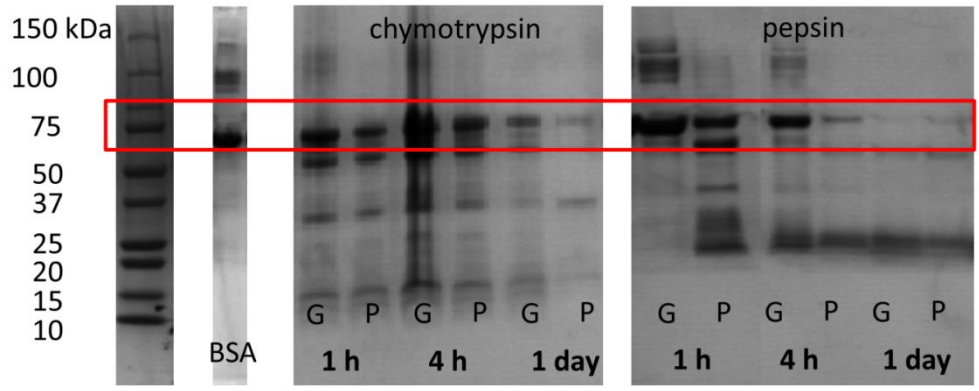

Figure 4.2: SDS-PAGE for BSA (30 µM) encapsulated in gels (G) and BSA alone (P) after incubation with two different enzymes; chymotrypsin and pepsin for 1 h, 4 h and 1 day. In 120 µL of gel (0.5% w/v) in different buffers (50 mM KH_2PO_4 (pH = 4.5) for pepsin and PBS for chymotrypsin), 10 µL (5 mg/ml, ≥1250 units/mg) of pepsin and 20 µL (2 mg/ml, ≥80 units/mg) of chymotrypsin were pipetted on top of the already formed gel and incubated at 37 °C.

4.2.3 Investigating the released proteins' functionality

After evaluating that the gel is providing efficient protection to the protein against proteolytic hydrolysis, a critical question is whether the functionality of the protein is preserved after encapsulation within the gel. This has also been a controversial topic for the polymeric gels [97]. Firstly, the integrity of all released proteins was tested with SDS-PAGE separation. As presented in Figure 4.3A, all four released proteins have the same molecular weight as the proteins that did not undergo gel encapsulation (represented by the same band on the SDS-PAGE). Furthermore, the protein's functionality is highly dependent on its secondary structure [221]. While circular dichroism would be a typical choice to study the secondary structure of proteins, in this system the strong CD activity of the gelator precludes the use of CD for the protein characterisation [200]. Considering this, we included a therapeutic protein, insulin and an enzyme, lysozyme in our study and assessed their activity after encapsulation [222].

To assess the bioactivity of insulin after the release through the gel, we used a cell-based functional assay. The HepG2 cells originate from a human liver carcinoma (one main target organ of insulin) and express abundant levels of the insulin receptor. A luciferase vector was transfected under the promoter fragment of the HMG CoA enzyme that is responsive to insulin [223-225]. The cell response to different doses of released insulin and insulin in solution was measured through luciferase activity. In Figure 4.3B, insulin released from the gel (red bars) is plotted against insulin in solution (green bars). No difference between the bioactivity of the natural insulin and the released insulin is observed and, importantly a clear dose-response was observed at ranges of concentration similar to those present in humans, both at fasting (normal range 2-25 μUI/ml taken as a reference the Mayo Clinic laboratory fasting values for the normal population[226]) and at post-prandial levels (approximately 30-230 μIU/ml [227]). There was no action of the released insulin on the mutated promoter bearing four point-mutations, where also there is no action of the natural insulin, indicating that the response was specific for the insulin receptor (SI, Figure 4.S6).

Lysozyme is an antimicrobial enzyme that selectively cleaves β-1,4-glycosidic bonds between *N*-acetylmuramic acid and *N*-acetylglucosamine present in bacterial cell walls [228]. The functionality of lysozyme has been previously assessed using *Micrococcus lisodeikticus* lyophilised cell walls as a substrate [222]. The lytic activity of the released lysozyme after encapsulation in the gel and free lysozyme are presented in Figure 4.3C. Both traces (green and red) follow the same trend and are both distinctly different from the control (black trace), demonstrating that released lysozyme has the similar activity as free lysozyme. Incubation of the cells with the gelator alone did not cause a change in absorbance, indicating that the gelator does

not affect the integrity of the cell wall and that a change in absorbance in the gelator/protein sample is due to lysozyme released from the gel.

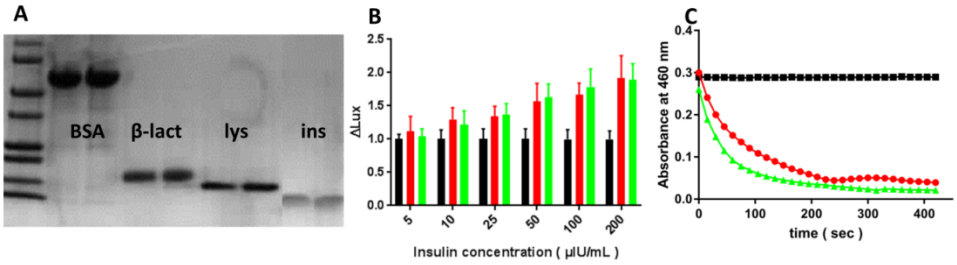

Figure 4.3: SDS-PAGE of different proteins (30 µM) BSA, β-lactoglobulin (β-lact), lysozyme (lys), insulin (ins) after encapsulation in the gel (0.5% w/v). Data are presented in pairs (first column control protein and second released protein). Dose response curve for human insulin was measured through luciferase activity;[229] gel alone (black trace), insulin released from gel in the presence of gelator (red trace) and insulin alone (green trace) (N=3 with 6 replicate measurements each). Turbidimetric assay of lysozyme; absorbance at 460 nm of *Micrococcus Lisodeikticus* lyophilised cell walls in the presence of gel alone (black trace), released protein (red trace) in the presence of gel, lysozyme control (green trace),(N=3).

4.2.4 Encapsulation of proteins into hydrogels in the nanoscale

The macroscopic data presented on the release of the different proteins and the degradation of the gel itself suggest that rather than physical encapsulation in the hydrophilic cavities within the 3D nanofibre network (the size of the protein did not seem to affect the release profiles, even if the size of the proteins is very different as shown in Figure 4.S2), chemical, non-covalent interactions between the proteins and the gel nanofibres are responsible for the retention of proteins within the gels.

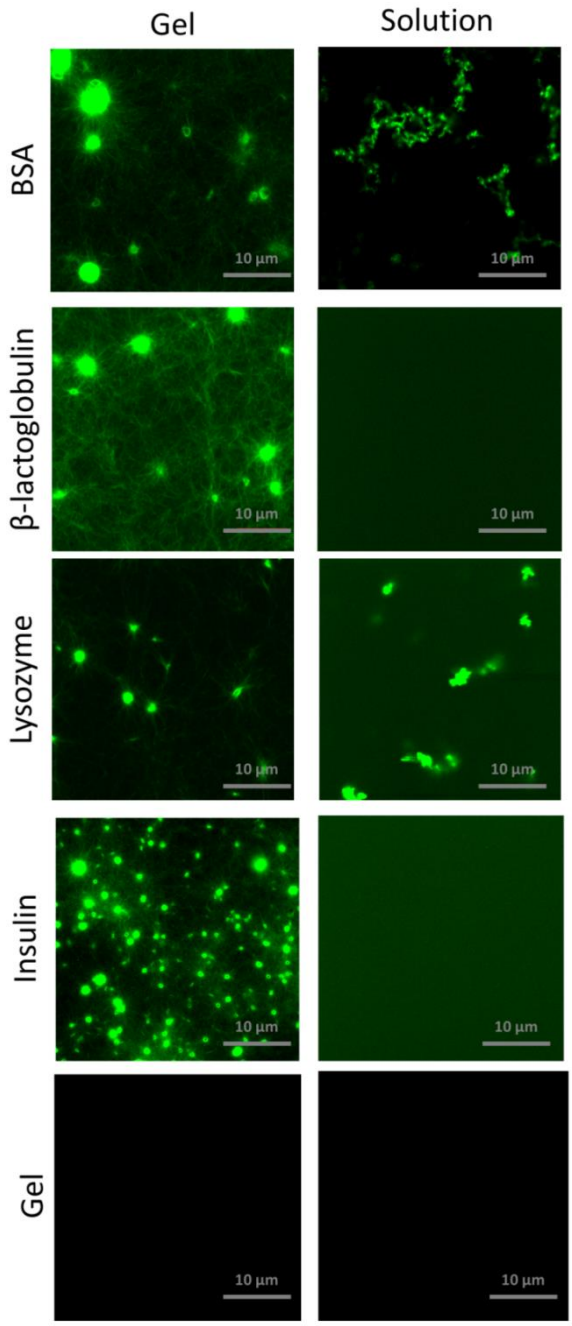

Figure 4.4: Fluorescence images of gels (concentration 0.5% w/v) (left column) and solutions (right column) containing (30 µM) protein labelled with fluorescamine in PBS for 4 h at 37 °C; BSA, beta-lactoglobulin, lysozyme, insulin and gel alone (from top to bottom). The 405 nm laser was set to 0.8%, emission detected at: 490 – 624 nm, channel colour (LUT) was set to green.

In order to investigate this in more detail and to elucidate the location of the proteins in the gel nanostructure, we used fluorescence microscopy and fluorescamine as a probe. Fluorescamine is a well-established dye in protein

quantification as it reacts with primary amines and forms fluorescent complexes, consequently it is selective for the proteins and not the gelator [230]. Hence, the gel fibres alone are not fluorescent (at λ_{exc}=405 nm) and only become visible in fluorescence microscopy because fluorescent proteins associate with them (Figure 4.4). The dispersed points giving strong fluorescence signals across the fibre network are most likely due to protein and/or dye associated with fibre bundles (crossover points) or dye/protein aggregates. Additionally, the gelator was shown to inhibit protein aggregation, ruling out the possibility that the fluorescent fibres are due to protein aggregation and not the association of proteins with the gel fibres.[231] Note that the size of the observed features does not correspond to their actual dimensions). The diameters of the fibres (254 nm) observed in fluorescence microscopy are considerably larger than expected (~13 nm)[200] which is attributed to instrumental limitations (Raleigh/Abbe criteria, signal to background and signal to noise (of the detector) ratio.

Further to this, the intrinsic fluorescence of both the proteins and the gel was used for further evaluation of the interaction of the protein with the fibres [232]. The proteins' intrinsic fluorescence is due to the presence of aromatic amino acids and any change in their surrounding environment can result in a change in their fluorescence [232]. The gelator is non-fluorescent in solution but it fluoresces in the assembled state, as previously reported [200]. As presented in Figure 4.5, emission spectra were recorded for the gel after the encapsulation of the protein, the gel and the protein alone, after excitation at two wavelengths that have been widely used for the excitation of proteins, 275 nm for the general excitation of the three aromatic amino acids and 295 nm for the specific excitation of tryptophan (human insulin has no tryptophan, so no emission after excitation at 295 nm is detected).

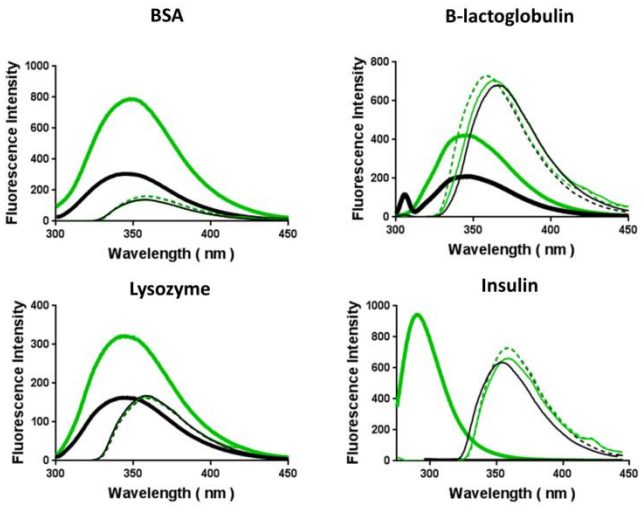

Figure 4.5: Fluorescence emission spectra for gels (at concentration 0.5% w/v) containing four different proteins (30 μM) and the gel alone in PBS (30 μM for all proteins in gel and solution, apart from insulin which is 3 μM to allow recording of samples of insulin in gel and solution with the same instrumental settings). In every graph; protein containing gel after excitation at 295 nm (black solid), protein containing gel after excitation at 275 nm (green solid), protein in solution after at 295 nm (black bold), protein in solution after excitation at 275 nm (green bold), gel without protein after excitation at 295 nm (black dashed), gel without protein after excitation at 275 nm (green dashed). The two minor peaks between 400 nm and 450 nm on the spectra of the gels containing β-lactoglobulin and insulin have been identified as artefacts and not related to the protein/gel intrinsic fluorescence.

Compared to the spectra obtained from protein solutions, the fluorescence emission spectra of all four different proteins in the gels shift and fully overlap with the emission spectra of the gel without the proteins. This suggests that the proteins' intrinsic fluorescence is fully quenched due to their association with the fibres and only the fluorescence of the gel is detected. This may be the result of a change in the environment of the aromatic amino acids in the protein structure and indicates that these aromatic amino acids are directly involved in the fibre-protein interactions.

To understand if the presence of the protein is affecting the diameter of the fibre, we performed Small Angle X-Ray Scattering (SAXS) measurements of the gels with proteins, the proteins in solution and the gel alone (Figure 4.7). SAXS has been previously used to investigate the structures of supramolecular gels[141] as well as the

effect that molecules encapsulated in the fibre have on the fibre diameter [105]. The gel sample was fitted to a flexible cylinder model (as previously reported for similar systems)[105] revealing a fibre radius of 73.2 Å, in good agreement with previously published data [200]. Since fluorescence microscopy images showed that the proteins locate themselves on the fibres yielding cylindrical geometries, the SAXS patterns obtained from protein containing gels were fitted to a flexible cylinder model in the same manner as the gel sample that did not contain proteins, yielding fibre radii of 91.2 ± 0.4 Å (BSA), 66.6 ± 0.4 Å (β-lactoglobulin), 71.1 ± 0.9 Å (lysozyme) and 67.6±0.9 Å (insulin). The fitting parameters are presented in SI, Table S1. Compared to the other proteins, BSA was the protein with the highest MW and the only one that significantly increases the fibre radius compared to the other proteins confirming that there is an ordered association of the protein with the fibre. The other proteins likely associate with the fibres by arranging themselves in a non-ordered, amorphous structure surrounding the main gel fibre which would not be detectable by X-ray scattering.

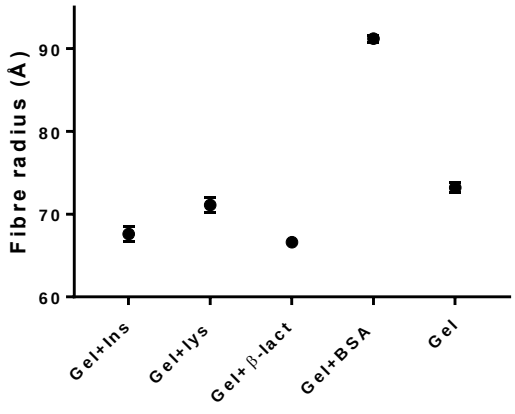

Figure 4. 7: Fibre radii determined from SAXS data obtained from gels (at concentration 0.5% w/v) with the four different proteins (30 μM) and the gel alone in PBS at room temperature. The data points represent the average fitted values of the radii and standard errors of the fitted values are also presented as error bars.

4.2.5 Understanding the encapsulated molecules' release *in vitro*

As mentioned earlier, supramolecular gels can encapsulate a range of different molecules with different molecular weights, hydrophobicity/hydrophilicity, and charges [9, 46, 108]. The present gel can encapsulate different proteins through their direct association with the fibres whereas in previous work it was shown that a small hydrophobic dye can be encapsulated in the hydrophobic core of the fibres of this gelator [200]. Here, we use a small hydrophobic dye, 1,1'-Dioctadecyl-3,3,3',3'-Tetramethylindocarbocyanine Perchlorate (DiI), and a fluorescently labelled protein, cyanine 5-BSA (Cy5-BSA), to compare their release profiles *in vitro* and *in vivo*. The fluorescent probes were selected due to the good contrast they demonstrated in In Vivo Imaging System (IVIS)®.

In order to study the release of the encapsulated molecules *in vitro*, we performed real time fluorescence microscopy. Gels after the encapsulation of DiI and Cy5-BSA, were incubated with PBS at 37 °C for 48 h. Images were captured at t=0 min, 10 min, 24 h and 48 h and are presented Figure 4.8. For t=0 min, in both cases the fluorescent molecules directly associate with the fibres. It is important to highlight again that the gel alone is not fluorescent and the fluorescence signal is exclusively associated with the presence of the encapsulated molecule (Cy5-BSA or DiI).

At t=0 min, in both cases there is an extensive fluorescent network of fibres with dispersed points giving strong fluorescence signals, most likely due to protein and/or dye associated with fibre bundles (crossover points) or dye/protein aggregates (note that the size of the observed features does not correspond to their actual dimensions due to the method's limitations). After 10 min, we focused on the gel-

PBS interface, where fluorescent fibres were observed to leave the bulk gel and the protein aggregates were released (Figure 4.8, zoom in at 10 min).

A similar observation was made with DiI encapsulated in the gel where fluorescent fibres as well as dye aggregates left the bulk gel. After 1 day, in both cases the bulk gel has been fully eroded leaving smaller gel fragments floating in the medium. In the case of Cy5-BSA, fluorescent structures of different sizes (<20 μm) and shapes are floating in the medium whereas in the case of DiI encapsulating gel, significantly larger gel fragments were visible with diameters of more than 100 μm, suggesting that fibres are held together for longer in the latter. In the case of DiI encapsulating gel fragments, fibres were protruding out in the gel-medium interface, suggesting the interfacial erosion of the gel through single fibres (SI, Figure 4.S8).

4.2.6 Understanding the encapsulated molecules' release *in vivo*

To date, a limited number of nucleoside-based gelators have been tested *in vivo* [83, 116]. In this work, we used a nucleoside-based gel encapsulating a small hydrophobic dye (DiI) or Cy5-BSA in order to evaluate how these model molecules get released *in vivo*, how they affect the gel's properties as well as correlate the findings with *in vitro* data. At the same time, we acquired preliminary insight into the safety of the material *in vivo* and its potential as a drug delivery system.

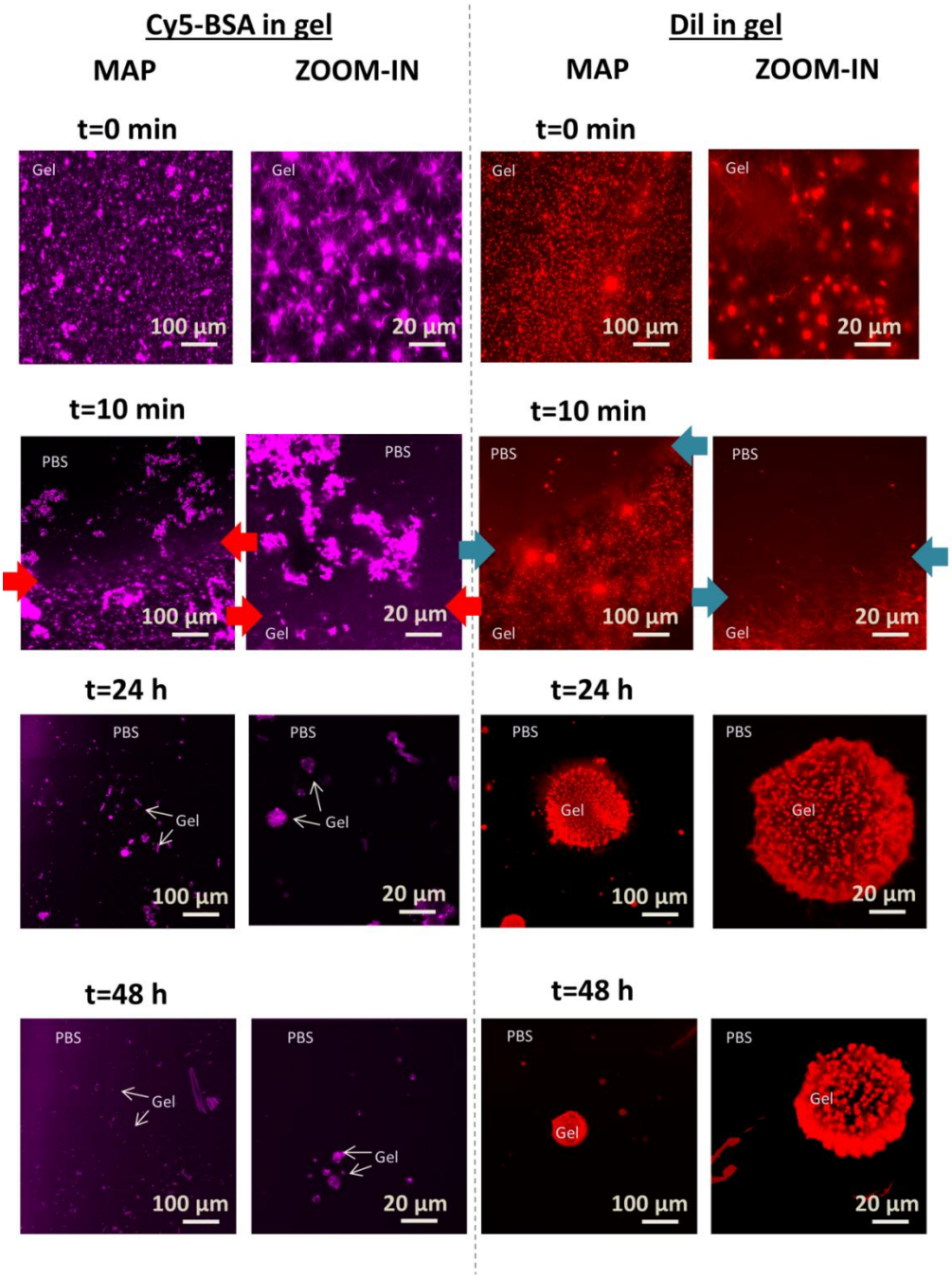

Figure 4.8: Fluorescence microscopy images of gels (0.5% w/v) encapsulating Cy5-BSA at a final concentration of 15 µM (left) and hydrophobic dye (Dil) at a final concentration of 8.3 µM (right) at after incubation with PBS at 37 ˚C at different time points (t=0 min, 10 min, 24 h, 48 h). The arrows indicate the gel-PBS interface. In each case a large area image (map) and a zoom in image were recorded. For the Cy5 labelled protein, 647 nm laser was set to 4%, emission detected at 654 – 752 nm, channel colour (LUT) was set to magenta; for Dil, 561 nm laser was set to 0.1%, emission detected at 561 – 624nm.

Hydrogels containing Cy5-BSA and DiI, Cy5-BSA in solution and plain gel were injected subcutaneously into mice. In Figure 4.9A, IVIS® images of the mice are presented at different time points (0 hr, 1 h, 24 h and 2 weeks after subcutaneous injection) for gels encapsulating Cy5-BSA (top) and DiI (bottom). In both cases the fluorescence intensity faded out over time and was almost zero after two weeks (very low levels of fluorescence were detected probably due to association of the dye with tissue). No control group was injected with DiI in solution as DiI is highly hydrophobic and remains completely insoluble in PBS. Fluorescence data were extracted for quantification and are presented in Figure 4.9B. In all cases there was an increase in the fluorescence intensity during the first 4 hours, probably due to the gel reformation after the shear stress applied during injection. Another explanation could be equilibration phenomena of the fluorescent probe in the lipophilic tissue environment that has been previously reported [233]. After this period, fluorescence intensity started to drop as expected.

Fluorescence data of the gel containing Cy5-BSA and Cy5-BSA in solution (Figure 4.9B) demonstrates that that encapsulation in the gel increased retention of Cy5-BSA (approximately 3 days) compared to Cy5-BSA in solution. When comparing fluorescence data of Cy5-BSA and DiI after encapsulation in the gel (Figure 4.9B) clear differences between the two gel samples are observed. The gel with the dye DiI formed a compact gel that remained at the injection site for over 2 days and slowly disappeared over time. On the other hand, the gel encapsulating the protein did not form a compact gel and spread significantly in the tissue at the injection site. Further investigations using rheological measurements *in vitro* could potentially shed light into these questions. In both cases, the mice of both groups were healthy

when sacrificed after 2 weeks and there was no macroscopic trace of the gel in the tissue, indicating that the gel is biodegradable *in vivo* (Figure 4.9C).

The *in vitro* protein release data (Figure 4.1B) showed that the release of different encapsulated proteins from the gel followed the degradation of the gel. In the case of the encapsulated hydrophobic dye (Dil), *in vitro* release data were impossible to acquire due to the high hydrophobicity of the dye that tended to interact strongly with the containers and not remain in solution. Even when different solvents were used to extract the dye, exact quantification was not possible. The use of an alternative dye was not an option at this stage as in contrast to other dyes Dil demonstrated selective binding into the hydrophobic cavity of the fibres as well as provided with adequate contrast for IVIS®. Due to this, macroscopic images of the degradation of the gel encapsulating the dye and the gel alone are presented in Figure 4.S9, SI, over a course of 24 h. As the volume of the gel encapsulating Dil and the gel alone reduce in a similar manner over time, we conclude that the release of the dye follows the gel erosion as well and the gel completely degrades macroscopically within 1 day. The *in vitro* release data are in good agreement with the fluorescence microscopy images that show gel breakdown within 24 h (even if gel and media volumes are not the same, preventing us from quantitative comparisons). Additionally, the fluorescence microscopy images showed that the gel encapsulating the dye and the gel encapsulating the protein followed two different breakdown pathways; the first broke down into gel particles whereas the second into fibre bundles, suggesting that the forces holding the fibres together for the gel encapsulating the dye are stronger compared to the gel encapsulating the protein. Preliminary rheological investigations as presented in SI, Figure 4.S9 did not reflect this difference in the behavior of the two formulations. Further investigations using

rheological measurements *in vitro* could potentially shed light into these questions. As shown in Figure 4.9, although the same volume of gel was injected, gel encapsulating Cy5-BSA occupied a larger area in the animals after injection compared to gel encapsulating DiI suggesting that the ability of the gel to reform *in vivo* is different between the two formulations. Alternatively, this could be explained by the fact that the fluorescence intensity of Cy5 is stronger compared to that of DiI or that Cy5-BSA could diffuse quicker into the tissue compared to DiI.

In order to investigate if the gel causes any inflammation, cross-sections of the tissue at the site of injection of the gel alone were stained with haematoxylin and eosin imaged as shown in Figure 4.9D. Tissue and cell morphology appeared comparable to the control. There was no evidence of the gel depot itself or of cellular or tissue damage from the gel in the samples. Areas of haemorrhage or excessive immune cell infiltration (including cells such as mononuclear leukocytes and polymorphonuclear cells) were not visualised within any of the tissues assessed. The basic histological investigations indicated no damage to the cells within the tissue where the gel was injected. These samples were measured 2 weeks after injection, therefore at this stage we can conclude that no inflammation or tissue necrosis was observed, suggesting that the material does not cause any permanent damage to tissue. It is possible that a larger immune cell response could have been present in the days immediately following injection as is usual following injections of biomaterials[234 235-237].

4.3 Conclusions

So far, supramolecular gels have emerged as promising biomaterials for drug delivery. Here, we investigate for the first time different aspects of the behaviour of

a novel nucleoside-based gel *in vitro* and *in vivo* as a drug delivery system for a range of different therapeutically relevant molecules. We demonstrated that all the systems form stable, self-healing gels that release the encapsulated molecules in a sustained way through a process consistent with gel erosion. Regarding protein delivery, we clearly demonstrated a major advantage of these materials; the prevention of enzymatic degradation of the encapsulated protein against model proteolytic enzymes. Additionally, after *in vitro* release proteins (such as lysozyme and insulin) are shown to maintain their functionality. However, the material demonstrated no signs of inflammation or tissue necrosis during the course of these two weeks. Furthermore, in this work we present an in-depth, comprehensive understanding of the encapsulation and the release mechanism of a range of molecules for the first time for supramolecular gels that can provide unique information on the in vivo behaviour of the supramolecular gels as drug delivery systems. To conclude, this study provides a solid demonstration that bioactive molecules with different properties can significantly impact the nano- and macro-properties of supramolecular gels, establishing the need for mechanistic investigations in order for these materials to reach their maximum potential in the challenging drug delivery field.

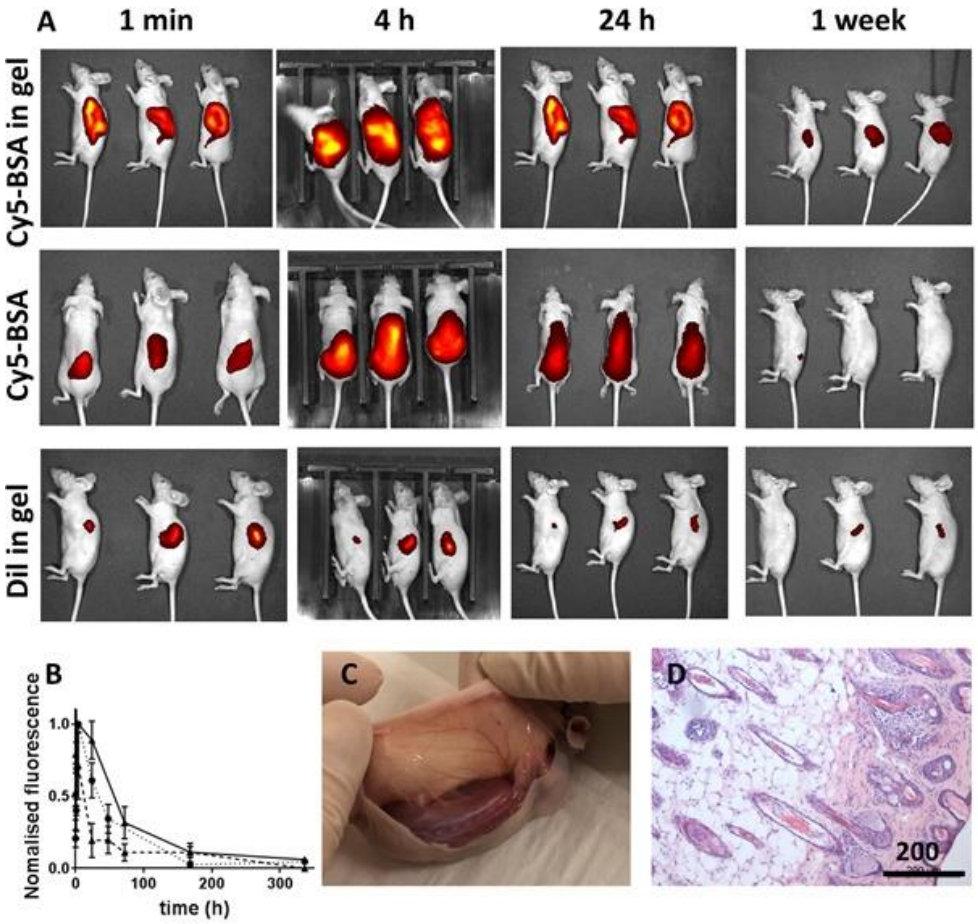

Figure4.9: *In vivo* data of gels encapsulating Dil and Cy5-BSA after subcutaneous injection in mice (N=3 for each group); (A) IVIS® images of the mice after injection of approximately 300 µl of gel (0.5% w/v) encapsulating Cy5-BSA (15 µM, top row), Cy5-BSA in solution (15 µM) and gel encapsulating a hydrophobic dye, Dil (8 µM). Images are presented in the same colour scale 6.00 x 10^8 - 1.00 x 10^{10} (ρ/sec/cm^2/sr) for the gel encapsulating Cy5-BSA and Cy5-BSA in solution and 3.50 x 10^8 - 7.00 x 10^9 (ρ/sec/cm^2/sr) for all the images of the gel with Dil. (B) Normalised to maximum fluorescence intensity (fluorescence signal is measured in radiance over the same region of interest for all images) of gel encapsulating Cy5-BSA (solid trace) and Cy5-BSA in solution (dotted trace) and gel encapsulating Dil (dashed trace) (N=3). (C) Macroscopic image of tissue where plain gel was injected; after two weeks the animals were sacrificed and the gel had completely degraded. No control group was injected. Dil in solution as Dil is highly hydrophobic and remains completely insoluble in PBS. (D) Photomicrograph showing normal cellular and tissue morphology. Haematoxylin and eosin were used to stain the tissue at the injection site 2 weeks after the injection of the control gel (without encapsulated molecule).

4.4 Experimental methods

4.4.1 Materials

2'-Deoxycytidine (lot #SLBN6031, 99% [high-performance liquid chromatography (HPLC)]), pepsin from porcine gastric mucosa (#P7012, lyophilized powder, ≥2,500 units/mg protein (E1%/280)), lysozyme from chicken egg white lyophilized powder (product # L6876, protein ≥90 %, ≥40,000 units/mg protein), β-lactoglobulin B from bovine milk (≥90% (PAGE) product # L8005), Bovine Serum Albumin lyophilised powder, essentially fatty acid free and essentially globulin free, ≥99% ((agarose gel electrophoresis), product #A028) 1,1'-Dioctadecyl-3,3,3',3'-tetramethylindocarbocyanine perchlorate 97% (product #468495) and fluorescamine [(product # 47614) BioReagent, suitable for fluorescence, ≥99.0% (UV)], C4129 α-Chymotrypsin from bovine pancreas, Type II, lyophilized powder, ≥40 units/mg protein, (product # C4129), Micrococcus lisodeikticus lyophilised cells, Dulbecco's Phosphate Buffered Saline Modified, (without calcium chloride and magnesium chloride, liquid, sterile-filtered, suitable for cell culture D8537) were purchased from Sigma Aldrich. Polyacrylamide gels 4–20% Mini-PROTEAN® TGX™ Precast Protein Gels, 12-well, 20 µl (#4561095) and Quick Start™ and Bradford 1x Dye Reagent (#5000205) were purchased from Bio-Rad. Cyanine5 NHS ester was purchased from Lumiprobe. Insuman Rapid 100 IU/ml solution for injection in a cartridge was purchased from Sanofi. SnakeSkin™ Dialysis Tubing was purchased from Thermofisher Scientific (Waltham, Massachusetts, United States), MWCO 3.5 kDa. For Fluorescence Microscopy Cellview cell culture slide (Item No.: 543079) were purchased from Greiner Bio-one. The gelator was synthesized according to previously published work. Analysis of the gelator was performed by NMR and liquid

chromatography−mass spectrometry (LC−MS) (Supporting Information Figures 4.S11 and 4.S12), and purity was determined as 98% (LC−MS). [51]

4.4.2 Gel preparation

Certain amount of gelator was weighed out in 2 ml HPLC vial and dispersed with PBS in order to get a final concentration of 0.5% w/v. The vial was carefully sealed and the gelator was heated up to 100 ˚C till complete dissolution. The sealed vial was immersed in a water bath at 37 ˚C for 1 min before opening (allowing for water condensation) and certain amount of protein was pipetted in to achieve final protein concentration of 30 µM. For protein-gel association studies, stock solutions of proteins were prepared in PBS (Bovine Serum Albumin 27 mg/ml, Lysozyme 5.75 mg/ml, β-lactoglobulin, Insulin 2 mg/ml) and 40 µl of protein stock solution was pipetted into 500 µl of gelator at 37 ˚C. For the Real Time Fluorescence Microscopy and the in vivo study 13.5 mg/ml stock solution of Cy5-BSA in PBS (the labelling protocol is described further) were prepared and 48 µl of protein stock solution were pipetted into 552 µl gelator (37 ˚C), then a stock solution of 5 mg/ml DiI in ethanol was prepared and 3 µl were pipetted into 600 µl of warm gelator.

4.4.3 Release studies of proteins

500 µL of gel containing protein in 2 ml HPLC vials were incubated with 1 ml PBS at 37 ˚C. The supernatant was removed at different time points (1, 2, 4, 6, 14 and 24 h) and replaced with fresh PBS. The protein concentration was determined using the Bradford colorimetric assay [215]. For lysozyme and β-lactoglobulin, 20 µl of supernatant at each time point was premixed with 200 µl Bradford reagent, for Bovine Serum Albumin 20 µl of supernatant were premixed with 200 µl of Bradford reagent and for Insulin 100 µl of supernatant with 100 µl of Bradford reagent and

absorbance at 595 nm was measured using a Tecan Spark 10 M/ 20 M plate reader. Ratios of supernatant:reagent were determined in order to provide with a linear calibration curve (Supplementary Information Figure 4.S10). For each data point an average of 4 repeats is presented for the calibration curve and an average of 3 repeats for the protein release study.

4.4.4 Gel degradation study

500 µL of gel in 2 ml HPLC vials were incubated with 1 ml PBS at 37 ˚C. The supernatant was removed at different time points (the same as the protein release study; 1, 2, 4, 6, 14 and 24 h) and replaced with fresh PBS. 40 µl of supernatant were premixed with 160 µl of methanol and the absorbance was measured at 295 nm in a quartz 96 well-plate using a Tecan Spark 10 M/ 20 M plate reader. For each data point an average of 4 repeats is presented for the calibration curve (Supplementary Information Figure 4.S9) and an average of 3 repeats for the gel degradation study.

4.4.5 Fluorescence spectroscopy

600 µL of gel (with or without proteins prepared as explained above) were added to a 2 mm path length cuvette. Fluorescence spectra were recorded at a Cary Eclipse fluorescence spectrophotometer. The spectra were recorded with a scan rate of 30 nm/min, averaging time 1 s, and data interval 0.5 nm using different emission and excitation slits; for BSA (excitation slit 2.5 nm and emission slit 5 nm), β-lactoglobulin (excitation slit 5 nm and emission slit 5 nm), lysozyme (excitation slit 2.5 nm and emission slit 5 nm), insulin (excitation slit 5 nm and emission slit 5 nm). Samples were excited in all cases at 275 nm and 295 nm. Gels (concentration 5 mg/ml) with

proteins (30 μM) were prepared and compared to protein solution in PBS (30 μM for all proteins apart from insulin that is 3 μM).

4.4.6 Fluorescence microscopy

15 μl of warm gelator solution (concentration 0.5% w/v) where the encapsulating molecule has already been added were pipetted in the well and the first image (t=0 min) was recorded. 400 μl of PBS were added and the well was transferred to 37 ˚C and images were recorder at t=10 min, 24 h, 48 h.

Gels were made and imaged in Cellview multiwell , glass bottom slides (0.17mm, category 1.5, product no: 543079). Fibres / gels and suspensions were visualized and scanned with the confocal unit of a Zeiss Elyra PS1 LSM780 microscope. Two different objectives were used, water immersion C-Apochromat 63x/1.2 W Korr M27 for scanning the gels and solutions labelled with fluorescamine, and alpha-Plan-Apochromat 100x/1.46 oil objective for DiI and Cy5 labelled proteins and time laps experiments. Fluorescent dyes were detected with the following settings: for fluorescamine, 405 nm laser was set to 0.8%, emission detected at: 490 – 624 nm, channel colour (LUT) was set to green; for Cy5 labelled proteins, 647 nm laser was set to 4%, emission detected at 654 – 752 nm, channel colour (LUT) was set to magenta; for DiI, 561 nm laser was set to 0.1%, emission detected at 561 – 624 nm. To reduce noise, and reveal more details, for all the scans line averaging of 2, and slow scan of 6.3 μs dwell time was applied during scanning. Images and videos were exported using Zeiss Zen 2012 SP5, histogram values (display of the image brightness) was set to the same for the samples belonging to the same experiment.

4.4.7 Protein Labelling

0.4 mg Cyanine5 NHS ester were dissolved in 200 µl DMSO and 6 mg Bovine Serum Albumin were dissolved in 1800 µl $NaHCO_3$ 0.1 M (pH 8.3). The reaction was left under stirring overnight and the mixture was left to dialyse for 7 days using a 3.5 kDa dialysis tubing. After dialysis, the labelled protein was analysed by size exclusion chromatography (SEC) using a TSK gel G3000SWXL (300 × 7.8 mm) column (TOSOH, Tokyo, Japan), running on a HPLC system. The protein was isocratically eluted in DPBS at a flow rate of 1 mL min^{-1}. Fluorescence was recorded at λ_{em} = 666 nm, with excitation fixed at λ_{ex} = 644 nm. The chromatogram is presented in Figure 4.S13.

4.4.8 Enzymatic degradation study

120 µL of warm gelator solution (0.5% w/v) in different buffers [50 mM KH2PO4 (pH = 4.5) for pepsin and PBS for chymotrypsin] were pipetted into 1.5 ml plastic Eppendorf tubes and Bovine Serum Albumin (in PBS) was added, as described earlier, to achieve a final concentrations of 30 µM. 10 µL (5 mg/ml) of pepsin and 20 µl (2 mg/ml) were pipetted on top of the already formed gel and incubated for 1 h, 4 h and 24 h at 37 ˚C. Enzyme concentrations were selected in order to allow us to qualitatively assess the prevention of protein degradation, in a time course of 24 h. At the previously mentioned time points, the enzymes were quenched after the addition of 80 µl SDS-PAGE Reducing Sample Buffer (RSB), plus 10 µl of HCl 1 M in the case of chymotrypsin, and the samples were denatured by heating at 100 ˚C for 5 min prior to gel loading. 10 µL of sample were pipetted into a 4–20% Mini-PROTEAN® TGX™ Precast Protein Gel which was run in a standard running buffer (25 mM Tris, 192 mM glycine, 0.1% SDS). Gels were incubated in InstantBlue® (Expedeon, UK). RSB contained 75 mM Tris–HCl, pH 6.8, 10% glycerol, 2% SDS, 0.05% bromophenol blue, 2.5% β-mercaptoethanol.

4.4.9 Samples for Small Angle X-ray scattering (SAXS)

Samples for Small Angle X-ray scattering (SAXS) were prepared in 1.5 mm borosilicate glass capillaries (Capillary Tube Supplies Ltd) and sealed with a UV-curable adhesive (Norland Optical Adhesive). SAXS measurements were taken on a SAXSLab Ganesha 300XL instrument using a CuKα source (1.54 Å) and a Pilatus 300K detector. Data collection was performed over a Q range of 0.007-0.25 $Å^{-1}$, with an exposure time of 7200 seconds per sample. A correction for tube thickness and curvature was applied during measurement, and a capillary of buffer was run in order to perform background subtraction. The data were fitted using the SasView 4.1 software package.

4.4.10 Atomic Force Microscopy

Gel solutions were prepared as previously described for the gel degradation study (see 'Gel degradation study' section). The supernatant after 4 h incubation was extracted and 40 µl were pippeted onto mica. Mica was transferred on preheated at 37 °C AFM stage. Adequate amount (approximately 50 µl) of PBS were added to immerse fully the AFM tip in liquid. Imaging was performed under Peak Force mode using the Bruker FastScan Dimension with ScanAnalyst AFM.

4.4.11 Lysozyme functionality assay

A turbidimetric enzymatic assay was performed by measuring the decrease in optical density of an aqueous suspension of Micrococcus lysodeikticus lyophilised cells, a natural substrate for lysozyme, in PBS. Gel with lysozyme was prepared as described before and 0.5 ml of gel was incubated with 1 ml of PBS at 37 °C for 24 h until gel erosion. The final concentration of lysozyme in the dispersion produced was 37 µg/mL. PBS (20 mL) solution was added to 10 mg of lyophilised cells. 300 µL of this

substrate suspension were added to 150 µL of solution and the decrease in optical density at λ = 460 nm was measured as a function of time. Free gelator and free lysozyme were used as controls at the same concentration as in the samples after incubation at the same conditions as lysozyme in the gel. All kinetic experiments were carried out in triplicate.

4.4.12 Evaluation of the insulin bioactivity in human cells

The HepG2 cell line was obtained from ECACC (UK, distributed by SIGMA) and cultured in growth medium: EMEM (1 g glucose/L, SIGMA, UK) supplemented with 10 % FBS (GIBCO, Thermo South America), 1% Non-essential amino acids (GIBCO, Thermo Grand Island USA), 2 mM L-Glutamine (SIGMA Brazil), 1% Penicillin-Streptomycin (SIGMA Israel). HepG2 originated from a human liver carcinoma, a bona-fide insulin target organ, and are enriched in Insulin Receptor expression (https://www.proteinatlas.org/ENSG00000171105-INSR/cell). Cells were passaged once per week by trypsinization (10x Trypsin solution, SIGMA USA) for 5 minutes and passage through an 18 gauge needle to obtain a single cell suspension. They were used between passages 3 and 20.

For transfection, Viafect (Promega, Madison USA), and Turbofect (Thermo, Lithuania) were compared by measuring the efficiency of transfection of a commercial plasmid preparation of pMAXGFP (Lonza, Köhln Germany) following the standard recommended protocols. Efficiency was calculated measuring the number of GFP fluorescent cells respect to the total number of cells stained with Hoescht 33258 (SIGMA Israel). Apoptosis measured as condensed Hoescht+ cells was also measured and discarded for efficiency. Since Viafect obtained a >95% efficiency

while Turbofect approached 65% all subsequent experiments were performed using Viafect.

MW48 plates (Costar, Thermo NY USA) were previously coated with 100 µg/ml Type I collagen solution in PBS (stock solution: 4 mg/ml, SIGMA St Louis MO USA) and washed three times with PBS (SIGMA St Louis MO USA). For each assay, 24000 HepG2 cells/well were seeded on these wells in growth medium, and allowed to grow for one full day. Next day, a transfection mix of DNA plasmid (85 ng of promoter+35 ng empty RSV plasmid/well), Viafect transfection reagent (1.5 µL/well) and EMEM (23.5 µL/well) was prepared for all wells combined and incubated for 20 min. The plasmids used were: pSynSRE-T-luc (Addgene, Cambridge USA) containing the −324 to −225 bp fragment of the hamster HMG-CoA synthase promoter containing the SRE elements upstream of the minimal HMG-CoA synthase TATA box (−28 to +39) pSynSRE-Mut-T-luc bearing four point mutations in that promoter SRE elements[223-224]. It has been previously shown that Insulin regulates HMG-CoA synthase expression through those SRE sites in human cells, and its action abolished in the mutated promoter[225] .

Meanwhile, cell medium was replaced by growth medium plus 2 mM metformin (SIGMA, Steinheim Germany). Metformin helps to reduce the basal luciferase expression while the cells were under transfection. Subsequently, 25 µL of the transfection mix was pipetted per well and incubated during 6 hours. After three washes with warm PBS were performed and changed to deprived medium (as growth medium but with only 0.5% FBS) including the insulin/vehicle to test (5-200 µIU/ml or equivalent vehicle volume). Each condition was tested in six-eight replicates. After 20 hr, wells were washed three times with PBS followed by addition of 40 µL PassiveLysis Buffer/well (Promega, Madison USA) for 20 min. Lysates were

collected and frozen at -20 °C. Luciferase activity was assayed as described[238] using 15 µL of lysate in a Mithras microplate reader (LB940, Berthold, Bad Wildbad Germany). Experiments were repeated three times.

Statistics and figures were performed with GraphPad 7 by applying first a Kolmogorov-Smirnov normality test and, being normally distributed, following by an unpaired t-test to assess significance. Insulin –Vehicle concentrations were plotted in parallel graphics comparing the normal SynSRE-T-luc and the mutated SynSRE-Mut-T-luc promoter (SI, Figure 4.S6).

4.4.13 Rheology studies

Rheology was carried out using an Anton Paar MCR302 Modular Compact Rheometer. A four bladed vane geometry was used with a diameter of 8.5 mm and length 8.5 mm in a cup with a diameter of 14.5 mm. The solution of gelator was prepared in 7 mL aluminium cups to a final sample volume of 2 mL, as per the method described above. Once the gel was prepared, the sample vial was mounted in the lower plate (cup) of the rheometer; the vane (attached to the upper part) was lowered into place, at a depth of 2 mm. This arrangement gave a total sample depth of approximately 16 mm in the 14.5 mm diameter cup which allowed positioning of the vane in the centre of the sample. All rheological measurements were carried out in 7 mL aluminium vials to allow for heating at 37 ˚C of the sample prior to measurement. Time dependant recovery measurements were carried out by alternating the strain between 5% and 500%; conditions that could guarantee a stable gel at the lower strain and complete deformation at the higher strain. The strains were applied in 20 min (0.2%) and 30 sec (500%), followed by 30 min (0.2%)

cycles. The frequency (5 rad/sec) and temperature (37 ˚C) were kept constant throughout.

4.4.14 *In vivo* study

This study was conducted under the Animals (Scientific Procedures) Act 1986 UK Home Office Licence number PPL P435A9CF8, 19b and given ethical approval by the University of Nottingham AWERB. NCRI guidelines for the welfare and use of animals in cancer research, LASA good practice guidelines and FELASA working group on pain and distress guidelines were followed. ARRIVE Guidelines were followed in the reporting of the animal studies. 12 female CD-1 NuNu mice (12 weeks old) were obtained from Charles River (UK). Mice were maintained in IVCs (Tecniplast UK) within a barriered unit illuminated by fluorescent lights set to give a 12 h light-dark cycle (on 07.00, off 19.00), as recommended in the United Kingdom Home Office Animals (Scientific Procedures) Act 1986. The room was air-conditioned by a system designed to maintain an air temperature range of 21 ± 2 °C and a humidity of 55% + 10%. Mice were housed in social groups during the procedure with irradiated bedding and provided with autoclaved nesting materials and environmental enrichment. Daily monitoring of general health and well-being and weights was undertaken.

After injections of the different formulations, fluorescence signal was measured at 0 hr, 1 h, 2 h, 4 h, 24 h and 72 h followed by weekly imaging through IVIS Spectrum. The gels were prepared with concentration 5 mg/ml, 0.025 mg/Ml Dil or 1 mg/mL Cy5-BSA. The gel containing Dil contained 0.5% v/v ethanol in order to solubilise the hydrophobic dye. 4 different groups of mice were used: (1) gels containing Dil, (2) gels containing Cy5-BSA, (3) gel alone, and (4) Cy5-BSA in solution.

For the data processing the Living Image Software was used. Rectangular regions of interest (ROI) were drawn including the area occupied by the gel at t= 0 h. The same ROIs were used for the other time points. Fluorescence intensity values were extracted in radiance (ρ/sec/cm^2/sr) and presented in the same colour scale.

4.4.15 Inflammation markers at the site of injection

All samples (samples with gel, N=3 and a control with no gel injected) were embedded in optimal cutting temperature (OCT) compound using liquid nitrogen cooled isopentane. Sections 7 µm thick were cut from each block on a crystat (Leica, Germany) and mounted on polysilinated microscope glass slides (Menzel Gläser Polysine®; Thermo-Scientific, Germany). Following embedding and sectioning, tissue sections were fixed in 4% paraformaldehyde for 5 min and stained using haematoxylin and eosin (H&E). H&E staining was achieved by immersing samples for 2.5 min in haematoxylin, 15 s in 1% acetic industrial methylated spirits, 15 s in ammoniated water and 4 min in eosin. Following staining were dehydrated through an ethanol series (50, 70, 90, 95 and 100% ethanol for 5 min each followed by 2X xylene immersions) and glass coverslips were mounted using DPX. Following staining, tissue and cell morphology was analysed. The observer was blinded to the sample identification to avoid subconscious bias. Images were captured using a Leica CTR500 microscope (Leica Microsystems, Germany) with bright field light. For each sample several sections 200 µm apart were analysed at 5X, 10X, 20X, 40X and 60X magnifications and photomicrographs captured.

4.6 Supplementary Information

4.6.1 Structure of the hydrogelator

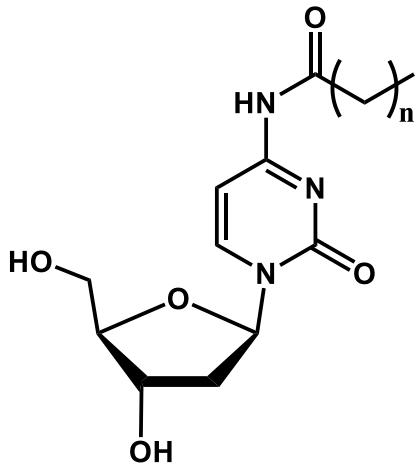

Figure 4.S1: Structure of *N*[4]-octanoyl-2'-deoxycytidine (n=6).

4.6.2 Different proteins used for gel encapsulation

Properties for the four different proteins are presented below; molecular weight (MW), isoelectric point (pI) and charge at physiological pH 7.4. Here, the properties of insulin are presented for the monomer even if the formulation used in this study was Insuman Rapid® that was found to assemble into hexamers that would disassemble into dimers/monomers in a concentration dependent fashion.[239] In the present study insulin is included as a model therapeutic protein and since its release profile did not deviate from the release profile of the other proteins, the assembly state of insulin in the supramolecular gel formulation was not further investigated.

		MW	pI	Charge at pH = 7.4
BSA	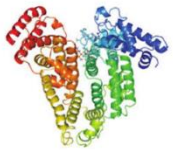	66,500	4.7	-
β-lactoglobulin		18,400	5.1	-
Lysozyme	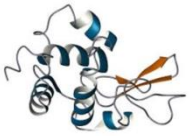	14,300	11.35	+
Insulin	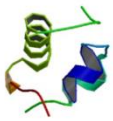	5,800	5.8	-

Figure 4.S2: Model proteins with different properties that were encapsulated in the gel. Images were extracted from Protein Data Bank (PDB) entries; Bovine Serum Albumin (BSA)- entry code 3V03, β-lactoglobulin (β-lact)- entry code 3BLG, lysozyme (lys) -entry code 1GXV, human insulin (ins)- entry code 3I3Z.

4.6.3 Formation of stable gels

Figure 4.S3: Macroscopic images of gels with and without proteins; gel, gel with Bovine Serum Albumin (BSA), gel with β-lactoglobulin (β-lact) , gel with lysozyme (lys) and gel with insulin (ins), from left to right.

4.6.4 Effect of protein on the gel's stiffness

For supramolecular gels and especially for peptide-based gelators, it has been reported that the presence of proteins can significantly alter the architecture and the mechanical properties (either make the gel stronger[122] or weaker[121]) of the co-assembled gels.[122] Here, we perform rheology measurements on the gels encapsulating different proteins and the gel alone to assess if the presence of the protein influences the properties of the gel.

The storage moduli for gels containing different proteins, as defined in the linear region during the first 20 min of the measurement at a 0.2% strain, are shown in Figure 4.S4. The mean values of the storage moduli seem to be lower for the gels in the presence of proteins as compared to gel without protein but are proven to be only statistically significantly smaller for insulin (ANOVA ($P<0.05$), $N = 5$). Considering that proteins are present in the same concentrations and the fact that insulin has a several fold smaller molecular weight (even in the hexameric form the MW is significantly smaller to BSA), it seems that it is not primarily the mass of the protein that is interfering with the gel formation, but a combination of the different properties of the protein.

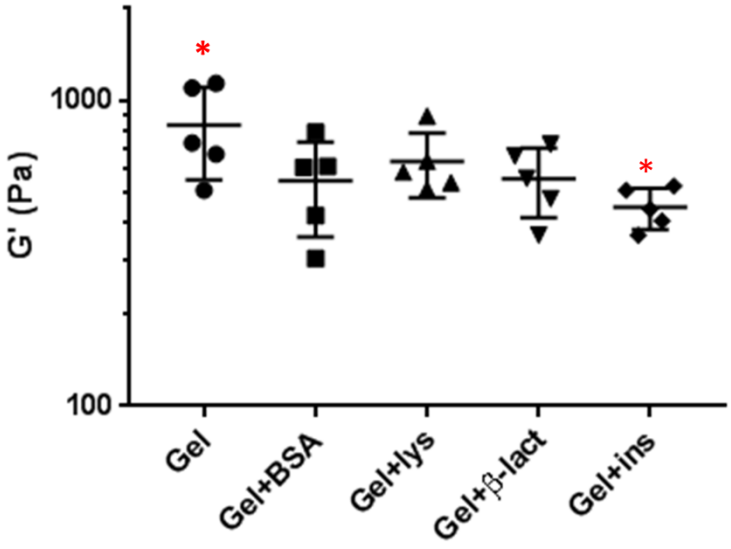

Figure 4.S4: Storage modulus values (G') from the linear region during 20 min at strain γ=0.2% and frequency ω=5 rad/sec from gels (at concentration 0.5% w/v) with the four different proteins (30 μM) and the gel alone in PBS at 37 °C (* significant difference -ANOVA (P<0.05) N=5).

4.6.5 Gel erosion

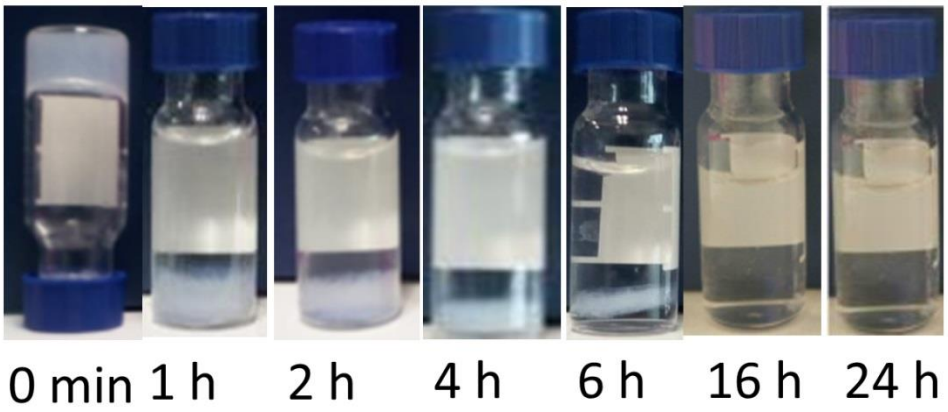

Figure 4.S5: Macroscopic images of gels exposed to PBS at 37 °C for different time periods (0 min, 1 h, 2 h, 4 h, 6 h, 16 h and 24 h), showing a gradual change in appearance as the gel degrades over time.

4.6.6 Insulin functionality assay

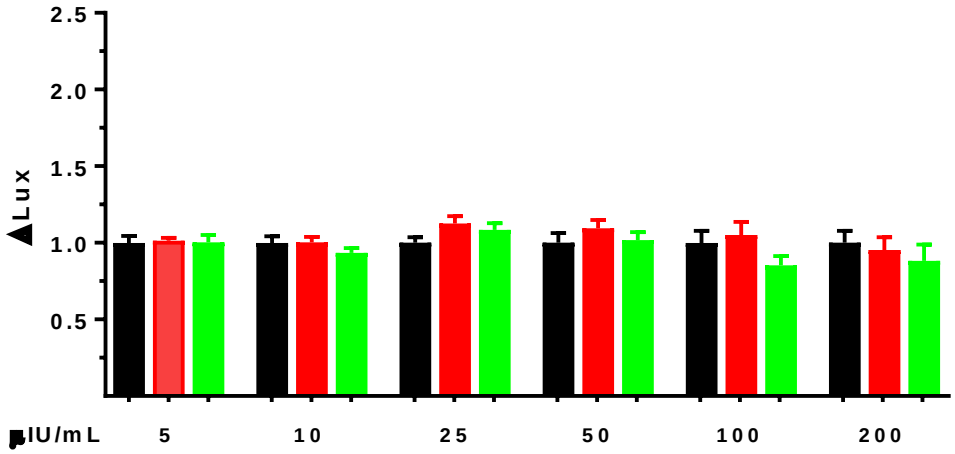

Figure 4.S6: Graph for different human insulin concentrations measured through luciferase activity on the HepG2 cell line with a mutated promoter showing no response;[229] gel alone (black trace), insulin released from gel in the presence of gelator (red trace) and insulin alone (green trace) (N=3 with 6 replicate measurements each). There was no action of the released insulin on the mutated promoter, where also there is no action of the natural insulin, indicating that the response was specific for the insulin receptor.

4.6.7 SAXS data of gels with different encapsulated molecules

All data had a buffer background subtracted and were fitted to a flexible cylinder model. In this model, either the SLD or the scale parameter need to be fixed; as such, the SLDs were calculated and fixed and the scale was allowed to refine. The length of the fibres is outside of the range which can be detected within the q range of the instrument, therefore it was fixed to be 300 nm. A Schulz polydispersity was applied to each data set. The output parameters of the model fits are shown in Table 4.S1.

Gel alone

The fit for the gel alone gave a radius of 7.3 nm and a Kuhn length of 8 nm. The radius agrees well with the radius observed by SANS (6.5 nm),[200] particularly when

the polydispersity is taken into account. The short Kuhn length indicates that the fibres within the gel alone are highly flexible.

Gel and proteins (Lysozyme, β-lactoglobulin, Insulin)

The values of the radii for the gels with lysozyme, insulin and beta lactoglobulin range between 6.5 nm and 7.1 nm which are comparable to the gel alone. The polydispersity is similar to that of the gel in all cases, being ~0.4. The Kuhn lengths are similar to that of the gel, indicating no significant stiffening. There is a pronounced peak at high q in both lysozyme and beta-lactoglobulin samples which is not present in the gel alone which is likely indicative of protein aggregates. These correspond to values of 36 nm and 13 nm respectively.

Gel and BSA

A comparison of all the samples shows that the gel with BSA deviates in its scattering most significantly from the gel alone, or the gel with other proteins. The Kuhn length and radius, as well as polydispersity are the highest of all the samples. There is also a peak at high q corresponding to a value of 18 nm which can likely be attributed to protein aggregation.

Gel and DiI (1,1'-Dioctadecyl-3,3,3',3'-tetramethylindocarbocyanine perchlorate)

The radius of the gel sample with the dye added shows an increase of the radius to 8.3 nm and a similar polydispersity to the gels with protein (except the gel + BSA). The Kuhn length is increased to 30 nm, suggesting a slight stiffening of the fibres compared to the gel alone. The high q peak is also prominent in this sample.

Table 4.S1: The model fit parameters generated by fitting the SAXS pattern of gels formed on the different surfaces with a Kratky-Porod flexible cylinder model in the SasView-4.1 analysis package.

Sample	Scale	Length / nm	Kuhn Length / nm	Radius	PD	Reduced Chi^2
Gel	0.004	300	8.0	7.3	0.39	1.3
Gel + BSA	1.04	300	75	9.2	0.54	1.3
Gel + Insulin	0.005	300	8.5	6.5	0.44	1.2
Gel + Lysozyme	0.01	300	11	7.1	0.46	1.3
Gel + β-lactoglobulin	0.06	300	11.7	6.7	0.40	1.8
Gel + Dil	0.01	300	30	8.3	0.39	1.1

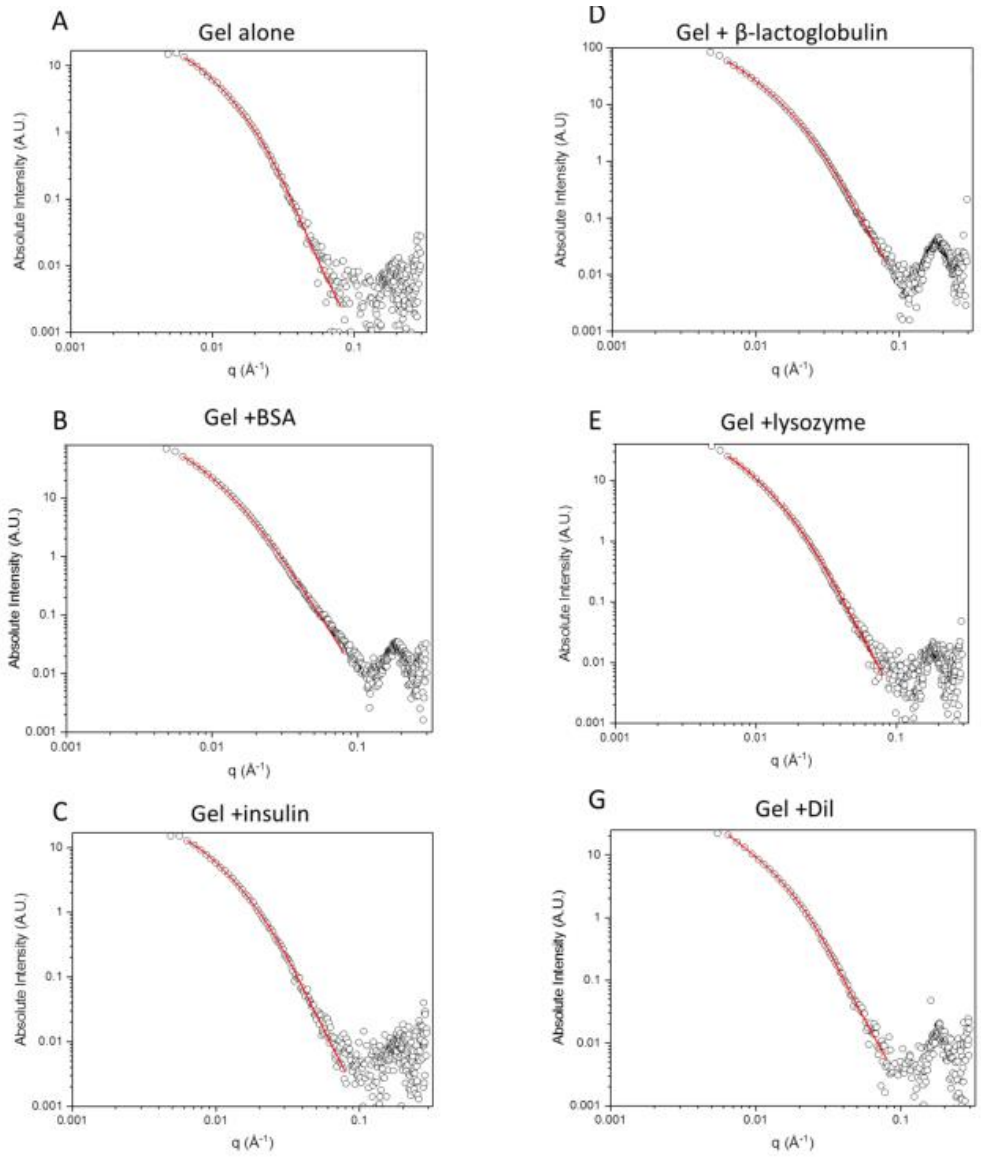

Figure 4.S7: SAXS patterns of gels (0.5% w/v) (with and without proteins, (30 µM)), the solid line on the pattern is a fit to the data with a Kratky-Porod flexible cylinder model. Data were fitted between 0.006 $Å^{-1}$ and 0.08 $Å^{-1}$.

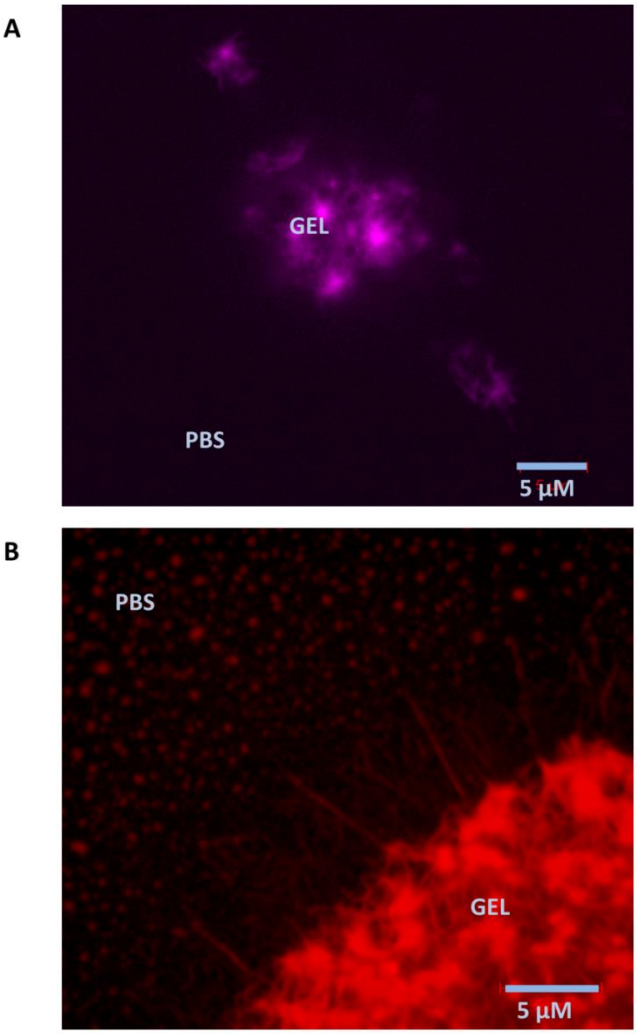

Figure 4.S8: Fluorescence microscopy images (high magnification) demonstrating the single fibres protruding out of the gel into the medium (PBS); (A) gels (0.5% w/v) encapsulating Cy5-BSA at a final concentration of 15 µM captured at 2 h incubation with PBS at 37 ˚C and (B) hydrophobic dye (DiI) at a final concentration of 8.3 µM captured after incubation with PBS for 17 h at 37 ˚C at different time points. For the Cy5 labelled protein, 647 nm laser was set to 4%, emission detected at 654 – 752nm, channel colour (LUT) was set to magenta; for DiI, 561 nm laser was set to 0.1%, emission detected at 561 – 624nm.

4.6.8 *In vitro* release of gel encapsulating a hydrophobic dye

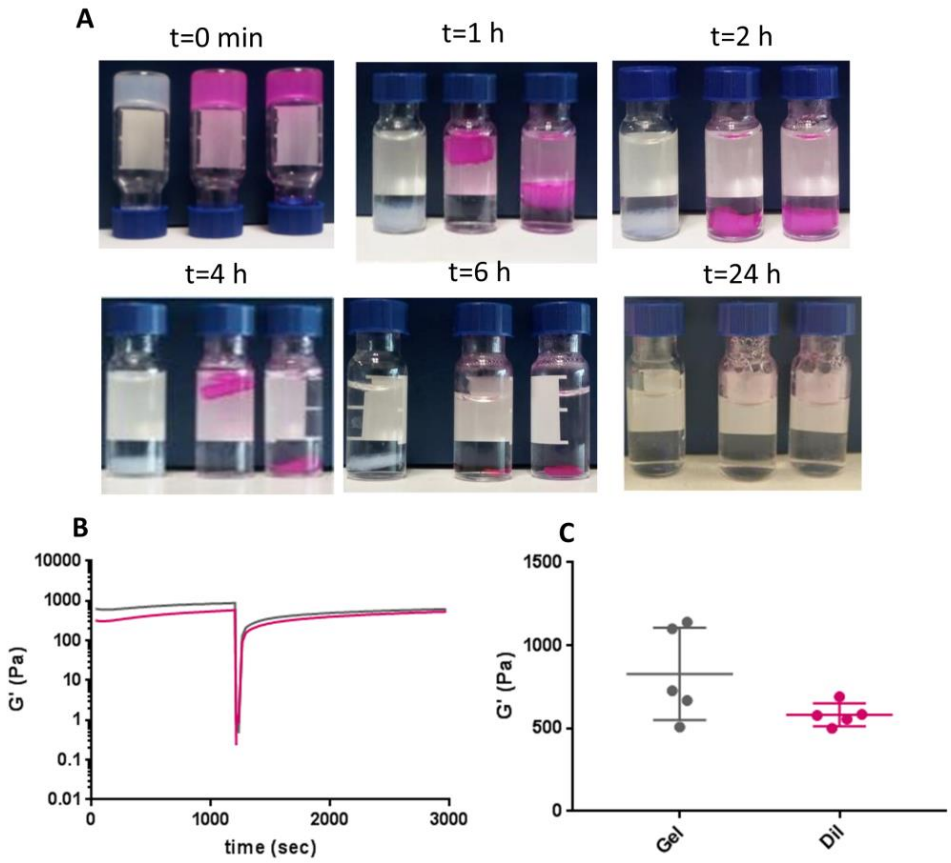

Figure 4.S9: (A) Macroscopic images of the *in vitro* erosion profile of the gel encapsulating the hydrophobic dye, DiI (pink gel) at concentration 8.3 µm/ml compared to plain gel (colourless gel) at different time points. Gels were subject to the same process as the protein in-vitro release data of the gels with proteins presented in Figure 4.3 0.5 ml of gel (0.5 % w/v) was incubated with 1 ml PBS at 37 ˚C. (B) Oscillatory rheology time recovery data of the gel with (DiI) and gel alone (grey trace) for number of repeats N=5. Data were recorded for 20 min (γ= 0.2 %, ω=5 rad/s) and then the gel was disrupted for 30 sec (γ=500%, ω=5 rad/s), the gel was left to reform for 30 min (γ= 0.2 %, ω=5 rad/s) at 37 ˚C. (C) Storage modulus values determined through the linear region of the time dependent measurements for the first 20 min are presented for the gel encapsulating the DiI and gel alone.

4.6.9 Calibration curves

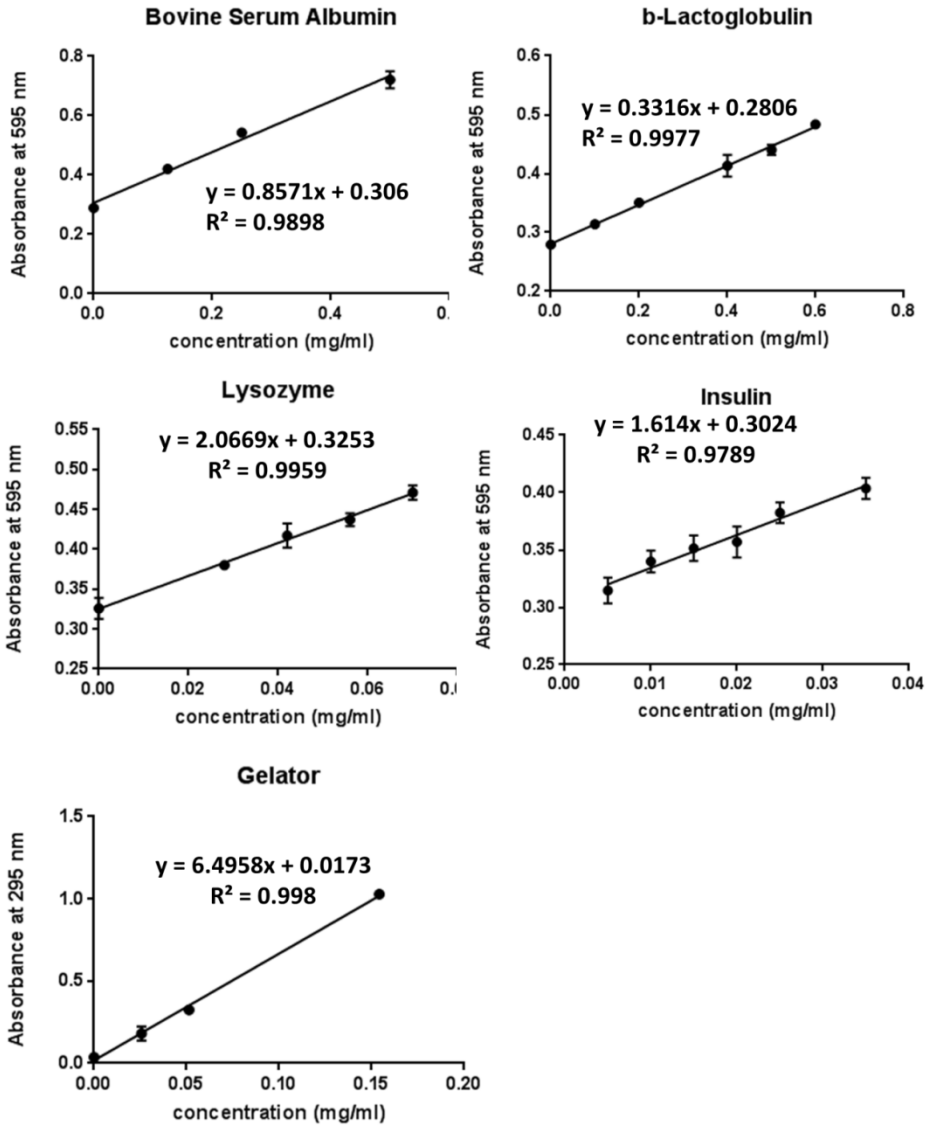

Figure 4.S10: Calibration curves for proteins and gel quantification in release studies. Proteins are quantified through the Bradford assay.

4.6.10 Structural characterisation of the gelator

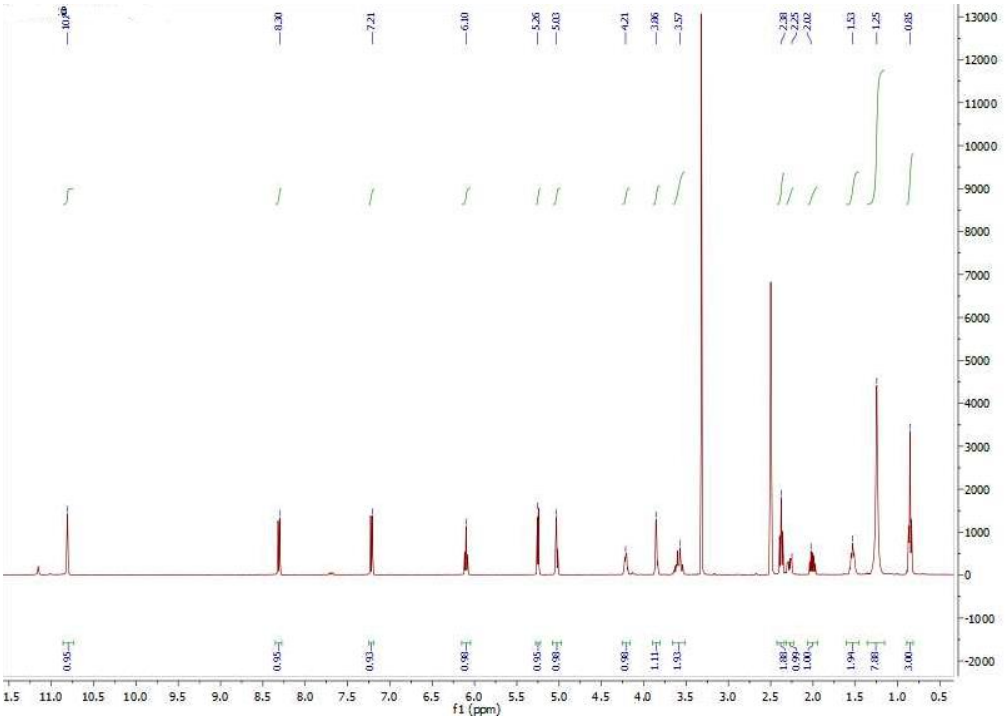

Figure 4.S11: ^{1}H NMR spectrum of *N*^{4}-octanoyl-2'-deoxycytidine in deuterated DMSO. Details of the peak assignment can be found in previously published work.[51]

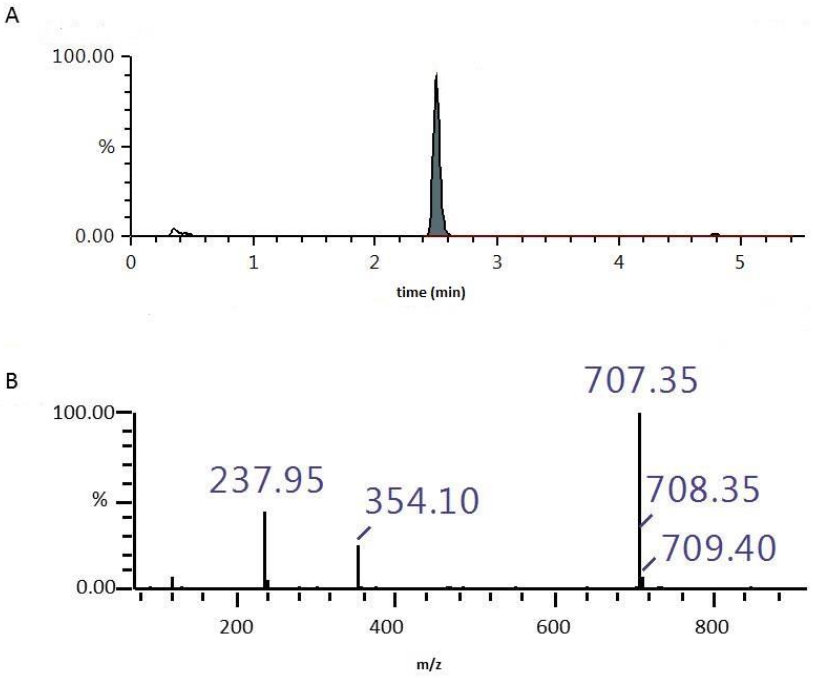

Figure 4.S12: LC-MS analysis of N^4-octanoyl-2'-deoxycytidine in methanol. Purity determined from the chromatogram as 99% (by height) and 98% (by area) by UV at 254 nm (A). MS spectrum with main ions detected at m/z 237.95 [N^4-octanoyl-cytosine + H]$^+$, 354.10 [M+H]$^+$ and 707.35 [2M + H]$^+$.

4.6.11 Purity of Cy5-labelled Bovine Serum Albumin

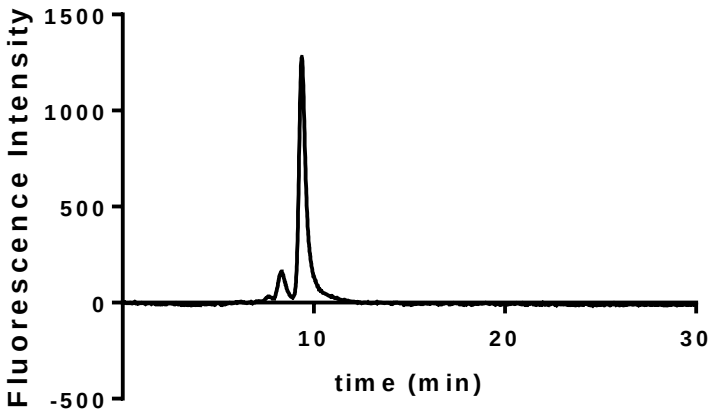

Figure 4.S13: Size Exclusion Chromatogram of Cy5-BSA recording emission at λ_{em} = 666 nm, with excitation fixed at λ_{ex} = 644 nm. The peak at t= 8.3 min corresponds to the Cy5-BSA. Minor peaks between t=7 and t=9 min correspond to BSA dimer and trimer, which have been previously observed in commercial BSA and have been correlated to intermolecular disulphide bridges.[240-241] No peak was detected for the non-bound dye at the later time points, indicating the purity of the labelled protein.

4.7 General Conclusions

In Chapter 4, we investigated how the presence of different encapsulated molecules can affect the properties of supramolecular gels. In the presence of a hydrophobic small molecule and proteins with different properties (MW, pI), a nanoscopic network of entangled fibres was formed that gave stable gels macroscopically. The encapsulated molecules interacted non-covalently with the gel fibres and got released after the degradation of the gel. The gels were injected subcutaneously in mice that were healthy when sacrificed after two weeks. The gel degraded within two weeks and there were no signs of inflammation at the site of injection. This work demonstrates one of the first mechanistic investigations of how supramolecular gels encapsulate and release bioactive molecules *in vitro* and *in vivo,* highlighting the promising potential of supramolecular gels as biodegradable and biocompatible drug delivery systems.

Chapter 5

Conclusions and Future work

5.1 Conclusions

This work was conducted on three parallel interdependent axis: i) the mechanism and the driving forces regulating the self-assembly, ii) the design of simple model-interfaces that can explain how different chemical functionalities interfere with the self-assembly and alter the physical and mechanical gel properties and iii) the understanding and development of supramolecular gels as drug delivery systems encapsulating a range of molecules from small hydrophobic dyes to bulky biomolecules such as proteins *in vitro* and *in vivo*. In our studies we used a family of nucleoside-based gelators, previously synthesized by our group, that have been shown to form stable gels in different mixtures of organic solvents and water. [51, 133] Mainly we focused on the one member of the family that forms a stable, self-healing hydrogel, the N^4-octanoyl-2'-deoxycytidine.[51] The absence of any solvent is particularly favourable for the encapsulation of biomolecules that tend to denature and reduce/lose their functionality such as proteins in the presence of organic solvents.

These three strands of work, (i) mechanism of self-assembly, (ii) characterisation of interfacial interactions between gelators and chemical functionalities and (iii) the development of supramolecular gels as drug delivery systems, are interconnected and an understanding of all the three areas is required in order for a supramolecular gel to evolve into an optimized drug delivery system. Here, we employed a ''bottom-up'' approach starting from establishing the mechanism of the self-assembly of the

gelator alone and eventually building up our understanding as the complexity of the system under study was increasing.

5.1.1 Understanding the mechanism of the self-assembly of a nucleoside-based gelator

In Chapter 2, we employed experimental analytical techniques together with molecular dynamics simulations to identify the mechanistic pathway that the nucleoside-based self-assembling molecules follow to form the nanoarchitectures that macroscopically result in the self-supporting gel. The molecules of the cytidine-based gelator directed by hydrophobic/solvophobic forces orient themselves in order to form cylindrical fibres with the aliphatic chain towards the inside of the fibre and the hydrophilic sugars protruding towards the outside surface of the fibre. The aromatic nucleobases stack together through π-π stacking interactions while hydrogen bonds through the sugar or the nucleobase stabilise the structure. Through these molecular orientations a hydrophobic core is generated within the fibres whereas the surrounding of the fibre constitutes a very polar environment where solvent molecules reside. This distinct dual hydrophobic/hydrophilic environment will constitute the basis for the potential applications of these materials in drug delivery in the encapsulation of molecules with different properties. Finally, this study presented a solid demonstration of the complementarity of the experimental and MD approaches, that both provide with essential information in order to build the different steps in the self-assembly process. These mechanistic aspects that have been hardly investigated for nucleic acid-based hydrogels in general and especially for cytidine-based hydrogels have never been explored, contribute in building fundamental understanding for these materials paving the way for tailored drug delivery systems. Having established a

comprehensive understanding of the self-assembly mechanism for this family of gelators, we moved on to more complex systems and exposed the gel to simple, well-described chemically modified surfaces in order to model the interactions on simple interfaces.

5.1.2 Understanding the interfacial interactions between gelator molecules and different chemical entities

In Chapter 3, we aimed to understand how different chemical functionalities related to the gelators' structure can influence the self-assembly formation. Different interfaces between different gelators (members of the family of gelators consisting of 2'-deoxycytidine (or cytidine) conjugated to alkyl chains with different number of carbons and surfaces with different chemical groups were generated and studied with different surface-sensitive techniques. In the first part, thin gel films of N^4-tetradecanoyl-cytidine were generated on two very different surfaces (a very hydrophobic and a very hydrophilic one) to demonstrate with AFM imaging and AFM nanoindentation measurements that the physical (fibre diameter) and mechanical properties of dry films are significantly different on the two surfaces. This preliminary study established for the first time that different chemistries immobilized on flat surfaces can have a significant effect on the supramolecular structures, The value of the conclusions generated in this first study was limited by two important factors: (1) gel films were studied in the dry state and (2) even if the gel thickness was very low (< 1 μm), data information was accessed through the air-gel interface and not the gel-substrate. In the second part, gel films of different 2'-deoxycytidine gelators were formed on surfaces with a range of different chemistries. Different surface properties related to the surface chemistry (surface descriptors) were calculated and measured for these surfaces and the key

parameters that relate directly to the self-assembled structures formed were identified through linear regression analyses. The logP value and the polar surface area (PSA) of the surfaces were found to linearly relate to the diameter of the fibre bundles of the N^4-tetradecanoyl-2'-deoxycytidine. These findings correlate hydrophobic surfaces with lower degrees of fibre bundling and highlight again the influence that hydrophobicity has on amphiphilic self-assembling systems. Overall in this chapter, unique information into these interfacial interactions was given that has not been accessed in previous studies in the field. Further to this, it was established that different chemical functionalities can affect the properties of the self-assembled structures suggesting that encapsulated molecules with complex chemistries are likely to interact with the self-assembled gelator and impact its final properties. Moving on to the next level of complexity, we proceed to composite gel systems where we encapsulate different molecules and study the properties of the bulk gel. The interactions between different encapsulated molecules and this cytidine-based gel as well as their effect on the final gels will be discussed in Chapter 4.

5.1.3 A 2'-deoxycytinde-based gelator as a drug delivery system

In Chapter 4, we investigated different aspects of the behaviour of a novel nucleoside-based gel *in vitro* and *in vivo* as a drug delivery system for a range of therapeutically relevant molecules with different properties. Firstly, proteins with different properties (MW, pI) were encapsulated in the gel and released in a sustained way following the erosion profile of the gel. Fluorescence microscopy and spectroscopy as well as Small Angle X-ray scattering were used to demonstrate that the proteins were directly associated with the gel's fibres. At the same time, in the presence of proteolytic enzymes, it was shown that the gel protects the

encapsulated proteins integrity against enzymatic degradation. In vivo, after two weeks the gel had completely degraded, there was no toxicity and no signs of inflammation, demonstrating the biodegradability of the material. Furthermore, in this work we present an in-depth, comprehensive understanding of the encapsulation and the release mechanism of a range of molecules for supramolecular gels that can provide with novel, unique information on the *in vivo* behaviour of the supramolecular gels as drug delivery systems. Finally, this study provides a solid demonstration of how bioactive molecules with different properties can significantly impact the supramolecular gels nano- and macro- properties, establishing the need for mechanistic investigations in order for these materials to reach their maximum potential in the challenging drug delivery field.

To conclude, the work included in this thesis aimed to contribute to the understanding of the gelation principles, characterise how different interactions are represented structurally on simple interfaces and finally describe and understand mechanistically the potential of supramolecular gels as depot drug delivery systems for sustained release of molecules with different properties. In Chapter 2, the mechanism of the self-assembly for this class of amphiphilic gelators was established and the importance of the hydrophobic forces and the π-π stacking as the driving forces of the self-assembly were identified. Driven by these forces the gelator molecules orient themselves, generating a hydrophobic core. These observations are in line with the mechanistic principles underlying other more well-described gelators, for example peptide-based ones, that have so far attracted significant attention in the biomedical field. Nucleoside-based hydrogelators are also bio-derived molecules that are stable against proteolytic degradation, an important issue with peptide-based gelators. In Chapter 3, when different surface descriptors

were assessed as the ones that directly relate to the formation of higher order structures, logP (that directly estimates the hydrophobicity of the surface) as well as the presence of aromatic rings were found to significantly relate with the higher order associations, confirming the importance of the findings in Chapter 3. As identified in Chapter 2, hydrophobic interactions and π-π stacking are driving the self-assembly whereas at the same time a highly hydrophobic interface or the interfacial presence of aromatic rings can affect the characteristics of the higher order structures (Chapter 3). In Chapter 4, among the interactions mediating the encapsulation of different molecules, hydrophobic interactions and π-π stacking were again identified to play an important role. In the case of the small hydrophobic molecule, it was shown that it was directly encapsulated in the hydrophobic core, whereas in the case of bigger more hydrophilic proteins, π-π stacking was demonstrated to contribute in the association of these molecules with the gel fibres. Finally, hydrophobic interactions and π-π stacking govern the first and higher order self-assembled structure formation, whereas they mediate the encapsulation of different compounds into the self-assembled hydrogels.

Overall, in this work the amphiphilicity of the gelators, and especially the presence of the hydrophobic moiety, is emerging as the key factor for the gel formation and the potential uses of these systems in the drug delivery. Having approached the system through different perspectives, the same conclusion arose every time: the presence of the hydrophobic domain in the solid phase is holding the self-assembled structures together, whereas at the same time is responsible (potentially other non-covalent forces are contributing as well) for the generation of the non-covalent interactions (hydrophobic and π-π stacking) with the encapsulated molecules that hold them associated with the fibrillar network. Even if the importance of the

amphiphilic nature of the molecules as well as the duality of the environments of supramolecular gels have been vastly exploited in drug delivery,[9, 46, 108] this was mostly done empirically but also scarcely used to design tailored drug delivery systems.

5.2 Future perspectives

The component of modelling the interfacial interactions between gelators and substrates with desirable properties is of great importance in the present work (chapter 3). The attempt to simplify the complexity of biologically relevant bio-interfaces has been a challenging task and only a solid proof of concept has been achieved during these three years. This work achieved to (i) generate and characterise a range of surfaces with different chemistries (but similar roughness), (ii) establish a toolkit to structurally characterise the interfacial architectures formed in the dry and wet state and the nanomechanical properties in the dry state, and ultimately (iii) demonstrate that specific interactions can be initiated from the interfaces, at the moment solely structurally described in the wet state. Following the characterization of the nanomechanical properties of the dry gels, further work should include the characterisation of the nanomechanical properties of the gels in the wet state.

In addition to this, in this work, among the pool of different surface properties (chemistry, curvature, roughness and charge etc.), we only investigated the effect of different chemistries on the self-assembly. At the same time we tried to rule out (to allow for systematic analysis) other important surface properties that would provide with particularly exciting insight into the way other therapeutically relevant components with applications in tissue engineering and drug delivery affect the

properties of the supramolecular gels. For example modelling interfaces with different properties such as different degrees of curvature/shapes, roughness and charge could give precious information on how supramolecular gels interact with cells, or nanoparticles. For example, unpublished data from our group demonstrated that when nanocapsules of different sizes (80 nm to 250 nm) were encapsulated in the supramolecular gels they disrupted the gel formation and much higher concentrations of the gelator were required for the gel to form. In the presence of the nanocapsules, the gels were stiffer compared to the gels alone as observed by rheology measurements of the bulk gel. Nanocapsules and other polymeric nanoparticles are complex systems that consist of different sizes (as well as distributions of sizes) and very complex external surfaces. Modelling these systems on the interface and eventually the bulk gel as well as understanding how the different components/properties/characteristics mechanistically contribute to the properties of the final composite systems would be a very exciting question to answer.

The final objective of this work was the demonstration of this supramolecular gel's advantages as a drug delivery system. In the last chapter, model molecules were used to investigate and understand the material *in vivo*, but time did not allow for an *in vivo* assessment of its efficacy with pharmacologically active molecules. Therapeutic antibodies would be interesting to be encapsulated and demonstrate their therapeutic efficacy after release in animal models. Small therapeutic hydrophobic molecules such as doxorubicin could also be encapsulated and evaluated in vivo. These molecules structurally resembling to this class of gelators could potentially co-assemble with the gelator molecules and produce materials with novel, exciting behaviour and unique properties.

Another scientifically challenging area of the self-assembly that has not been investigated for pharmacological applications is the area of multicomponent supramolecular gels (consisting of different LMWGs). For several years there has been a lot interest around multicomponent supramolecular gels (two or more LMWGs) that even if initially appeared complex to understand,[15, 242] landmark work[124, 243-244] demonstrated that mixtures of two or more gelators can controllably result in uniquely organised structures that can provide with new ways to tune their properties. Several self-assembling prodrugs have been widely reported.[9] For example, recently published work from our group demonstrated a series of pharmacologically active derivatives of gemcitabine and lamivudine that self-assembled into stable gels.[245] Combining two different self-assembling molecules together, a simple gelator and a prodrug gelator or two prodrug gelators, responsive to different triggers if possible, could lead to drug delivery systems that could release different active ingredients in different release profiles with improved therapeutic efficacies.

Furthermore, this work (Chapter 4) demonstrated that in the same material (not simultaneously) therapeutic molecules with very different properties could be encapsulated (from small hydrophobic molecules to large biomolecules). Regarding this, it would be interesting to encapsulate two therapeutic molecules with different properties in the same gel at the same time, for example a large therapeutic biomolecule such as an antibody and a small hydrophobic one such as doxorubicin and explore the properties of the final formulation as well as the combined therapeutic effect in vivo.

Additionally, in chapter 4 we reported a property of the N^4-octanoyl-2'-deoxycytidine that has not been reported for other nucleoside—based gelators that

have been tested *in vivo*;[83, 116] the ability to break down in vivo and leave no macroscopic traces of the gels. This *in vivo* behaviour demonstrates the material's *in vivo* biodegradability but on the other hand (*in vitro* data showed gel erosion within 24 hours), relatively longer (several days to weeks) *in vivo* stability would be desirable. An interesting way to address this issue would be to generate hybrid gels combining LMWG with polymers as has been previously suggested.[246] Previous pioneering work in the field[246-249] demonstrated that these hybrid gels have promising applications in drug delivery as they can yield robust, responsive systems where each of their components maintains its own characteristic properties. In an important piece of work, it was clearly demonstrated that the presence of agarose can stiffen the supramolecular gel as well as provide with an extra level of control in the release of the pharmaceutically active component (heparin).[250] Following a similar approach, it would be of particular interest to combine the N^4-octanoyl-2'-deoxycytidine with different polymers that yield gels themselves (agarose or gelatin) and study the properties of the advanced composite systems.

Supramolecular gels are a fascinating class of materials with unique potential to finely tune their properties. Their unusual responsiveness to various external stimuli (yielding different responses) requires detailed investigations of the principles underlying the mechanism behind it. Once this holistic mechanistic picture is elucidated, creativity and imagination are the only components required to exploit the potential of these materials.

References

1. Pilpel, N., Properties of Organic Solutions of Heavy Metal Soaps. *Chemical Reviews* **1963,** *63*, 221-234.
2. Flory, P.J., Introductory lecture. *Faraday Discussions of the Chemical Society* **1974,** *57*, 7-18.
3. Weiss, R. G., Preface to the molecular and polymer gels; materials with self-assembled fibrillar networks special issue. ACS Publications: 2009.
4. Rubinstein, M.; Colby, R. H., *Polymer physics*. Oxford University Press New York: 2003; Vol. 23.
5. Sangeetha, N. M.; Maitra, U., Supramolecular gels: Functions and uses. *Chemical Society Reviews* **2005,** *34*, 821-836.
6. Steed, J. W., Supramolecular gel chemistry: developments over the last decade. *Chemical Communications* **2011,** *47*, 1379-1383.
7. Amabilino, D. B.; Smith, D. K.; Steed, J. W., Supramolecular materials. *Chemical Society Reviews* **2017,** *46*, 2404-2420.
8. Branco, M. C.; Schneider, J. P., Self-assembling materials for therapeutic delivery. *Acta Biomaterialia* **2009,** *5*, 817-831.
9. Skilling, K. J.; Citossi, F.; Bradshaw, T. D.; Ashford, M.; Kellam, B.; Marlow, M., Insights into low molecular mass organic gelators: a focus on drug delivery and tissue engineering applications. *Soft Matter* **2014,** *10*, 237-256.
10. Du, X.; Zhou, J.; Shi, J.; Xu, B., Supramolecular hydrogelators and hydrogels: from soft matter to molecular biomaterials. *Chemical Reviews* **2015,** *115*, 13165-13307.
11. Escuder, B.; Miravet, J. F., *Functional molecular gels*. Royal Society of Chemistry: 2013.
12. Estroff, L. A.; Hamilton, A. D., Water gelation by small organic molecules. *Chemical Reviews* **2004,** *104*, 1201-1218.
13. Draper, E. R.; Adams, D. J., Low-molecular-weight gels: the state of the art. *Chem* **2017,** *3*, 390-410.
14. Nuthanakanti, A.; Srivatsan, S. G., Hierarchical self-assembly of switchable nucleolipid supramolecular gels based on environmentally-sensitive fluorescent nucleoside analogs. *Nanoscale* **2016,** *8*, 3607-3619.
15. Raeburn, J.; Adams, D. J., Multicomponent low molecular weight gelators. *Chemical Communications* **2015,** *51*, 5170-5180.
16. Lin, Y. C.; Weiss, R. G., Liquid-crystalline solvents as mechanistic probes. 24. A novel gelator of organic liquids and the properties of its gels. *Macromolecules* **1987,** *20*, 414-417.
17. Gupta, J. K.; Adams, D. J.; Berry, N. G., Will it gel? Successful computational prediction of peptide gelators using physicochemical properties and molecular fingerprints. *Chemical Science* **2016,** *7*, 4713-4719.
18. Adams, D. J.; Mullen, L. M.; Berta, M.; Chen, L.; Frith, W. J., Relationship between molecular structure, gelation behaviour and gel properties of Fmoc-dipeptides. *Soft Matter* **2010,** *6*, 1971-1980.
19. Hirst, A. R.; Coates, I. A.; Boucheteau, T. R.; Miravet, J. F.; Escuder, B.; Castelletto, V.; Hamley, I. W.; Smith, D. K., Low-molecular-weight

gelators: elucidating the principles of gelation based on gelator solubility and a cooperative self-assembly model. *Journal of the American Chemical Society* **2008,** *130*, 9113-9121.
20. Terech, P.; Weiss, R. G., Low molecular mass gelators of organic liquids and the properties of their gels. *Chemical reviews* **1997,** *97*, 3133-3160.
21. Weiss, R. G.; Terech, P., *Molecular gels: materials with self-assembled fibrillar networks*. Springer Science & Business Media: 2006.
22. Mukkamala, R.; Weiss, R. G., Physical Gelation of Organic Fluids by Anthraquinone− Steroid-Based Molecules. Structural Features Influencing the Properties of Gels. *Langmuir* **1996,** *12*, 1474-1482.
23. Mukkamala, R.; Weiss, R. G., Anthraquinone–steroid based gelators of alcohols and alkanes. *Journal of the Chemical Society, Chemical Communications* **1995,** 375-376.
24. Zweep, N.; van Esch, J. H., *The Design of Molecular Gelators*. Royal Society of Chemistry: Cambridge, UK: 2013; Vol. 1.
25. Tachibana, T.; Kambara, H., The sense of twist in the fibrous aggregates from 12-hydroxystearic acid and its alkali metal soaps. *Journal of Colloid and Interface Science* **1968,** *28*, 173-174.
26. Terech, P., Small-angle-scattering study of 12-hydroxystearic physical organogels and lubricating greases. *Colloid and polymer science* **1991,** *269*, 490-500.
27. Yoza, K.; Amanokura, N.; Ono, Y.; Akao, T.; Shinmori, H.; Takeuchi, M.; Shinkai, S.; Reinhoudt, D. N., Sugar-Integrated Gelators of Organic Solvents—Their Remarkable Diversity in Gelation Ability and Aggregate Structure. *Chemistry–A European Journal* **1999,** *5*, 2722-2729.
28. Gronwald, O.; Shinkai, S., Sugar-integrated gelators of organic solvents. *Chemistry–A European Journal* **2001,** *7*, 4328-4334.
29. Hanabusa, K.; Kobayashi, H.; Suzuki, M.; Kimura, M.; Shirai, H., Organogel from L-leucine-containing surfactant in nonpolar solvents. *Colloid and Polymer Science* **1998,** *276*, 252-259.
30. Debnath, S.; Shome, A.; Dutta, S.; Das, P. K., Dipeptide-Based Low-Molecular-Weight Efficient Organogelators and Their Application in Water Purification. *Chemistry–A European Journal* **2008,** *14*, 6870-6881.
31. Simeone, L.; Milano, D.; De Napoli, L.; Irace, C.; Di Pascale, A.; Boccalon, M.; Tecilla, P.; Montesarchio, D., Design, Synthesis and Characterisation of Guanosine-Based Amphiphiles. *Chemistry–A European Journal* **2011,** *17*, 13854-13865.
32. Godeau, G.; Barthélémy, P., Glycosyl-nucleoside lipids as low-molecular-weight gelators. *Langmuir* **2009,** *25*, 8447-8450.
33. Wang, G.; Hamilton, A. D., Low molecular weight organogelators for water. *Chemical Communications* **2003,** 310-311.
34. Matteucci, M.; Bhalay, G.; Bradley, M., A combinatorial approach to the synthesis of cystine based organogelators. *Journal of peptide science* **2004,** *10*, 318-325.
35. Suzuki, M.; Yumoto, M.; Kimura, M.; Shirai, H.; Hanabusa, K., A Family of Low-Molecular-Weight Hydrogelators Based on L-Lysine Derivatives with a Positively Charged Terminal Group. *Chemistry–A European Journal* **2003,** *9*, 348-354.

36. Suzuki, M.; Yumoto, M.; Kimura, M.; Shirai, H.; Hanabusa, K., Hydrogel Formation Using New L-Lysine-Based Low-Molecular-Weight Compounds with Positively Charged Pendant Chains. *Helvetica Chimica Acta* **2003,** *86*, 2228-2238.
37. Suzuki, M.; Hanabusa, K., L-Lysine-based low-molecular-weight gelators. *Chemical Society Reviews* **2009,** *38*, 967-975.
38. Ryan, D. M.; Anderson, S. B.; Senguen, F. T.; Youngman, R. E.; Nilsson, B. L., Self-assembly and hydrogelation promoted by F 5-phenylalanine. *Soft Matter* **2010,** *6*, 475-479.
39. Ryan, D. M.; Doran, T. M.; Anderson, S. B.; Nilsson, B. L., Effect of C-terminal modification on the self-assembly and hydrogelation of fluorinated Fmoc-Phe derivatives. *Langmuir* **2011,** *27*, 4029-4039.
40. Mahler, A.; Reches, M.; Rechter, M.; Cohen, S.; Gazit, E., Rigid, self-assembled hydrogel composed of a modified aromatic dipeptide. *Advanced Materials* **2006,** *18*, 1365-1370.
41. Orbach, R.; Mironi-Harpaz, I.; Adler-Abramovich, L.; Mossou, E.; Mitchell, E. P.; Forsyth, V. T.; Gazit, E.; Seliktar, D., The rheological and structural properties of Fmoc-peptide-based hydrogels: the effect of aromatic molecular architecture on self-assembly and physical characteristics. *Langmuir* **2012,** *28*, 2015-2022.
42. Yang, Z.; Liang, G.; Ma, M.; Gao, Y.; Xu, B., Conjugates of naphthalene and dipeptides produce molecular hydrogelators with high efficiency of hydrogelation and superhelical nanofibers. *Journal of Materials Chemistry* **2007,** *17*, 850-854.
43. Chen, L.; Revel, S.; Morris, K.; C. Serpell, L.; Adams, D. J., Effect of molecular structure on the properties of naphthalene− dipeptide hydrogelators. *Langmuir* **2010,** *26*, 13466-13471.
44. Kiyonaka, S.; Sugiyasu, K.; Shinkai, S.; Hamachi, I., First thermally responsive supramolecular polymer based on glycosylated amino acid. *Journal of the American Chemical Society* **2002,** *124*, 10954-10955.
45. Yan, N.; He, G.; Zhang, H.; Ding, L.; Fang, Y., Glucose-based fluorescent low-molecular mass compounds: creation of simple and versatile supramolecular gelators. *Langmuir* **2009,** *26*, 5909-5917.
46. Peters, G. M.; Davis, J. T., Supramolecular gels made from nucleobase, nucleoside and nucleotide analogs. *Chemical Society Reviews* **2016,** *45*, 3188-3206.
47. Moreau, L.; Barthélémy, P.; El Maataoui, M.; Grinstaff, M. W., Supramolecular assemblies of nucleoside phosphocholine amphiphiles. *Journal of the American Chemical Society* **2004,** *126*, 7533-7539.
48. Park, S. M.; Lee, Y. S.; Kim, B. H., Novel low-molecular-weight hydrogelators based on 2′-deoxyuridine. *Chemical Communications* **2003,** 2912-2913.
49. Park, S. M.; Shen, Y.; Kim, B. H., Water gelation abilities of alkylbenzyltriazole-appended 2′-deoxyribonucleoside and ribonucleoside. *Organic & biomolecular chemistry* **2007,** *5*, 610-612.
50. Park, S. M.; Kim, B. H., Ultrasound-triggered water gelation with a modified nucleoside. *Soft Matter* **2008,** *4*, 1995-1997.

51. Skilling, K. J.; Kellam, B.; Ashford, M.; Bradshaw, T. D.; Marlow, M., Developing a self-healing supramolecular nucleoside hydrogel. *Soft Matter* **2016,** *12*, 8950-8957.
52. Snip, E.; Shinkai, S.; Reinhoudt, D. N., Organogels of a nucleobase-bearing gelator and the remarkable effects of nucleoside derivatives and a porphyrin derivative on the gel stability. *Tetrahedron letters* **2001,** *42*, 2153-2156.
53. Godeau, G.; Bernard, J.; Staedel, C.; Barthélémy, P., Glycosyl–nucleoside–lipid based supramolecular assembly as a nanostructured material with nucleic acid delivery capabilities. *Chemical Communications* **2009,** 5127-5129.
54. Li, X.; Kuang, Y.; Lin, H. C.; Gao, Y.; Shi, J.; Xu, B., Supramolecular nanofibers and hydrogels of nucleopeptides. *Angewandte Chemie* **2011,** *123*, 9537-9541.
55. Du, X.; Zhou, J.; Shi, J.; Xu, B., Supramolecular hydrogelators and hydrogels: from soft matter to molecular biomaterials. *Chem. Rev* **2015,** *115*, 13165-13307.
56. Rodrigues, M.; Calpena, A. C.; Amabilino, D. B.; Garduño-Ramírez, M. L.; Pérez-García, L., Supramolecular gels based on a gemini imidazolium amphiphile as molecular material for drug delivery. *Journal of Materials Chemistry B* **2014,** *2*, 5419-5429.
57. Howe, E. J.; Okesola, B. O.; Smith, D. K., Self-assembled sorbitol-derived supramolecular hydrogels for the controlled encapsulation and release of active pharmaceutical ingredients. *Chemical Communications* **2015,** *51*, 7451-7454.
58. Jonkheijm, P.; van der Schoot, P.; Schenning, A. P.; Meijer, E., Probing the solvent-assisted nucleation pathway in chemical self-assembly. *Science* **2006,** *313*, 80-83.
59. Avrami, M., Kinetics of phase change. I General theory. *The Journal of Chemical Physics* **1939,** *7*, 1103-1112.
60. Avrami, M., Kinetics of phase change. II transformation-time relations for random distribution of nuclei. *The Journal of Chemical Physics* **1940,** *8*, 212-224.
61. Avrami, M., Granulation, phase change, and microstructure kinetics of phase change. III. *The Journal of chemical physics* **1941,** *9*, 177-184.
62. Weiss, R. G., The past, present, and future of molecular gels. What is the status of the field, and where is it going? *Journal of the American Chemical Society* **2014,** *136*, 7519-7530.
63. Huang, X.; Terech, P.; Raghavan, S. R.; Weiss, R. G., Kinetics of 5α-cholestan-3β-yl N-(2-naphthyl) carbamate/n-alkane organogel formation and its influence on the fibrillar networks. *Journal of the American Chemical Society* **2005,** *127*, 4336-4344.
64. Liu, X. Y.; Sawant, P. D., Mechanism of the formation of self-organized microstructures in soft functional materials. *Advanced Materials* **2002,** *14*, 421-426.
65. Li, J.-L.; Yuan, B.; Liu, X.-Y.; Wang, R.-Y.; Wang, X.-G., Control of crystallization in supramolecular soft materials engineering. *Soft Matter* **2013,** *9*, 435-442.

66. Ramos Sasselli, I.; Halling, P. J.; Ulijn, R. V.; Tuttle, T., Supramolecular fibers in gels can be at thermodynamic equilibrium: a simple packing model reveals preferential fibril formation versus crystallization. *ACS nano* **2016,** *10*, 2661-2668.
67. Terech, P., Metastability and sol phases: two keys for the future of molecular gels? *Langmuir* **2009,** *25*, 8370-8372.
68. Raeburn, J.; Cardoso, A. Z.; Adams, D. J., The importance of the self-assembly process to control mechanical properties of low molecular weight hydrogels. *Chemical Society Reviews* **2013,** *42*, 5143-5156.
69. Tantakitti, F.; Boekhoven, J.; Wang, X.; Kazantsev, R. V.; Yu, T.; Li, J.; Zhuang, E.; Zandi, R.; Ortony, J. H.; Newcomb, C. J., Energy landscapes and functions of supramolecular systems. *Nature materials* **2016,** *15*, 469.
70. Grzybowski, B. A.; Wilmer, C. E.; Kim, J.; Browne, K. P.; Bishop, K. J., Self-assembly: from crystals to cells. *Soft Matter* **2009,** *5*, 1110-1128.
71. Grzybowski, B. A.; Fitzner, K.; Paczesny, J.; Granick, S., From dynamic self-assembly to networked chemical systems. *Chemical Society Reviews* **2017,** *46*, 5647-5678.
72. Grzybowski, B. A.; Stone, H. A.; Whitesides, G. M., Dynamic self-assembly of magnetized, millimetre-sized objects rotating at a liquid–air interface. *Nature* **2000,** *405*, 1033.
73. Ulijn, R. V.; Moore, B. D.; Janssen, A. E.; Halling, P. J., A single aqueous reference equilibrium constant for amide synthesis–hydrolysis. *Journal of the Chemical Society, Perkin Transactions 2* **2002,** 1024-1028.
74. Jayawarna, V.; Ali, M.; Jowitt, T. A.; Miller, A. F.; Saiani, A.; Gough, J. E.; Ulijn, R. V., Nanostructured hydrogels for three-dimensional cell culture through self-assembly of fluorenylmethoxycarbonyl–dipeptides. *Advanced Materials* **2006,** *18*, 611-614.
75. Tang, C.; Smith, A. M.; Collins, R. F.; Ulijn, R. V.; Saiani, A., Fmoc-diphenylalanine self-assembly mechanism induces apparent p K a shifts. *Langmuir* **2009,** *25*, 9447-9453.
76. Raeburn, J.; Mendoza-Cuenca, C.; Cattoz, B. N.; Little, M. A.; Terry, A. E.; Cardoso, A. Z.; Griffiths, P. C.; Adams, D. J., The effect of solvent choice on the gelation and final hydrogel properties of Fmoc–diphenylalanine. *Soft Matter* **2015,** *11*, 927-935.
77. Wang, H.; Yang, Z.; Adams, D. J., Controlling peptidebased hydrogelation. *Materials Today* **2012,** *15*, 500-507.
78. Liu, C.; Jin, Q.; Lv, K.; Zhang, L.; Liu, M., Water tuned the helical nanostructures and supramolecular chirality in organogels. *Chemical Communications* **2014,** *50*, 3702-3705.
79. Jin, Q.; Zhang, L.; Liu, M., Solvent-polarity-tuned morphology and inversion of supramolecular chirality in a self-assembled pyridylpyrazole-linked glutamide derivative: nanofibers, nanotwists, nanotubes, and microtubes. *Chemistry–A European Journal* **2013,** *19*, 9234-9241.
80. Liang, G.; Yang, Z.; Zhang, R.; Li, L.; Fan, Y.; Kuang, Y.; Gao, Y.; Wang, T.; Lu, W. W.; Xu, B., Supramolecular hydrogel of a D-amino acid dipeptide for controlled drug release in vivo. *Langmuir* **2009,** *25*, 8419-8422.
81. Jones, C. D.; Steed, J. W., Gels with sense: supramolecular materials that respond to heat, light and sound. *Chemical Society Reviews* **2016,** *45*, 6546-6596.

82. Wang, Y.; Tang, L.; Yu, J., Investigation on the assembled structure–property correlation of supramolecular hydrogel formed from low-molecular-weight gelator. *Journal of colloid and interface science* **2008,** *319*, 357-364.
83. Ramin, M. A.; Sindhu, K. R.; Appavoo, A.; Oumzil, K.; Grinstaff, M. W.; Chassande, O.; Barthélémy, P., Cation Tuning of Supramolecular Gel Properties: A New Paradigm for Sustained Drug Delivery. *Advanced Materials* **2017,** *29*.
84. Lloyd, G. O.; Steed, J. W., Anion-tuning of supramolecular gel properties. *Nature chemistry* **2009,** *1*, 437.
85. Yan, X.; Li, S.; Cook, T. R.; Ji, X.; Yao, Y.; Pollock, J. B.; Shi, Y.; Yu, G.; Li, J.; Huang, F., Hierarchical self-assembly: well-defined supramolecular nanostructures and metallohydrogels via amphiphilic discrete organoplatinum (II) metallacycles. *Journal of the American Chemical Society* **2013,** *135*, 14036-14039.
86. Colquhoun, C.; Draper, E. R.; Schweins, R.; Marcello, M.; Vadukul, D.; Serpell, L. C.; Adams, D. J., Controlling the network type in self-assembled dipeptide hydrogels. *Soft Matter* **2017,** *13*, 1914-1919.
87. Adams, D. J., Does Drying Affect Gel Networks? *Gels* **2018,** *4*, 32.
88. Yang, B.; Adams, D. J.; Marlow, M.; Zelzer, M., Surface-Mediated Supramolecular Self-assembly of Protein, Peptide and Nucleoside Derivatives: From Surface Design to Underlying Mechanism and Tailored Functions. *Langmuir* **2018**, *34,* 15109–15125.
89. Saiani, A.; Mohammed, A.; Frielinghaus, H.; Collins, R.; Hodson, N.; Kielty, C.; Sherratt, M.; Miller, A., Self-assembly and gelation properties of α-helix versus β-sheet forming peptides. *Soft Matter* **2009,** *5*, 193-202.
90. Kumaraswamy, P.; Lakshmanan, R.; Sethuraman, S.; Krishnan, U. M., Self-assembly of peptides: influence of substrate, pH and medium on the formation of supramolecular assemblies. *Soft Matter* **2011,** *7*, 2744-2754.
91. Korolkov, V. V.; Allen, S.; Roberts, C. J.; Tendler, S. J., Surface mediated L-phenylalanyl-L-phenylalanine assembly into large dendritic structures. *Faraday discussions* **2013,** *166*, 257-267.
92. Huang, R.; Su, R.; Qi, W.; Zhao, J.; He, Z., Hierarchical, interface-induced self-assembly of diphenylalanine: formation of peptide nanofibers and microvesicles. *Nanotechnology* **2011,** *22*, 245609.
93. Mayans, E.; Fabregat, G.; Juárez, R.; Cativiela, C.; Puiggalí, J.; Alemán, C., Surface Mediated Hierarchical Assemblies of Highly Hydrophobic Phenylalanine-Based Peptides. *ChemistrySelect* **2017,** *2*, 1133-1139.
94. Raeburn, J.; Pont, G.; Chen, L.; Cesbron, Y.; Lévy, R.; Adams, D. J., Fmoc-diphenylalanine hydrogels: understanding the variability in reported mechanical properties. *Soft Matter* **2012,** *8*, 1168-1174.
95. Christoff-Tempesta, T.; Lew, A. J.; Ortony, J. H., Beyond Covalent Crosslinks: Applications of Supramolecular Gels. *Gels* **2018,** *4*, 40.
96. Cui, H.; Webber, M. J.; Stupp, S. I., Self-assembly of peptide amphiphiles: From molecules to nanostructures to biomaterials. *Peptide Science* **2010,** *94*, 1-18.
97. Vermonden, T.; Censi, R.; Hennink, W. E., Hydrogels for protein delivery. *Chemical Reviews* **2012,** *112*, 2853-2888.

98. Xing, B.; Yu, C.-W.; Chow, K.-H.; Ho, P.-L.; Fu, D.; Xu, B., Hydrophobic interaction and hydrogen bonding cooperatively confer a vancomycin hydrogel: a potential candidate for biomaterials. *Journal of the American Chemical Society* **2002,** *124*, 14846-14847.
99. van Bommel, K. J.; van der Pol, C.; Muizebelt, I.; Friggeri, A.; Heeres, A.; Meetsma, A.; Feringa, B. L.; van Esch, J., Responsive cyclohexane-based low-molecular-weight hydrogelators with modular architecture. *Angewandte Chemie* **2004,** *116*, 1695-1699.
100. Bhuniya, S.; Seo, Y. J.; Kim, B. H., (S)-(+)-Ibuprofen-based hydrogelators: an approach toward anti-inflammatory drug delivery. *Tetrahedron letters* **2006,** *47*, 7153-7156.
101. Li, J.; Kuang, Y.; Shi, J.; Gao, Y.; Zhou, J.; Xu, B., The conjugation of nonsteroidal anti-inflammatory drugs (NSAID) to small peptides for generating multifunctional supramolecular nanofibers/hydrogels. *Beilstein journal of organic chemistry* **2013,** *9*, 908.
102. Vegners, R.; Shestakova, I.; Kalvinsh, I.; Ezzell, R. M.; Janmey, P. A., Use of a gel-forming dipeptide derivative as a carrier for antigen presentation. *Journal of peptide science* **1995,** *1*, 371-378.
103. Nagai, Y.; Unsworth, L. D.; Koutsopoulos, S.; Zhang, S., Slow release of molecules in self-assembling peptide nanofiber scaffold. *Journal of controlled release* **2006,** *115*, 18-25.
104. Koutsopoulos, S.; Unsworth, L. D.; Nagai, Y.; Zhang, S., Controlled release of functional proteins through designer self-assembling peptide nanofiber hydrogel scaffold. *Proceedings of the National Academy of Sciences* **2009,** *106*, 4623-4628.
105. Soukasene, S.; Toft, D. J.; Moyer, T. J.; Lu, H.; Lee, H.-K.; Standley, S. M.; Cryns, V. L.; Stupp, S. I., Antitumor activity of peptide amphiphile nanofiber-encapsulated camptothecin. *ACS nano* **2011,** *5*, 9113-9121.
106. Naskar, J.; Palui, G.; Banerjee, A., Tetrapeptide-based hydrogels: for encapsulation and slow release of an anticancer drug at physiological pH. *The Journal of Physical Chemistry B* **2009,** *113*, 11787-11792.
107. Moorkens, E.; Meuwissen, N.; Huys, I.; Declerck, P.; Vulto, A. G.; Simoens, S., The market of biopharmaceutical medicines: A snapshot of a diverse industrial landscape. *Frontiers in pharmacology* **2017,** *8*, 314.
108. Li, Y.; Wang, F.; Cui, H., Peptide-based supramolecular hydrogels for delivery of biologics. *Bioengineering & translational medicine* **2016,** *1*, 306-322.
109. Nishimura, A.; Hayakawa, T.; Yamamoto, Y.; Hamori, M.; Tabata, K.; Seto, K.; Shibata, N., Controlled release of insulin from self-assembling nanofiber hydrogel, PuraMatrix™: application for the subcutaneous injection in rats. *European Journal of Pharmaceutical Sciences* **2012,** *45*, 1-7.
110. Zhang, S.; Zhao, X.; Spirio, L., PuraMatrix: self-assembling peptide nanofiber scaffolds. *Scaffolding in tissue engineering* **2005**, 217-238.
111. Tokunou, T.; Miller, R.; Patwari, P.; Davis, M. E.; Segers, V. F.; Grodzinsky, A. J.; Lee, R. T., Engineering insulin-like growth factor-1 for local delivery. *The FASEB Journal* **2008,** *22*, 1886-1893.
112. Guo, H.; Cui, G.; Yang, J.; Wang, C.; Zhu, J.; Zhang, L.; Jiang, J.; Shao, S., Sustained delivery of VEGF from designer self-assembling peptides

improves cardiac function after myocardial infarction. *Biochemical and biophysical research communications* **2012,** *424*, 105-111.
113. Rajangam, K.; Behanna, H. A.; Hui, M. J.; Han, X.; Hulvat, J. F.; Lomasney, J. W.; Stupp, S. I., Heparin binding nanostructures to promote growth of blood vessels. *Nano letters* **2006,** *6*, 2086-2090.
114. Branco, M. C.; Pochan, D. J.; Wagner, N. J.; Schneider, J. P., Macromolecular diffusion and release from self-assembled β-hairpin peptide hydrogels. *Biomaterials* **2009,** *30*, 1339-1347.
115. Branco, M. C.; Pochan, D. J.; Wagner, N. J.; Schneider, J. P., The effect of protein structure on their controlled release from an injectable peptide hydrogel. *Biomaterials* **2010,** *31*, 9527-9534.
116. Ramin, M. A.; Latxague, L.; Sindhu, K. R.; Chassande, O.; Barthélémy, P., Low molecular weight hydrogels derived from urea based-bolaamphiphiles as new injectable biomaterials. *Biomaterials* **2017,** *145*, 72-80.
117. Kaplan, J.; Barthélémy, P.; Grinstaff, M., Self-assembled nanofiber hydrogels for mechanoresponsive therapeutic anti-TNFα antibody delivery. *Chemical Communications* **2016,** *52*, 5860-5863.
118. Allain, V.; Bourgaux, C.; Couvreur, P., Self-assembled nucleolipids: from supramolecular structure to soft nucleic acid and drug delivery devices. *Nucleic acids research* **2011,** *40*, 1891-1903.
119. Sreenivasachary, N.; Lehn, J. M., Structural Selection in G-Quartet-Based Hydrogels and Controlled Release of Bioactive Molecules. *Chemistry–An Asian Journal* **2008,** *3*, 134-139.
120. Plank, T. N.; Davis, J. T., AG 4· K+ hydrogel that self-destructs. *Chemical Communications* **2016,** *52*, 5037-5040.
121. Nagy-Smith, K.; Yamada, Y.; Schneider, J. P., Protein release from highly charged peptide hydrogel networks. *Journal of Materials Chemistry B* **2016,** *4*, 1999-2007.
122. Javid, N.; Roy, S.; Zelzer, M.; Yang, Z.; Sefcik, J.; Ulijn, R. V., Cooperative self-assembly of peptide gelators and proteins. *Biomacromolecules* **2013,** *14*, 4368-4376.
123. Yu, G.; Yan, X.; Han, C.; Huang, F., Characterization of supramolecular gels. *Chemical Society Reviews* **2013,** *42*, 6697-6722.
124. Morris, K. L.; Chen, L.; Raeburn, J.; Sellick, O. R.; Cotanda, P.; Paul, A.; Griffiths, P. C.; King, S. M.; O'Reilly, R. K.; Serpell, L. C., Chemically programmed self-sorting of gelator networks. *Nature communications* **2013,** *4*, 1480.
125. Escuder, B.; LLusar, M.; Miravet, J. F., Insight on the NMR study of supramolecular gels and its application to monitor molecular recognition on self-assembled fibers. *The Journal of organic chemistry* **2006,** *71*, 7747-7752.
126. Nuthanakanti, A.; Srivatsan, S. G., Surface-tuned and metal ion-responsive supramolecular gels based on nucleolipids. *ACS Applied Materials & Interfaces* **2017**.
127. Ramalhete, S. M.; Nartowski, K. P.; Sarathchandra, N.; Foster, J. S.; Round, A. N.; Angulo, J.; Lloyd, G. O.; Khimyak, Y. Z., Supramolecular amino acid based hydrogels: probing the contribution of additive molecules using NMR spectroscopy. *Chemistry-A European Journal* **2017,** *23*, 8014-8024.

128. Šaman, D.; Kolehmainen, E., Studies on supramolecular gel formation using DOSY NMR. *Magnetic Resonance in Chemistry* **2015,** *53*, 256-260.
129. Duncan, D. C.; Whitten, D. G., 1H NMR Investigation of the Composition, Structure, and Dynamics of Cholesterol− Stilbene Tethered Dyad Organogels. *Langmuir* **2000,** *16*, 6445-6452.
130. Wallace, M.; Iggo, J. A.; Adams, D. J., Probing the surface chemistry of self-assembled peptide hydrogels using solution-state NMR spectroscopy. *Soft matter* **2017,** *13*, 1716-1727.
131. Segarra-Maset, M. D.; Escuder, B.; Miravet, J. F., Selective Interaction of Dopamine with the Self-Assembled Fibrillar Network of a Molecular Hydrogel Revealed by STD-NMR. *Chemistry-A European Journal* **2015,** *21*, 13925-13929.
132. Wallace, M.; Adams, D. J.; Iggo, J. A., Analysis of the mesh size in a supramolecular hydrogel by PFG-NMR spectroscopy. *Soft Matter* **2013,** *9*, 5483-5491.
133. Skilling, K. J.; Ndungu, A.; Kellam, B.; Ashford, M.; Bradshaw, T. D.; Marlow, M., Gelation properties of self-assembling N-acyl modified cytidine derivatives. *Journal of Materials Chemistry B* **2014,** *2*, 8412-8417.
134. Iwaura, R.; Yoshida, K.; Masuda, M.; Ohnishi-Kameyama, M.; Yoshida, M.; Shimizu, T., Oligonucleotide-templated self-assembly of nucleotide bolaamphiphiles: DNA-like nanofibers edged by a double-helical arrangement of A–T base pairs. *Angewandte Chemie International Edition* **2003,** *42*, 1009-1012.
135. Chen, L.; Morris, K.; Laybourn, A.; Elias, D.; Hicks, M. R.; Rodger, A.; Serpell, L.; Adams, D. J., Self-assembly mechanism for a naphthalene− dipeptide leading to hydrogelation. *Langmuir* **2009,** *26*, 5232-5242.
136. Nordén, B.; Rodger, A.; Dafforn, T., *Linear dichroism and circular dichroism*. The Royal Society of Chemistry: 2010.
137. Sprecher, C. A.; Johnson, W. C., Circular dichroism of the nucleic acid monomers. *Biopolymers* **1977,** *16*, 2243-2264.
138. Bulheller, B. M.; Rodger, A.; Hirst, J. D., Circular and linear dichroism of proteins. *Physical Chemistry Chemical Physics* **2007,** *9*, 2020-2035.
139. Gao, Y.; Berciu, C.; Kuang, Y.; Shi, J.; Nicastro, D.; Xu, B., Probing nanoscale self-assembly of nonfluorescent small molecules inside live mammalian cells. *ACS nano* **2013,** *7*, 9055-9063.
140. Raeburn, J.; Chen, L.; Awhida, S.; Deller, R. C.; Vatish, M.; Gibson, M. I.; Adams, D. J., Using molecular rotors to probe gelation. *Soft Matter* **2015,** *11*, 3706-3713.
141. Guilbaud, J.-B.; Saiani, A., Using small angle scattering (SAS) to structurally characterise peptide and protein self-assembled materials. *Chemical Society Reviews* **2011,** *40*, 1200-1210.
142. Sivia, D. S., *Elementary scattering theory: for X-ray and neutron users*. Oxford University Press: 2011.
143. Svergun, D. I.; Koch, M. H., Small-angle scattering studies of biological macromolecules in solution. *Reports on Progress in Physics* **2003,** *66*, 1735.
144. Frederix, P. W.; Patmanidis, I.; Marrink, S. J., Molecular simulations of self-assembling bio-inspired supramolecular systems and their connection to experiments. *Chemical Society Reviews* **2018,** *47*, 3470-3489.

145. Anderson, K. M.; Day, G. M.; Paterson, M. J.; Byrne, P.; Clarke, N.; Steed, J. W., Structure calculation of an elastic hydrogel from sonication of rigid small molecule components. *Angewandte Chemie International Edition* **2008,** *47*, 1058-1062.
146. Hsu, C.-H.; Jeng, U.-S.; Lee, H.-Y.; Huang, C.-M.; Liang, K.; Windover, D.; Lu, T.-M.; Jin, C., Structural study of a low dielectric thin film using X-ray reflectivity and grazing incidence small angle X-ray scattering. *Thin Solid Films* **2005,** *472*, 323-327.
147. Rabolt, J.; Jurich, M.; Swalen, J., Infrared reflection-absorption studies of thin films at grazing incidence. *Applied Spectroscopy* **1985,** *39*, 269-272.
148. Flores, S. M.; Toca-Herrera, J. L., The new future of scanning probe microscopy: Combining atomic force microscopy with other surface-sensitive techniques, optical microscopy and fluorescence techniques. *Nanoscale* **2009,** *1*, 40-49.
149. Woodruff, D. P., *Modern techniques of surface science*. Cambridge university press: 2016.
150. Good, R. J., Contact angle, wetting, and adhesion: a critical review. *Journal of adhesion science and technology* **1992,** *6*, 1269-1302.
151. Smith, A. M.; Williams, R. J.; Tang, C.; Coppo, P.; Collins, R. F.; Turner, M. L.; Saiani, A.; Ulijn, R. V., Fmoc-Diphenylalanine Self Assembles to a Hydrogel via a Novel Architecture Based on π–π Interlocked β-Sheets. *Advanced Materials* **2008,** *20*, 37-41.
152. Iwaura, R.; Yoshida, K.; Masuda, M.; Yase, K.; Shimizu, T., Spontaneous fiber formation and hydrogelation of nucleotide bolaamphiphiles. *Chemistry of materials* **2002,** *14*, 3047-3053.
153. Roviello, G. N.; Oliviero, G.; Di Napoli, A.; Borbone, N.; Piccialli, G., Synthesis, self-assembly-behavior and biomolecular recognition properties of thyminyl dipeptides. *Arabian Journal of Chemistry* **2018**.
154. Ma, M.; Kuang, Y.; Gao, Y.; Zhang, Y.; Gao, P.; Xu, B., Aromatic− aromatic interactions induce the self-assembly of pentapeptidic derivatives in water to form nanofibers and supramolecular hydrogels. *Journal of the American Chemical Society* **2010,** *132*, 2719-2728.
155. Fu, I. W.; Markegard, C. B.; Chu, B. K.; Nguyen, H. D., Role of hydrophobicity on self-assembly by peptide amphiphiles via molecular dynamics simulations. *Langmuir* **2014,** *30*, 7745-7754.
156. Han, S.; Cao, S.; Wang, Y.; Wang, J.; Xia, D.; Xu, H.; Zhao, X.; Lu, J. R., Self-assembly of short peptide amphiphiles: the cooperative effect of hydrophobic interaction and hydrogen bonding. *Chemistry–A European Journal* **2011,** *17*, 13095-13102.
157. Elemans, J. A.; Rowan, A. E.; Nolte, R. J., Mastering molecular matter. Supramolecular architectures by hierarchical self-assembly. *Journal of Materials Chemistry* **2003,** *13*, 2661-2670.
158. Aggeli, A.; Nyrkova, I. A.; Bell, M.; Harding, R.; Carrick, L.; McLeish, T. C.; Semenov, A. N.; Boden, N., Hierarchical self-assembly of chiral rod-like molecules as a model for peptide β-sheet tapes, ribbons, fibrils, and fibers. *Proceedings of the National Academy of Sciences* **2001,** *98*, 11857-11862.

159. Adler-Abramovich, L.; Gazit, E., The physical properties of supramolecular peptide assemblies: from building block association to technological applications. *Chemical Society Reviews* **2014,** *43*, 6881-6893.
160. Busseron, E.; Ruff, Y.; Moulin, E.; Giuseppone, N., Supramolecular self-assemblies as functional nanomaterials. *Nanoscale* **2013,** *5*, 7098-7140.
161. Johnson, E. K.; Adams, D. J.; Cameron, P. J., Peptide based low molecular weight gelators. *Journal of Materials Chemistry* **2011,** *21*, 2024-2027.
162. Baillet, J.; Desvergnes, V.; Hamoud, A.; Latxague, L.; Barthélémy, P., Lipid and Nucleic Acid Chemistries: Combining the Best of Both Worlds to Construct Advanced Biomaterials. *Advanced Materials* **2018,** *30*.
163. Maisani, M.; Ziane, S.; Ehret, C.; Levesque, L.; Siadous, R.; Le Meins, J. F.; Chevallier, P.; Barthélémy, P.; De Oliveira, H.; Amédée, J., A new composite hydrogel combining the biological properties of collagen with the mechanical properties of a supramolecular scaffold for bone tissue engineering. *Journal of tissue engineering and regenerative medicine* **2017,** *12:e1489-e1500.*
164. Angelerou, M. G. F.; Sabri, A.; Creasey, R.; Angelerou, P.; Marlow, M.; Zelzer, M., Surface-directed modulation of supramolecular gel properties. *Chemical Communications* **2016,** *52*, 4298-4300.
165. Schaaf, P.; Vigier-Carrière, C.; Boulmedais, F.; Jierry, L., Surface-assisted self-assembly strategies leading to supramolecular hydrogels. *Angewandte Chemie* **2017**.
166. Bogliotti, N.; Ritter, A.; Hebbe, S.; Vasella, A., Oligonucleotide Analogues with Integrated Bases and Backbones. Part 19. *Helvetica chimica acta* **2008,** *91*, 2181-2202.
167. Banerjee, P.; Pyne, A.; Pal, S.; Karan, C. K.; Sarkar, N., Self-assembling behavior of pyrimidine analogues: Unveiling the factors behind morphological diversity. *Journal of colloid and interface science* **2018,** *522*, 63-73.
168. Thota, N.; Jiang, J., Computational amphiphilic materials for drug delivery. *Frontiers in Materials* **2015,** *2*, 64.
169. Manandhar, A.; Kang, M.; Chakraborty, K.; Tang, P. K.; Loverde, S. M., Molecular simulations of peptide amphiphiles. *Organic & biomolecular chemistry* **2017,** *15*, 7993-8005.
170. Yuan, C.; Li, S.; Zou, Q.; Ren, Y.; Yan, X., Multiscale simulations for understanding the evolution and mechanism of hierarchical peptide self-assembly. *Physical Chemistry Chemical Physics* **2017,** *19*, 23614-23631.
171. Pan, D.; Tang, C.; Fan, X.; Li, Y.; Yang, X.; Jin, H.; Guan, Z.; Yang, Z.; Zhang, L., Thymidine-based amphiphiles and their bonding to DNA. *New Journal of Chemistry* **2013,** *37*, 1122-1127.
172. Lepeltier, E.; Bourgaux, C.; Rosilio, V. r.; Poupaert, J. H.; Meneau, F.; Zouhiri, F.; Lepêtre-Mouelhi, S.; Desmaële, D.; Couvreur, P., Self-assembly of squalene-based nucleolipids: relating the chemical structure of the bioconjugates to the architecture of the nanoparticles. *Langmuir* **2013,** *29*, 14795-14803.
173. Fichman, G.; Gazit, E., Self-assembly of short peptides to form hydrogels: Design of building blocks, physical properties and technological applications. *Acta biomaterialia* **2014,** *10*, 1671-1682.

174. Hughes, M.; Birchall, L. S.; Zuberi, K.; Aitken, L. A.; Debnath, S.; Javid, N.; Ulijn, R. V., Differential supramolecular organisation of Fmoc-dipeptides with hydrophilic terminal amino acid residues by biocatalytic self-assembly. *Soft Matter* **2012,** *8*, 11565-11574.
175. Maitra, U.; Mukhopadhyay, S.; Sarkar, A.; Rao, P.; Indi, S., Hydrophobic pockets in a nonpolymeric aqueous gel: observation of such a gelation process by color change. *Angewandte Chemie International Edition* **2001,** *40*, 2281-2283.
176. Greenspan, P.; Mayer, E. P.; Fowler, S. D., Nile red: a selective fluorescent stain for intracellular lipid droplets. *The Journal of cell biology* **1985,** *100*, 965-973.
177. Gels, M., Materials with self-assembled fibrillar networks, ed. RG Weiss and P. Terech. Springer, Dordrecht: 2006.
178. Angulo, J.; Enríquez-Navas, P. M.; Nieto, P. M., Ligand–receptor binding affinities from saturation transfer difference (STD) NMR spectroscopy: the binding isotherm of STD initial growth rates. *Chemistry-A European Journal* **2010,** *16*, 7803-7812.
179. Iqbal, S.; Rodríguez-LLansola, F.; Escuder, B.; Miravet, J. F.; Verbruggen, I.; Willem, R., HRMAS 1H NMR as a tool for the study of supramolecular gels. *Soft Matter* **2010,** *6*, 1875-1878.
180. Mears, L. L.; Draper, E. R.; Castilla, A. M.; Su, H.; Dietrich, B.; Nolan, M. C.; Smith, G. N.; Doutch, J.; Rogers, S.; Akhtar, R.; Cui, H.; Adams, D. J., Drying affects the fiber network in low molecular weight hydrogels. *Biomacromolecules* **2017,** *18*, 3531-3540.
181. Baldelli Bombelli, F.; Berti, D.; Keiderling, U.; Baglioni, P., Giant polymerlike micelles formed by nucleoside-functionalized lipids. *The Journal of Physical Chemistry B* **2002,** *106*, 11613-11621.
182. Hess, B.; Kutzner, C.; Van Der Spoel, D.; Lindahl, E., GROMACS 4: algorithms for highly efficient, load-balanced, and scalable molecular simulation. *Journal of chemical theory and computation* **2008,** *4*, 435-447.
183. Reif, M. M.; Hünenberger, P. H.; Oostenbrink, C., New interaction parameters for charged amino acid side chains in the GROMOS force field. *Journal of chemical theory and computation* **2012,** *8*, 3705-3723.
184. Reif, M. M.; Winger, M.; Oostenbrink, C., Testing of the GROMOS force-field parameter set 54A8: structural properties of electrolyte solutions, lipid bilayers, and proteins. *Journal of chemical theory and computation* **2013,** *9*, 1247-1264.
185. Berendsen, H. J.; Postma, J. P.; van Gunsteren, W. F.; Hermans, J., Interaction models for water in relation to protein hydration. In *Intermolecular forces*, Springer: 1981; pp 331-342.
186. Hess, B., P-LINCS: A parallel linear constraint solver for molecular simulation. *Journal of Chemical Theory and Computation* **2008,** *4*, 116-122.
187. Miyamoto, S.; Kollman, P. A., SETTLE: an analytical version of the SHAKE and RATTLE algorithm for rigid water models. *Journal of computational chemistry* **1992,** *13*, 952-962.
188. Bussi, G.; Donadio, D.; Parrinello, M., Canonical sampling through velocity rescaling. *The Journal of chemical physics* **2007,** *126*, 014101.

189. Berendsen, H. J.; Postma, J. v.; van Gunsteren, W. F.; DiNola, A.; Haak, J., Molecular dynamics with coupling to an external bath. *The Journal of chemical physics* **1984,** *81*, 3684-3690.
190. Humphrey, W.; Dalke, A.; Schulten, K., VMD: Visual Molecular Dynamics. *Journal of Molecular Graphics* **1996,** *14*, 33-38.
191. Williams, R. J.; Mart, R. J.; Ulijn, R. V., Exploiting biocatalysis in peptide self-assembly. *Peptide Science: Original Research on Biomolecules* **2010,** *94*, 107-117.
192. Gooding, J. J.; Mearns, F.; Yang, W.; Liu, J., Self-assembled monolayers into the 21st century: recent advances and applications. *Electroanalysis: An International Journal Devoted to Fundamental and Practical Aspects of Electroanalysis* **2003,** *15*, 81-96.
193. Blunt, M. O.; Russell, J. C.; del Carmen Gimenez-Lopez, M.; Taleb, N.; Lin, X.; Schröder, M.; Champness, N. R.; Beton, P. H., Guest-induced growth of a surface-based supramolecular bilayer. *Nature chemistry* **2011,** *3*, 74.
194. Williams, R. J.; Smith, A. M.; Collins, R.; Hodson, N.; Das, A. K.; Ulijn, R. V., Enzyme-assisted self-assembly under thermodynamic control. *Nature nanotechnology* **2009,** *4*, 19.
195. Johnson, E. K.; Chen, L.; Kubiak, P. S.; McDonald, S. F.; Adams, D. J.; Cameron, P. J., Surface nucleated growth of dipeptide fibres. *Chemical Communications* **2013,** *49*, 8698-8700.
196. Lee, S. S.; Tang, S. B.; Smilgies, D. M.; Woll, A. R.; Loth, M. A.; Mativetsky, J. M.; Anthony, J. E.; Loo, Y. L., Guiding crystallization around bends and sharp corners. *Advanced Materials* **2012,** *24*, 2692-2698.
197. Dong, X.; Gusev, A.; Hercules, D. M., Characterization of polysiloxanes with different functional groups by time-of-flight secondary ion mass spectrometry. *Journal of the American Society for Mass Spectrometry* **1998,** *9*, 292-298.
198. Domke, J.; Radmacher, M., Measuring the elastic properties of thin polymer films with the atomic force microscope. *Langmuir* **1998,** *14*, 3320-3325.
199. Oyen, M., Mechanical characterisation of hydrogel materials. *International Materials Reviews* **2014,** *59*, 44-59.
200. Angelerou, M.; Frederix, P. W.; Wallace, M.; Yang, B.; Rodger, A.; Adams, D. J.; Marlow, M.; Zelzer, M., A supramolecular nucleoside-based gel: Molecular dynamics simulation and characterization of its nanoarchitecture and self-assembly mechanism. *Langmuir* **2018**, *14,* 6912-6921.
201. Als-Nielsen, J.; Jacquemain, D.; Kjaer, K.; Leveiller, F.; Lahav, M.; Leiserowitz, L., Principles and applications of grazing incidence x-ray and neutron scattering from ordered molecular monolayers at the air-water interface. *Physics Reports* **1994,** *246*, 251-313.
202. Renaud, G.; Lazzari, R.; Leroy, F., Probing surface and interface morphology with grazing incidence small angle X-ray scattering. *Surface Science Reports* **2009,** *64*, 255-380.
203. Lee, S.; Jo, W.; Cho, Y. c.; Lee, H. H.; Lee, G. W., Solution electrostatic levitator for measuring surface properties and bulk structures of

an extremely supersaturated solution drop above metastable zone width limit. *Review of Scientific Instruments* **2017,** *88*, 055101.
204. Tresset, G., The multiple faces of self-assembled lipidic systems. *PMC biophysics* **2009,** *2*, 3.
205. Nicklin, C.; Arnold, T.; Rawle, J.; Warne, A., Diamond beamline I07: a beamline for surface and interface diffraction. *Journal of synchrotron radiation* **2016,** *23*, 1245-1253.
206. Wang, J.-X.; Lei, Q.; Luo, G.-F.; Cai, T.-T.; Li, J.-L.; Cheng, S.-X.; Zhuo, R.-X.; Zhang, X.-Z., Controlled arrays of self-assembled peptide nanostructures in solution and at interface. *Langmuir* **2013,** *29*, 6996-7004.
207. Pedersen, J. S.; Schurtenberger, P., Scattering functions of semiflexible polymers with and without excluded volume effects. *Macromolecules* **1996,** *29*, 7602-7612.
208. Chen, W.-R.; Butler, P. D.; Magid, L. J., Incorporating intermicellar interactions in the fitting of SANS data from cationic wormlike micelles. *Langmuir* **2006,** *22*, 6539-6548.
209. Hoffman, A. S., Hydrogels for biomedical applications. *Advanced drug delivery reviews* **2012,** *64*, 18-23.
210. Gupta, P.; Vermani, K.; Garg, S., Hydrogels: from controlled release to pH-responsive drug delivery. *Drug discovery today* **2002,** *7* (10), 569-579.
211. Qiu, Y.; Park, K., Environment-sensitive hydrogels for drug delivery. *Advanced drug delivery reviews* **2001,** *53*, 321-339.
212. Mart, R. J.; Osborne, R. D.; Stevens, M. M.; Ulijn, R. V., Peptide-based stimuli-responsive biomaterials. *Soft Matter* **2006,** *2*, 822-835.
213. Li, X.; Du, X.; Li, J.; Gao, Y.; Pan, Y.; Shi, J.; Zhou, N.; Xu, B., Introducing D-amino acid or simple glycoside into small peptides to enable supramolecular hydrogelators to resist proteolysis. *Langmuir* **2012,** *28*, 13512-13517.
214. Li, X.; Du, X.; Gao, Y.; Shi, J.; Kuang, Y.; Xu, B., Supramolecular hydrogels formed by the conjugates of nucleobases, Arg-Gly-Asp (RGD) peptides, and glucosamine. *Soft Matter* **2012,** *8*, 7402-7407.
215. Kruger, N. J., The Bradford method for protein quantitation. In *The protein protocols handbook*, Springer: 2002; pp 15-21.
216. Barichello, J. M.; Morishita, M.; Takayama, K.; Nagai, T., Absorption of insulin from Pluronic F-127 gels following subcutaneous administration in rats. *International journal of pharmaceutics* **1999,** *184*, 189-198.
217. Wang, P. L.; Johnston, T. P., Sustained-release interleukin-2 following intramuscular injection in rats. *International journal of pharmaceutics* **1995,** *113*, 73-81.
218. Neurath, H., Evolution of proteolytic enzymes. *Science* **1984,** *224*, 350-357.
219. Gráf, L.; Szilágyi, L.; Venekei, I., Chymotrypsin. In *Handbook of Proteolytic Enzymes (Third Edition)*, Elsevier: 2013; 2626-2633.
220. Smith, M. E.; Morton, D. G., *The Digestive System: Systems of the Body Series*. Elsevier Health Sciences: 2011.
221. Berg, J.; Tymoczko, J.; Stryer, L.; Stryer, L., Biochemistry, Ed 5th. WH Freeman, New York: 2002.
222. Shugar, D., The measurement of lysozyme activity and the ultra-violet inactivation of lysozyme. *Biochimica et biophysica acta* **1952,** *8*, 302-309.

223. Dooley, K. A.; Millinder, S.; Osborne, T. F., Sterol regulation of 3-hydroxy-3-methylglutaryl-coenzyme A synthase gene through a direct interaction between sterol regulatory element binding protein and the trimeric CCAAT-binding factor/nuclear factor Y. *Journal of Biological Chemistry* **1998,** *273*, 1349-1356.
224. Smith, J. R.; Osborne, T.; Brown, M. S.; Goldstein, J. L.; Gil, G., Multiple sterol regulatory elements in promoter for hamster 3-hydroxy-3-methylglutaryl-coenzyme A synthase. *Journal of Biological Chemistry* **1988,** *263*, 18480-18487.
225. Harris, I. R.; Höppner, H.; Siefken, W.; Wittern, K.-P.; Farrell, A. M., Regulation of HMG-CoA synthase and HMG-CoA reductase by insulin and epidermal growth factor in HaCaT keratinocytes. *Journal of investigative dermatology* **2000,** *114*, 83-87.
226. Mayo Clinic Laboratory. Serum Insulin range of values for normal population at fasting. . https://www.mayomedicallaboratories.com/test-catalog/Clinical+and+Interpretive/62990.
227. Melmed, S.; Polonsky, K.; Larsen, P.; Kronenberg, H., Williams Textbook of Endocrinology. *Philadelphia, PA: Saunders Elsevier* **2011**.
228. Rees, A. R.; Sternberg, M. J., From Cells to Atoms: An illustrated introduction to molecular biology. Wiley-Blackwell, **1984**.
229. Bravo, S. B.; Garcia-Rendueles, M. E.; Garcia-Rendueles, A. R.; Rodrigues, J. S.; Perez-Romero, S.; Garcia-Lavandeira, M.; Suarez-Fariña, M.; Barreiro, F.; Czarnocka, B.; Senra, A., Humanized medium (h7H) allows long-term primary follicular thyroid cultures from human normal thyroid, benign neoplasm, and cancer. *The Journal of Clinical Endocrinology & Metabolism* **2013,** *98*, 2431-2441.
230. Udenfriend, S.; Stein, S.; Boehlen, P.; Dairman, W.; Leimgruber, W.; Weigele, M., Fluorescamine: a reagent for assay of amino acids, peptides, proteins, and primary amines in the picomole range. *Science* **1972,** *178*, 871-872.
231. Johnson, L.; Angelerou, M. G. F.; Surikutchi, B. T.; Allen, S.; Zelzer, M.; Marlow, M., Low molecular weight nucleoside gelators: A platform for protein aggregation inhibition. *Molecular pharmaceutics* **2018**.
232. Royer, C. A., Probing protein folding and conformational transitions with fluorescence. *Chemical reviews* **2006,** *106*, 1769-1784.
233. Son, A. R.; Park, S. H.; Jang, J. Y.; Kim, K.; Kim, B. J.; Yin, X. Y.; Kim, J. H.; Min, B. H.; Han, D. K.; Kim, M. S., Direct chemotherapeutic dual drug delivery through intra-articular injection for synergistic enhancement of rheumatoid arthritis treatment. *Scientific reports* **2015,** *5*, 14713.
234. Anderson, J. M., Biological responses to materials. *Annual review of materials research* **2001,** *31*, 81-110.
235. Anderson, J. M.; Shive, M. S., Biodegradation and biocompatibility of PLA and PLGA microspheres. *Advanced drug delivery reviews* **1997,** *28*, 5-24.
236. Anderson, J. M., In vivo biocompatibility of implantable delivery systems and biomaterials. *European journal of pharmaceutics and biopharmaceutics* **1994,** *40*, 1-8.
237. Motulsky, A.; Lafleur, M.; Couffin-Hoarau, A.-C.; Hoarau, D.; Boury, F.; Benoit, J.-P.; Leroux, J.-C., Characterization and biocompatibility of

organogels based on L-alanine for parenteral drug delivery implants. *Biomaterials* **2005,** *26*, 6242-6253.
238. Garcia-Rendueles, A.; Rodrigues, J.; Garcia-Rendueles, M.; Suarez-Fariña, M.; Perez-Romero, S.; Barreiro, F.; Bernabeu, I.; Rodriguez-Garcia, J.; Fugazzola, L.; Sakai, T., Rewiring of the apoptotic TGF-β-SMAD/NFκB pathway through an oncogenic function of p27 in human papillary thyroid cancer. *Oncogene* **2017,** *36*, 652.
239. Gast, K.; Schüler, A.; Wolff, M.; Thalhammer, A.; Berchtold, H.; Nagel, N.; Lenherr, G.; Hauck, G.; Seckler, R., Rapid-Acting and Human Insulins: Hexamer Dissociation Kinetics upon Dilution of the Pharmaceutical Formulation. *Pharmaceutical research* **2017,** *34*, 2270-2286.
240. Rombouts, I.; Lagrain, B.; Scherf, K. A.; Lambrecht, M. A.; Koehler, P.; Delcour, J. A., Formation and reshuffling of disulfide bonds in bovine serum albumin demonstrated using tandem mass spectrometry with collision-induced and electron-transfer dissociation. *Scientific reports* **2015,** *5*, 12210.
241. Barone, G.; Capasso, S.; Del Vecchio, P.; De Sena, C.; Fessas, D.; Giancola, C.; Graziano, G.; Tramonti, P., Thermal denaturation of bovine serum albumin and its oligomers and derivatives pH dependence. *Journal of Thermal Analysis and Calorimetry* **1995,** *45*, 1255-1264.
242. Heeres, A.; van der Pol, C.; Stuart, M.; Friggeri, A.; Feringa, B. L.; van Esch, J., Orthogonal self-assembly of low molecular weight hydrogelators and surfactants. *Journal of the American Chemical Society* **2003,** *125*, 14252-14253.
243. Draper, E. R.; Adams, D. J., Supramolecular fibres: Self-sorting shows its true colours. *Nature chemistry* **2016,** *8*, 737.
244. Moffat, J. R.; Smith, D. K., Controlled self-sorting in the assembly of 'multi-gelator'gels. *Chemical Communications* **2009,** 316-318.
245. Skilling, K. J.; Stocks, M. J.; Kellam, B.; Ashford, M.; Bradshaw, T. D.; Burroughs, L.; Marlow, M., Nucleoside-Based Self-Assembling Drugs for Localized Drug Delivery. *ChemMedChem* **2018**.
246. Cornwell, D. J.; Smith, D. K., Expanding the scope of gels–combining polymers with low-molecular-weight gelators to yield modified self-assembling smart materials with high-tech applications. *Materials Horizons* **2015,** *2*, 279-293.
247. Cornwell, D. J.; Okesola, B. O.; Smith, D. K., Hybrid polymer and low molecular weight gels–dynamic two-component soft materials with both responsive and robust nanoscale networks. *Soft Matter* **2013,** *9*, 8730-8736.
248. Cornwell, D. J.; Okesola, B. O.; Smith, D. K., Multidomain Hybrid Hydrogels: Spatially Resolved Photopatterned Synthetic Nanomaterials Combining Polymer and Low-Molecular-Weight Gelators. *Angewandte Chemie International Edition* **2014,** *53*, 12461-12465.
249. Wang, J.; Wang, Z.; Gao, J.; Wang, L.; Yang, Z.; Kong, D.; Yang, Z., Incorporation of supramolecular hydrogels into agarose hydrogels—a potential drug delivery carrier. *Journal of Materials Chemistry* **2009,** *19*, 7892-7896.
250. Vieira, V. M.; Hay, L. L.; Smith, D. K., Multi-component hybrid hydrogels–understanding the extent of orthogonal assembly and its impact on controlled release. *Chemical science* **2017,** *8*, 6981-6990.